UNIVERSITY OF CALIFORNIA, SAN DIEGO

Ultraviolet resonance Raman and fluorescence studies of folded and unfolded conformations of the membrane protein OmpA

A dissertation submitted in partial satisfaction of the
requirements for the degree Doctor of Philosophy

in

Chemistry

by

Katheryn Marie Sanchez

Committee in charge:

Professor Judy E. Kim, Chair
Professor Robert E. Continetti
Professor Douglas Magde
Professor Melvin Okamura
Professor Mark Thiemens
Professor Hector Viadiu-Ilarraza

2010

The Dissertation of Katheryn Marie Sanchez is approved, and it is acceptable in quality and form for publication on microfilm and electronically:

_____

_____

_____

_____

_____

_____

Chair

University of California, San Diego

2010

DEDICATION

This dissertation is dedicated to

My husband, Andrew. Thank you for your unending love, support, and patience. Thank you for being my best friend and cheerleader always. Without you, I would not have survived graduate school.

My parents, Alan and Holly Holderness. Thank you for all of your love, (mental, emotional, and financial) support, and encouragement with all of my life decisions. Mom, thank you for suggesting I take a chemistry class in the first place.

My sister, Brynn Marie Ervin, and the rest of my family and friends, Kyle, Josh & Megan, Jennifer & James, Lane & Carole, Monique, Katrina. You have given me all the love and support a girl could ever ask for.

TABLE OF CONTENTS

LIST OF ABBREVIATIONS

DMPC: 1,2-dimyristoyl-*sn*-glycero-3-phosphocholine

DPPC: 1,2-dipalmitoyl-*sn*-glycero-3-phosphocholine

DMPE: 1,2-dimyristoyl-*sn*-glycero-3-phosphoethanolamine

kDa: kilodalton

LPS: lipopolysaccharides

OG: octyl-glucopyranoside

OmpA: Outer Membrane Protein A

Phe: phenylalanine

SASA: solvent accessible surface area

SDS-PAGE: sodium dodecyl sulfate polyacrylamide gel electrophoresis

Ti:Sapph: Titanium Sapphire

Trp: tryptophan

Tyr: tyrosine

UVRR: Ultraviolet resonance Raman

WT: wild type

LIST OF FIGURES

LIST OF TABLES

ACKNOWLEDGEMENTS

I would like to express my deepest gratitude to my advisor Professor Judy Kim. It has been a wonderful experience working with you. Thank you for all of your expertise, excitement, motivation, and guidance during graduate school. You have been an inspiration to us all.

I would also like to thank my past and present lab members Diana Schlamadinger, Jon Gable, Tiffany Neary, Hannah Shafaat, Tim Tirrell, and Eric Smoll, and our postdoctoral researchers Dr. Vanessa Oklejas, and Dr. Christina Stuart, for their support in times of triumph, crises, and surviving day-to-day life in the lab. Thank you for all of the scientific discussions at the coffee cart and the pub. I especially want to thank the undergraduate researchers who have helped with the expression of OmpA. Without these hardworking individuals, it would have taken me twice as long to finish. From being to end: Jon Gable, Tiffany Neary, Nadhia Gotama, Ruben Carmona, William Gaieck, Beijing Wu, and Cyril Gary.

I greatly appreciate my friends at UCSD who were always up for a break: Dr. John Savee, Dr. Ryan Sullivan, Dr. Jamie Matthews, Dr. Anna Cogen, Dustin Huard, Lauren Brothers, Dr. Christina Stuart, and Dr. Nancy Santagata. Thank you for all of the lunches, coffee breaks, and therapy sessions- You are truly great friends.

A special thanks to Professor Bob Continetti, who rented me space in his lab for six months during my second year. A special thanks to Professor Doug Magde, who took the time to train me on his laser system and teach me all he knows about dynamic light scattering.

Chapter 3, in part, is a reprint of the material as it appears in Biochemistry 47, 2008. Sanchez, Katheryn M.; Gable, Jonathan E.; Schlamadinger, Diana E.; Kim, Judy E. American Chemical Society 2008. The dissertation author was the primary investigator and author of this paper.

Chapter 5, in part, is a reprint of the material as it appears in Journal of Physical Chemistry B 112, 2008. Sanchez, Katheryn M.; Neary, Tiffany J.; Kim, Judy E. American Chemical Society 2008. The dissertation author was the primary investigator and author of this paper.

Chapter 6, in part, is currently in preparation for publication. The dissertation author was the primary investigator and author of this material.

VITA

2003	Bachelor of Science in Chemistry, University of California, Riverside
2003-2004	Teaching Assistant, University of California, San Diego
2004-2009	Research Assistant, University of California, San Diego
2005	Master of Science in Chemistry, University of California, San Diego
2010	Doctor of Philosophy in Physical Chemistry, University of California, San Diego

PUBLICATIONS

"*Förster Resonance Energy Transfer and Conformational Stability of Proteins*", K. M. Sanchez, D. E. Schlamadinger, J. E. Gable, and J. E. Kim,
J. Chem. Ed. **85**, 125 (2008).

"*Ultraviolet Resonance Raman Spectroscopy of Folded and Unfolded States of an Integral Membrane Protein*", K. M. Sanchez, T. J. Neary, and J. E. Kim,
J. Phys. Chem. B **112**, 9507 (2008).

"*Effects of Tryptophan Microenvironment, Soluble Domain, and Vesicle Size on the Thermodynamics of Membrane Protein Folding: Lessons from the Transmembrane Protein OmpA*", K. M. Sanchez, J. E. Gable, D. E. Schlamadinger, and J. E. Kim,
Biochemistry **47**, 12844 (2008).

"*Ultraviolet Resonance Raman Spectroscopy of a β-sheet Peptide A Model for Membrane Protein Folding*", H. S. Shafaat, K. M. Sanchez, T. J. Neary, and J. E. Kim, *J. Raman Spectrosc*. **8**, 1060 (2009).

"*Selective antimicrobial action is provided by phenol-soluble modulins derived from* Staphylococcus epidermidis*, a normal resident of the skin*", A. L. Cogen, K. Yamasaki, K. M. Sanchez, R. A. Dorschner, Y. Lai, D. T. MacLeod, J. W. Torpey, M. Otto, V. Nizet, J. E. Kim, and R. L. Gallo, *J. Invest. Dermatol*. 2009, online.

PRESENTATIONS

52nd Annual Biophysical Meeting, February 2008, "*Spectroscopic Folding Studies of an Integral Membrane Protein*". Poster presentation.

56th Annual Western Spectroscopy Association Conference, January 2009, "Ultraviolet resonance Raman studies of membrane protein folding". Oral presentation.

ABSTRACT OF THE DISSERTATION

Ultraviolet resonance Raman and fluorescence studies of folded and unfolded conformations of the membrane protein OmpA

by

Katheryn Marie Sanchez

Doctor of Philosophy in Chemistry

University of California, San Diego, 2010

Professor Judy E. Kim, Chair

This dissertation focuses on the folding dynamics of a bacterial membrane protein, Outer Membrane Protein A (OmpA), using fluorescence and Ultraviolet resonance Raman spectroscopy. Our model β-barrel membrane protein, OmpA, contains five native anchoring Tryptophan residues. The spectroscopic properties of trp residues are highly sensitive to the local environment, making it an ideal probe for membrane protein folding studies. Utilizing trp fluorescence, refolding studies were performed on single trp mutants of OmpA to determine the thermodynamic stability of these trp mutants. The important noncovalent interactions that promote stability in OmpA are pairwise aromatic interactions and hydrogen bonds with the N_1H moiety of trp. Refolding studies were also performed on truncated single-trp mutants, in which the soluble domain of the protein was removed. These studies resulted in increased stability

relative to the full-length protein and suggest the absence of the soluble domain may destabilize the unfolded transmembrane domain.

Ultraviolet resonance Raman spectroscopy (UVRR) is a powerful vibrational technique that can selectively probe different biological chromophores depending on excitation wavelength. Excitation wavelength dependence studies were performed on OmpA using wavelengths from 206.5 nm – 236.5 nm. This study determined an optimal excitation wavelength of 228-nm to selectively enhance signal from trp residues in OmpA. Additionally, UVRR was used to monitor changes in trp environmental hydrophobicity, hydrogen bonding, and dihedral torsion angle in different conformations of OmpA. The first UVRR spectra were collected of OmpA in a highly scattering environment and show differences in folded and unfolded conformations of the protein, showing the applicability of this technique to study membrane protein folding. UVRR spectra were collected of trp mutants of OmpA at different time points in the folding/insertion process to determine the types of noncovalent interactions with trp residues, and the folding timescales these interactions occur. Our results indicate noncovalent interactions start to form within the first 20 minutes after initiation of folding into DMPC vesicles and continue to show subtle changes over the course of the folding process. Additionally, there is evidence for interactions between trp residues and lipids, inter-residue hydrogen bonding, and amino-aromatic interactions.

Chapter 1

Introduction to Membrane Protein Folding

1.1 Protein Misfolding and Disease

Thousands of different proteins are found in cells, and are responsible for a variety of functions ranging metabolism, intra- and intercellular communication, and regulation of intracellular concentrations.[1] The correctly folded three-dimensional structure of a protein is correlated to its function; loss of structure results in loss of function. All of the information required for a protein to correctly fold into its functional secondary and tertiary structures is encoded in its primary sequence.[2] According to the "Thermodynamic Hypothesis" proposed by Anfinsen in the 1950's, "the three-dimensional structure of a native protein in its normal physiological milieu (solvent, pH, ionic strength, presence of other components such as metal ions or prosthetic groups, temperature, and other) is the one in which the Gibbs free energy of the whole system is lowest".[2] Hence, there should be one correctly folded, native structure with the lowest energy. Many thermodynamic, structural, and functional studies have shown this to be true. Both soluble proteins and membrane proteins do reside in the free energy minimum under normal physiological conditions, as hypothesized by Anfinsen.[3,4]

Despite the prevalence of normal, functioning proteins in the cell, mutations occur in the primary sequence and can lead to aberrant protein structures. Aberrations can arise from missense mutations (point mutations where a single nucleotide is changed resulting in a codon for a different amino acid residue), short in-frame deletions, or short in-frame

additions. A majority of these mutations affect protein assembly or folding, trafficking, and function.[5] Partially unfolded proteins can further evolve into insoluble aggregates forming large structures with extensive hydrogen bonding networks that are difficult for the cell machinery to destroy, and can accumulate in human tissue, such as the brain, liver, or spleen. Misfolding of both soluble and membrane proteins can occur. Misfolded membrane proteins has been associated with diseases such as cystic fibrosis, Alzheimer's, and diabetes.[1,6,7]

It is understandable why the scientific and medical communities are interested in protein folding/misfolding problem due to its implications in human disease. Although these misfolded structures can be vastly different than the native functional form, they remain energetically stable. In fact, the difference in energy between the stable form and misfolded forms is often quite small. Understanding the mechanisms of folding/misfolding, and the factors that stabilize these structures may help to solve the protein folding problem. Small-molecule drugs and peptides can be designed to bind to aggregates or misfolded proteins in the hopes of destabilizing these structures, thereby preventing or reversing the effects of protein-misfolding diseases.

1.2. Membrane Protein folding

Soluble proteins are not the only type of proteins in cells that misfold and form insoluble aggregates in tissue. Proteins that associate with or reside in the membrane are referred to as peripheral or integral membrane protein, respectively. These membrane proteins (MPs) can also form insoluble aggregates that are implicated in human disease.[5,6] Despite the prevalence and importance of membrane proteins in biological

systems, there is a large discrepancy in the number of folding studies done on membrane protein systems in comparison to soluble proteins.

Our understanding of membrane protein folding is lacking compared to soluble protein folding mechanisms mainly due to experimental difficulties in handling MPs. First and foremost, membrane proteins are hydrophobic moieties and will aggregate in aqueous solutions. MPs are difficult to express, resulting in lower sample yields, thereby making it difficult to obtain large quantities of protein for folding studies. MPs require the addition of detergent or lipid bilayers to trigger protein folding. Due to the hydrophobic nature of these proteins, they require extensive sample preparation with protein expression and purification procedures under highly denaturing conditions.

In addition to these experimental difficulties, the bilayer itself adds another layer if complexity. The addition of a synthetic lipid bilayer (vesicles) is frequently used to refold membrane proteins. The bilayer introduces scattering artifacts in spectroscopic measurements, and scale upwards with increasing size. It also affects measured thermodynamic parameters of membrane proteins and protein folding efficiencies. Lipid composition can greatly affect measured parameters. Head-group size and compositions (neutral, negative, positive), chain-length, saturated or unsaturated hydrocarbon tails, and vesicle size and curvature can drastically change experimental results.[8-10]

Another deterrent for studying membrane protein folding is the lack of known high resolution crystal structures for membrane proteins. The first crystal structure of a protein was determined in 1960, and was of the soluble protein myoglobin. The first crystal structure of a membrane protein was collected twenty-five years later (1985) of the photosynthetic reaction center in purple bacterium. As of 2009, there are only 182

unique crystals structures of membrane proteins compared to over 55,000 crystal structures of soluble proteins according to the RCSB Protein Data Bank.

Many questions arise in the study membrane protein folding. How does the polypeptide chain fold into its functional form and insert into the membrane without loss of function? What are the factors (specific residues, non-covalent interactions, bilayer composition) that affect the stability of these proteins in the membrane? Integral membrane proteins exhibit characteristics that are different from their soluble counterparts, which allow them to fold and stabilize in the core of a very hydrophobic moiety, the lipid bilayer.

Both experimental and theoretical studies have been applied to study this complex topic in research. Computational studies can probe folding pathways and energy landscape theory, or they can be applied to structure-prediction studies.[11] Thermodynamic studies can determine factors affect protein stability by determining Gibbs Free energies of protein mutants.[12,13] Spectroscopic techniques such as circular dichroism, absorption, fluorescence, infrared, or Raman spectroscopy, and NMR, can provide a wealth of knowledge on protein structure, function, or thermodynamic properties of folded and unfolded states.[14-16] There is a wide rage of experimental and theoretical techniques that can be applied to solve different parts of the protein folding puzzle. Separately, these techniques can only provide a small piece of the puzzle; together, they can provide a much better understanding of membrane protein folding.

There are two structural folding motifs found in membrane proteins: α-helical units or β-barrels. Figure 1.1 shows two representative membrane proteins, the alpha-helical Bacteriorhodopsin, and the beta-barrel Outer Membrane Protein A, with the rough

placement in the bilayer. Typical water/bilayer interfaces are ~ 15 Å, while the hydrophobic core of the membrane is ~30 Å.[17] Both structural motifs follow general steps along the folding pathway: protein binding to the membrane, folding into the secondary and tertiary structures, and insertion into the membrane (partitioning).[17-20] However, the folding and insertion mechanism for each motif is quite different. Alpha-helical membrane proteins form a large portion of their secondary structure upon association with the membrane, and are able to insert as separate units. After insertion into the membrane, the final tertiary and quaternary structures form.[21] Discussion of protein folding will be limited to β-barrel membrane protein folding, since this is the focus of this dissertation. Alpha helical membrane protein folding has been studied in great detail elsewhere and will not be discussed here.[18,22,23] The β-barrel membrane protein have been shown to folds and insert into the membrane in a concerted process.[20] The formation of the beta-barrel structure is coincident with insertion into the membrane.

1.3 Model Membrane Protein System: OmpA

The membrane protein investigated in this dissertation is Outer Membrane Protein A (OmpA). It is frequently used as a model system to study membrane protein folding because it is relatively easy to express and spontaneously refolds into synthetic lipid bilayers from a denatured state. The ease of reversibility of folding/unfolding processes makes it an ideal candidate for β-barrel membrane protein folding studies. OmpA is one of the most abundant proteins found in the outer membrane of *E. coli*. There are 325 residues that form a monomeric transmembrane β-barrel. It has a variety of functions, and can act as a non-specific pore, phage receptors, and provides structural support in the membrane.[24-26] OmpA has two distinct domains: a transmembrane domain and a

periplasmic (or soluble) domain. The transmembrane is made up of ~170 residues on the N-terminus that forms the barrel from 8 anti-parallel β-sheets. The remaining ~150 residues reside outside the membrane in the periplasm, and forms the soluble C-terminus. Figure 1.2 shows the crystal structure of the transmembrane domain of OmpA, with a cartoon depiction of the soluble tail, showing its approximate location in the membrane.[27,28] The structure of the soluble tail has not been determined. The native aromatic amino acids in the transmembrane domain of the protein are highlighted. The five native tryptophan residues located at amino acid position 7, 15, 57, 102, and 143 (indicated as W7, W15, W57, W102, and W143) are shown in blue; the 13 native tyrosine residues in the transmembrane domain are shown in green.

1.4 Previous Studies of OmpA

OmpA has been studied by a variety of groups and techniques for over 20 years, and these results provide a strong foundation for membrane protein folding studies. In 1990, a study by Jähnig showed the spontaneous refolding of OmpA after denaturation.[29] Reversibility of the unfolding/refolding process is necessary for thermodynamic stability measurements. In this early work by Jähnig, OmpA was denatured by boiling in sodium dodecyl sulfate (SDS) and successfully refolded in a nonionic detergent. When denatured and refolded OmpA were separated via SDS gel-electrophoresis, an interesting observation arose: OmpA displayed different migration rates in the presence or absence of SDS + heat. Denatured OmpA migrated on the gels with an apparent molecular weight of ~35 KDa, while the folded protein migrated at an apparent molecular weight of ~30 KDa.[29] Figure 1.3 shows a prototypical SDS gel electrophoresis of wild type OmpA in various conditions from the Jähnig work; this gel clearly illustrates the different

migration rates of denatured and refolded protein. A trypsin-digested fragment of OmpA was also distinguishable from denatured or refolded protein and migrated at ~24 kDa. This difference in migration rates was attributed to differences in structure. The folded protein was more compact and therefore had a smaller apparent molecular weight. This technique has since been adapted to many OmpA folding studies to monitor changes in tertiary structure in the presence or absence of denaturant. It has also been used extensively for refolding/unfolding curves to measure thermodynamic stabilities of protein.[30,31]

A compilation of studies from many groups have proposed folding/insertion mechanisms of OmpA over the years. One of the early questions that arose was whether OmpA inserts into the membrane in a directional manner. Does one side of the protein always insert first? *In vitro* folding studies performed by Surrey and Jähnig in 1992 used trypsin digestion to show directional insertion of OmpA into synthetic lipid bilayers.[32] When protein was folded in vesicle, trypsin only cleaved the peripheral portion of OmpA, suggesting the soluble part of the protein remained outside the vesicle after insertion. They concluded that the protein inserted in the same direction every time. Their interpretation of the directional insertion of OmpA into a lipid bilayer is shown in Figure 1.4.

Further advancement of the folding mechanism was achieved by Kleinschmidt and Tamm via isolation of folding intermediates using native tryptophan fluorescence.[30] In 1996, they determined four kinetically distinguishable steps in the folding and insertion process of OmpA by monitoring folding reaction as a function of temperature. Based on their results, they presented a simple folding and insertion pathway in the

membrane, which is shown in Figure 1.5. The first step consists of a kinetically unresolved hydrophobic collapse of the unfolded protein (U) to a water soluble-intermediate (I_W). This intermediate has two available pathways: adsorption to lipid bilayer (I_{M1}) or aggregation (A). After adsorption to the bilayer, the reaction proceeds to form the next membrane-bound intermediate (I_{M2}). The protein finally folds to form the native state (N). Estimates for the timescales of these events is estimated as sub-seconds to hours.

In 1999, Kleinschmidt and Tamm proposed that OmpA folds and inserts into the membrane by a concerted folding/insertion mechanism.[20] These studies monitored tryptophan fluorescence quenching using brominated lipids. Translocation rates of these trp residues through the membrane, and distances from the bilayer center were determined for each trp residue in OmpA. It was determined that the four trp residues at the top of the barrel (Trp-15, Trp-57, Trp-102, and Trp-143) showed similar translocation rates and final distances from bilayer center, suggesting the four β-loops that form the barrel travel through the lipid bilayer on similar timescales. This result provided evidence for a concerted folding/insertion mechanism of OmpA that has been generally accepted.

OmpA has been shown to spontaneously refold in the presence of detergent or lipid vesicles.[20,33] The folding mechanism of OmpA is likely different in micelles compared to lipid bilayers. Molecular dynamic (MD) simulations have been performed on OmpA to compare the structures and dynamics in detergent micelles and lipid bilayers.[34] The first MD simulation of protein-micelle aggregates of OmpA was performed by Bond and Sansom in 2003.[34] Their study showed different dynamics for

OmpA in micelles or lipid bilayers. OmpA showed increased mobility and enhanced flexibility in micelles. In addition to enhanced flexibility, the formation of a continuous pore through the center of OmpA was observed in the presence of micelles. Figure 1.6 shows a simulation of OmpA in micelles and in lipid bilayers.

Additional studies have been reported to monitor the formation of OmpA secondary and tertiary structure in micelles or vesicles using a multitude of spectroscopic techniques. Fluorescence, SDS-gel electrophoresis, and circular dichroism studies had been performed to monitor the effects of detergent and vesicle composition on the thermodynamic properties and folding kinetics of OmpA. Formation of secondary structure of OmpA required detergents concentrations above the critical micelle concentration (CMC) of the lipid.[33,35] The thermodynamic properties and folding kinetics of OmpA are also sensitive to bilayer composition, head-group, chain length, and saturated/unsaturated hydrocarbon tails.[9,31] Systematic studies showed that free energy depends on vesicle curvature and hydrophobic mismatch.

Steady-state and time-resolved fluorescence and anisotropy studies were performed on OmpA to elucidate the environment near the native trp residues.[36] Excited state lifetimes and mobility of each native trp residue were measured in unfolded and folded environments. Excited state lifetimes increased when OmpA was folded, with trp exhibiting longer lifetimes in micelles than in lipid bilayers. Anisotropy (related to mobility) of trp residues increased when OmpA was folded in micelles, and further increase when OmpA was folded in vesicles. These and other results determined different environments for trp residues for OmpA unfolded in buffer, folded in micelles, and folded in lipid bilayers.

1.5 Factors that influence protein structure and stability

Since many misassembled proteins linked to diseases are similar in stability to their natively folded counterpart, it is important to understand the factors that contribute to the overall stability of a protein. While the primary sequence (covalent structure) determines the three-dimensional structure of a protein, the main forces responsible for stabilizing this structure include a wide range of covalent and non-covalent interactions that cooperatively maintain the protein's functional structure. Individually, these interactions may not be significant, but collectively are very important to the overall stability of a protein. These interactions can occur among neighboring residues, solvent molecules, metal cofactors, and additionally for membrane proteins, with the lipid bilayer (head-groups, hydrocarbon centers, and/or the water-bilayer interface). Although most studies that determine stabilizing interactions typically focus on soluble proteins, these same factors have been shown to stabilize the structures of membrane proteins.[37]

Disulfide bonds and bonds to metal cofactors are two types of covalent interactions that promote protein stability. Electrostatic effects are also prominent in some protein systems. These can be thought of as simple electrostatic interactions between charged residues in the protein or between a charged residue and solvent molecules, and can be classified as salt-bridges or ion-pairings. Another important driving force for protein folding is the hydrophobic effect.[3] Stated simply, nonpolar residues have a strong aversion to water molecules and will cluster together separated from water.[38] Lipid/protein interactions also play a large part in membrane protein stability.[37] In addition, there are many other types of non-covalent interactions that are responsible for formation of stable protein structures, namely hydrogen bonds, aromatic-

aromatic or aromatic-amine interactions, cation-π interactions, and for membrane proteins in particular, the driving force of partitioning into the membrane. These are discussed in detail below. Tabulated non-covalent interactions with energy contributions to protein stability are found in Table 1.1.

1.5.1 Hydrogen Bonds

The most prevalent and perhaps one of the most important non-covalent interactions are hydrogen bonds. Hydrogen bonds contribute ~ 1 to 7 kcal/mol, depending on the type of donor-acceptor pair involved and the distance and angle between them.[39,40] Extensive hydrogen-bonding networks are the dominant forces behind stabilizing protein secondary structure. These hydrogen bonds form between backbone N-H (amide) hydrogens and C=O (carbonyl) oxygens. For alpha-helical segments, hydrogen bonds form between every i and (i + 4) amino acid residue on the same chain (intra-strand H-bonding). Beta-sheet structures are formed via hydrogen bonds from N-H group from one strand and the C=O groups from another strand (inter-strand H-bonding).[41,42] Hydrogen bonds can also occur between many other types of donor-acceptor pairs, between amino acid side-chains and/or main chains, such as C-H···O, N-H···O, C-H···π, O-H···π, or S-H···π.[40,43-46] It is important to recognize that many of the hydrogen bonds that form in proteins do not follow typical hydrogen-bonding parameters. The lengths of the H-bonds in proteins cover a wide range, and are typically longer than the "normal" H-bond, and the geometry between the donor-acceptor pair is often bent from the preferable linear geometry.[46]

Transmembrane spanning regions of integral membrane proteins have been shown to traverse the membrane only when there is complete backbone-backbone

hydrogen bonding because the penalty for crossing the hydrophobic barrier is too high. This large driving force for H-bond formation may explain why unfolded proteins are not found unfolded in the bilayer.[4,47,48] Although H-bonds are the most prevalent non-covalent interaction in proteins, it has been shown that it is not necessarily the dominant folding force for soluble proteins.[49] If hydrogen bonds were the dominant folding force, then any solvent that could form stronger hydrogen bonds with the peptide backbone would completely unfold the protein. Since this is not the case, there are other classes of non-covalent interactions that provide the driving force for protein folding.

1.5.2 Aromatic residues at the water-bilayer interface

There is a strong tendency for aromatic amino acid residues, tryptophan, tyrosine, and phenylalanine to cluster at the water-bilayer interface in the membrane, and have been shown to play a role in anchoring the protein in the membrane.[50-53] This can be seen in OmpA, Figure 1.2. Aromatic residues can enhance stability due to interfacial interactions arising from the unique amphipathic nature of these residues. Both tryptophan and tyrosine can form hydrogen bonds with the –NH group, and –OH group, respectively. In addition to the hydrogen bonding partners, the aromatic rings allow possible π-π interactions and cation-π interactions to help stabilize structure. Thermodynamic studies have shown favorable partitioning of these aromatic residues into hydrophobic solvents, and can contribute ~ 1 to 4 kcal/mol to protein stability.[54,55]

1.5.3. Aromatic interactions with neighboring residues

Not only can these aromatic residues provide stability at the water-bilayer interface, but they can also form non-covalent interaction with other aromatic residues, amino acid side chains, and/or the protein backbone. Studies on soluble proteins have

found favorable interactions among aromatic residues located within ~ 4.5 – 7 Å of aromatic centroids.[56] More than half of aromatic residues were found to be involved in favorable aromatic-aromatic interactions that stabilized protein tertiary structure. These interactions were found to contribute ~ 1 to 3 kcal/mol in the folded protein.[56,57] These included Trp-X (X = Trp, Tyr, or Phe), Tyr-X (X = Trp, Tyr, Phe) and Phe-X (X = Trp, Tyr, Phe) interactions, in all geometries.

Another type of important interaction involving aromatic residues are termed amino-aromatic interactions.[58,59] These interactions involve side-chain amino groups with aromatic side chains. The amino groups Asn, Gln, and His are preferentially located near the π-electron cloud of the aromatic residues, Trp, Tyr, and Phe. Typical interaction distances are ~3.4 – 6 Å between amino group and ring centroids. It has been shown that these are favorable interactions in protein folding and can contribute ~1.5 to 4 kcal/mol to stability.[59]

Another non-covalent interactions involving aromatic residues are Cation-π interactions.[60,61] This type of interaction can be thought of as simple electrostatic attractions between cations and the π face of aromatic moieties like benzene, or aromatic amino acids (tryptophan, tyrosine, and phenylalanine). The type of cation involved can be simple ions, like Li^+, K^+, or Na^+, or more complex molecules like NH_4^+ and $N(CH_3)_4^+$. In protein systems, the likely cation-π pairs are the side chains of Lys, and Arg with the aromatic clouds of Trp, Tyr, or Phe. Due to the preference for aromatic residues at the water-bilayer interface, it is likely that this type of interaction can also occur between the choline heads groups of lipids with the π-face of the aromatic residue. Cation-π interactions can contribute ~4.0 kcal/mol to the overall stability of the protein.[61]

1.5.4 Partitioning Energies

There is a large change in environment for residues upon transfer from an aqueous environment in the unfolded protein, to the hydrophobic environment of the membrane in a folded protein. Partition energies have been calculated to determine the energetics of individual residues crossing the bilayer. The major driving force behind membrane partitioning was previously assumed to be the hydrophobic effect, but is now considered to be more complex, and may depend on both an enthalpic and entropic contribution to the transfer free energy.[62] Numerous studies have been done to determine the partition energy for all the amino acid residues from octanol-to-water, partition energies of short peptides into bilayers with various residues, and solvation energies of peptide backbone with amino acid contributions.[62-64] As is expected, hydrophobic residues, like Leu, Ile, Phe, Trp, and Tyr have partition energies that reflect a preference in the membrane, while polar or charged residues have partition energies that reflect a preference for the aqueous phase. Tabulated Free energies of transfer (bilayer interface → water) for the 20 amino acids located in a short peptide (AcTrp-Leu-X-Leu-Leu) are found in Table 1.2.[64]

1.6 Experimental investigation of OmpA folding

Chapters in this dissertation describe experimental approaches to studying the folding and insertion mechanism of a bacterial integral membrane protein, Outer Membrane Protein A (OmpA). This work focused on determining the important molecular interactions that contribute to protein stability in the membrane, and the evolution of these interactions during a folding event. Chapter 2 describes the experimental techniques utilized to study OmpA in folded and unfolded conformations

and different environments, by using native tryptophan residues in OmpA as the spectroscopic probe for these studies. Thermodynamic studies of OmpA were performed using fluorescence spectroscopy of native tryptophan in the protein. The results of these thermodynamic studies are discussed in Chapter 3. The stabilities of various mutants of OmpA were determined, using native and non-native trp residues. The trends in stabilities are discussed in terms of the specific non-covalent interactions that influence protein stability in the membrane.

In addition to fluorescence thermodynamic studies of OmpA, the vibrational technique called ultraviolet resonance Raman (UVRR) spectroscopy was used to monitor changes in tryptophan vibrational modes in folded and unfolded states in OmpA. UVRR is an inelastic scattering technique that allowed us to study the vibrational changes of aromatic residues in the protein upon folding and/or insertion into the membrane. Strong enhancement of Raman scattering occurs when the excitation wavelength corresponds to an electronic transition of a molecule, allowing for high selectivity and sensitivity. Chapter 4 investigates the wavelength dependence of aromatic residues in OmpA and is compared to aqueous model compounds. The wavelength dependence was performed in the Trp-less mutant, to probe tyrosine residues in OmpA, and of the single-trp mutant Trp-57, to probe tryptophan residues in OmpA. These results highlight the selective enhancement of protein backbone (secondary structure) or aromatic residues, depending on the excitation wavelength, and determined the excitation wavelength with the largest enhancement of tryptophan vibrational modes in OmpA.

Further UVRR studies were applied to study the remaining tryptophan residues in OmpA, folded in vesicles, and unfolded in buffer, using the optimum excitation

wavelength determined in Chapter 4. These steady-state UVRR experiments are discussed in Chapter 5. UVRR kinetics experiments were also performed to monitor vibrational changes of trp associated with the folding/insertion mechanism into synthetic lipid bilayers. These kinetics experiments show the evolution of molecular interactions between specific tryptophan residues with the surrounding protein or bilayer, and are discussed in Chapter 6. General conclusions of OmpA membrane protein folding experiments, and future experiments of membrane protein folding/insertion are found in Chapter 7.

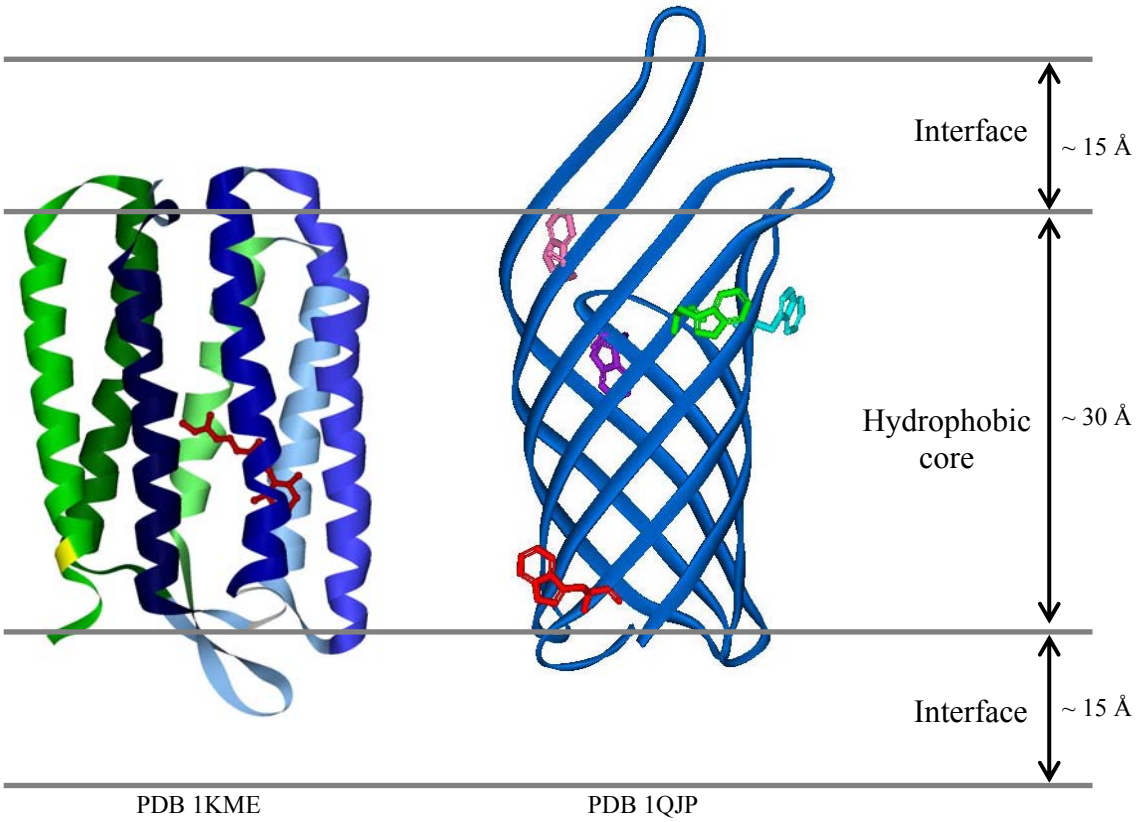

Figure 1.1: Representation of the lipid bilayer, with the aqueous water/bilayer interfaces (complex mixture of lipid head groups and water molecules), and the hydrophobic core (lipid aliphatic chains) in the membrane. On the left is the crystal structure of the alpha-helical membrane protein Bacteriorhodopsin (bR) showing the retinal prosthetic group; on the right is the crystal structure of the β-barrel membrane protein Outer Membrane Protein A (OmpA) with the native tryptophan residues highlighted. Placement of proteins in bilayer is rough estimate.

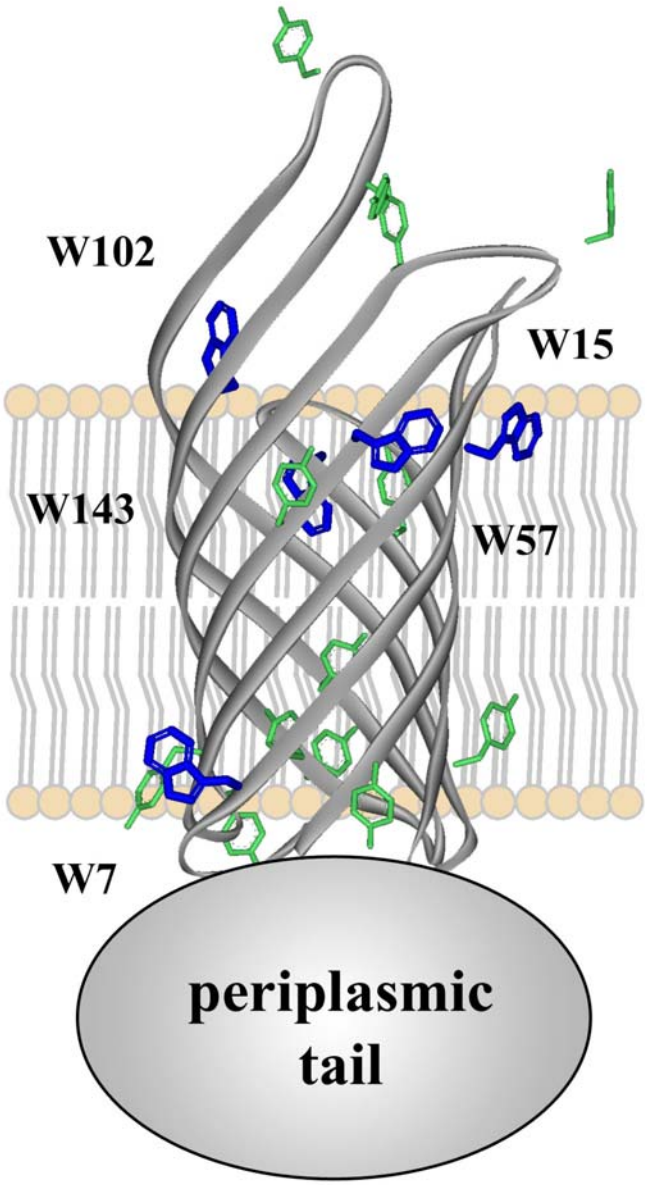

Figure 1.2: The crystal structure of the transmembrane portion of OmpA (PDB 1QJP), with a cartoon representation of the periplasmic tail, in a bilayer. The aromatic amino acids are highlighted and are shown clustered at the water-bilayer interface. The five native tryptophan residues are shown in blue (labeled as W7, W15, W57, W102, and W143); the 13 native tyrosine residues are shown in green.

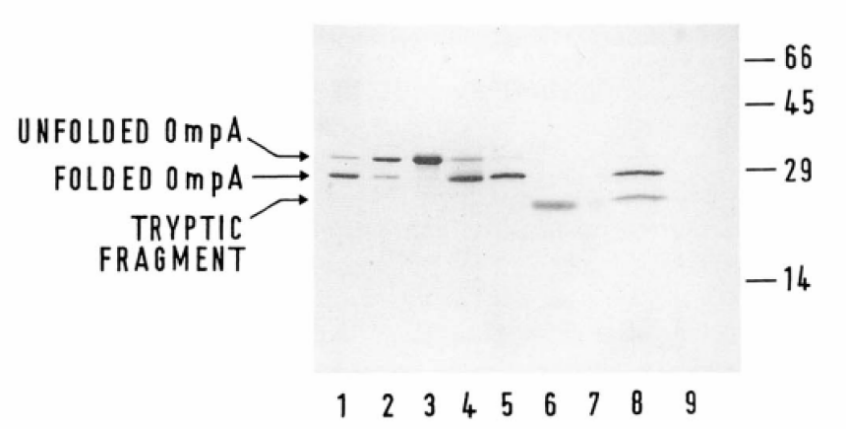

Figure 1.3: Representative SDS-PAGE gels of wild type OmpA in different conditions. Unfolded OmpA runs with a molecular weight of ~35 KDa; folded OmpA runs with a molecular weight of ~ 30 KDa; Trysin digested fragments of OmpA run with a molecular weight of ~24 KDa. Folded OmpA (in SDS, not boiled) in Lane 1; unfolded OmpA (in SDS, boiled) in Lane 2; refolded OmpA in detergent (OG) in Lane 4; refolded OmpA in vesicle (DMPC) in Lane 5; unfolded and digested OmpA (reconstituted in OG/SDS, boiled and digested with trysin) in Lane 6; folded and digested OmpA (reconstituted in DMPC and digested with trypsin) in Lane 8. Reproduced from Reference 29.

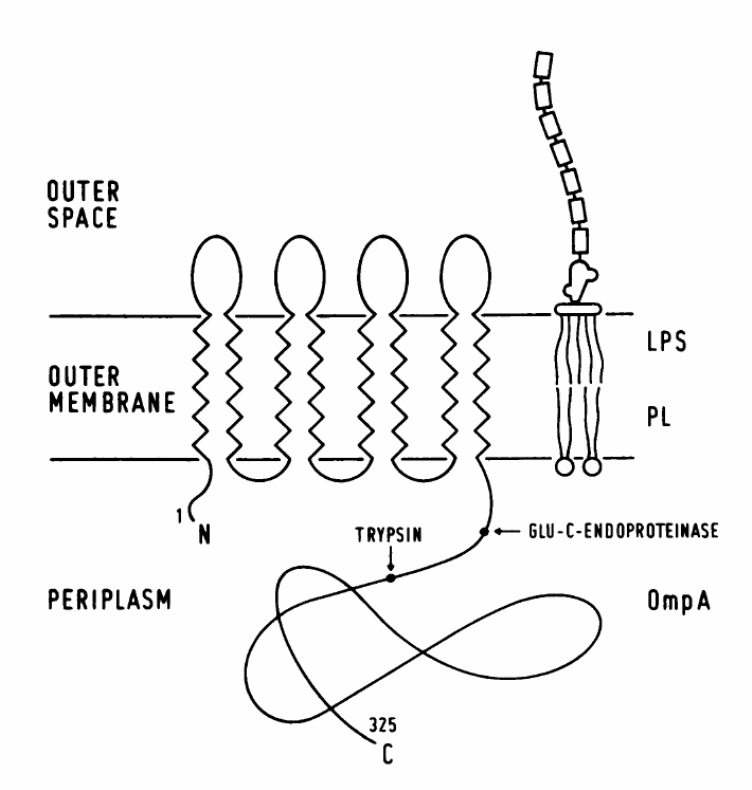

Figure 1.4: Drawing showing directional insertion of OmpA into the membrane, with labeled membrane topology, including lipopolysaccharides (LPS) and phospholipids (PL); cleavage sites for trypsin and Glu-C endoproteinase are labeled. Reproduced from Reference 32.

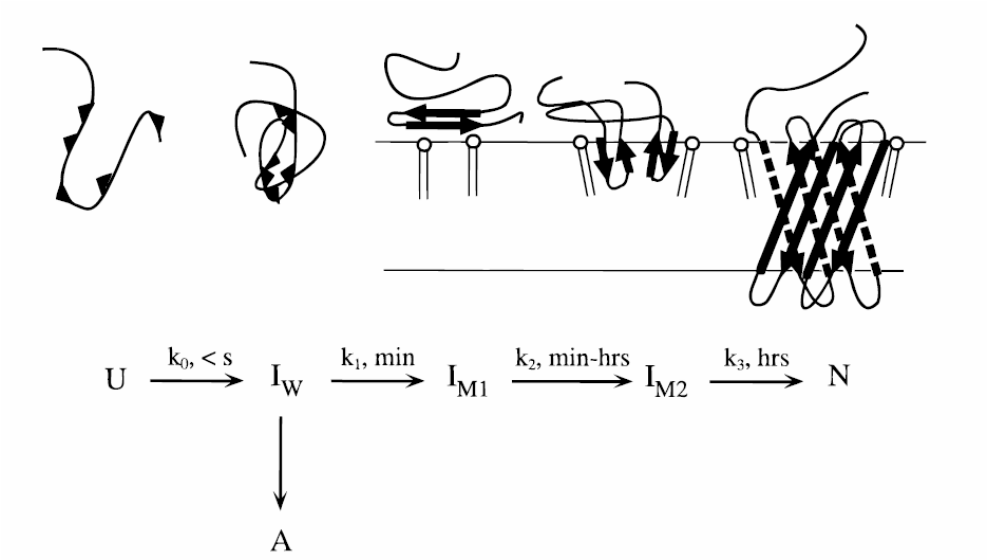

Figure 1.5: The folding pathway of OmpA proposed by Kleinschmidt and Tamm in 1996. The unfolded protein (U) undergoes a kinetically unresolved hydrophobic collapse to the water-soluble intermediate (I_W). Two pathways exist: irreversible aggregation (A) or adsorption to the membrane surface (I_{MI}). I_{M1} converts into the second membrane-associated intermediate, I_{M2}, followed by the final stages of insertion and folding to the final native state (N). Reproduced from Reference 31.

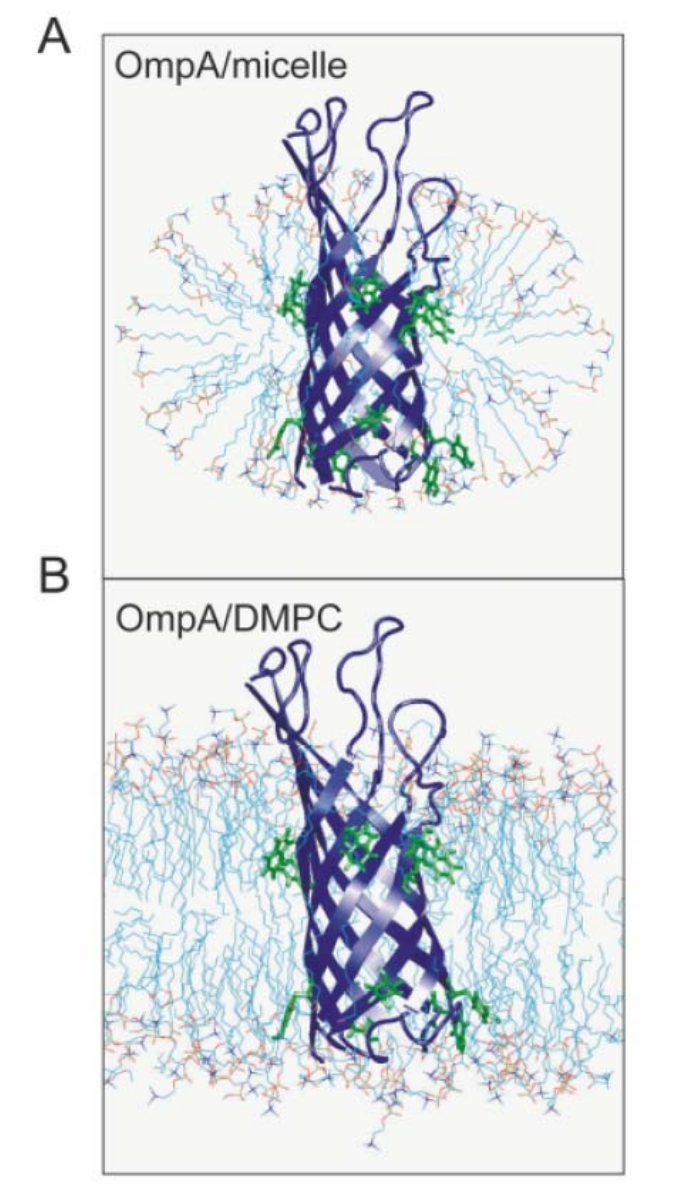

Figure 1.6: Molecular dynamics simulations for OmpA in micelles (A), or in DMPC lipid bilayer (B). Oxygen atoms are colored in red, hydrocarbon tails are cyan, and aromatic side-chains in OmpA are shown in green. Water was omitted for clarity. Reproduced from Reference 34.

Table 1.1: Summary of non-covalent interactions in proteins, with energy contributions to the overall protein stability.

Non-covalent Interaction	Energy Contribution (kcal/mol)
hydrogen bond	1 - 7
aromatic-bilayer	1 - 4
aromatic-aromatic	1 - 3
aromatic-amine	1.5 - 4
cation-π	1 - 4

Table 1.2: Free energies of transfer of Ac-Trp-Leu-X-Leu-Leu peptide from the bilayer interface to water. Whole residue contributions to partitioning, including side-chain and backbone contributions. Negative values indicate preference for aqueous environment, positive values indicate preference for hydrophobic environment. Modified from Reference 64.

X-residue	Abbreviation	Delta G (kcal/mol)
Alanine	Ala	-0.17
Arginine	Arg	-0.81
Asparagine	Asn	-0.42
Aspartic acid	Asp	-1.23
Cysteine	Cys	0.24
Glutamine	Gln	-0.58
Glutamic acid	Glu	-2.02
Glycine	Gly	-0.01
Histidine	His	-0.17
Isoleusine	Ile	0.31
Leusine	Leu	0.56
Lysine	Lys	-0.99
Methionine	Met	0.23
Phenylalanine	Phe	1.13
Proline	Pro	-0.45
Serine	Ser	-0.13
Threonine	Thr	-0.14
Tryptophan	Trp	1.85
Tyrosine	Tyr	0.94
Valine	Val	-0.07

1.7 References

(1) Bross, P.; Corydon, T. J.; Andresen, B. S.; Jorgensen, M. M.; Bolund, L.; Gregersen, N. *Human Mutation* **1999**, *14*, 186.

(2) Anfinsen, C. B. *Science* **1973**, *181*, 223.

(3) Dill, K. A. *Biochem.* **1990**, *29*, 7133.

(4) White, S. H.; Wimley, W. C. *Annu. Rev. Biophys. Biomol. Struct.* **1999**, *28*, 319.

(5) Sanders, C. R.; Myers, J. K. *Annu. Rev. Biophys. Biomol. Struct.* **2004**, *33*, 25.

(6) Sanders, C. R.; Nagy, J. K. *Curr. Op. Struct. Biol.* **2000**, *10*, 438

(7) Dobson, C. M. *Trends Biochem. Sci.* **1999**, *24*, 329.

(8) Gruner, S. M. *Proc. Natl. Acad. Sci. U.S.A.* **1985**, *82*.

(9) Hong, H.; Tamm, L. K. *Proc. Natl. Acad. Sci. U.S.A.* **2004**, *101*, 4065.

(10) Allen, S. J.; Curran, A. R.; Templer, R. H.; Meijberg, W.; Booth, P. J. *J. Mol. Biol.* **2004**, *342*, 1293.

(11) Onuchic, J. N.; Luthey-Schulten, Z.; Wolynes, P. G. *Annu. Rev. Phys. Chem.* **1997**, *48*, 545.

(12) Rose, G. D.; Wolfenden, R. *Annu. Rev. Biophys. Biomol. Struct.* **1993**, *22*, 381.

(13) Rose, G. D.; Geselowitz, A. R.; Lesser, G. L.; Lee, R. H.; Zehfus, M. H. *Science* **1985**, *229*, 834.

(14) Royer, C. A. *Chem. Rev.* **2006**, *106*, 1769.

(15) Pace, N. C. *Methods Enzymol.* **1986**, *131*, 266.

(16) Schellman, J. A. *Biopolymers* **1978**, *17*, 1305.

(17) Bowie, J. U. *Nature* **2005**, *438*, 581.

(18) Lau, F. W.; Bowie, J. U. *Biochem.* **1997**, *36*, 5884.

(19) Booth, P. J.; Curnow, P. *Curr. Op. Struct. Biol.* **2006**, *16*, 480.

(20) Kleinschmidt, J. H.; den Blaauwen, T.; Driessen, A. J. M.; Tamm, L. K. *Biochemistry* **1999**, *38*, 5006.

(21) Popot, J.; Engelman, D. *Biochem.* **1990**, *29*, 4031.

(22) Renthal, R. *Biochem.* **2006**, *45*, 14559.

(23) Booth, P. J.; Templer, R. H.; Meijberg, W.; Allen, S. J.; Curran, A. R.; Lorch, M. *Crit. Rev. in Biochem. and Mol. Biol.* **2001**, *36*, 501.

(24) Sugawara, E.; Nikaido, H. *J. Mol. Biol.* **1992**, *267*, 2507.

(25) Wang, Y. *Biochem. Biophys. Res. Comm.* **2002**, *292*, 396.

(26) Morona, R.; Klose, M.; Henning, U. *J. Bacteriol.* **1984**, *159*, 570.

(27) Pautsch, A.; Schulz, G. E. *Nat. Struct. Biol.* **1998**, *5*, 1013.

(28) Pautsch, A.; Schulz, G. E. *J. Mol. Biol.* **2000**, *298*, 273.

(29) Dornmair, K.; Kiefer, H.; Jahnig, F. *J. Biol. Chem.* **1990**, *265*, 18907.

(30) Kleinschmidt, J. H.; Tamm, L. K. *Biochem.* **1996**, *35*, 12993.

(31) Kleinschmidt, J. H.; Tamm, L. K. *J. Mol. Biol.* **2002**, *324*, 319.

(32) Surrey, T.; Jahnig, F. *Proc. Natl. Acad. Sci. U.S.A.* **1992**, *89*, 7457.

(33) Kleinschmidt, J. H.; Wiener, M. C.; Tamm, L. K. *Protein Science* **1999**, *8*, 2065.

(34) Bond, P. J.; Sansom, M. S. P. *J. Mol. Biol.* **2003**, *329*, 1035.

(35) Ohnishi, S.; Kameyama, K. *Biochim. Biophys. Acta* **2001**, *1515*, 159.

(36) Kim, J. E.; Arjara, G.; Richards, J. H.; Gray, H. B.; Winkler, J. R. *J. Phys. Chem. B* **2006**, *110*, 17656.

(37) Domene, C.; Bond, P. J.; Deol, S. S.; Sansom, M. S. P. *J. Am. Chem. Soc.* **2003**, *125*, 14966.

(38) Chandler, D. *Nature* **2005**, *437*, 640.

(39) Weiss, M. S.; Brandl, M.; Suhnel, J.; Pal, D.; Hilgenfeld, R. *Trends Biochem. Sci.* **2001**, *26*, 521.

(40) Steiner, T.; Koellner, G. *J. Mol. Biol.* **2001**, *305*, 535.

(41) Pauling, L.; Corey, R. B.; Branson, H. R. *Proc. Natl. Acad. Sci. U.S.A.* **1951**, *37*, 205.

(42) Pauling, L.; Corey, R. B. *Proc. Natl. Acad. Sci. U.S.A.* **1951**, *37*, 729.

(43) Fabiola, G. F.; Krishnaswamy, S.; Nagarajan, V.; Pattabhi, V. *Acta Cryst.* **1997**, *D53*, 316.

(44) Brandl, M.; Weiss, M. S.; Jabs, A.; Suhnel, J.; Hilgenfeld, R. *J. Mol. Biol.* **2001**, *307*, 357.

(45) Derewenda, Z. S.; Lee, L.; Derewenda, U. *J. Mol. Biol.* **1995**, *252*, 248.

(46) Scheiner, S.; Kar, T.; Pattanayak, J. *J. Am. Chem. Soc.* **2002**, *124*, 13257.

(47) White, S. H. *Adv. Protein Chem.* **2006**, *72*, 157.

(48) Liu, Y.; Bolen, D. W. *Biochem.* **1995**, *34*, 12884.

(49) Singer, S. J. *Adv. Protein Chem.* **1962**, *17*, 1.

(50) van der Wel, P. C. A.; Reed, N. D.; Greathouse, D. V.; Koeppe II, R. E. *Biochem.* **2007**, *46*, 5714.

(51) Schiffer, M.; Chang, C. H.; Stevens, F. J. *Protein Engineering* **1992**, *5*, 213.

(52) Ridder, A. N. J. A.; Morein, S.; Stam, J. G.; Kuhn, A.; de Kruijff, B.; Killian, J. A. *Biochem.* **2000**, *39*, 6521.

(53) Sun, H.; Greathouse, D. V.; Andersen, O. S.; Koeppe II, R. E. *J. Biol. Chem.* **2008**, *283*, 22233.

(54) Yau, W.-M.; Wimley, W. C.; Gawrisch, K.; White, S. H. *Biochemistry* **1998**, *37*, 14713.

(55) Hong, H.; Park, S.; Flores Jimenez, R. H.; Rinehart, D.; Tamm, L. K. *J. Am. Chem. Soc.* **2007**, *129*, 8320.

(56) Burley, S. K.; Petsko, G. A. *Science* **1985**, *229*, 23.

(57) Serrano, L.; Bycroft, M.; Fersht, A. R. *J. Mol. Biol.* **1991**, *218*, 465.

(58) Burley, S. K.; Petsko, G. A. *FEBS Lett.* **1986**, *203*, 139.

(59) Duan, G.; Smith Jr., V. H.; Weaver, D. F. *J. Phys. Chem. A* **2000**, *104*, 4521.

(60) Dougherty, D. A. *Science* **1996**, *271*, 163.

(61) Gallivan, J. P.; Dougherty, D. A. *Proc. Natl. Acad. Sci. U.S.A.* **1999**, *96*, 9459.

(62) Wimley, W. C.; White, S. H. *Biochemistry* **1993**, *32*, 6307.

(63) Wimley, W. C.; Creamer, T. P.; White, S. H. *Biochemistry* **1996**, *35*, 5109.

(64) Wimley, W. C.; White, S. H. *Nat. Struct. Biol.* **1996**, *3*, 842.

Chapter 2

Spectroscopic Probe and Experimental Methods

2.1 Spectroscopic Probe: Tryptophan Residues in Outer Membrane Protein A

Aromatic residues, such as tryptophan (trp), tyrosine (tyr), and phenylalanine (phe) are often clustered at the water-bilayer interface in membrane proteins and peptides, and are thought to play a role in anchoring proteins and peptides in the membrane.[1-4] Tryptophan fluorescence is highly sensitive to environment, and display different emission maxima and quantum yields depending on the solvent. It is often used as a reporter for solvent exposure in proteins.[5] Trp residues in aqueous environments (exposed to solvent) display emission maxima of ~350-355 nm; trp in modest hydrophobic environment (partially buried) display emission maxima of ~ 340 nm; trp in hydrophobic environments (fully buried) display emission maxima of ~330 nm. Representative tryptophan fluorescence in an aqueous and hydrophobic environment is shown in Figure 2.1. This sensitivity makes trp residues an ideal spectroscopic probe for studying membrane protein folding.

2.2 Tryptophan residues in OmpA

Our model membrane protein is OmpA. It contains many aromatic residues clustered at the water-bilayer interface, as seen in Figure 1.2. The location of the five native tryptophan residues and the thirteen tyrosines in the transmembrane region are highlighted. The native trp residues are located at amino acid position 7, 15, 57, 102, and 143. Each trp residue is located on a different strand of the β-barrel. The trp at position 7

is located at the N-terminus and remains on the periplasmic side of the membrane. The remaining trp residues at positions 15, 57, 102, and 143 are located at the top of the barrel, on the cytoplasmic side of the membrane. Because our *in vitro* refolding studies are performed using pre-formed vesicles, unfolded protein is initially localized outside the vesicle and inserts into it during the folding process; this directional folding in which Trp-7 remains on the extra-vesicle side while the four other trp residues are located on the intra-vesicle side has been demonstrated previously.[6]

These native tryptophan residues were used as intrinsic spectroscopic probes in thermodynamic and kinetic folding studies of OmpA. Single-trp containing mutants were made by replacing four of the five native trp residues with the spectroscopically silent phenylalanine residue. Since each trp residue is located on a different location on the protein, single-trp containing mutants allowed for site specific investigation of different locations of OmpA during the folding process. These single-trp containing OmpA mutants will be referred to throughout this dissertation as Trp-7, Trp-15, Trp-57, Trp-102, and Trp-143. Due to the large number of tyrosine residues that contribute to the spectroscopic signatures of OmpA, a trp-less version was made in which all five native trp residues were replaced with phenylalanine residues. This is referred to as Trp-less OmpA. Signal from Trp-less mutant could then be subtracted from signal from the single-trp containing mutants to remove any tyrosine contribution.

Only one native trp residue resides at the bottom of the barrel, while four are located at the top. In order to probe another location on the bottom of the barrel, a non-native trp mutant was created by replacing a phe residue at position 170 with a trp

residue. Trp-170 is located at the bottom of the barrel in the same region as Trp-7, but is situated at the boundary between the transmembrane and soluble domains.

Truncated versions of the full-length single-trp mutants were also made to determine the effects of the soluble tail on the thermodynamic and kinetic folding studies of OmpA. In these truncated mutants, the soluble tail was removed, leaving the transmembrane domain only. The single-trp truncated mutants are referred to throughout is dissertation as Trp-7t, Trp-15t, Trp-57t, Trp-102t, Trp-143t, and Trp-170t. A truncated version of the wild type OmpA was also made, and is referred to as WTt.

2.3 Techniques

2.3.1 Preparation of Small Unilamellar Vesicles (SUVs)

Small unilamellar vesicles (SUVs) were prepared using an adaptation of a previously published procedure.[7] A stock solution (20 mg/mL) of 1,2-dimyristoyl-sn-glycero-3-phosphocholine (DMPC, Avanti Polar Lipids) in chloroform was dried under a stream of argon and resuspended in phosphate buffer (20 mM KP_i, pH 7.3) to a final lipid concentration of 5 mg/mL. SUVs (~50 nm diameter) were made by sonication of the lipid solution with a Branson ultrasonicator microtip. The sonicated solution was passed through a 0.22 μm filter to remove titanium dust and other particulates. The SUVs were further diluted to a final concentration of 1 mg/mL for all experiments. Vesicle solutions were equilibrated overnight at 37 º C and used the following day.

2.3.2 Steady-State Fluorescence and Absorption spectroscopy

OmpA refolding was monitored by tryptophan fluorescence. Steady-state fluorescence measurements were collected using 290 nm excitation were performed with a Jobin Yvon-SPEX Fluorolog FL3-11 spectrofluorometer. Samples were maintained at

30 °C, which is above the phase transition temperature for DMPC vesicles. The emission wavelength range was 305 – 500 nm, in 1-nm increments, and 10sec integration times. Absorbance measurements were recorded on an Agilent UV-visible spectrophotometer, in a 200-μL small volume quartz cuvette. Protein concentrations were calculated using ε_{280} values of 54 400 $M^{-1}cm^{-1}$, 32 300 $M^{-1}cm^{-1}$, 26 000 $M^{-1}cm^{-1}$, and 26 810 M^{-1} cm^{-1} for wild-type, single-trp, truncated single-trp, and trp-less mutants of OmpA, respectively.[8]

2.3.3 Dynamic Light Scattering

Dynamic light scattering (DLS) was used to determine vesicle diameters. The apparatus has been described in detail elsewhere.[9] Two populations with corresponding average diameters were obtained for each sample. The fraction of reported population was > 80% unless specified. Vesicle size was measured as a function of vesicle concentration from 0.1 to 1 mg/ml to ensure appropriate conditions for our measurements; these control experiments indicated variation of <20% in vesicle diameter across this concentration range.

2.3.4 UV resonance Raman Spectroscopy

A tunable Ti:Sapphire laser (Photonics Industries) pumped by a frequency-doubled Nd:YLF laser was used in the current experiments. The 1-kHz, >1-Watt, 912 nm fundamental output beam was collimated into a lithium triborate (LBO) crystal for second harmonic generation; the resulting 460nm beam was then passed through a β-barium borate (BBO) crystal to produce >10-mW of the 228 nm excitation beam. The UV beam was isolated via a Pellin-Broca prism, and focused by two cylindrical lenses (200mm and 50mm focal lengths) to a spot size of ~230μm x ~75μm at the sample. The power at the sample was ~4-mW. Scattered light was collected in a 135° backscattering

geometry by a UV compound lens and focused onto the entrance slit of a prism-based prefilter. This prefilter has been described elsewhere, and allows for acquisition of UVRR spectra to within 200 cm^{-1} of the Rayleigh line.[10] Raman scattered light was dispersed in a 0.5-meter spectrograph (JY Horiba, Spex 500M with 3600 gr/mm holographic grating), and imaged onto a CCD detector (Roper Scientific, Pixis 400B). The spectral response was determined by a deuterium lamp, and the bandpass and accuracy (based on ethanol peaks) of the detection system are <14 cm^{-1} and ±1 cm^{-1}, respectively. Figure 2.2 shows a rough diagram of the UVRR laser system.

Protein solution was pumped through a vertically-mounted, 200μm i.d. quartz microcapillary at a rate of 0.42 mL/min to minimize sample degradation due to exposure to UV light, and was discarded after a single-pass through the laser beam to eliminate artifacts from photolyzed protein. Five-minute UVRR spectra were collected for protein samples under the following conditions: folded in DMPC SUVs, or unfolded in KP_i buffer. Spectra of all buffer solutions without OmpA were also acquired and subtracted from the corresponding OmpA spectra. Fluorescence and absorption spectra were measured before and after photolysis.

2.4 Data analysis

2.4.1 Fluorescence and absorption spectra

Data analysis for fluorescence and absorbance spectra was performed using Igor Pro (Wavemetrics) software. Fluorescence and absorbance spectra were corrected by subtracting the appropriate buffer + urea from the protein-containing sample. Fraction subtraction was employed when necessary, and was typically for fluoresce spectra

containing vesicles because of irreproducible scattering artifacts. In general, however, a one-to-one subtraction was used of buffer + urea from sample from the sample spectra.

2.4.2 UVRR spectra

Data analysis for UVRR spectra was performed using Igor Pro (WaveMetrics) software. A typical data workup is as follows:

1. Individual 1-minute spectra were collected. Representative 1-minute spectra of phosphate buffer are shown in Figure 2.3.

2. Cosmic rays were removed manually and the resulting spectra were summed.

3. Buffer contribution was removed by fractional subtraction in the form of:

Protein sample – x*(buffer + urea) blank – y*(buffer) blank

Where buffer + urea blank is a spectrum of buffer with appropriate urea concentration, and buffer is a spectrum of KP_i buffer. Representative summed spectra for OmpA and blanks are shown in Figure 2.4.

4. A residual baseline was interpolated and subtracted from background-corrected spectrum of OmpA from step #3, shown in Figure 2.5.

5. The resulting UVRR spectra were normalized for acquisition time and laser power.

6. When appropriate, final spectra were scaled for Y9a intensity (~1179 cm^{-1}).

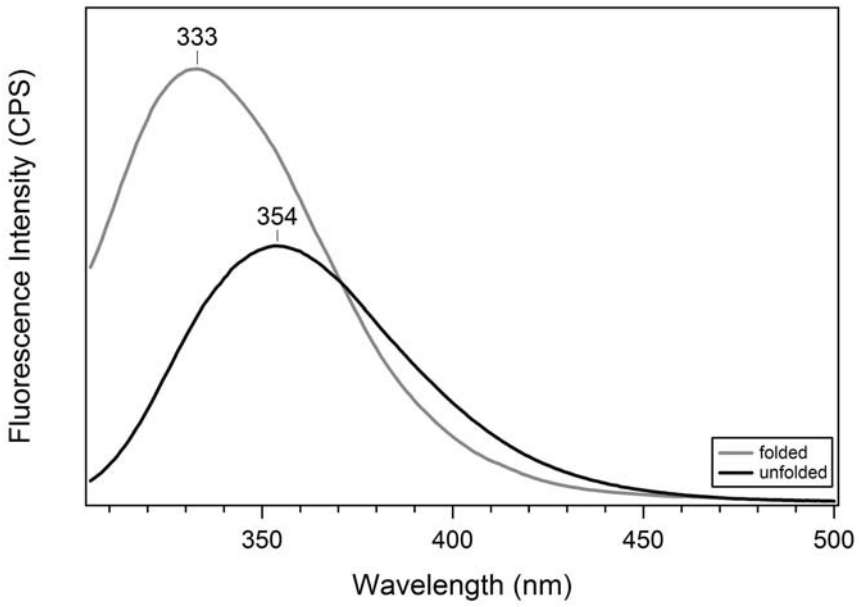

Figure 2.1: Tryptophan fluorescence spectra of wild type OmpA. Unfolded protein (black curve) has an emission maximum of 354 nm; folded protein (gray curve) has an emission maximum of 333 nm.

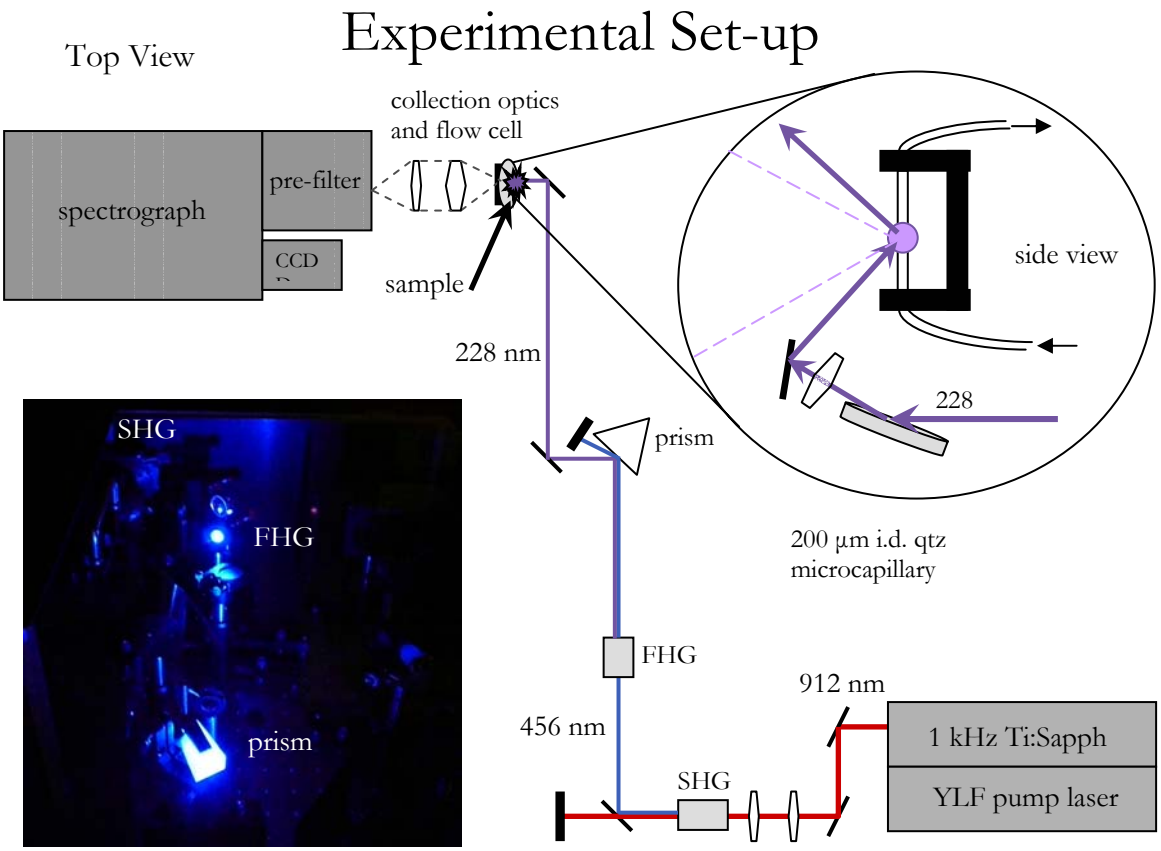

Figure 2.2: UVRR laser set-up, showing path of the laser beam. Here, the Ti:Sapphire fundamental (912 nm) light is frequency doubled using two doubling crystals, to produce 228-nm light. Isolated 228-nm light is sent to the capillary flow cell, seen in the blow-up diagram. Scattered light is collected at 135º backscattering geometry and sent through the pre-filter to remove contribution from Rayleigh scattered light. Raman scattered light is dispersed through a spectrograph and collected using a CCD detector.

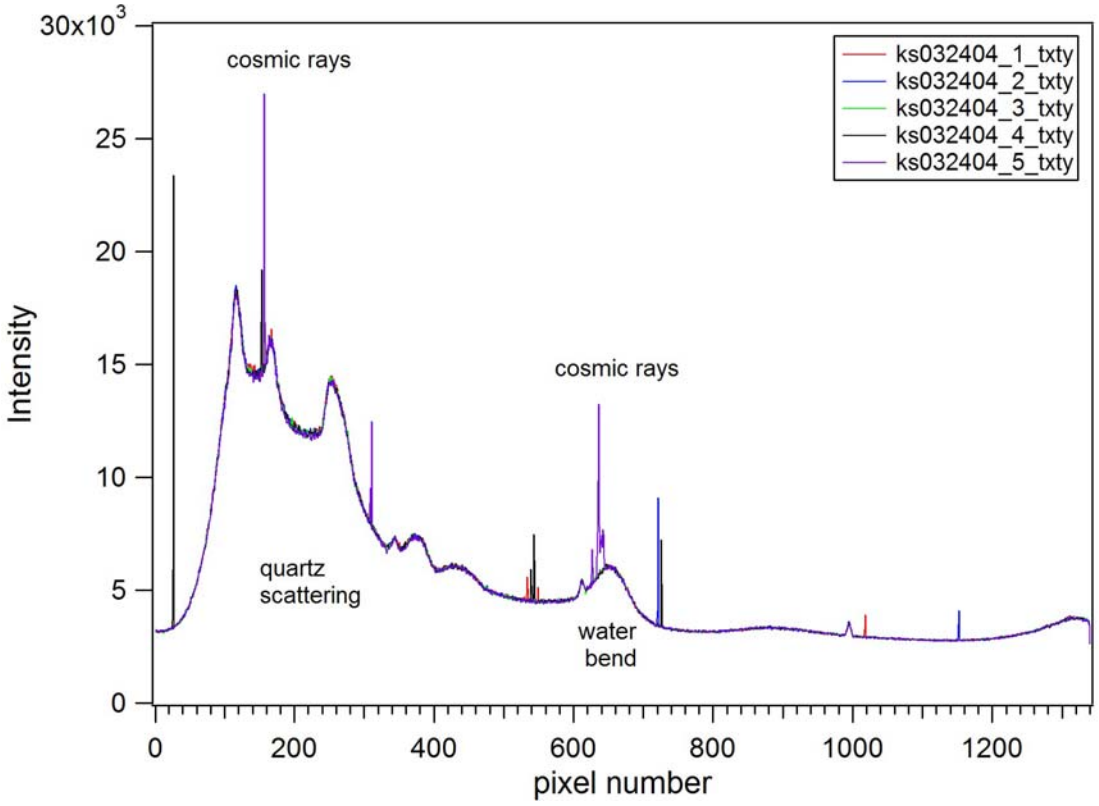

Figure 2.3: Representatice raw UVRR spectra of phosphate buffer, showing individual 1-min spectra, with UV power ~4 mW. The graph shows Raman intensity versus CCD pixel number (1 – 1340). Contribution of capillary, water, and buffer peaks are seen. Cosmic rays appear as sharp features, and are typically 1 – 2 pixels wide.

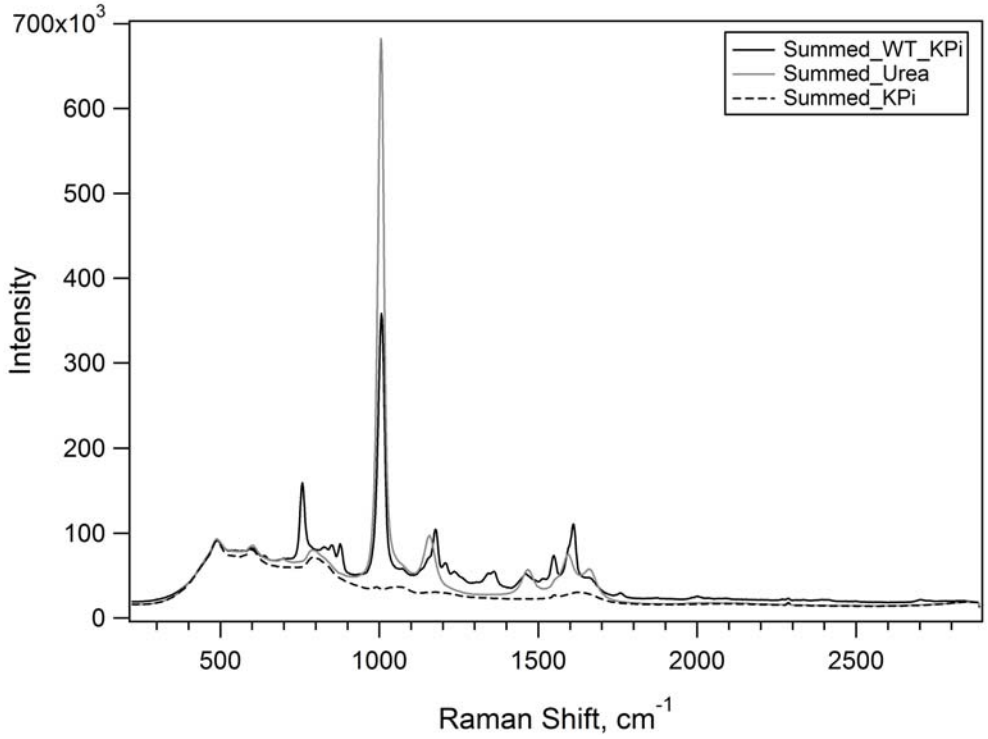

Figure 2.4: Representative summed spectra of WT OmpA in KP_i buffer (solid black line), 1 M urea in KP_i buffer (solid gray line), and KPi_i buffer (dashed black line). Trp and tyr peaks are distinguishable from those of urea and the capillary.

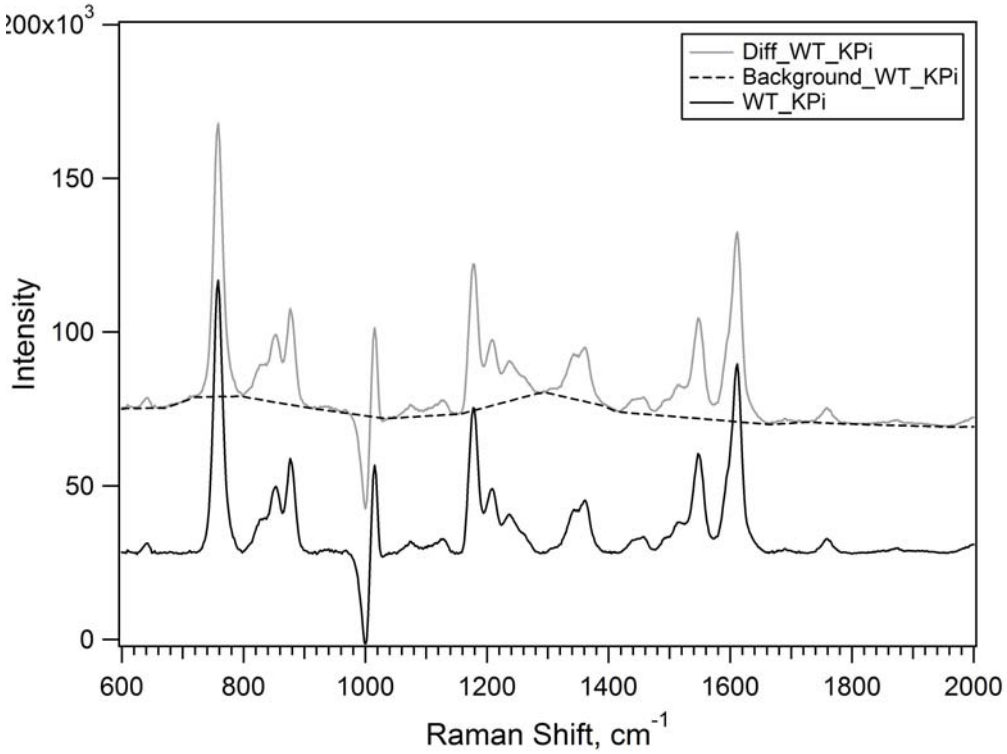

Figure 2.5: Representative difference spectra, showing buffer subtracted protein (dotted), interpolated background (dash), and final (buffer and background removed) spectra (solid). Spectra are offset for clarity. Subtraction is as follows:
Diff_WT_KPi = Summed_WT_KPi – 0.51*Summed_Urea – 0.4*Summed_KPi
WT_KPi = Diff_WT_KPi – Background_WT_KPi

2.5 References

(1) Sun, H.; Greathouse, D. V.; Andersen, O. S.; Koeppe II, R. E. *J. Biol. Chem.* **2008**, *283*, 22233.

(2) Yau, W.-M.; Wimley, W. C.; Gawrisch, K.; White, S. H. *Biochemistry* **1998**, *37*, 14713.

(3) van der Wel, P. C. A.; Reed, N. D.; Greathouse, D. V.; Koeppe II, R. E. *Biochem.* **2007**, *46*, 5714.

(4) Liu, W.; Caffrey, M. *Biochem.* **2006**, *39*, 11713.

(5) Burnstein, E. A.; Vedenkina, N. S.; Ivkova, M. N. *Photochem. and Photobiol.* **1973**, *18*, 263.

(6) Surrey, T. J., F. *Proc. Natl. Acad. Sci. U.S.A.* **1992**, *89*, 7457.

(7) Surrey, T.; Jahnig, F. *Proc. Natl. Acad. Sci. U.S.A.* **1992**, *89*, 7457.

(8) Sanchez, K. M.; Gable, J. E.; Schlamadinger, D. E.; Kim, J. E. *Biochemistry* **2008**, *47*, 12844.

(9) Toal, S. J.; Jones, K. A.; Magde, D.; Trogler, W. C. *J. Am. Chem. Soc.* **2005**, *127*, 11661.

(10) Kaminaka, S.; Mathies, R. A. *Appl. Spect.* **1998**, *52*, 469.

Chapter 3

Effects of Tryptophan Microenvironment, Soluble Domain, and Vesicle Size on the Thermodynamics of Membrane Protein Folding: Lessons from the Transmembrane Protein OmpA

3.1 Introduction

Membrane proteins adopt unique three-dimensional structures in cell membranes to be biologically active. Like soluble proteins, membrane proteins that form aberrant structures lead to a number of prevalent diseases, such as cystic fibrosis and type II diabetes.[1,2] A great deal of experimental and theoretical research has recently been devoted towards elucidating the molecular mechanisms, thermodynamics, and kinetics of protein folding in lipid bilayers.[3-7] Despite these efforts, our knowledge of membrane protein folding remains inferior to our fundamental understanding of soluble protein folding. A number of factors contribute to the inherent difficulties in the study of membrane protein folding. First, in contrast to soluble proteins, a limited number of membrane protein systems are available to serve as models for membrane protein folding.[5-8] An additional challenge is the membrane itself; lipid bilayers are complex systems, with a high degree of chemical heterogeneity.[6,9] Finally, the limited availability of membrane protein structures inhibits rapid expansion of experimental and theoretical work in this area.

A few α-helical and β-barrel membrane proteins and peptides have been studied to provide insight into the driving forces relevant to membrane protein folding. The energetically expensive process of dehydrating the peptide bond is balanced by two critical events: the formation of secondary-structure hydrogen bonds in the bilayer and

favorable hydrophobic interactions. Peptide backbone stabilization in the form of extensive hydrogen bond networks dominates the formation of secondary structure; this large driving force may provide the physical basis for why unfolded proteins are not found within a bilayer.[10] Hydrogen bonds involving side chains are also critical, and have been analyzed for soluble proteins.[11,12] Hydrophobic interactions have been quantified in the form of measured free energies of transfer from water to bilayer interface or to *n*-octanol on White-Wimley hydrophobicity scales.[6,13,14] Aromatic amino acids also play critical roles in the stability of proteins and are considered to be anchoring residues for membrane proteins.[15,16] Hence, the aromatic residues trp, tyr, and phe are found predominantly at the bilayer-water interface.[17-21]

Outer Membrane Protein A (OmpA) is a monomeric, 325-residue integral membrane protein found in the outer membrane of Gram-negative bacteria (Figure 3.1 inset). It is one of the most abundant proteins in the outer membrane, and is reported to have a variety of functions, such as acting as a nonspecific pore, providing membrane stability, and serving as a receptor.[22,23] OmpA consists of a transmembrane β-barrel constructed from eight anti-parallel β-sheets and a soluble C-terminal domain located in the periplasm.[24] The relative ease with which wild-type and mutant OmpA can be overexpressed in *E. coli* combined with the success with which OmpA spontaneously folds into a membrane bilayer or micelles make OmpA an ideal candidate for β-barrel membrane protein folding studies.[25-27] The existence of five native tryptophan residues that are sensitive reporters of conformational state provides an additional advantage of working with OmpA for membrane protein folding studies: Steady-state fluorescence

experiments may be used to directly determine relative populations of folded and unfolded states.

The *in vitro* folding mechanism of OmpA has been studied by several groups and techniques. Electronic spectroscopy, including fluorescence and circular dichroism, as well as vibrational techniques have yielded structural and kinetic information.[25-31] Effects of temperature, bilayer composition, and bilayer curvature on the folding of OmpA have been investigated.[25,29,32] Conversion between narrow and large pore sizes of OmpA folded in planar bilayers has also been reported.[33,34] These and other previous studies have helped establish successful conditions for performing folding experiments and have expanded our general understanding of β-barrel membrane protein folding.

Here, we present fluorescence data to shed light on conformational stabilities of wild-type and mutant OmpA folded in small unilamellar vesicles (SUVs), and discuss the observed trends in terms of important non-covalent interactions. An important goal is to elucidate molecular interactions of interfacial tryptophan residues that are critical for membrane protein stability. In the current studies, mutations have been made on wild-type OmpA to produce single-trp containing mutants, where four of the five native tryptophan residues have been replaced with phenylalanine residues. A similar study was recently reported by the Tamm group in which one or two aromatic amino acids was replaced by alanine to determine the contribution of tryptophan, tyrosine, or phenylalanine on conformational stability.[35] In addition to the contribution of amphiphilic tryptophan residues to membrane protein stability, we compare refolding curves in the presence and absence of the soluble C-terminus. Surprisingly, the free energy of unfolding is greater when the soluble domain is removed, highlighting the

importance of the unfolded state in these measurements of stability. Finally, we report dynamic light scattering measurements to elucidate changes in vesicle size in the presence of urea and/or protein, and probe changes in protein conformational stability as a function of vesicle diameter.

3.2 Materials and Methods

3.2.1 Preparation of single-tryptophan containing mutants

Site-directed mutagenesis was performed on a plasmid encoding for the single-tryptophan mutant at position 7 of Outer Membrane Protein A (OmpA) to produce additional full-length mutants with single trp residues in the other native positions.[26] In these single-trp mutants, the remaining four native trp residues were mutated to phenylalanine residues. These quadruple mutants are referred to throughout the text as the single-trp mutants Trp-7 (W7), Trp-15 (W15), Trp-57 (W57), Trp-102 (W102), and Trp-143 (W143) for mutants with a trp residue at position 7, 15, 57, 102, or 143, respectively. Truncated versions of these OmpA single-trp mutants were generated by introducing a stop codon at position 177 to cleave the periplasmic domain (147 residues), resulting in single-trp, transmembrane-spanning, truncated mutants Trp-7t (W7t), Trp-15t (W15t), Trp-57t (W57t), Trp-102 (W102t), and Trp-143 (W143t). PCR products were transformed into XL1-Blue supercompetent cells; the resulting DNA was extracted using a Qiagen Miniprep Kit. All sequences were verified before expression.

3.2.2 Expression, isolation, and purification of OmpA

Previously published procedures were adapted to isolate and purify wild-type OmpA and OmpA mutants.[25,28] A detailed description of this procedure can be found in Appendix A. Wild-type OmpA, containing five native tryptophan residues, was obtained

from *E. coli* strain JF701 (Genetic Stock Center, Yale University). Cells were initially grown overnight in sterile media (1% bactotryptone, 0.5% yeast extract, and 25 μg/mL streptomycin) at 37 °C before transferring to fresh LB containing 25 μg/mL streptomycin. Single-trp mutants of OmpA were overexpressed in an $OmpA^-$ and $OmpF^-$ *E. coli* strain JF733 (Genetic Stock Center, Yale University). Cells containing the appropriate plasmid for the mutant OmpA protein were initially grown overnight at 37 °C in sterile LB media with 0.5% glucose and 50 μg/mL ampicillin and then transferred to fresh LB containing 50 μg/mL ampicillin. Overexpression of OmpA was induced with 1 mM isopropyl β-D-thiogalactopyranoside (IPTG).

Wild-type and mutant OmpA were isolated and purified by the following procedure. Defrosted cells were placed in an ice bath and resuspended in a cold solution of 0.75 M sucrose in 10 mM tris-HCl buffer (pH 7.8). A solution of cold 20 mM EDTA with lysozyme (0.5 mg/mL) was added over a period of one minute. Phenylmethanesulphonylfluoride (PMSF) was also added. The solution was stirred in an ice bath until cells dissolved, and sonicated in an ice bath with a standard horn tip. After intact cells and other particulates were removed, the cell lysis was centrifuged and the resulting red-brown pellets containing OmpA was redissolved in pre-extraction buffer (3.5 M urea, 20 mM tris-HCl, pH 9, 0.05% 2-mercaptoethanol) in a 50 °C water bath to solubilize peripheral membrane proteins. This solution was centrifuged and the pellets containing OmpA were dissolved in a 1:1 mixture of 2-propanol: extraction buffer (8 M urea, 20 mM tris-HCl, 0.05% 2-mercaptoethanol, pH 8.5). The solution was stirred in a 50 °C water bath until pellets dissolved, and solubilized OmpA was isolated via centrifugation from the lipid membrane. The supernatant containing crude OmpA was

purified by anion exchange chromatography. OmpA was eluted using a linear concentration gradient of up to 200 mM NaCl in urea buffer (8M urea, 15 mM tris-HCl, 0.5% 2-mercaptoethanol, pH 8.5) over 20 column volumes. Fractions containing purified protein were combined, washed, and concentrated via ultrafiltration (Amicon, PM-10 for full-length protein, and YM-3 for truncated). Stock protein samples were stored as unfolded protein in 8 M urea, 20 mM KP_i, pH 7.3 buffer at -80 °C. SDS-PAGE was used to determine a purity of ~90%.

3.2.3 Preparation of unilamellar vesicles

Small unilamellar vesicles (SUVs) were prepared using an adaptation of a previously published procedure.[25] A stock solution (20 mg/mL) of 1,2-dimyristoyl-sn-glycero-3-phosphocholine (DMPC, Avanti Polar Lipids) in chloroform was dried under a stream of argon and resuspended in phosphate buffer (20 mM KP_i, pH 7.3) to a final lipid concentration of 5 mg/mL. SUVs (~50 nm diameter) were made by sonication of the lipid solution with a Branson ultrasonicator microtip. The sonicated solution was passed through a 0.22 μm filter to remove titanium dust and other particulates. The SUVs were further diluted to a final concentration of 1 mg/mL for all experiments. Vesicle solutions were equilibrated overnight at 37 º C and used the following day.

Small and large unilamellar vesicles were also made by extrusion.[36] Stock DMPC solutions were dried and resuspended in KP_i buffer as discussed above. Resuspended lipid solutions were passed through an extruder with a membrane of appropriately sized pores to produce nominal vesicle diameters of 50, 100, 200, and 400 nm. A gravity-flow size-exclusion column (Bio-Rad, 10DG) was used to separate the vesicles based on size. Dynamic light scattering experiments were performed to measure

the average vesicle size for each fraction. Appropriately combined fractions with DLS-determined diameters of ~70, ~120, ~200, and ~300 nm were diluted to a final concentration of 1 mg/mL. The population of the nominally 400 nm vesicles was ~50% (300 nm) and ~50% >1 μm. Vesicle solutions were equilibrated overnight at 37 º C and used the following day.

3.2.4 Steady-state fluorescence and absorption spectroscopy

OmpA refolding was monitored by tryptophan fluorescence. Steady-state fluorescence measurements with 290 nm excitation were performed with a Jobin Yvon-SPEX Fluorolog FL3-11 spectrofluorometer. Samples were maintained at 30 °C, which is above the phase transition temperature for DMPC. Absorbance measurements were recorded on an Agilent UV-visible spectrophotometer. Protein concentrations were calculated using ε_{280} values of 54 400 $M^{-1}cm^{-1}$, 32 300 $M^{-1}cm^{-1}$, and 26 000 $M^{-1}cm^{-1}$ for wild-type, single-trp, and truncated single-trp mutants of OmpA, respectively.

3.2.5 Equilibrium refolding and unfolding of OmpA

Stock solutions of 20 mM KP_i buffer (pH 7.3), 10 M urea in 20 mM KP_i buffer (pH 7.3), and appropriately sized vesicles were used to prepare 1 mg/mL vesicle samples with urea concentrations ranging from 0-8 M. Stock solution of unfolded protein was added to these vesicle solutions to a final OmpA concentration of ~ 4 μM for fluorescence experiments and ~12 uM for gel electrophoresis (SDS-PAGE) measurements. Blank samples (urea, KPi, and vesicles) containing no protein were also prepared. Fluorescence spectra of blank samples were subtracted from spectra of protein samples to remove contributions from buffer. Urea concentrations were determined from refractive index measurements using an Abbe 3L Bausch & Lomb refractometer.[37] A

time-dependence study was performed and determined that a 12 hour incubation period was sufficient to reach equilibrium conditions. All protein and blank samples for fluorescence and SDS-PAGE experiments were equilibrated overnight at 37 ºC. SDS-PAGE experiments were performed to confirm that the folding of OmpA is reversible using an adaptation of a previously published method.[32] The differential mobility of folded (30 kDa) and unfolded (35 kDa) protein was utilized for these gel-shift assays. For unfolding studies, unfolded stock protein was diluted into SUVs and incubated at 37 ºC for refolding to occur. The solution was diluted 2x in appropriate urea solutions to a final protein concentration of ~12 uM. For refolding studies, the stock unfolded protein was diluted into solutions with SUV and varying urea concentrations. All refolding and unfolding samples were loaded onto 12.5% gels (full-length protein) or 15% gels (truncated protein). Unfolding gels of the truncated protein indicated a minor population (<15%) of the protein remained unfolded in low urea concentrations and folded at high urea concentrations.

3.2.6 Determination of the effective free energy of unfolding for OmpA mutants

Gel-shift assays indicated fully reversible folding/unfolding conditions for full-length OmpA, and >85% reversibility for truncated OmpA under our experimental conditions. Due to the reversibility of refolding, all calculated free energies determined from the refolding curves are the effective free energies of unfolding. Emission maxima were determined for all protein samples, and the resulting plot of fraction unfolded, *f*, vs urea concentration were fit to a reversible, two-state model for protein unfolding.[38,39]

3.2.7 Dynamic Light Scattering Measurements

Dynamic light scattering (DLS) was used to determine vesicle diameters. The apparatus has been described in detail elsewhere.[40] Measurements were made using the 514.5-nm laser line from an argon ion laser with the samples held at a constant temperature of 30 °C. Ten autocorrelation traces were collected and averaged for each sample. Autocorrelation functions, $g(\tau)$, determined from DLS were calculated using the relationship $g(\tau) = \exp(-t/\tau)$, where t is the correlation time, and τ is the characteristic lifetime of a particle diffusing within a defined volume.[41] The translational diffusion constant, D_T, can be calculated from the following relationship: $\tau^{-1} = 2D_T q^2$. The scattering vector, q, is defined by $q = (4\pi n_s/\lambda)\sin(\theta/2)$, where λ is the excitation wavelength, n_s is the solvent refractive index, and θ is the scattering angle ($\theta = 90$ °). The diffusion constant, D_T, is defined by $D_T = kT/6\pi\eta R_h$, where η is the viscosity of the medium and R_h is the hydrodynamic radius of the particle. Particles were assumed to be spherical. The value of η was assumed to be 0.798×10^{-2} poise for water and scaled appropriately for changes in viscosity with increasing urea.[42] The average characteristic lifetime, τ, of each sample obtained from experimental measurements was used to calculate R_h of the vesicles. Two populations with corresponding average diameters were obtained for each sample. The fraction of reported population was > 80% unless specified. Vesicle size was measured as a function of vesicle concentration from 0.1 to 1 mg/ml to ensure appropriate conditions for our measurements; these control experiments indicated variation of <20% in vesicle diameter across this concentration range and this error has been included in Figure 3.3.

3.3 Results

3.3.1 Refolding Curves

Tryptophan fluorescence spectroscopy was used to determine conformational stabilities of single-trp mutants of OmpA in synthetic lipid bilayers. The single-trp residue in Trp-15, Trp-57, Trp-102, and Trp-143, is located on the β-barrel near the extracellular (intra-vesicle) region, while the trp residue in Trp-7 is located closer to the periplasmic (extra-vesicle) side. Each trp is located along a different strand, except for Trp-7 and Trp-15 which are located along the same strand. Representative trp emission spectra of OmpA folded in vesicle (λ_{max} = ~330 nm) and unfolded in 8 M urea (λ_{max} = ~350 nm) are illustrated in Figure 3.1. This shift in emission maximum upon addition of denaturant was used to monitor the relative populations of folded and unfolded protein.

Refolding curves of wild-type and single-trp mutants of OmpA are displayed in Figure 3.2A. Wild-type OmpA was determined to be the most stable, with a $\Delta G^{\circ}_{H_2O}$ value of 10.5 kcal/mol. Full-length mutants had lower free energies of unfolding compared to wild-type OmpA, with $\Delta G^{\circ}_{H_2O}$ values ranging between 2.4 and 6.7 kcal/mol. Trp-15 and Trp-102 mutants had $\Delta G^{\circ}_{H_2O}$ values of 4.8 and 4.7 kcal/mol, respectively, while Trp-57 and Trp-143 mutants had $\Delta G^{\circ}_{H_2O}$ values of 2.4 and 2.8 kcal/mol, respectively. The most stable mutant appears to be the single-trp mutant Trp-7, with a $\Delta G^{\circ}_{H_2O}$ value of 6.7 kcal/mol. Despite the fact that Trp-7 has a similar C_m value (~3 M urea) as Trp-15 and Trp-102, Trp-7 has a greater overall conformational stability due to its larger *m*-value. Tabulated fitting parameters, *m* and C_m, and resulting $\Delta G^{\circ}_{H_2O}$ values are summarized in Table 1.

Refolding curves were also determined for the truncated single-trp mutants that lack the soluble domain. These curves are shown in Figure 3.2B. Truncated mutants had free energy of unfolding values that ranged from 3.9 to 11.1 kcal/mol. The most stable mutants were Trp-102t and Trp-7t, with $\Delta G^{\circ}_{H_2O}$ values of 11.1 and 9.4 kcal/mol, respectively. Trp-143t was also stable, with $\Delta G^{\circ}_{H_2O}$ of 7.2 kcal/mol. Even though Trp-7t and Trp-143t have almost identical C_m values of ~3.1 M urea, the higher stability for Trp-7t can be traced to its larger *m*-value. However, given the difficulty of these experiments, our estimates of error (see below) prevent us from making definitive assessments of the relative stabilities of Trp-7t and Tr-143t at this time. $\Delta G^{\circ}_{H_2O}$ values for Trp-57t and Trp-15t were determined to be 5.3, and 4.8 kcal/mol, respectively. Fitting parameters and $\Delta G^{\circ}_{H_2O}$ values for the truncated mutants are summarized in Table 3.1. In general, the truncated mutants were more stable than their full-length counterparts: $\Delta G^{\circ}_{H_2O}$ values for Trp-7 and Trp-57 increased by ~3 kcal/mol, $\Delta G^{\circ}_{H_2O}$ for Trp-143 increased by ~4 kcal/mol, and $\Delta G^{\circ}_{H_2O}$ for Trp-102 increased by ~6.5 kcal/mol upon removal of the soluble tail. In contrast to these mutants, $\Delta G^{\circ}_{H_2O}$ for Trp-15 decreased only ~ 1 kcal/mol when the periplasmic tail was eliminated; this difference for Trp-15 vs. Trp-15t falls within our experimental uncertainty and is therefore negligible.

3.3.2 Determination of vesicle size

DLS measurements determined vesicle size and stability to ensure reproducibility for the current protein unfolding studies. Fluorescence and DLS measurements were performed on the same day using solutions from the refolding studies for six mutants

Trp-57, Trp-57t, Trp-102, Trp-102t, Trp-143, and Trp-143t. A representative data set for Trp-143 OmpA is shown in Figure 3.3.

Diameters of vesicle-only solutions were measured with increasing urea concentration (0-8 M). The initial stock vesicle solution contained ~50 nm SUVs. Vesicle diameters remained ~50 nm in low concentrations of urea (< 1 M), and increased to ~100-300 nm at greater concentrations of urea (> 1 M). This trend was observed for all six vesicle-only (blank) solutions. Vesicle diameters were also measured in the presence of OmpA with increasing concentrations of urea. Vesicle diameters in protein-containing solutions followed the same trend as blank solutions. Diameters remained ~50 nm in low urea concentrations (< 1 M), and increased to ~80-300 nm at higher concentrations of urea (> 1 M). Similar trends of increased vesicle size with increasing urea concentration were also found for the Trp-57, Trp-57t, Trp-102, and Trp-102t mutants (data not shown).

3.3.3 Effects of small and large unilamellar vesicles on thermodynamic stability of OmpA

Refolding curves were measured for the single-trp mutant, Trp-15t, using small unilamellar vesicles (SUVs) and large unilamellar vesicles (LUVs) to test the effects of vesicle size on thermodynamic stability. Figure 3.4 shows refolding curves of Trp-15t OmpA using nominally 50, 100, 200, and 400 nm diameter vesicles. Actual vesicle diameters were ~70, ~120, ~200, and ~300 nm, respectively. For the latter sample, ~ 50% of the population exhibited an average diameter of ~ 300 nm and the remaining population had a very large average diameter (> 1 μm). Measurements were taken 6, 12, and 24 hours after the addition of protein to determine equilibrium conditions. The data

shown were measured after a 24-hour incubation period. The greatest stability was measured for solutions containing 50 nm vesicles, with $\Delta G^{\circ}_{H_2O}$ of 3.9 kcal/mol, followed by solutions using ~100 and ~200 nm diameter vesicles which yielded the same value of 3.4 kcal/mol and is <15% lower than the value for 50 nm vesicles. Folding into nominally 400 nm diameter vesicles resulted in the lowest measured $\Delta G^{\circ}_{H_2O}$ value of 2.2 kcal/mol. These measurements of conformational stabilities as a function of vesicle size combined with the range of urea concentrations over which OmpA unfolds indicates that the largest source of systematic error is the change in vesicle size over the urea concentrations of interest; therefore, we estimate an error of <15% in our reported values in Table 1.

3.4 Discussion

3.4.1 Full-length mutants

Non-covalent interactions are crucial to the stability of membrane proteins. Important forces that drive a peptide or protein towards a membrane include non-polar (hydrophobic) interactions, electrostatic interactions between residues and charged lipid head groups, formation of secondary structure, and electrostatic effects because of differences in the dielectric constants of water and the membrane.[6,43] A large variety of critical side-chain and backbone hydrogen bonds have been reported.[44-46] The current study probes the thermodynamic stabilities associated with the five native tryptophan residues in wild-type and single-trp mutants of OmpA. Five native trp residues give rise to the refolding curve of wild-type OmpA, and hence provide an estimate of the global stability of the protein. In contrast, single-trp OmpA mutants in which four native trp

residues are replaced with phe residues provide a unique opportunity to probe the effects of the trp environment on the overall stability of the protein.

The aromatic residues tryptophan, tyrosine, and phenylalanine contribute significantly to the thermodynamic stability of membrane proteins because of strong interactions with neighboring aromatic residues and favorable water-to-bilayer partition energies.[13,14,16,35] Individual trp residues provide greater contribution to membrane protein stability relative to phe residues; however both are energetically favored in the membrane and are able to participate in pairwise interactions with aromatic residues.[35] Previous studies of OmpA showed similar secondary structure and trp environments when comparing wild-type and the single-trp mutants; therefore, it is likely that the range of conformational stabilities reported here for the single-trp mutants can be attributed to differences in local environment of trp residues as opposed to modification in global protein structure.[26,28]

As seen in Figure 3.2 and Table 3.1, the full-length single-trp mutants of OmpA were found to be less stable than wild-type OmpA. This result is consistent with removal of four of the five native anchoring trp residues. The change in free energy upon transfer of an individual trp residue from water to lipid bilayer is -1.85 kcal/mol; the analogous value for a phe residue is -1.13 kcal/mol.[13] Trp and phe energy contributions determined from previous thermodynamic stability experiments on OmpA mutants showed an average contribution of -2.0 and -1.0 kcal/mol, respectively.[35] Our results indicate that OmpA is destabilized 3.8 to 8.1 kcal/mol upon substitution of four trp residues for phe residues and are consistent with these previous reports; trp residues provide a greater contribution to the stability of OmpA relative to phe residues.

Three important molecular interactions involving trp residues are considered in the current study of single-trp mutants. First, the role of pairwise aromatic interactions has been shown to be critical to membrane protein stability. While it was previously suggested that the exact identity of aromatic amino acid involved in these interactions is not crucial, our results support a picture in which a trp residue is optimum for the aromatic pocket near Trp-7, but may not be critical in the pairwise interactions involving Trp-143 and Trp-57.[35] Second, hydrogen-bonding of the indole heteroatom provides stability in the transmembrane domain; this hydrogen bond is important in Trp15. Finally, the unique amphiphilic nature of trp plays an important role for interfacial stabilization of Trp102 relative to phe and tyr residues. These topics are discussed in detail below.

3.4.2 Stability of W7: Pairwise aromatic interactions

Neighboring aromatic residues may interact in pairwise fashion to contribute to the stability of proteins. Typical interaction distances of 4.5 to 7.0 Å between aromatic residue centroids in soluble proteins contribute up to 2 kcal/mol towards the stability of a protein.[16] These pairwise interactions were recently investigated in OmpA and were estimated to be on the same order as those found for soluble proteins.[35] The region near Trp-7 has the greatest number of neighboring aromatic residues, Tyr8, Tyr43, Tyr168, and Phe170 (~ 7 Å between aromatic centroids). Our results support a picture in which a trp (and not phe) residue at position 7 is ideally suited for this aromatic pocket in the protein; mutant Trp-7 is the most stable of all full-length single-trp species. This result modifies the previous report that suggested that these important pairwise interactions may not depend on the type of aromatic residue involved; here, our results illustrate that

maintaining a trp residue at position 7 while replacing the remaining four native trp residues with phe residues decreases the $\Delta G^{\circ}_{H_2O}$ the least amount (by 3.8 kcal/mol) relative to the wild-type protein.[35,46] This destabilization of W7 relative to WT can be attributed to removal of the hydrogen bond at position 15 and removal of the amphiphilic trp residue at position 102 (see below).

Other pairwise interactions exist in OmpA. W143 has two neighboring aromatic residues, Phe132 and Tyr141, and W57 has one neighboring aromatic residue, Tyr55, within ~ 7 Å of the indole centroid. These pairwise aromatic interactions contribute to the stability for OmpA. However, it is not clear that that the trp-to-phe mutation in positions 143 or 57 causes significant destabilization of the protein as was observed in the case of position 7. W143 and W57 are the least stable of all full-length single-trp mutants; this enhanced instability can be attributed to the combined effects of the loss of Trp7 in the aromatic pocket, loss of the hydrogen bond at position 15, and removal of the amphiphilic trp residue at position 102. In contrast, W15 and W102 have no neighboring aromatic residues; these observations are summarized in Table 3.2.

3.4.3 Stability of W15: Hydrogen bonding

The mutant W15 is one of the next highest in stability following W7. A variety of side-chain hydrogen bonds in proteins have been described, including bonding between N-H, O-H, and C-H donor groups and N-, O-, and π– acceptor groups.[11,12] A range of hydrogen bonding energies has been reported, and the typical value for biological systems is on the order of a few kcal/mol. The crystal structure of OmpA indicates a likely hydrogen bond between Trp15 and the side chain of Asn33. Specifically, the distance between the heteroatom in indole and the carbonyl oxygen of Asn33 is less than

2.9 Å. The presence of this hydrogen bond likely contributes to the stability of W15, and we estimate the hydrogen-bond strength of Trp15 to be ~ 2 kcal/mol. The measured decrease in stability of W15 relative to WT is attributable to loss of Trp7 in the aromatic pocket and loss of amphiphilic stability at position 102. The observation that W15 is less stable than W7 supports a picture in which stabilization due to Trp7 in the aromatic pocket (< 4 kcal/mol, see below) is more significant than stabilization due to Trp15 hydrogen bond (~2 kcal/mol). These values are consistent with Hong *et al*,which determined that the trp residue at position 7 contributes 3.6 kcal/mol, and the trp residue at position 15 contributes 2.0 kcal/mol to the stability of the protein.[35]

3.4.4 Stability of W102: Amphiphilic nature of tryptophan

In addition to contributions from interacting aromatic pairs and hydrogen-bonding partners, contributions from neighboring residues to the stability of tryptophan residues in OmpA were also investigated. Local partition energies for transfer from the bilayer to water to mimic protein unfolding were calculated using the White-Wimley interfacial hydrophobicity scale, which includes side-chain and backbone contributions.[13] For hydrophobic residues, this partition energy is a positive value, and for hydrophilic residues, this value is typically negative. These calculations were performed to provide an estimate of the partition energy of the region surrounding each trp residue. All neighboring residues within a 7 Å radius of the trp were included in the determination of the local partition energies, and are tabulated in Table 2 under ΔG_{part}. This radius typically included 12 or 13 residues surrounding a given trp and included residues located on different strands of the β-barrel relative to the location of the trp.

The region with the largest partition energy is Trp7 (3.23 kcal/mol), and the region near Trp102 has the smallest partition energy (-1.38 kcal/mol).[13] The large positive partition energy for W7 is consistent with Trp7 being located in a highly hydrophobic environment: W7 displays the most blue-shifted emission maximum as well as a large *m*-value, suggesting that Trp7 undergoes a large increase in solvent exposure upon unfolding relative to the other trp positions.[47] The region around Trp102 is the only region with a calculated negative partition energy, indicating a thermodynamic preference for this region to be in aqueous environment. This calculated negative partitioning energy for W102 is due to the presence of Gln75, Arg103, and Asp116.

Trp102 is found on a large loop that is likely in the interior of the vesicle due to the known directional insertion of OmpA.[25] However, there is no evidence that Trp102 is solvent-exposed in the folded form despite it being the only trp residue located on a loop, that faces the interior of the barrel, and has a calculated negative partition energy. In fact, W102 remains in a hydrophobic region, evidenced by fluorescence experiments. The emission maximum of W102 folded in vesicle is 332 nm, which is identical to the emission maxima of the other trp residues located on the same side of the barrel, W15, W57, and W143. This similarity in emission maxima indicates a similar degree of hydrophobicity surrounding these trp residues. For W102, the local hydrophobicity can be attributed to neighboring nonpolar residues including Ala74, Met100, Val101, and Ala104, as opposed to the hydrophobic environment of the lipid bilayer. In addition to similar steady-state emission, the kinetics of refolding and the fluorescence lifetime of W102 were found to be similar to those of W15, W57, and W143.[26,28]

The presence of both hydrophobic and hydrophilic residues in the local vicinity of Trp102 is consistent with the amphiphilic nature of tryptophan residues, and the substitution of trp for phe in this region may destabilize OmpA. The $\Delta G^{\circ}_{H_2O}$ value of W102 is similar to that of W15; in the case of W102, loss of the hydrogen bond at position 15 and loss of Trp7 in the aromatic pocket destabilizes this mutant relative to WT. However, the observation that W102 and W15 have similar values for $\Delta G^{\circ}_{H_2O}$ indicates that the energetic contributions from the amphiphilic nature of Trp102 and hydrogen-bonding ability of Trp 15 are similar, and each may contribute ~2 kcal/mol to overall protein stability.

3.4.5 Stability of W143 and W57

The least stable full-length mutants, W143 and W57, lack all three stabilizing effects discussed above. Namely, these mutants do not have Trp7 in the aromatic pocket, lack a hydrogen-bonded side chain at position 15, and do not possess the optimized amphiphilic trp residue in the unique loop region near Trp102. The absence of these effects results in the greatest destabilization of ~8 kcal/mol relative to WT. The observation that the $\Delta G^{\circ}_{H_2O}$ values are similar for W143 and W57 despite the presence of two or one neighboring aromatic residues, respectively, suggests that the trp-to-phe mutation has not perturbed the energetics of these pairwise interactions significantly. This implication helps provide an upper estimate of ~4 kcal/mol to the stabilization effect of Trp7.

3.4.6 Truncated Mutants

OmpA contains two distinct regions, the transmembrane domain located in the membrane which contains all five native trp residues, and the soluble periplasmic domain located in the exterior portion of the vesicle. There is no published structure of the C-terminal periplasmic tail of OmpA. A previous circular dichroism study of full-length and truncated mutants of OmpA showed a decrease in molar ellipticity and red-shift of the CD peak to ~216 nm when the soluble tail was removed.[28] The origin of this variation in CD spectra is not known. While it was previously suggested that the soluble C-terminus may possess β-sheet structure, the observed CD changes are also consistent with a random coil soluble domain. Other studies demonstrated that OmpA forms two pores in planar bilayers: a small pore that involves the N-terminus domain only, and a large pore that requires both the N- and C-terminal domains.[33,34] We are unable to determine whether the soluble domain possesses secondary structure or whether an entirely new folded structure is formed in SUVs in the presence of the C-terminal domain; we are applying UV resonance Raman spectroscopy to probe changes in vibrational structures between full-length and truncated mutants.

Results from the current study indicate that removal of the soluble domain results in a greater free energy of unfolding for the transmembrane domain. The $\Delta G^{\circ}_{H_2O}$ values for four of the five full-length mutants increased by >2.7 kcal/mol upon removal of the soluble tail. The trend in $\Delta G^{\circ}_{H_2O}$ values of the full-length mutants was not identical to the trend for the $\Delta G^{\circ}_{H_2O}$ values of the truncated mutants. This variation may indicate structural differences of the transmembrane domain upon removal of the soluble tail as well as reflect our experimental uncertainty. Previous studies have probed the

differential stabilities of the transmembrane and soluble domains of a membrane protein, but to our knowledge, this is the first report of direct measurements of the effect of a soluble domain on the conformational stability of a transmembrane domain.[48,49]

Our result that the $\Delta G^{\circ}_{H_2O}$ values increase upon removal of a significant (soluble) portion of the protein is surprising, and may be explained by one of the following scenarios in a simplified two-state picture consisting of folded and unfolded states of the transmembrane region. First, it is possible that the covalently bound soluble domain *destabilizes* the *folded* transmembrane domain such that removal of this energetically expensive soluble domain overall stabilizes the folded transmembrane portion. We have no experimental evidence or examples in literature to support this case and therefore, believe that this is an unlikely scenario. Second, the soluble domain may *stabilize* the *unfolded* transmembrane domain by, for example, providing favorable hydrophobic interactions in solution. Removal of this energetically favorable soluble domain destabilizes the unfolded transmembrane portion, resulting in the observed increase in $\Delta G^{\circ}_{H_2O}$. Other studies on the effects of the denatured state on the free energies of unfolding for soluble proteins have been reported.[50-52] Currently, tryptophan emission studies on OmpA mutants do not show significant variations in fluorescence maxima of the unfolded transmembrane domain of the full-length and truncated protein; however stabilization provided by the soluble domain may not necessarily impact the emission properties of the native tryptophan residues in the unfolded state. Finally, the structure of the transmembrane domain may be different in the absence of the soluble C-terminus. For example, the transmembrane domain may be imbedded deeper into the bilayer when

the soluble tail is removed. We do not have evidence to support a significant change in global protein structure upon truncation of the C-terminus, but do not dismiss the possibility. Based on our preliminary findings, we hypothesize that the second scenario is the most likely explanation for the increase in free energy of unfolding upon removal of the soluble tail; however, it is clear that more in-depth studies must be pursued.

3.4.7 Effects of denaturant on SUVs

To complement these studies of OmpA thermodynamics, we investigated the effects of denaturant and protein on SUVs. Previous studies have shown that factors such as bilayer composition, chain-length, and bilayer curvature affect protein folding and assembly mechanisms in the membrane.[29,32,53,54] In fact, conformational stabilities of OmpA ranged from ~2 to 6 kcal/mol depending on lipid composition, head-group size, and chain-length.[29] From these studies, it is apparent that the properties of the bilayer can greatly affect the stability of the protein. Some important factors to consider are the following: Does the presence of a denaturant and/or folded protein affect the properties of the vesicles? How do the macroscopic properties of vesicles affect measurements of protein stability?

Urea has been shown to traverse the bilayer through a solubility-diffusion controlled mechanism, indicating equilibrium urea concentrations on the inside and outside of the vesicle in our experimental time-scale.[55] Previous studies illustrated no change in vesicle size over a twelve hour period in the presence of ~100 mM urea and little to no change in vesicle structure up to 3 M urea; our results are consistent with these previous works in that low concentrations of urea (< 1M) do not affect vesicle size.[56-58] However, at urea concentrations typical of unfolding studies, there is an increase in

vesicle size; in blank solutions, the presence of > 1 M urea caused an increase in vesicle diameter with a high degree of variability in size (Figure 3.3). It appears that the presence of urea enhances vesicle fusion. A similar increase in vesicle diameter was observed in vesicle solutions containing protein and urea. This result suggests the protein itself does not cause vesicle fusion. Instead, the observed change in size is due to denaturant. It is not clear from our results that the presence of protein directly affects vesicle size as has been previously reported.[59]

3.4.8 Effects of SUV size on $\Delta G^{\circ}_{H_2O}$

Figure 3.4 illustrates that $\Delta G^{\circ}_{H_2O}$ values vary by less than 15% when determined with nominally 50, 100, or 200 nm diameter vesicles. Measurements of $\Delta G^{\circ}_{H_2O}$ with 400 nm vesicles, however, resulted in a >40% decrease in observed $\Delta G^{\circ}_{H_2O}$ value. It is not clear if this decrease is significant since the scattering became more pronounced and we have not thoroughly characterized these larger vesicles. Nonetheless, these results illustrate the importance of characterizing the effect of denaturant and protein on vesicle properties in these measurements of membrane protein conformational stabilities; the largest source of experimental error may be associated with the change in vesicle properties in the presence of denaturant.

3.5 Summary

The conformational stabilities of single-trp mutants of OmpA were measured and found to be less than that of wild-type OmpA: The mutants are destabilized ~ 4 kcal/mol (Trp-7), ~6 kcal/mol (Trp-15 and Trp-102), and ~8 kcal/mol (Trp-43 and Trp-57) relative to WT. The trends in free energies of unfolding for the different mutants are likely due to

a combination of non-covalent interactions, summarized in Table 3.2. Neighboring aromatic residues interact favorably to contribute to the stability of a protein. The presence of a specific trp residue is especially important in the aromatic pocket surrounding Trp-7, and we estimate an upper limit of ~4 kcal/mol for the stabilizing effect of Trp-7. The stability of Trp-15 may be explained in terms of a hydrogen bond, which may provide ~2 kcal/mol of stabilization. The relatively high stability of Trp-102 cannot be explained in terms of energetically favorable pairwise aromatic interactions or hydrogen-bonding partners, of which it has neither. The calculated bilayer-to-water partition energy near Trp-102 is negative, indicating the local prevalence of hydrophilic residues, but the experimentally observed fluorescence maximum suggests a hydrophobic pocket. A likely explanation for the relatively high stability of Trp-102 is the unique amphiphilic nature of the trp residue; substitution of trp for phe in this region reduces the stability of the protein by ~2 kcal/mol. Removal of the soluble domain appears to destabilize the unfolded transmembrane domain of the protein, resulting in the enhanced values for $\Delta G^{\circ}_{H_2O}$ for the truncated proteins. This surprising result highlights the importance of the energetics of the unfolded state in measurements of overall protein conformational stability. DLS results presented here indicate that vesicle diameters increase in the presence of urea. In contrast, the presence of protein does not greatly affect vesicle size. $\Delta G^{\circ}_{H_2O}$ values changed < 15% when vesicles in the size range between 50 and 200 were used. These and other findings may have important implications for future studies of membrane protein folding.

3.6 Continued Studies

After publication of this data, thermodynamic refolding studies were performed on the new mutants Trp-170, Trp-170t, and WTt (wild type truncated) and are discussed in terms of these same non-covalent interactions as previously discussed. In addition to the new mutants, refolding studies were also performed again on the wild type OmpA to obtain more accurate data. The non-native trp residue at position 170 (Trp-170) is located in the membrane domain at the interface between the transmembrane and soluble domains, on a neighboring strand by Trp-7 in the same hydrophobic pocket. The location of Trp-170 in OmpA can be found in Figure 6.4 of this dissertation. The refolding curves for these new mutants are shown in Figure 3.5. The refolding curves for all of the mutants are included for comparison. Tabulated fitting parameters and thermodynamic values for all of the mutants are in Table 3.3.

Trp-170 has the highest calculated thermodynamic stability of all the trp residues, with a value of 10.4 kcal/mol. This value is comparable to that obtained for wild type OmpA, and suggests that the addition of a trp residue at position 170 will increase the stability of the wild type protein. The pairwise aromatic interactions that stabilize Trp-7 also stabilize Trp-170. The region in OmpA, near Trp-7 and Trp-170, has the greatest number of neighboring aromatic residues, Trp7, Tyr8, Tyr43, Tyr168, and Phe170 (~ 7 Å between aromatic centroids). These results support a picture in which a trp at position 170 will anchor this region of protein in the membrane, and therefore will increase its stability. This result also substantiates our claim that the pairwise interactions between aromatic residues does depend on the type of aromatic residue involved. Truncating the Trp-170 mutant (Trp-170t) destabilized the protein by 4 kcal/mol, and resulted in a $\Delta G^{\circ}_{H_2O}$ value of 6.3 kcal/mol.

The new refolding curve for wild type OmpA captured the midpoint in the transition, and gave a new $\Delta G^{\circ}_{H_2O}$ value of 8.7 kcal/mol. Although this is smaller than our previous calculated value of 10.5 kcal/mol, it is still within experimental error. Truncating the wild type protein to produce WTt, stabilized the protein by 2 kcal/mol. The refolding curve of truncated WT (WTt) resulted gave a $\Delta G^{\circ}_{H_2O}$ value of 10.2 kcal/mol. Although this is within our experimental error, it supports our claim that the removal of the soluble domain destabilizes the unfolded transmembrane domain of the protein, and in general, results in the enhanced values for $\Delta G^{\circ}_{H_2O}$ for the truncated proteins.

3.7 Acknowledgement

We thank Tiffany J. Neary for assistance with protein expression, Dustin Huard and Professor Akif Tezcan for help with gel-shift assays, and Professor Doug Magde for use of his DLA apparatus. We thank Beijing Wu for help with protein expression and the refolding curves for the new mutants W170 and W170t, and repeating the refolding curve of Wild-Type OmpA.

Chapter 3, in part, is a reprint of the material as it appears in *Biochemistry* **47**, 12844 (2008). Sanchez, K. M.; Gable, J. E.; Schlamadinger, D. E.; Kim, J. E., American Chemical Society, 2008. The dissertation author was the primary investigator and author of this paper.

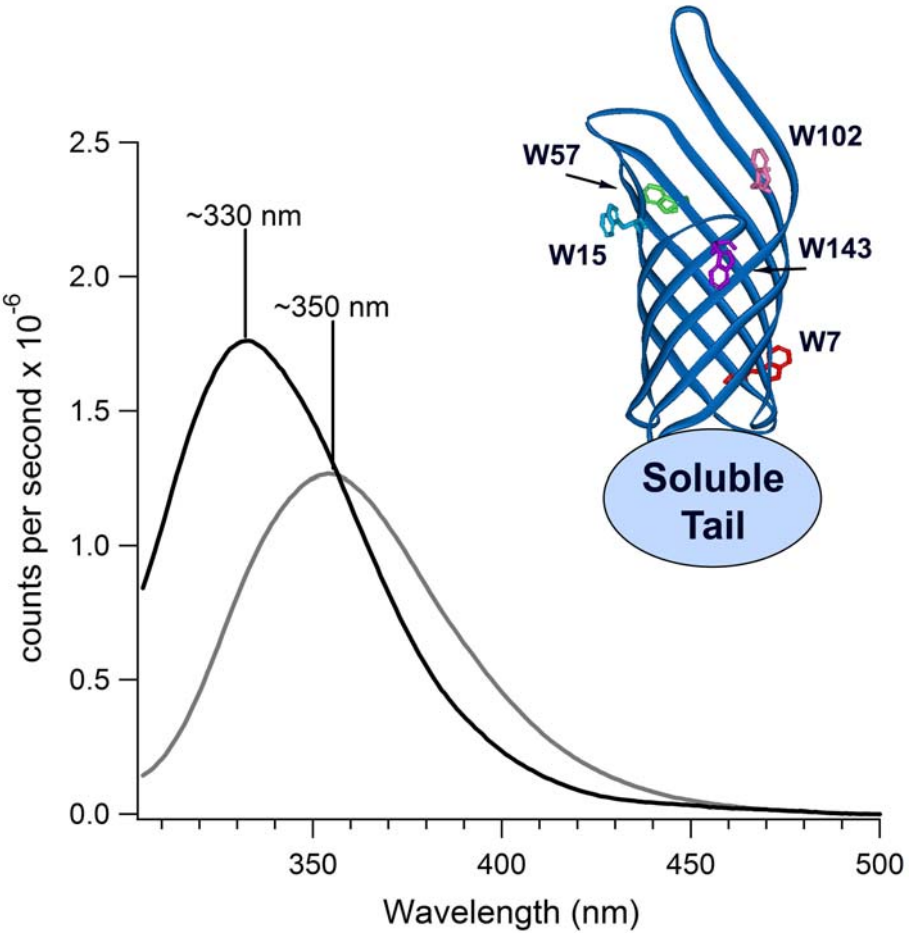

Figure 3.1: Representative tryptophan fluorescence spectra of folded (dark solid curve, λ_{max} ~330 nm) and unfolded protein (light solid curve, λ_{max} ~350 nm). Inset, crystal structure of the transmembrane portion of wild-type OmpA (PDB 1QJP), with a cartoon representation of the soluble periplasmic domain. The five native tryptophan residues, W7, W15, W57, W102, and W143, are highlighted.

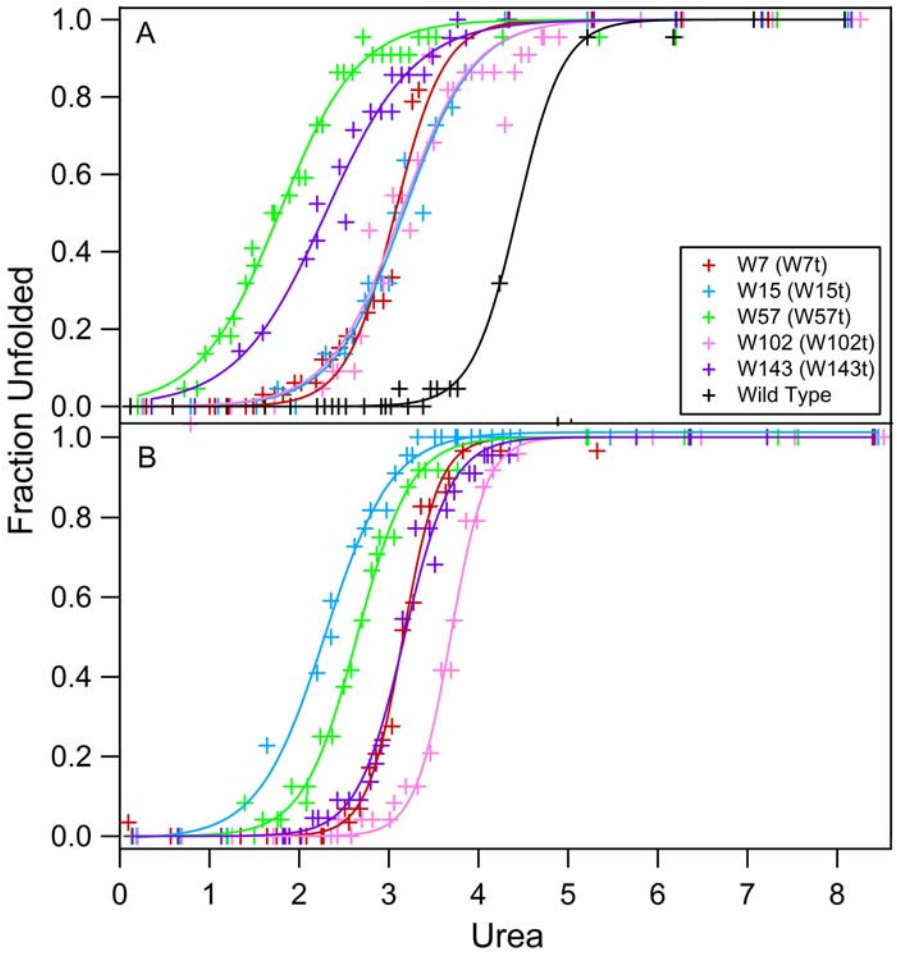

Figure 3.2: Denaturant-induced refolding curves of wild-type and full-length single-trp mutants (A) and single-trp truncated mutants (B) of OmpA along with fits (solid curves).

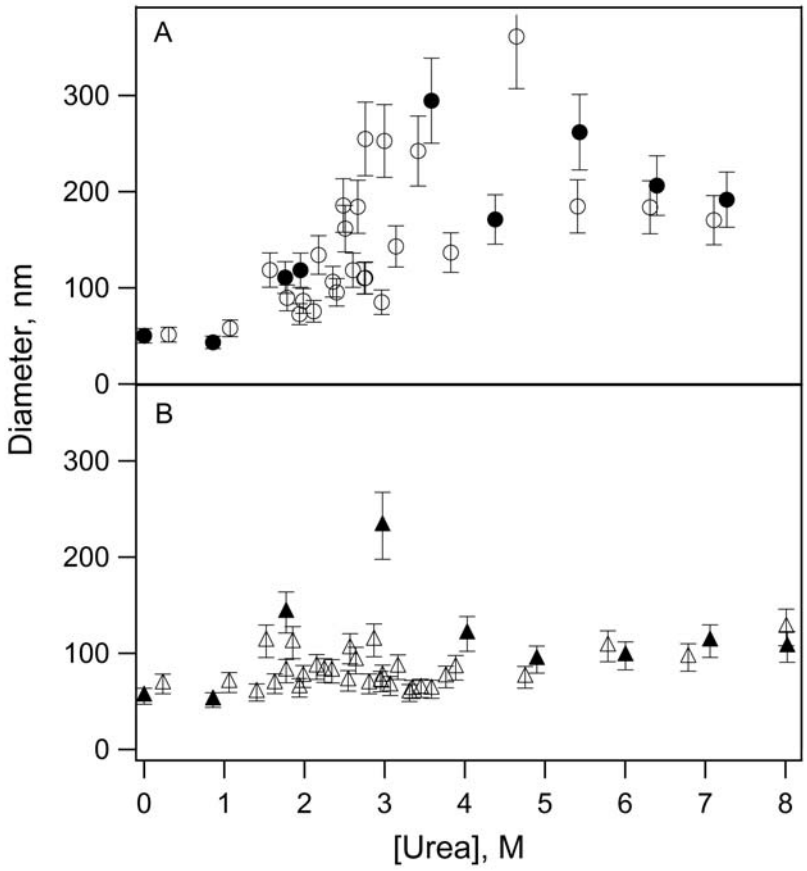

Figure 3.3: Representative vesicle diameters of samples used in refolding curve studies. Open symbols indicate vesicle samples containing 4 μM of protein; solid symbols indicate vesicle samples without protein (blanks).

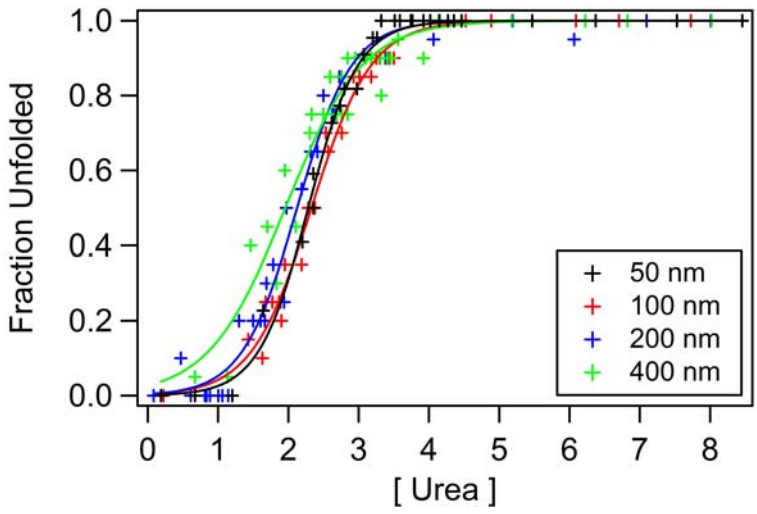

Figure 3.4: Refolding curves of W15t OmpA using nominally 50, 100, 200, and 400 nm diameter vesicles. Fits are solid curves.

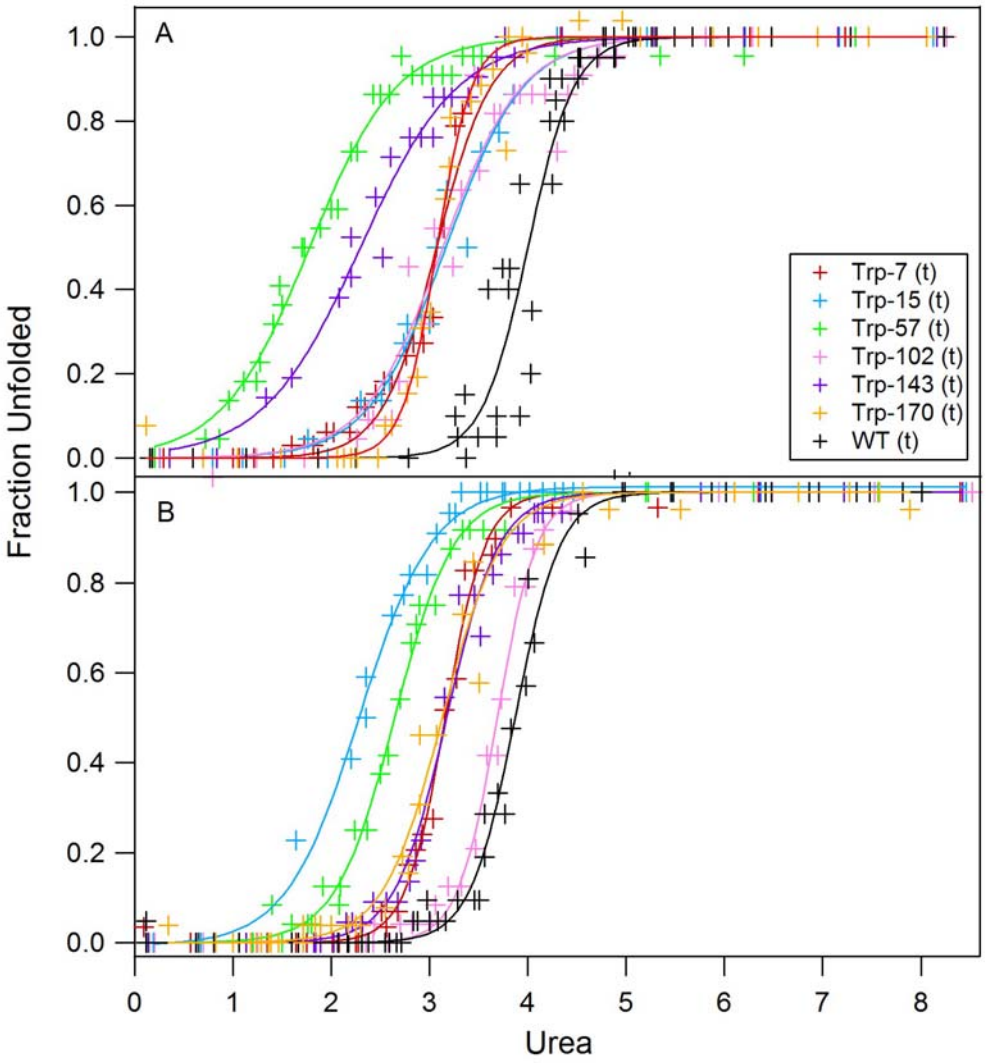

Figure 3.5: Denaturant-induced refolding curves of wild-type and full-length single-trp mutants (A) and single-trp truncated mutants (B) of OmpA along with fits (solid curves), containing refolding curves for the new mutant Trp-170, Trp-170t, and WTt, and a revised refolding curve for WT OmpA.

Table 3.1: Fitting parameters and thermodynamic values determined from refolding curves of wild-type and single-trp OmpA mutants.

	Unfolding Curve Parameters		
	m kcal/mol M^{-1}	C_m M	$\Delta G^{\circ}_{H_2O}$ kcal/mol
W7	2.18	3.07	6.7 +/- 1.0
W7t	2.98	3.16	9.4 +/- 1.4
W15	1.53	3.17	4.8 +/- 0.7
W15t	1.70	2.28	3.9 +/- 0.6
W57	1.36	1.78	2.4 +/- 0.4
W57t	2.01	2.64	5.3 +/- 0.8
W102	1.51	3.13	4.7 +/- 0.7
W102t	3.00	3.69	11.1 +/- 1.7
W143	1.22	2.30	2.8+/- 0.4
W143t	2.28	3.17	7.2 +/- 1.1
WT	2.36	4.43	10.5 +/- 1.6

Table 3.2: Summary of energies ($\Delta G^{\circ}_{H_2O}$ and ΔG°_{part}) and non-covalent interactions for the single-trp mutants of OmpA. $\Delta G^{\circ}_{H_2O}$ values are from current experiments; ΔG°_{part} values are calculated from reference 15; number of aromatic residues is based on a ~7 Å radius centered on the aromatic centroid (PDB 1QJP); number of hydrogen bonds is based on a 3.5 Å radius centered on the indole nitrogen atom.

	Energy (kcal/mol)		Non-Covalent Interactions	
Mutants	$\Delta G^{\circ}_{H_2O}$	ΔG°_{part}	# of Aromatic Residues	# of H-Bonds
W7	6.7	3.2	4	0
W15	4.8	2.0	0	1
W102	4.7	-1.4	0	0
W143	2.8	2.2	2	0
W57	2.4	0.7	1	0

Table 3.3: Revised fitting parameters and thermodynamic values determined from refolding curves of wild-type and single-trp OmpA mutants. Table contains new data collected after publication of this paper.

	Unfolding Curve Parameters		
	m kcal/mol M^{-1}	C_m M	$\Delta G^{\circ}_{H_2O}$ kcal/mol
W7	2.18	3.07	6.7 +/- 1.0
W7t	2.98	3.16	9.4 +/- 1.4
W15	1.53	3.17	4.8 +/- 0.7
W15t	1.70	2.28	3.9 +/- 0.6
W57	1.36	1.78	2.4 +/- 0.4
W57t	2.01	2.64	5.3 +/- 0.8
W102	1.51	3.13	4.7 +/- 0.7
W102t	3.00	3.69	11.1 +/- 1.7
W143	1.22	2.30	2.8+/- 0.4
W143t	2.28	3.17	7.2 +/- 1.1
W170	3.40	3.07	10.4 +/- 0.9
W170t	2.00	3.13	6.3 +/- 0.5
WT	2.28	3.82	8.74 +/- 1.1
WTt	2.64	3.87	10.2 +/- 0.7

Table 3.4: Revised summary of energies ($\Delta G^{\circ}_{H_2O}$ and ΔG°_{part}) and non-covalent interactions for the single-trp mutants of OmpA. $\Delta G^{\circ}_{H_2O}$ values are from current experiments; ΔG°_{part} values are calculated from reference 14; number of aromatic residues is based on a ~7 Å radius centered on the aromatic centroid (PDB 1QJP); number of hydrogen bonds is based on a 3.5 Å radius centered on the indole nitrogen atom. The new mutant, Trp-170, is added for completion.

	Energy (kcal/mol)		Non-Covalent Interactions	
Mutants	$\Delta G^{\circ}_{H_2O}$	ΔG°_{part}	# Aromatic Residues	# of H-bonds
W170	10.4	3.0	4	0
W7	6.7	3.2	4	0
W15	4.8	2.0	0	1
W102	4.7	-1.4	0	0
W143	2.8	2.2	2	0
W57	2.4	0.7	1	0

3.8 References

(1) Sanders, C. R.; Myers, J. K. *Annu. Rev. Biophys. Biomol. Struct.* **2004**, *33*, 25.

(2) Aridor, M.; Balch, W. E. *Nature Medic.* **1999**, *5*, 745.

(3) Im, W.; Brooks, C. L. *J. Mol. Biol.* **2004**, *337*, 513.

(4) Bond, P. J.; Cutherbertson, J. M.; Deol, S. S.; Sansom, M. S. P. *J. Am. Chem. Soc.* **2004**, *126*, 15948.

(5) Booth, P. J.; Templer, R. H.; Meijberg, W.; Allen, S. J.; Curran, A. R.; Lorch, M. *Crit. Rev. in Biochem. and Mol. Biol.* **2001**, *36*, 501.

(6) White, S. H.; Wimley, W. C. *Annu. Rev. Biophys. Biomol. Struct.* **1999**, *28*, 319.

(7) MacKenzie, K. R. *Chem. Rev.* **2006**, *106*, 1931.

(8) Tamm, L. K.; Hong, H.; Liang, B. *Biochim. Biophys. Acta* **2004**, *1666*, 250.

(9) Lee, A. G. *Biochim. Biophys. Acta* **2003**, *1612*, 1.

(10) White, S. H. *Adv. Protein Chem.* **2006**, *72*, 157.

(11) Weiss, M. S.; Brandl, M.; Suhnel, J.; Pal, D.; Hilgenfeld, R. *Trends Biochem. Sci.* **2001**, *26*, 521.

(12) Steiner, T.; Koellner, G. *J. Mol. Biol.* **2001**, *305*, 535.

(13) Wimley, W. C.; White, S. H. *Nat. Struct. Biol.* **1996**, *3*, 842.

(14) Wimley, W. C.; Creamer, T. P.; White, S. H. *Biochemistry* **1996**, *35*, 5109.

(15) Burley, S. K.; Petsko, G. A. *FEBS Lett.* **1986**, *203*, 139.

(16) Burley, S. K.; Petsko, G. A. *Science* **1985**, *229*, 23.

(17) Domene, C.; Bond, P. J.; Deol, S. S.; Sansom, M. S. P. *J. Am. Chem. Soc.* **2003**, *125*, 14966.

(18) Babakhani, A.; Gorfe, A. A.; Gullingsrud, J.; Kim, J. E.; McCammon, J. A. *Biopolymers* **2007**, *85*, 490.

(19) Yau, W.-M.; Wimley, W. C.; Gawrisch, K.; White, S. H. *Biochemistry* **1998**, *37*, 14713.

(20) Reithmeier, R. A. F. *Curr. Opin. Struct. Biol.* **1995**, *5*, 491.

(21) Killian, J. A.; von Heijne, G. *Trends Biochem. Sci.* **2000**, *25*, 429.

(22) Sugawara, E.; Nikaido, H. *J. Mol. Biol.* **1992**, *267*, 2507.

(23) Wang, Y. *Biochem. Biophys. Res. Comm.* **2002**, *292*, 396.

(24) Koebnik, R.; Locher, K. P.; Van Gelder, P. *Molec. Microbiol.* **2000**, *37*, 239.

(25) Surrey, T.; Jahnig, F. *Proc. Natl. Acad. Sci. U.S.A.* **1992**, *89*, 7457.

(26) Kleinschmidt, J. H.; den Blaauwen, T.; Driessen, A. J. M.; Tamm, L. K. *Biochemistry* **1999**, *38*, 5006.

(27) Dornmair, K.; Kiefer, H.; Jahnig, F. *J. Biol. Chem.* **1990**, *265*, 18907.

(28) Kim, J. E.; Arjara, G.; Richards, J. H.; Gray, H. B.; Winkler, J. R. *J. Phys. Chem. B* **2006**, *110*, 17656.

(29) Hong, H.; Tamm, L. K. *Proc. Natl. Acad. Sci. U.S.A.* **2004**, *101*, 4065.

(30) Ramakrishnan, M.; Qu, J.; Pocanschi, C. L.; Kleinschmidt, J. H.; Marsh, D. *Biochemistry* **2005**, *44*, 3515.

(31) Sanchez, K. M.; Neary, T. J.; Kim, J. E. *J. Phys. Chem. B* **2008**, *112*, 9507.

(32) Pocanschi, C. L.; Patel, G. J.; Marsh, D.; Kleinschmidt, J. H. *Biophys. J.* **2006**, *91*, L75.

(33) Arora, A.; Rinehart, D.; Szabo, G.; Tamm, L. K. *J. Biol. Chem.* **2000**, *275*, 1594.

(34) Zakharian, E.; Reusch, R. N. *Biochemistry* **2005**, *44*, 6701.

(35) Hong, H.; Park, S.; Flores Jimenez, R. H.; Rinehart, D.; Tamm, L. K. *J. Am. Chem. Soc.* **2007**, *129*, 8320.

(36) Hope, M. J.; Bally, M. B.; Webb, G.; Cullis, P. R. *Biochim. Biophys. Acta* **1985**, *812*, 55.

(37) Shirley, B. A. *Urea and Guanidine Hydrochloride Denaturation Curves*; Humana Press Inc.: Totowa, NJ, 1995; Vol. 40.

(38) Schellman, J. A. *Biopolymers* **1978**, *17*, 1305.

(39) Pace, N. C. *Methods Enzymol.* **1986**, *131*, 266.

(40) Toal, S. J.; Jones, K. A.; Magde, D.; Trogler, W. C. *J. Am. Chem. Soc.* **2005**, *127*, 11661.

(41) Berne, B. J.; Pecora, R. *Dynamic Light Scattering*; John Wiley and Sons: New York, 1976.

(42) Kawahara, K.; Tanford, C. *J. Biol. Chem.* **1966**, *241*, 3228.

(43) Ben-Tal, N.; BenShaul, A.; Honig, B. *Biophys. J.* **1996**, *70*, 1803.

(44) Scheiner, S.; Kar, T.; Pattanayak, J. *J. Am. Chem. Soc.* **2002**, *124*, 13257.

(45) Brandl, M.; Weiss, M. S.; Jabs, A.; Suhnel, J.; Hilgenfeld, R. *J. Mol. Biol.* **2001**, *307*, 357.

(46) Serrano, L.; Bycroft, M.; Fersht, A. R. *J. Mol. Biol.* **1991**, *218*, 465.

(47) Wrabl, J.; Shortle, D. *Nat. Struct. Biol.* **1999**, *6*, 876.

(48) Oikawa, K.; Lieberman, D. M.; Reithmeier, R. A. F. *Biochemistry* **1985**, *24*, 2843.

(49) Lau, F. W.; Bowie, J. U. *Biochem.* **1997**, *36*, 5884.

(50) Shortle, D. *FASEB Journal* **1996**, *10*, 27.

(51) Arai, M.; Kataoka, M.; Kuwajima, K.; Matthews, C. R.; Iwakura, M. *J. Mol. Biol.* **2003**, *329*, 779.

(52) Mok, Y.-K.; Elisseeva, E. L.; Davidson, A. R.; Forman-Kay, J. D. *J. Mol. Biol.* **2001**, *307*, 913.

(53) Curran, A. R.; Templer, R. H.; Booth, P. J. *Biochemistry* **1999**, *38*, 9328.

(54) Kleinschmidt, J. H.; Tamm, L. K. *J. Mol. Biol.* **2002**, *324*, 319.

(55) Finkelstein, A. *Journal of General Physiology* **1976**, *68*, 127.

(56) Pencer, J.; White, G. F.; Hallett, F. R. *Biophys. J.* **2001**, *81*, 2716.

(57) Kleinschmidt, J. H.; Tamm, L. K. *Biophys. J.* **2002**, *83*, 994.

(58) Feng, Y.; Quinn, P. J. *Chem. Phys. Lipids* **2002**, *114*, 149.

(59) Dini, L.; Di Giulio, A.; Pavan, A.; Ravagnan, G.; Mossa, G. *Biochim. Biophys. Acta* **1991**, *1062*, 108.

Chapter 4

UVRR excitation wavelength dependence: Selective enhancement of trp vibrational modes in OmpA

4.1 Introduction

The advent of lasers and commercially available Raman instrumentation in the late 1980s revolutionized the field of Raman spectroscopy.[1] With the use of resonance Raman (RR) spectroscopy, detailed structural and dynamic information can be obtained.[2-4] Theoretical and experimental studies using this technique have provided a wealth of information on vibrational modes of molecules.[2,5-10] In resonance Raman spectroscopy, the laser wavelength approaches an absorption band of a molecule of interest resulting in a large enhancement of the vibrational modes coupled to that electronic transition.[2] Resonance enhancement allows dilute samples as low as ~10^{-6} mol/L to be studied, and this ability is a highly desirable for sample limited systems like membrane proteins. Changing the wavelength of excitation can selectively enhances vibrations of different chromophores, and allows for systematic studies of a variety of small molecules in a macromolecule system.[11,12]

Resonance Raman experiments were hindered in the past by limitations of the excitation source. Continuous wave (CW) laser wavelengths typically have fundamental wavelengths in the visible region, thereby limiting resonance Raman studies to molecules with electronic transitions in this wavelength range. Many biological systems have visible absorption bands, such as heme and retinal groups, making Raman studies very

applicable for these systems.[13-15] The advent of pulsed lasers or high-powered CW lasers resulted in frequencies that were shifted using non-linear optics to second, third, and/or fourth harmonic wavelengths and enabled resonance Raman spectroscopy to be applied to biological systems with electronic transitions in the UV region.[11,16,17]

UV resonance Raman (UVRR) spectroscopy can selectively enhance signal from vibrational modes of protein backbone or aromatic amino acids depending on the wavelength of excitation: 193 – 210 nm for backbone enhancement and 225 – 240 nm for aromatic residues. Information on electronic excited states and symmetry of molecular vibrations can be obtained from enhancement patterns.[1,7,18,19] The extent of resonance enhancement is closely related to changes in ground and excite state structure.[20] The observed enhancement patterns can be obtained systematically changing the excitation wavelength and monitoring peak height for a set of modes. This analysis gives rise to Raman cross sections, σ, as a function of excitation wavelength, also known as a Raman excitation profile (REP).[20-23]

In the following experiments, Reps were determined for OmpA and model compounds. Raman cross sections were calculated for aqueous solutions of phenylalanine, tyrosine, and tryptophan.[20,21,23] Raman cross sections were also determined for tyrosine and tryptophan residues in OmpA and compared to the cross sections of the model compounds free in solution. It is likely that the excitation wavelength for aqueous solutions of aromatic residues will be different for aromatic residues in proteins due to local environment effects. Aromatic residues are located in complex microenvironments in proteins, and these environmental effects have been shown to influence Raman cross sections.[24]

The excitation wavelength range was 206.5 nm – 236.5 nm. The calculated Raman cross sections were plotted for trp and tyr modes. Trp-less mutant was studied to determine the optimal excitation wavelength for tyrosine residues in OmpA; Trp-57 mutant, with a single trp residue at position 57, was used to determine the optimal excitation wavelength for tryptophan residues in OmpA. To determine additional local environment effects, the excitation wavelength dependence was also performed on protein unfolded in aqueous buffer and protein folded in DMPC vesicles. The wavelength with the greatest enhancement of trp modes in OmpA was determined from these Raman excitation profiles

4.2 Materials & Methods

4.2.1. Preparation of OmpA mutants

The expression, isolation, and purification of Trp-57 and Trp-less OmpA mutants is described in detail in Appendix A.[25-27]

4.2.2. Unfolded and Folded Protein

Unfolded protein samples were made by dilution of stock unfolded protein into 20 mM KP_i buffer, pH 7.3. Spectroscopic measurements were made within 10 minutes after sample preparation to prevent aggregation of unfolded protein. Protein folded in SUVs was made by dilution of stock unfolded protein into 1 mg/mL ~50-nm diameter DMPC vesicles in 20 mM KP_i buffer, pH 7.3. Vesicle solutions containing protein were incubated at 37 ºC for ~ 4 hrs before spectroscopic measurements to ensure equilibrium conditions.

Protein concentrations were then calculated using ε_{280} values of 32 300 $M^{-1}cm^{-1}$ and 26 700 $M^{-1}cm^{-1}$ for Trp-57 and Trp-less mutants of OmpA, respectively.

Fluorescence spectra were also collected of all protein and blank solutions to verify folded or unfolded protein. Trp emission in a hydrophobic environment was ~333 nm for Trp-57 folded in DMPC vesicles; trp emission in a hydrophilic environment was ~355 nm for Trp-57 unfolded in KP_i buffer. Fluorescence and absorption spectra were measured before and after photolysis to determine sample degradation.

4.2.3. UVRR Spectroscopy

Excitation-wavelength dependence of trp and tyr residues in OmpA was performed using a tunable Titanium:sapphire laser (Photonics Industries). Details of the laser system can be found in Chapter 2. The Ti:Sapph laser was tuned to produce ~ 1 Watt of fundamental wavelengths ranging between 826 – 946 nm. The 206.5 – 236.5 nm UV beam has a spot size of ~230μm x ~75μm at the sample. The UV power was measured before the sample capillary and collection optics, and ranged from ~1 – 6 mW of power. The prefilter was manually adjusted to accommodate the UV excitation wavelengths to allow for acquisition of UVRR spectra to within 200 cm^{-1} of the Rayleigh line.[28] Fundamental IR wavelengths, UV wavelengths, prefilter slit, and intermediate (spectrograph) slit are tabulated in Table 4.1. A power dependence experiment ensured the Raman scattering was collected in the linear regime.

Samples were pumped through a vertically-mounted, 100μm i.d. quartz microcapillary, using a flow rate 0.16 mL/min to ensure fresh sample for each laser pulse, and discarded after a single-pass through the laser to eliminate artifacts from photolyzed protein. Collection times varied from 10 – 15 minutes depending on excitation wavelength, with longer collection times at the shorter wavelengths. UVRR spectra were collected of Trp-57 and Trp-less mutants folded in SUV, and unfolded in KP_i buffer. In

addition, UVRR spectra of buffer solutions, with and without 1 M urea, were also acquired and subtracted from the corresponding OmpA spectra.

4.2.4. Data analysis and calculation of Raman cross sections

Data were analyzed using Igor Pro (WaveMetrics) software. 50 mM sodium perchlorate was added to solutions of phe, tyr, and trp to be used as the internal standard for calculating Raman cross sections. Perchlorate could not be added to solutions containing OmpA because the effect of perchlorate on the protein is not known; in addition, the perchlorate peak could not be observed in OmpA spectra due to overlap with a strong urea mode at ~1000 cm^{-1}.

To calculate Raman cross section in OmpA, the average intensity of perchlorate peak at ~ 932 cm^{-1} was determined from other protein solutions collected on the same day. Specifically, perchlorate was added to solutions of cytochrome *c* and azurin; azurin was studied by another graduate student in the group. The absolute resonance Raman cross section for perchlorate was determined by correcting the raw data for detector response (using a deuterium lamp spectrum at each wavelength), pre-resonance enhancement, and self-absorption.[29] Another graduate student in the group performed the self-absorption corrections. Raman cross sections for the sample (σ_N) were calculated using the following relationship [21]:

$$\sigma_N = \sigma_S * \frac{I_N}{I_S}\left[\frac{(\nu_0 - \nu_S)}{(\nu_0 - \nu_N)}\right]^4 \frac{C_S}{C_N} \qquad (1)$$

where σ_S is the corrected Raman cross section of the internal standard; I_N and I_S are the peak height intensities of the vibrational bands of the sample (N) and the internal

standard (S), respectively; CS/C_N is the ratio of concentrations of the internal standard to the sample; ν_0 is the frequency of the incident radiation; ν_N and ν_S are the vibrational frequencies of the sample and the perchlorate standard Raman bands.

4.3. Results

The absorption spectra of the nominally 50 μM aqueous model compounds tryptophan, tyrosine, and phenylalanine in KP_i buffer are shown in Figure 4.1. By systematically changing the Raman excitation wavelength from 206.5 nm – 236.5 nm, we were able to monitor differences in vibrational mode intensities coupled to the main absorption bands in aromatic amino acids. The three main absorption bands consist of the $B_{a,b}$ band, and the two low-energy L_a, and L_b bands.[30] These absorption bands occur at different wavelengths for the three aromatic amino acids. For tryptophan specifically, the $B_{a,b}$ electronic transition occurs at ~220 nm, while the L_a, L_b electronic transitions are ~270nm, and ~280 nm, respectively.

4.3.1. Excitation Wavelength Dependence

4.3.1.1. Phenylalanine, Tyrosine, and Tryptophan

Figure 4.2 shows the UVRR spectra of phenylalanine (phe) vibrational modes with excitation wavelengths of 206.5 nm – 236.5 nm. Tabulated mode frequencies for phenylalanine are found in Table 4.2. The large feature at ~932 cm^{-1} is due to the internal standard, perchlorate. There are four main peaks that appear in the Raman spectra of phe, with frequencies of ~1000 cm^{-1}, ~1182 cm^{-1}, ~1586 cm^{-1}, and ~1606 cm^{-1}, arising from the F12, F9a, F8b, and F8a modes, respectively. Another peak at ~1207 cm^{-1} is apparent in the UVRR spectra at 220 nm; this peak has not been identified. At 236.5 nm excitation, no phe modes are enhanced.

Figure 4.3 shows the UVRR spectra of tyrosine (tyr) vibrational modes at excitation wavelengths from 206.5 nm – 236.5 nm. Tabulated mode frequencies for tyrosine are found in Table 4.2. The vibrational modes that contribute to the UVRR spectra of tyr are 2Y16a, Y1, Y9a, Y7a, Y8b, and Y8a, with frequencies of ~832 cm^{-1}, ~853 cm^{-1}, ~1180 cm^{-1}, ~1210 cm^{-1}, ~1601 cm^{-1}, and ~1617 cm^{-1}, respectively. The modes show different enhancement at the various wavelengths.

Figure 4.4 shows the UVRR spectra of tryptophan (trp) vibrational modes at different excitation wavelengths, from 206.5 nm – 236.5 nm. Tabulated mode frequencies for tryptophan are found in Table 4.2. The most noticeable vibrational modes of trp are the W18, W17, W16, W10, W7, W3, and W1 modes, with frequencies of ~762 cm^{-1}, ~880 cm^{-1}, ~1016 cm^{-1}, 1238 cm^{-1}, ~1361 cm^{-1}, ~1555 cm^{-1}, and ~1622 cm^{-1}, respectively. All modes are apparent in the UVRR spectrum collected at 206.5 nm excitation, but with significantly low signal. All of the trp modes have the highest intensities using 220 nm excitation.

4.3.1.2. Trp-less OmpA

The REP was determined for the Trp-less mutant to determine the optimum excitation wavelength for resonance enhancement of the tyrosine residues in OmpA. Figure 4.5 shows the UVRR spectra of Trp-less OmpA folded in DMPC vesicles at excitation wavelengths ranging from 206.5 – 236.5 nm. The Trp-less mutant contains 17 native tyr residues and 13 phenylalanine residues that contribute to the Raman spectrum of the Trp-less OmpA mutant. Varying contributions from signal from tyrosine, phenylalanine, or protein backbone vibrations are observed in the spectra at the different excitation wavelengths.

The dominant amide mode vibrations are the amide I, amide II, and amide III modes, with frequencies of ~1650 cm^{-1}, ~1560 cm^{-1}, and ~1250 cm^{-1}, respectively. The amide III mode at ~1250 cm^{-1} starts to appear in the UVRR spectrum at 215 nm excitation, and has the highest intensity at 206.5 nm excitation. The amide III intensity increases by a factor of 3, when the excitation wavelength changes from 210 nm to 206.5 nm. The amide I and amide II modes are observed in the spectra collected at 210 nm and 206.5 nm excitation. All three amide modes dominate the spectrum at 206.5 nm excitation, with minimal contribution from tyr or phe modes. The overlapping Y9a and/or F9a modes, both at ~1180 cm^{-1}, are still observed in the UVRR spectra at 206.5 nm excitation.

The UVRR spectra of Trp-less OmpA unfolded in KP_i buffer were also collected at different excitation wavelengths. UVRR wavelength dependent spectra of unfolded Trp-less is shown in Figure 4.6. Similar mode enhancements were found for tyr residues in unfolded protein, with largest intensities at 233 nm excitation. Amide backbone modes dominated spectrum at 206.5 nm excitation, with minimal contribution from tyr or phe modes, except for the Y9a/F9a modes.

4.3.1.3. Trp-57 OmpA

The excitation wavelength dependence was determined for the Trp-57 mutant to determine the optimum excitation wavelength for resonance enhancement of the tryptophan residues in OmpA. UVRR spectra were collected of the single-trp mutant Trp-57 folded in DMPC vesicles at excitation wavelengths ranging from 206.5 nm – 236.5 nm, and are shown in Figure 4.7. Trp-57 has 1 trp residue, 17 tyrosine residues, and 12 phenylalanine residues that contribute to the Raman spectra. Different

contributions from signal of tryptophan, tyrosine, phenylalanine, or protein backbone vibrations are observed at the different excitation wavelengths. The trp and tyr modes dominate the spectra with excitation wavelengths of 228, 230, 233, 236.5 nm, with no contribution from amide mode vibrations. The W18, W17, W7, and W3 modes are observed in the spectra with excitation wavelengths of 215 – 233 nm. There is no contribution from trp modes observed in the UVRR spectrum at 236.5 nm excitation, or at wavelengths shorter than 210 nm. The 2Y16a, Y1, Y9a, Y7a, Y8b, and Y8a modes are also apparent in the Raman spectra with excitation wavelengths of 215 nm or greater.

The three amide mode vibrations, amide I, amide II, and amide III, are found at ~1650 cm^{-1}, ~1560 cm^{-1}, and ~1250 cm^{-1}, respectively. Similar to the Trp-less mutant, the amide mode vibrations are clearly observable in the Raman spectra at 215 nm excitation, and are enhanced by a factor of 2 when the excitation wavelength is changed from 215 to 206.5 nm. The amide I, amide II, and amide III modes dominate the Raman spectrum at 206.5 nm excitation, with minimal contribution from the aromatic residue modes, except for the Y9a/F9a modes at ~1180 cm^{-1}.

The excitation wavelength dependence was also determined for Trp-57 unfolded in KP_i buffer. UVRR spectra were collected of Trp-57 unfolded in KP_i from 206.5 – 236.5 nm and is shown in Figure 4.8. Similar enhancement of trp, tyr, and amide mode vibrations were observed for unfolded Trp-57.

4.3.2. Raman Excitation Profiles (REPs)

The wavelength dependent UVRR spectra of phe, tyr, and trp in Figure 4.2, Figure 4.3, and Figure 4.4, respectively, were scaled to the intensity of the internal standard, perchlorate, at ~932 cm^{-1}. The scaled intensities of the Raman modes were

converted into Raman cross sections, using Equation 1. The calculated Raman cross sections were plotted versus wavelength to obtain Raman excitation profiles (REPs) for the phe, tyr, and trp modes in aqueous solutions and in the protein OmpA. All Y-axes for the Raman excitation profiles are scaled to the same range for easy comparison among the aromatic residues in aqueous solutions or in the protein.

4.3.2.1. Phe, Tyr, Trp REPs

The Raman cross sections were calculated for aqueous phenylalanine modes F12, F9a, F8b, and F8a. The Raman excitation profile for the phe modes are shown in Figure 4.9. The cross sections for all four phe modes do not change significantly, and remain small ($2 – 3 \times 10^{-28}$ cm^2/molecule sr) with excitation wavelengths between 225 nm – 236.5 nm. The cross sections increase to $3 – 8 \times 10^{-26}$ cm^2/molecule sr, with shorter excitation wavelengths, with the largest values found between 210 nm – 220 nm, depending on the mode. The F8a mode has the largest cross section of all four modes at these shorter wavelengths, while the F12 mode has the largest cross sections at excitation wavelengths ≥225 nm.

Raman cross sections were calculated for the aqueous tyrosine modes 2Y16a, Y1, Y9a, Y7a, Y8b, and Y8a. The Raman excitation profile for these modes is shown in Figure 4.10. There is a large variation in the Raman cross sections for the different tyr modes at the various wavelengths, with values ranging from $1 \times 10^{-25} – 3 \times 10^{-26}$ cm^2/molecule sr, at 206.5 nm and 236.5 nm, respectively. The values remain relatively small for all modes at all excitation wavelengths. The Y7a mode overall generally has the smallest Raman cross sections compared to the other tyr modes and remains relatively unchanged regardless of wavelength ($2 – 5 \times 10^{-26}$ cm^2/molecule sr).

The Raman cross sections were also calculated for aqueous tryptophan modes W18, W17, W16, W10, W7, W3, and W1 at the different excitation wavelengths. The Raman excitation profiles for trp modes are shown in Figure 4.11. The cross sections for the trp modes are much larger compared to those calculated for phe and tyr, with the highest values an order of magnitude larger than the highest values determined for tyr or phe modes. The largest trp mode cross sections are 1 x 10^{-24} cm^2/molecule sr, compared to values of 10^{-25} – 10^{-26} cm^2/molecule sr, for tyr and phe modes, respectively. The cross sections of all trp modes are small at 206.5 nm and 236.5 nm, and are the largest at 220 nm. In fact, all of the trp modes have the largest cross section at this wavelength. Our results are consistent with previous studies on Raman cross section determination.[20-22]

4.3.2.2. Trp-less OmpA REPs

Raman cross sections were determined for select tyr modes in Trp-less OmpA. The Raman excitation profiles for tyr modes in unfolded (open symbols) and folded (solid symbols) protein are shown in Figure 4.12. The intensities of the modes from the excitation wavelength dependence in Figure 4.5 and Figure 4.6 were used to calculate Raman cross sections. Cross sections were only calculated for the 2Y16a, Y1, Y9a, and Y8a modes because overlap with phe or backbone modes prevented analysis of the Y8b and Y7a modes. Raman cross sections for tyr residues in OmpA on average are similar in magnitude or ≤ one order of magnitude smaller than those determined for aqueous tyr. Typical Raman cross sections for tyr modes in OmpA are 1 – 0.5 x10^{-25} cm^2/molecule sr. The 2Y16a and Y1 modes have the lowest cross sections with values of 1 – 0.3 x 10^{-26} cm^2/molecule sr. The largest cross sections for tyr in the protein are found at 233 nm excitation. All four tyr modes have the largest cross sections at this wavelength. Raman

cross sections were calculated for unfolded protein. In general, the cross sections calculated for folded protein are larger than those calculated for unfolded protein. On average, the cross sections are ~3 – 10% larger in folded protein than in unfolded protein.

4.3.2.3. Trp-57 OmpA EPs

Raman cross sections were determined for select trp modes in the single-trp OmpA mutant, Trp-57. The intensities of the modes from the excitation wavelength dependence in Figure 4.7 and Figure 4.8 were used to calculate Raman cross sections. The Raman excitation profiles of trp modes in unfolded protein (open symbols) and folded protein (solid symbols) are shown in Figure 4.13. Due to spectral overlap with tyr, backbone, or urea modes, only the W18, W17, and W7 Raman cross sections could unambiguously be determined.

The W18 mode has the largest cross sections of all the modes for wavelengths between 215 nm – 236.5 nm, with values of 1 – 5 x 10^{-25} cm^2/molecule sr. The W7 mode has the lowest cross sections of all the modes, with values of 2 x 10^{-26} – 2 x 10^{-25} cm^2/molecule sr. Raman cross sections were calculated for trp modes unfolded in buffer, and folded in vesicle. Cross sections for W18 mode are ~10 – 40% larger in the folded protein wavelengths longer then 225 nm; W18 cross sections are ~10 % smaller in the folded protein at wavelengths < 225 nm. The W7 mode cross sections are also larger in the folded protein than unfolded protein, by ~5% on average. The W17 mode cross sections follow a different trend, and are smaller in the folded protein than unfolded protein, 1 – 10%.

4.4 Discussion

4.4.1 Aqueous Aromatic Amino Acids

A detailed analysis of Raman cross sections for aqueous solutions of phe, tyr, and trp have been done by a variety of groups, and will not be presented in great detail here. Different enhancement patterns are seen for tryptophan, tyrosine, and phenylalanine modes at different excitation wavelengths. These enhancement patterns result from coupling to different electronic states.[21,31] Despite the differences in enhancement patterns for the vibrational modes in the aromatic residues, the largest cross sections, strongest enhancement, for phenylalanine, tyrosine, and tryptophan in our wavelength range occurs at 220 nm excitation, consistent with previous studies.[20,21]

The largest cross sections for phe and tyr are found at excitation wavelengths below 200 nm, with strong enhancement from resonance with the $B_{a,b}$ absorption band (~190 nm). We were not able to achieve excitation wavelengths below 206.5 nm due to experimental limitations. Phe and Tyr modes in our experiments show strong enhancement at excitation wavelengths ~ 220 nm, consistent resonance with the L_a state, and enhancement from L_a - $B_{a,b}$ mixing. The trp vibrational modes show strong enhancement at 220 nm due to resonance with the B_b absorption band. Enhancement of modes due to the L_a band occurs with excitation close to ~270 nm.[21]

4.4.2. Aromatic Amino Acids in folded and unfolded OmpA

Excitation wavelength dependence was also used to determine Raman cross sections of select tyr and trp modes in the membrane protein OmpA with wavelengths ranging from 206.5 nm – 236.5 nm. Excitation with wavelengths of 225 nm – 235 nm selectively enhances vibrational modes coupled to the B_b, and $L_{a,b}$ electronic transitions.[11,21,23] The largest enhancement of trp and tyr modes in the protein occurred at excitation wavelengths of 228 nm, and 233 nm, respectively. This is significantly

different than the aqueous solutions of trp and tyr which have the largest mode enhancement at 220 nm.

Interpretation of the Raman excitation profiles for aromatic residues is more complex in the protein than for aqueous solutions, due to environmental effects of remaining amino acid side-chains in the protein and influence of the protein backbone.[24,32] Raman cross sections are sensitive to changes in the absorption spectrum. Since Raman bands gain intensity through resonance with an absorption band, shifts in the absorption bands due to environment will cause intensity changes of the Raman bands. For example, excitation at 228 nm is on the red side of the Raman excitation profile determined in Figure 4.11. If the B_b absorption band at ~220 nm red-shifts in the protein due to environmental effects, the Raman excitation profile will also red-shift, and cause greater enhancement of these modes with 228 nm excitation.

Our results show the environmental sensitivity of the tyr and trp cross sections due to effects of protein. Tyr Raman cross sections determined for Trp-less OmpA are comparable in magnitude to those determined for aqueous solutions. However, the tyr residues in OmpA are selectively enhanced at 233 nm excitation, and have the largest cross sections at this wavelength. Tyr modes in aqueous solutions show strong enhancement 220 nm excitation. The Raman cross sections for the trp modes in the protein are comparable to the cross sections of aqueous trp at shorter wavelengths (206.5 nm – 215 nm) and at longer wavelengths (228 nm – 236.5 nm). A large discrepancy exists between the cross sections of trp in the protein and aqueous trp is in the region of 220 – 225 nm, seen in Figures 4.11 and 4.13. Trp cross sections in the protein are significantly lower at these wavelengths compared to cross sections for aqueous trp

residues. These differences may result from large experimental error in calculating Raman cross sections, or result from environmental effects from protein residues and backbone. The largest Raman cross section for the W18 mode occurs at 228 nm excitation; the largest cross sections for the W17 and W7 modes occur at 215 nm excitation. Although the W7 mode appears to have significantly larger cross section at shorter wavelengths, it could result from spectral overlap with amide vibrations in the region that cause additional intensity in this region.

To determine any difference on Raman cross sections with hydrophobicity, Raman cross sections were calculated for protein unfolded in aqueous buffer (hydrophilic environment), and compared to cross sections for protein folded in synthetic lipid bilayer (hydrophobic environment). The W18 mode and W7 mode cross sections at longer excitation wavelengths (225 – 233 nm) are larger in a hydrophobic environment, and smaller in an aqueous environment. Some of the tyr modes also have larger cross sections in a hydrophobic environment (folded protein) compared to an aqueous environment. This difference in cross sections for tyr and trp residues in the protein is likely attributed to the influence of protein, and solvent (water) accessibility, both of which influence the absorption spectra of the molecule, and hence affect the Raman cross sections.

Amide vibrations of the protein backbone are selectively enhanced at 206.5 nm excitation. This is clearly observed in the Trp-57 OmpA UVRR spectra in Figure 4.14. Amide vibrations from protein backbone clearly dominate spectra at 206.5 nm excitation, while tyr and trp modes clearly dominate the spectra at 228 nm excitation. Excitation in the deep UV region, 206.5 nm significantly enhances amide vibrations of the protein

backbone. Strong enhancement of the amide modes are observed with excitation wavelengths approaching the amide $\pi \rightarrow \pi^*$ absorption band at ~195 nm. These amide modes are sensitive reporters of protein chain conformation and can be used to determine protein secondary structure. Deep UVRR excitation of soluble proteins has led basis spectra of secondary structure components of protein backbone, which can be used to analyze secondary structure information in proteins with no known crystal structure.[33,34] Future UVRR studies of full-length and truncated OmpA (which lacks the soluble domain of the protein) at 206.5 nm excitation (or lower) could shed light on changes and/or differences in secondary structure formation during insertion into synthetic lipid bilayers. Differences in UVRR spectra of full-length and truncated OmpA could help identify any secondary structure of the soluble tail.

4.5 Conclusions

We have presented the first UVRR excitation wavelength dependence of trp and tyr residues in the membrane protein OmpA, on the single-trp containing mutant, Trp-57, and the Trp-less mutant. Raman cross sections were calculated for select trp and tyr modes in the protein to determine the excitation wavelength with the greatest enhancement of trp modes in the protein. For comparison, the excitation wavelength dependence was also done on aqueous solutions of phe, tyr, and trp to determine the wavelength with the greatest enhancement of these modes in aqueous solutions. UVRR spectra were collected excitation wavelengths of 206.5 nm – 236.5 nm, and Raman excitation profiles were determined.

The aqueous solutions of phe, tyr, and trp show the greatest enhancement of the modes using an excitation wavelength of 220 nm. Excitation profiles determined for the

Trp-less mutant showed the greatest enhancement of tyr modes at 233 nm excitation. Excitation profiles of Trp-57 showed the greatest enhancement of the W18 mode at 228 nm excitation. To selectively enhance trp modes in OmpA, UVRR spectra of OmpA should be collected at 228 nm excitation.

4.6 Acknowledgements

I thank Hannah Shafaat for her assistance with self-absorption corrections and the UVRR experiments. I also thank Tiffany Neary for her assistance with the UVRR experiments.

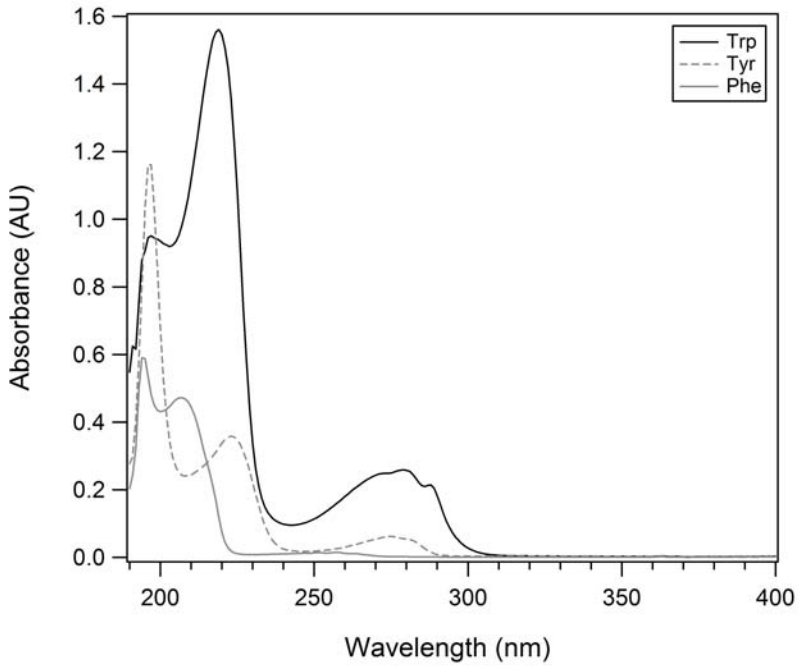

Figure 4.1: Absorption spectra of tryptophan (trp), tyrosine (tyr), and phenylalanine (phe) in aqueous buffer. The $B_{a,b}$ band is ~220 nm; the $L_{a,b}$ bands are at ~270 nm and ~280 nm.

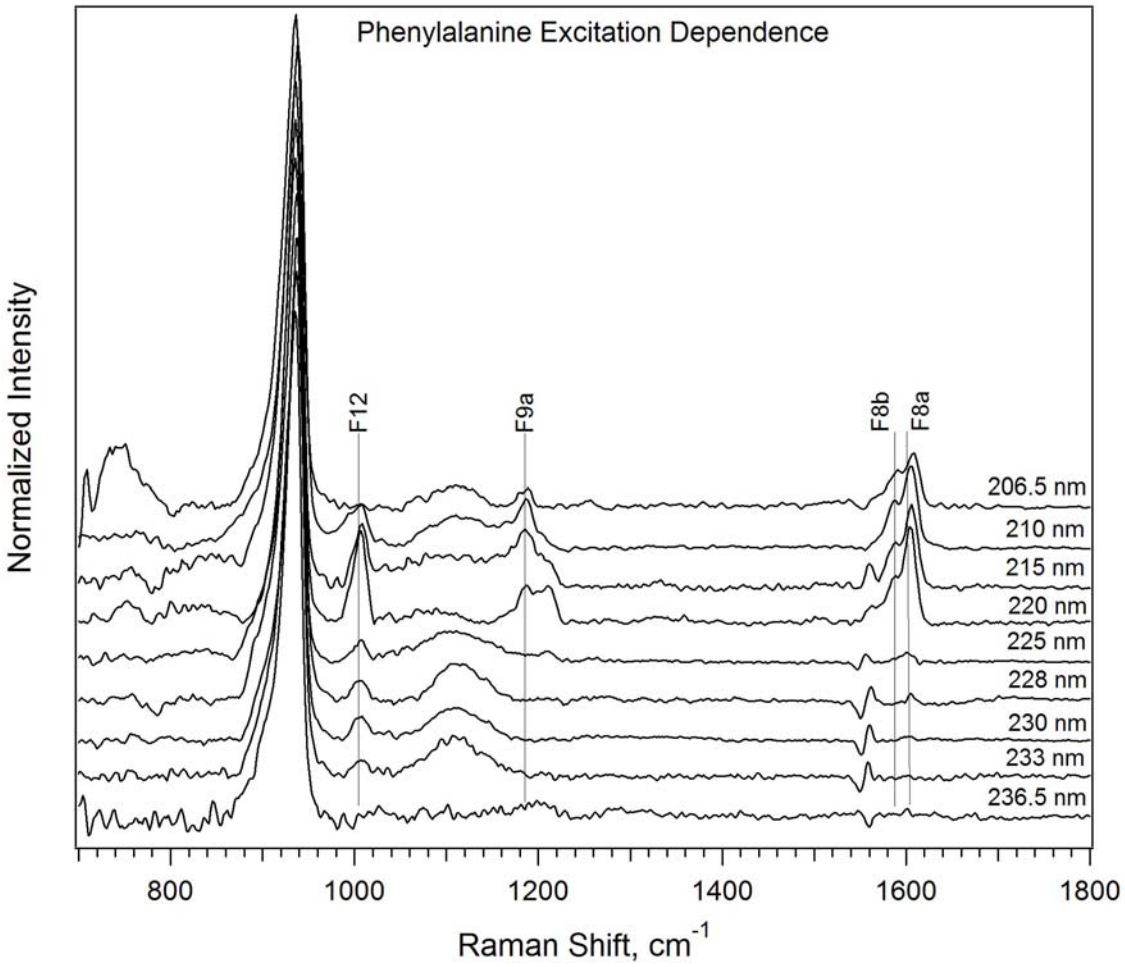

Figure 4.2: Resonance Raman spectra of aqueous phenylalanine with different excitation wavelengths. The peak at 932 cm^{-1} is due to the internal standard, perchlorate; all spectra are normalized to this peak. Derivative features at ~1550 cm^{-1} are due to incomplete subtraction of KP_i buffer. Some phe vibrational modes are indicated (F#).

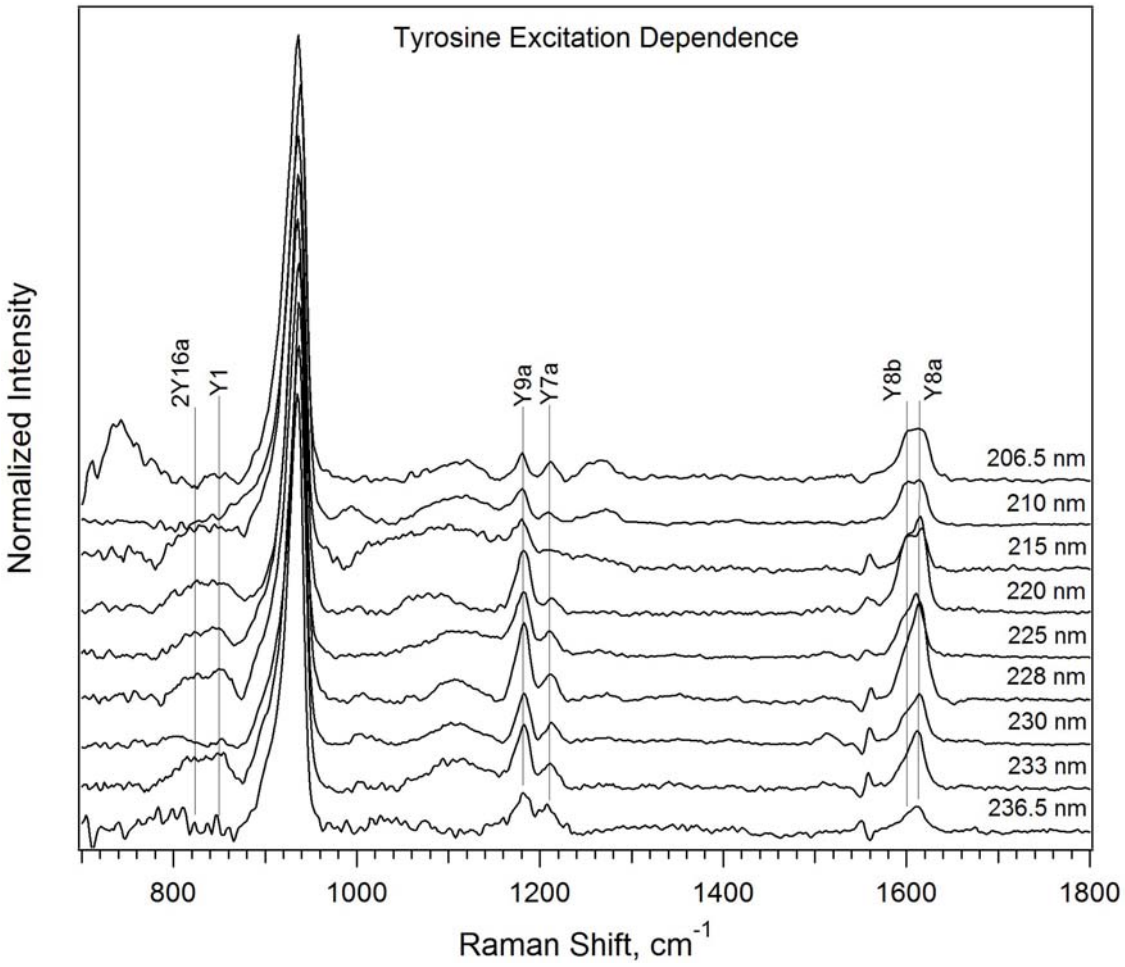

Figure 4.3: Resonance Raman spectra of aqueous tyrosine with different excitation wavelengths. The peak at 932 cm^{-1} is due to the internal standard, perchlorate; all spectra are normalized to this peak. Derivative features at ~1550 cm^{-1} are due to incomplete subtraction of KP_i buffer. Some tyr vibrational modes are indicated (Y#).

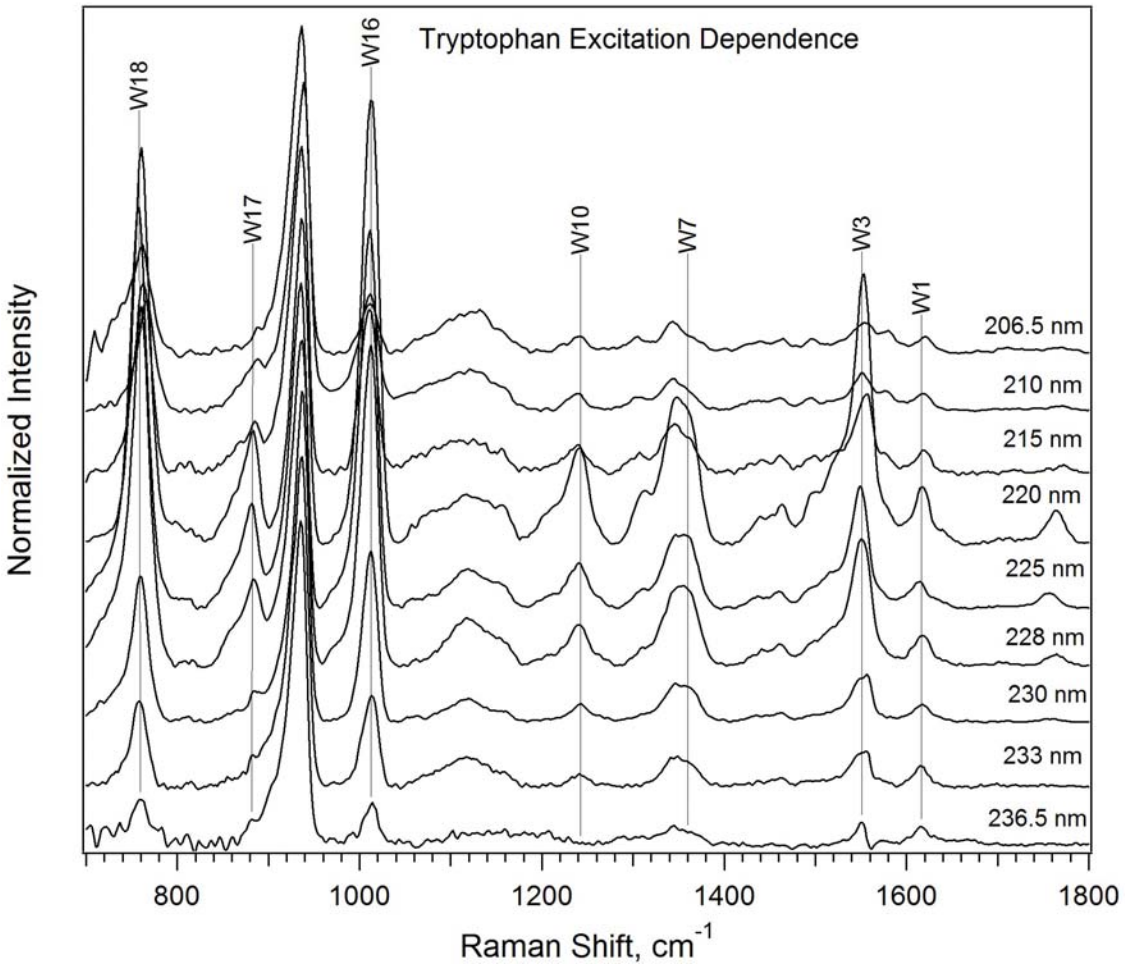

Figure 4.4: Resonance Raman spectra of aqueous tryptophan with different excitation wavelengths. The peak at 932 cm^{-1} is due to the internal standard, perchlorate; all spectra are normalized to this peak. Some trp vibrational modes are indicated (W#).

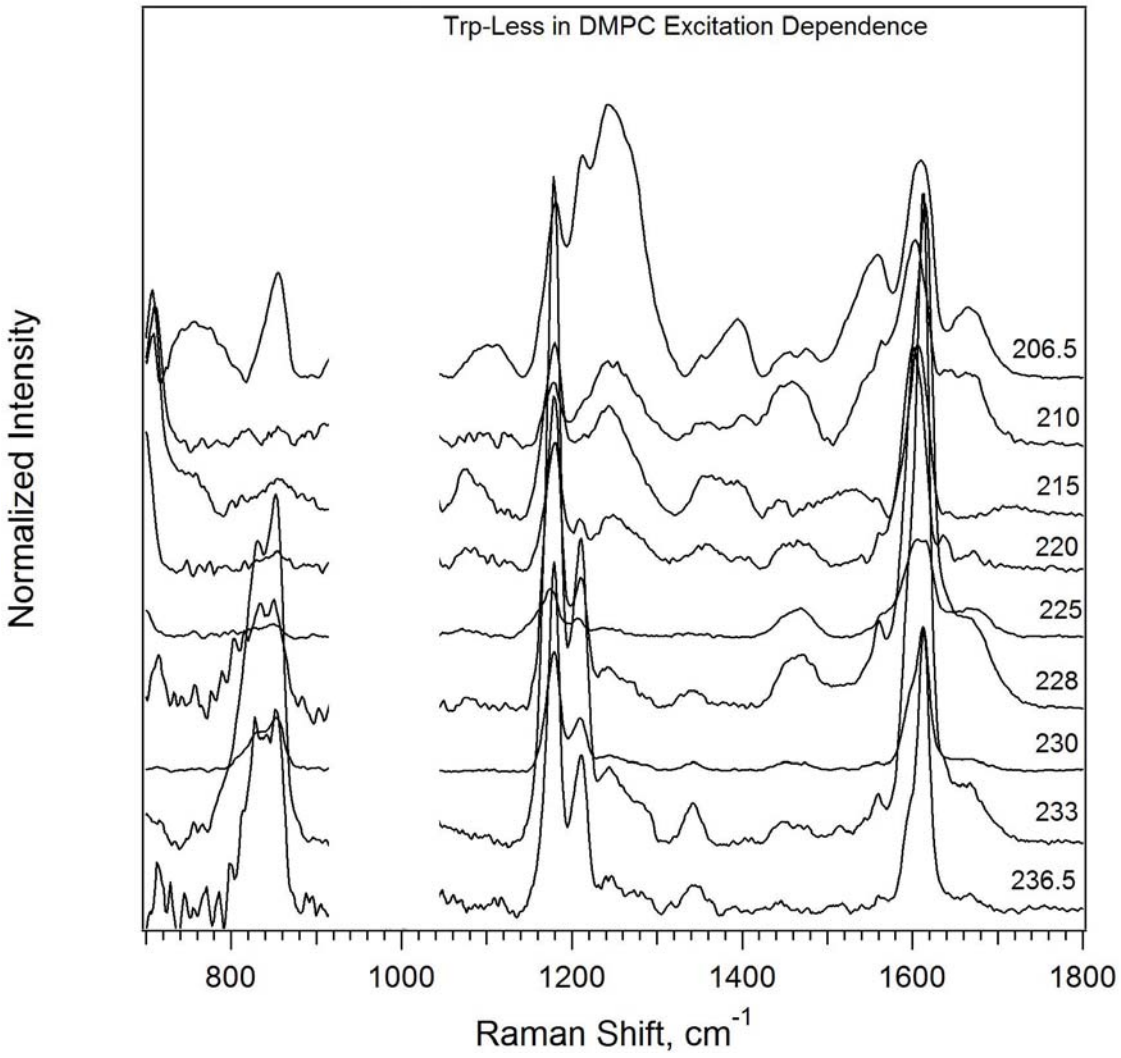

Figure 4.5: UVRR spectra of Trp-less OmpA mutant folded in DMPC vesicles with different excitation wavelengths.

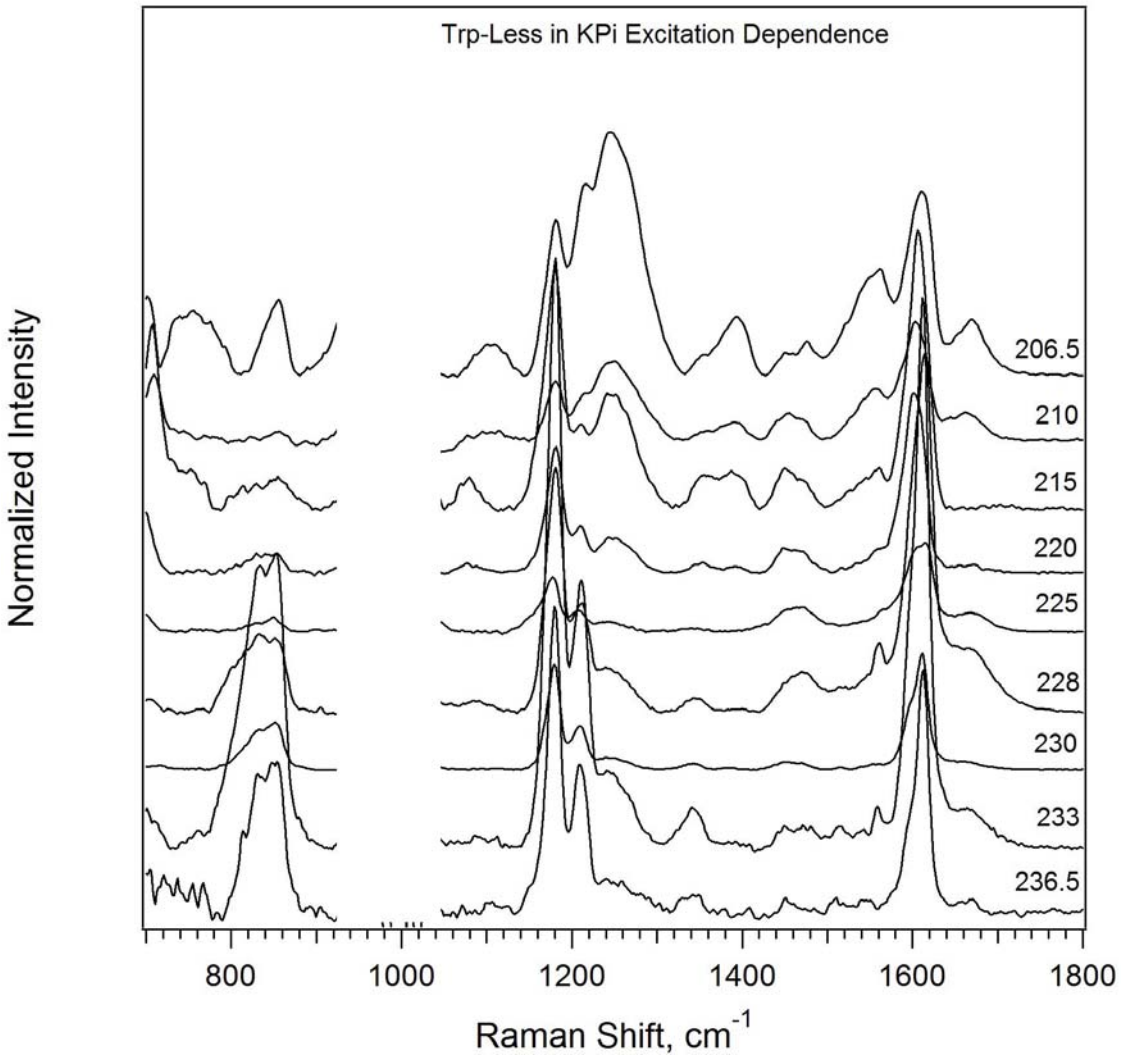

Figure 4.6: UVRR spectra of Trp-less OmpA mutant unfolded in KP_i buffer with different excitation wavelengths.

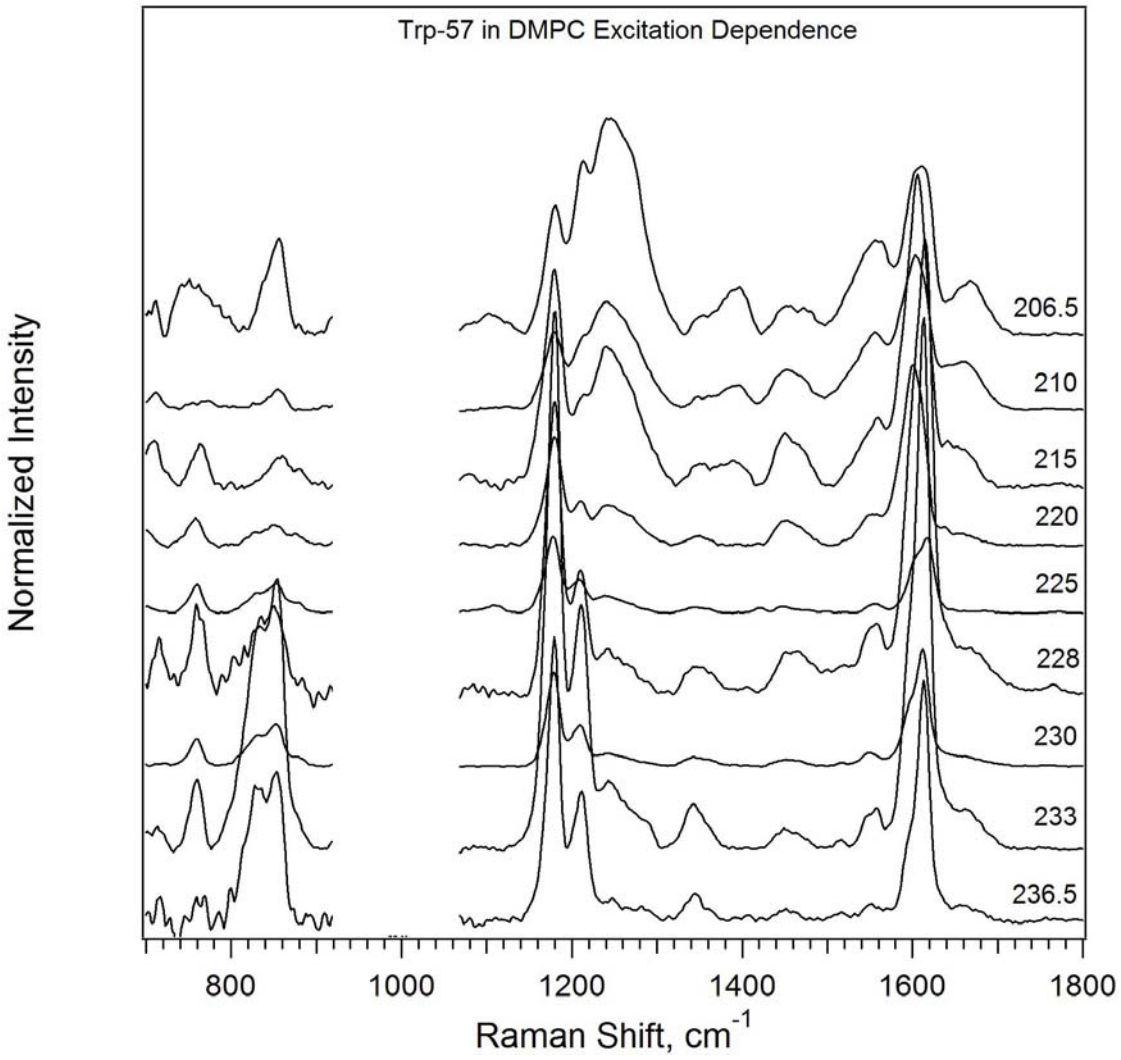

Figure 4.7: UVRR spectra of the single-trp mutant Trp-57 OmpA mutant folded in DMPC vesicles with different excitation wavelengths.

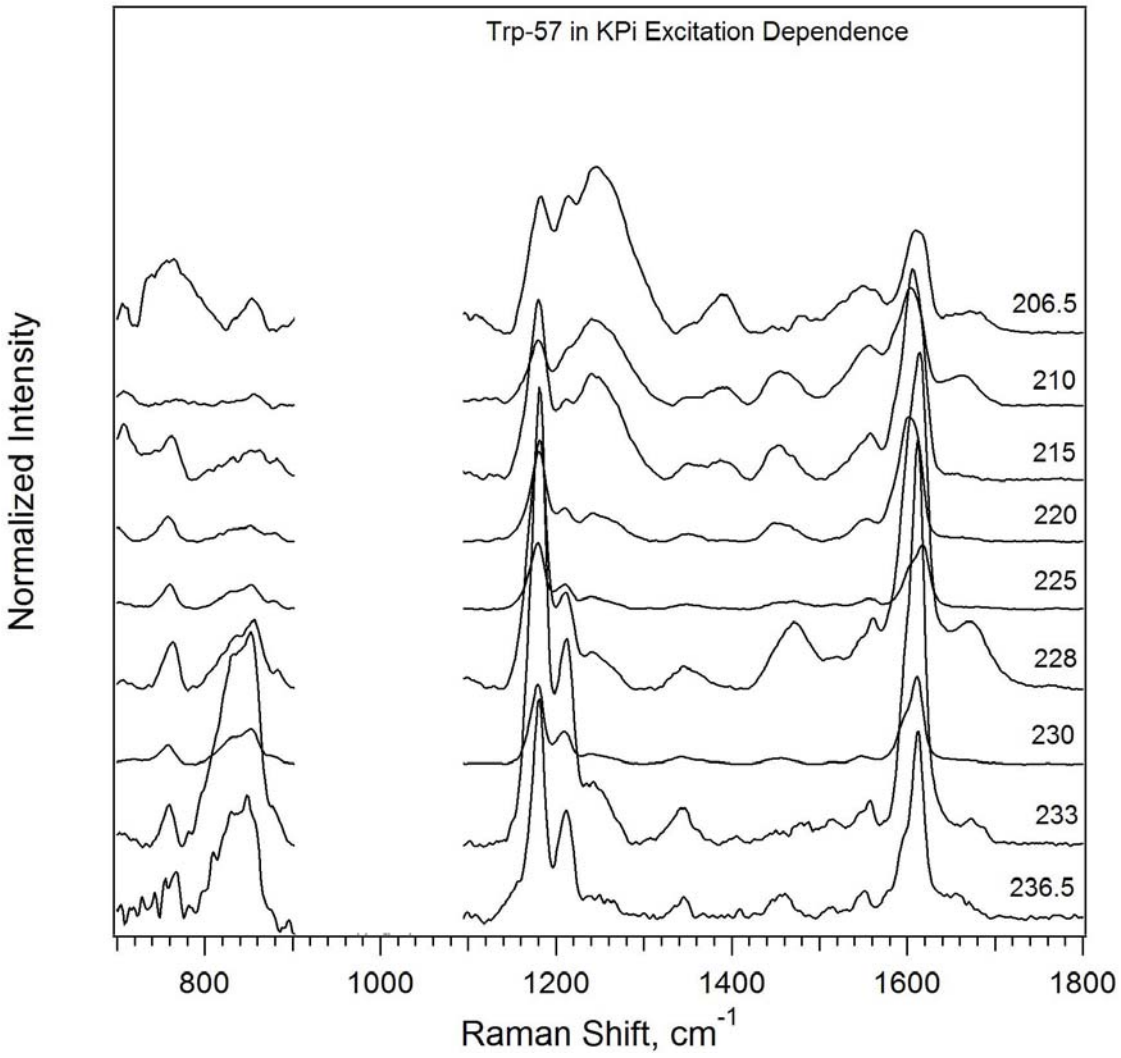

Figure 4.8: UVRR spectra of the single-trp mutant Trp-57 OmpA mutant unfolded in KP_i buffer with different excitation wavelengths.

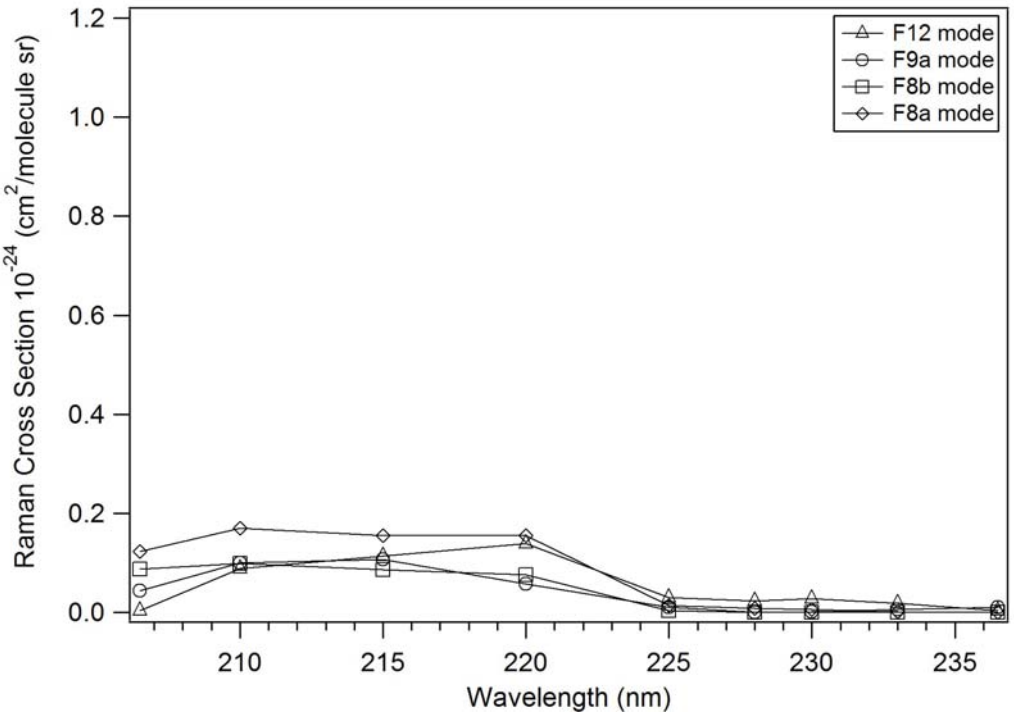

Figure 4.9: Phenylalanine resonance Raman excitation profile.

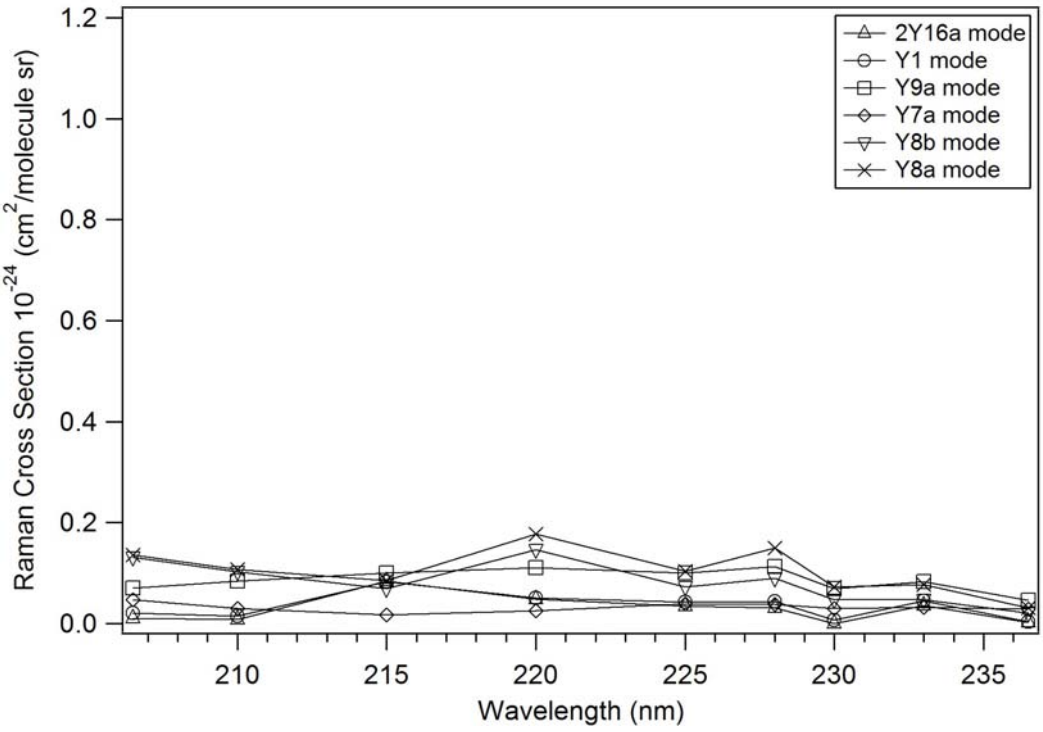

Figure 4.10: Tyrosine resonance Raman excitation profile.

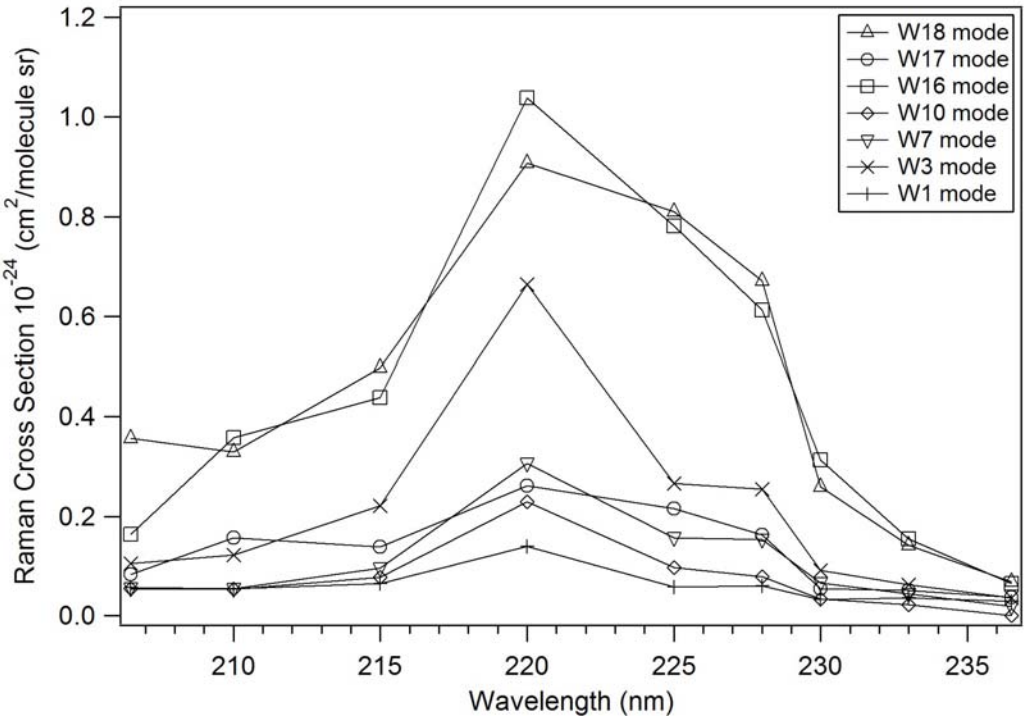

Figure 4.11: Tryptophan resonance Raman excitation profile.

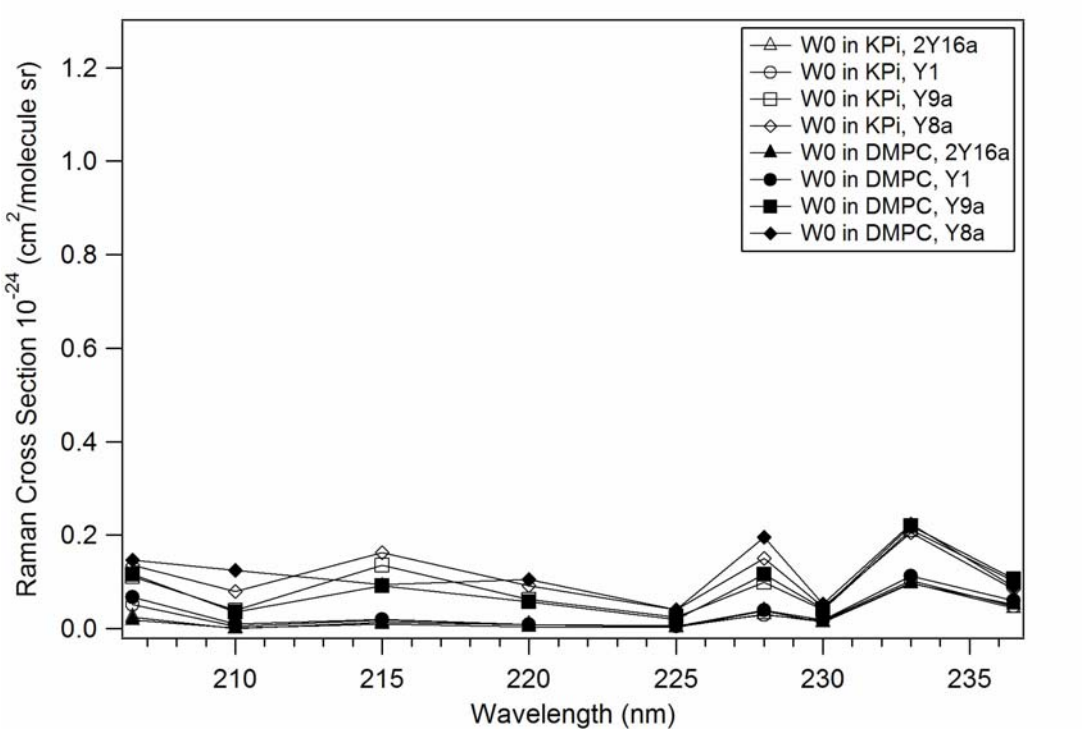

Figure 4.12: OmpA Trp-less, W0, resonance Raman excitation profile, unfolded in KP_i buffer (open symbols), and folded in DMPC vesicles (solid symbols). Raman cross sections of tyr (Y) modes in the protein are indicated.

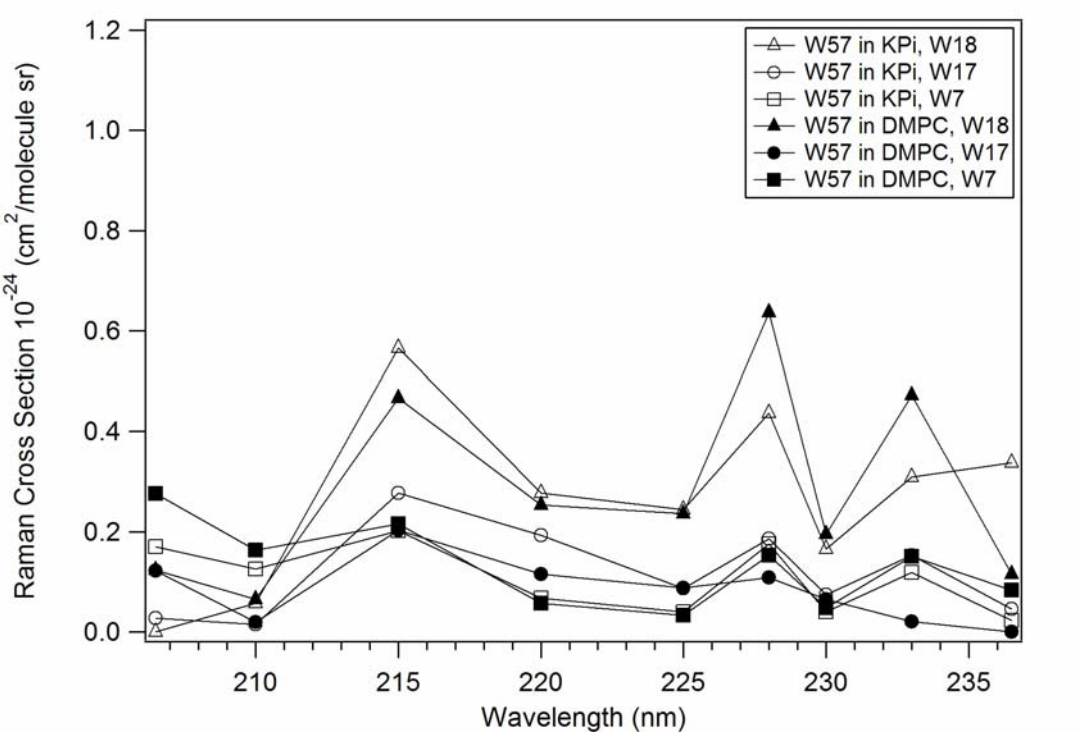

Figure 4.13: OmpA Trp-57, W57, resonance Raman excitation profile, unfolded in KP_i buffer (open symbols), and folded in DMPC vesicles (solid symbols). Raman cross sections of trp (w) modes in the protein are indicated.

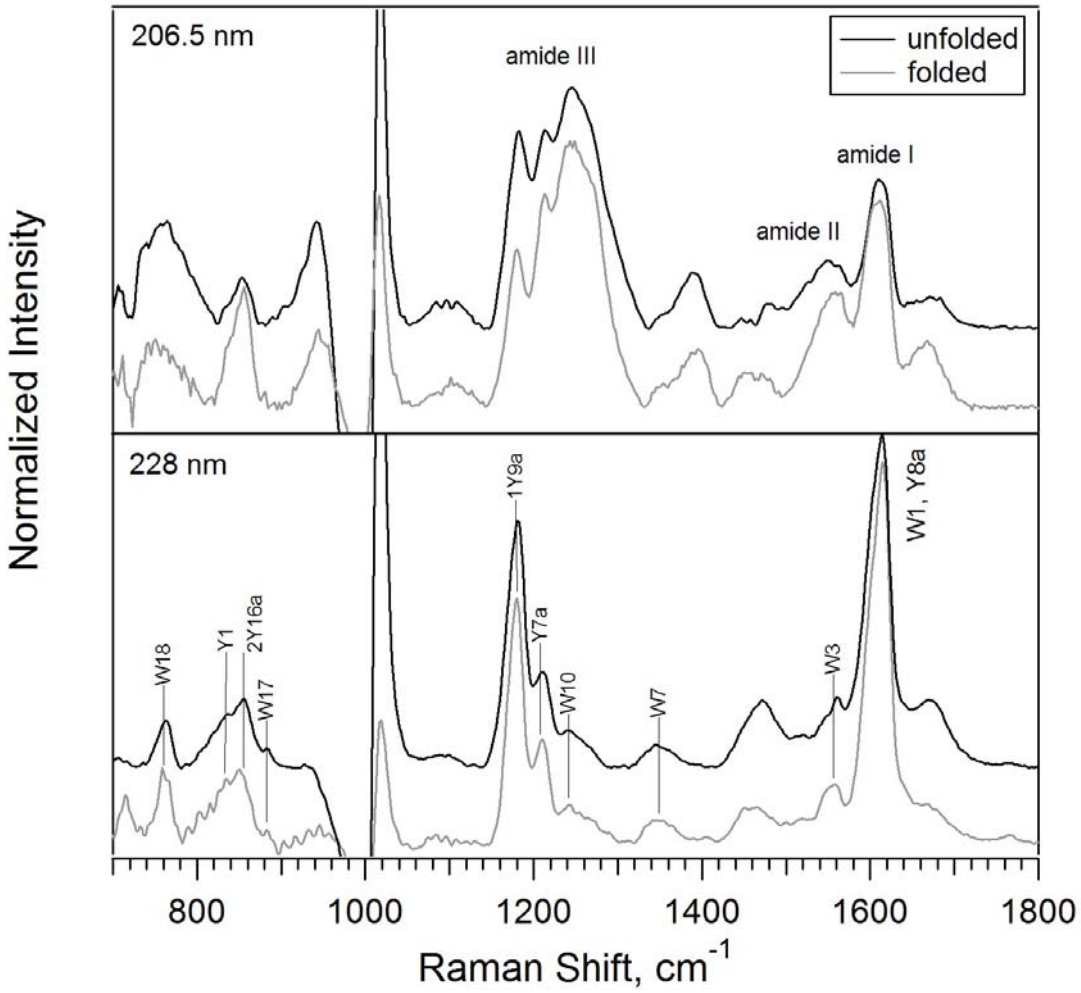

Figure 4.14: UVRR spectra pf Trp-57 with 206.5 nm and 228 nm excitation, unfolded in buffer (black curves), and folded in vesicle (gray curves), for comparison. The large feature at ~1000 cm^{-1} is due to incomplete subtraction of urea.

Table 4.1: UVRR experimental parameters for the different excitation wavelengths used in this study. The spectrograph was centered at the corresponding wavelengths. Prefilter and intermediate slits are reported. The power of the UV beam at the corresponding wavelengths is reported. The fourth harmonic of the fundamental (IR) wavelength is used to obtain the UV wavelengths. The Prefilter slit was adjusted to maintain ~10 – 14 cm^{-1} bandpass.

IR (nm)	UV (nm)	Spect. (nm)	Prefilter Slit (um)	Int. Slit (mm)	UV Power (mW)
826	206.5	642.89	90	3.00	1.0
840	210	654.09	100	3.00	4.2
860	215	668.40	100	2.80	6.3
880	220	681.60	110	2.20	4.3
900	225	697.50	110	2.13	4.2
912	228	707.67	110	2.13	4.0
920	230	714.30	110	2.13	4.0
932	233	722.74	110	1.80	4.0
946	236.5	733.29	110	1.90	3.1

Table 4.2: Vibrational mode frequencies of phenylalanine (F), tyrosine (Y), and tryptophan (W). Adapted from Reference 22.

	Frequency (cm^{-1})	Mode assignment
Phenylalanine	1000	F12
	1182	F9a
	1207	-
	1586	F8b
	1606	F8a
Tyrosine	832	2Y16a
	852	Y1
	1180	Y9a
	1210	Y7a
	1263	-
	1601	Y8b
	1617	Y8a
Tryptophan	762	W18
	880	W17
	1016	W16
	1127	W13
	1238	W10
	1305	W8
	1342	f.d.
	1361	W7
	1462	W5
	1496	W4
	1555	W3
	1575	W2
	1622	W1

4.7 References

(1) Spiro, T. G.; Grygon, C. A. *Journal of Molecular Structure* **1988**, *173*, 79.

(2) Clark, R. J. H.; Dines, T. J. *Angew. Chem. Int. Ed. Engl.* **1986**, *25*, 131.

(3) Clark, R. J. H.; Stewart, B. *Struct. Bonding* **1979**, *36*, 1.

(4) Efremov, E. V.; Ariese, F.; Gooijer, C. *Anal. Chim. Acta* **2008**, *606*, 119

(5) Albrecht, A. C. *J. Phys. Chem.* **1961**, *34*, 1476.

(6) Champion, P. M.; Albrecht, A. C. *Annu. Rev. Phys. Chem.* **1982**, *33*, 353.

(7) Spiro, T. G. *Accounts of Chemical Research* **1974**, *7*, 339.

(8) Spiro, T. G.; Stein, P. *Annu. Rev. Phys. Chem.* **1977**, *28*, 501.

(9) Shorygin, P. P. *Pure Appl. Chem.* **1962**, *4*, 87.

(10) Wang, Y.; Van Wart, H. E. *Methods Enzymol.* **1993**, *226*, 319

(11) Harada, I.; Takeuchi, H. *Raman and Ultraviolet Resonance Raman Spectra of Proteins and Related Compounds*; John Wiley & Sons, Ltd.: Chichester, 1986; Vol. 13.

(12) Tuma, R. *J. Ram. Spect.* **2005**, *36*, 307

(13) Spiro, T. G.; Strekas, T. C. *J. Am. Chem. Soc.* **1974**, *96*, 338

(14) Oseroff, A. R.; Callender, R. H. *Biochem.* **1974**, *13*, 4243.

(15) Hanlon, E. B.; Manoharan, R.; Koo, T.-W.; Shafer, K. E.; Motz, J. T.; Fitzmaurice, M.; Kramer, J. R.; Itzkan, I.; Dasari, R. R.; Feld, M. S. *Phys. Med. Biol.* **2000**, *45*, R1

(16) Chi, Z.; Asher, S. A. *Biochem.* **1999**, *38*, 8196.

(17) Austin, J. C.; Jordan, T.; Spiro, T. G. *Ultraviolet Resonance Raman Studies of Proteins and Related Model Compounds*; John Wiley and Sons: New York, 1993.

(18) Ferraro, J. R.; Nakamoto, K.; Brown, C. W. *Introductory Raman Spectroscopy*, Second ed.; Academic Press: San Diego, 2003.

(19) Benevides, J. M.; Overman, S. A.; Thomas, G. J. J. *J. Ram. Spect.* **2005**, *36*, 279

(20) Asher, S. A. L., M. ; Johnson, C.R. *J. Am. Chem. Soc.* **1986**, *108*, 3186.

(21) Fodor, S. P. S.; Copeland, R. A.; Grygon, C. A.; Spiro, T. G. *J. Am. Chem. Soc.* **1989**, *111*, 5509.

(22) Ludwig, M.; Asher, S. A. *J. Am. Chem. Soc.* **1988**, *110*, 1005.

(23) Sweeney, J. A.; Asher, S. A. *J. Phys. Chem.* **1990**, *94*, 4784.

(24) Chi, Z.; Asher, S. A. *J. Phys. Chem. B* **1998**, *102*, 9595

(25) Kleinschmidt, J. H.; den Blaauwen, T.; Driessen, A. J. M.; Tamm, L. K. *Biochemistry* **1999**, *38*, 5006.

(26) Kim, J. E.; Arjara, G.; Richards, J. H.; Gray, H. B.; Winkler, J. R. *J. Phys. Chem. B* **2006**, *110*, 17656.

(27) Sanchez, K. M.; Gable, J. E.; Schlamadinger, D. E.; Kim, J. E. *Biochemistry* **2008**, *47*, 12844.

(28) Kaminaka, S.; Mathies, R. A. *Appl. Spect.* **1998**, *52*, 469.

(29) Dudik, J. M.; Johnson, C. R.; Asher, S. A. *J. Chem. Phys.* **1984**, *82*, 1732

(30) Lakowicz, J. R. *Principles of Fluorescence Spectroscopy*, 3rd ed.; Springer: New York, 2006.

(31) Rava, R. P. S., T.G. *J. Phys. Chem.* **1985**, *89*, 1856.

(32) Matsuno, M.; Takeuchi, H. *Bull. Chem. Soc. Jpn* **1998**, *71*, 851.

(33) Huang, C. Y.; Balakrishnan, G.; Spiro, T. G. *J. Ram. Spect.* **2006**, *37*, 277.

(34) Chi, Z.; Chen, X. G.; Holtz, J. S.; Asher, S. A. *Biochem.* **1998**, *37*, 2854.

Chapter 5

UV Resonance Raman Spectroscopy of Folded and Unfolded States of an Integral Membrane Protein

5.1 Introduction

Membrane protein folding is an exploding area of research for experimentalists and theorists.[1-5] Despite recent efforts to elucidate the process of protein insertion into lipid bilayers, our knowledge of membrane protein folding remains inferior to our fundamental understanding of soluble protein folding. Experimental studies of the folding dynamics of membrane proteins and peptides are especially challenging because a limited number of membrane protein systems can realistically be studied, samples are difficult to prepare, and few experimental techniques are capable of providing structural details. In addition, techniques to initiate the folding reaction for membrane proteins have primarily been limited to rapid denaturant dilution methods. Finally, there is added complexity in the study of membrane protein folding due to properties of the bilayer itself. For example, curvature of the bilayer, nature of the phospholipid heads, composition of the lipids, and length of the hydrocarbon chains are important factors that affect the stability and folding mechanisms of membrane proteins.[3,6,7] These and other inherent obstacles have made the problem of membrane protein folding especially challenging.

One of the few membrane protein system that has been relatively well characterized is the robust bacterial integral membrane protein, Outer Membrane Protein A (OmpA). Here, we present the first UVRR spectra of OmpA under *in vitro* folding and

unfolding conditions. Folding into small unilamellar vesicles (SUV) and detergent micelles is spontaneous, and we have rigorously characterized the stability and size of the SUVs to ensure reproducible folding events.[8] Figure 1 displays the structure of OmpA, along with an expanded region of the atoms within 5Å of the tryptophan side chain of Trp-57. The *in vitro* folding mechanism of this 325-residue, monomeric, β-barrel protein has been studied via electronic spectroscopy, including fluorescence and circular dichroism,[7,9-11] as well as with non-specific vibrational techniques.[12,13] In addition, the effects of temperature, bilayer composition, and bilayer curvature have been investigated.[7,10,14] These previous studies have helped establish successful conditions for performing experiments and have expanded our general understanding of β-barrel membrane protein folding; however, critical molecular details remain missing.

UV resonance Raman (UVRR) spectroscopy is a powerful technique capable of providing highly specific and selective molecular detail in complex systems. UVRR has been applied to a variety of topics in biophysics, including folding of soluble proteins,[15-18] allosteric transitions,[19,20] activation of G-protein coupled receptors,[21,22] and ultrafast protein dynamics.[22-24] Variation of the excitation wavelength from ~195 to 240-nm allows for selective enhancement of Raman signal from peptide backbone or aromatic amino acids.[16,25,26] Extensive analysis of UVRR spectra of peptide backbone[27,28] and aromatic amino acids[28-31] have been reported. Off-resonance Raman studies of aromatic residues have also played a critical role in interpretation of UVRR spectra.[26,32,33] These and other Raman studies have established important empirical relationships between Raman frequencies/intensities and molecular detail, such as secondary structure, hydrogen bonding strength, microenvironment, and static structure. In particular,

systematic UVRR studies of tryptophan reveal spectral signatures that report upon local hydrophobicity, strength of indole N-H hydrogen bond, and torsional angle, χ2,1 about the C-2-C-3-Cβ-Cα linkage. The wealth of vibrational information makes UVRR studies of tryptophan an ideal probe in our studies of protein folding in a bilayer environment.

Tryptophan and other aromatic residues in membrane proteins are preferentially located at the bilayer-water interface[34-37] and can serve as membrane anchors. Therefore, it is likely that folding of a membrane protein causes significant modification in tryptophan vibrational structure and microenvironment. Comparison of UVRR spectra of wild-type OmpA (five native tryptophan residues), a single-trp mutant (Trp-57), and the trp-less mutant (Trp-less) enables systematic identification of vibrational changes from a single tryptophan residue in folded and unfolded protein states. In addition, structural differences of OmpA folded in detergent and folded in vesicles may be elucidated via UVRR. The current work provides the first set of residue-specific details associated with protein insertion into a synthetic bilayer and establishes a foundation for ongoing experimental studies of membrane protein folding.

5.2 Experimental Methods

5.2.1 Refolding and Unfolding of OmpA

OmpA samples were refolded into detergent micelles of *n*-octyl-β-D-glucopyranoside (OG) or SUVs. The final concentration of OmpA was ~ 20 μM based on UV-vis absorption measurements and the following calculated extinction coefficients: 54 390, 32 330, and 26 810 M^{-1} cm^{-1} for OmpA wild type, single-trp, and trp-less, respectively. For folding in detergent, stock OmpA was added to a 10 mg/mL solution of OG (20 mM KP_i, pH 7.3), and allowed to equilibrate for 30 minutes prior to

spectroscopic experiments. For folding in SUVs, stock OmpA was added to a 1 mg/mL solution of sonicated DMPC (20 mM KP_i, pH 7.3) and equilibrated for ~6 hrs before spectroscopic measurements were made. For unfolded OmpA, the stock solution was diluted to <1M urea in KP_i buffer solution. Protein conformational states were confirmed by the differential gel electrophoretic mobility of folded (30 kDa) and unfolded (35 kDa) OmpA and fluorescence spectroscopy;[10,11] trp emission in folded OmpA peaks near 330 nm while in unfolded protein, OmpA emits maximally at ~350 nm.[11]

5.2.2. UV resonance Raman spectroscopy

Detailed description of the laser system can be found in Chapter 2 of this dissertation. In short, 1-Watt of the 920-nm fundamental of a Ti:sapphire laser was sent through LBO and a BBO doubling crystals to generate ~10 mW of the fourth harmonic, 230 nm UV. The UV light was then sent to the sample, and collection optics. The spectral response was determined by a deuterium lamp, and the bandpass and accuracy (based on ethanol peaks) of the detection system are <14 cm^{-1} and ±1 cm^{-1}, respectively.

For 230-nm excitation: Protein solution was pumped through a vertically-mounted, 100μm i.d. quartz microcapillary at a rate of 0.16 mL/min to ensure fresh sample for each laser pulse, and discarded after a single-pass through the laser beam to eliminate artifacts from photolyzed protein. Ten-minute UVRR spectra were collected for wild-type and Trp-57 and Trp-less mutant OmpA solutions under the following conditions: folded in SUV, folded in detergent, and unfolded in KP_i buffer. Spectra of each of the three buffer solutions without OmpA were also acquired and subtracted from the corresponding OmpA spectra to obtain data shown in Figures 5.2 – 5.4. Fluorescence

and absorption spectra were measured before and after photolysis. Nominally ~20 μM protein was used. Data was analyzed using Igor Pro (WaveMetrics) software.

5.3 Results and Discussion

Typical raw spectra of folded and unfolded ~20 μM WT OmpA along with corresponding buffer spectra are shown in Figure 5.2. To our knowledge, these data are the first UVRR spectra of membrane proteins in highly-scattering synthetic vesicles. Despite intense Rayleigh scattering from SUVs (left-side of Figure 5.2), resonance Raman bands from OmpA are apparent in these ten-minute spectra. Raman signal from vibrational modes coupled to tryptophan L_{a-b}, and B_b electronic transitions are enhanced with 230-nm excitation.[26,29,30] Signal from residual urea (~0.8M), fused silica, and water are also evident. Linear dependence of Raman intensities for the W18 mode and 1005 cm^{-1} urea mode as a function of laser power up to 6.5-mW is shown as an inset.

Figure 5.3 shows the 230-nm UVRR spectra of folded and unfolded WT, Trp-57, and Trp-less OmpA after subtraction of appropriate buffer spectra and removal of residual scatter. For example, the top spectrum in Figure 5.3 was determined via the following analysis: [(raw OmpA in OG buffer – raw OG buffer) – residual scattering background]. The residual scattering background was determined by interpolation from a broad background spectrum after subtraction of buffer signal. The feature near 1000 cm^{-1} is due to urea and if relevant, overlapping W16 peak at ~1013 cm^{-1}; upon dilution of the stock solution of OmpA in 8M urea/KP_i into appropriate folding or unfolding buffers, residual (~0.8M) urea remained. Despite our attempt to replicate the residual urea concentrations in analogous, protein-free buffer solutions, it was difficult to

quantitatively eliminate signal from urea without simultaneously over- or under-subtracting other features, such as the water bend peak at ~1640 cm^{-1}.

The OmpA UVRR spectra in Figure 5.3 show strong signal from the seventeen native tyrosine residues in WT, Trp-57, and Trp-less OmpA. Strong enhancements are also observed for the native tryptophan residues in WT and Trp-57 OmpA.[26] Comparison of the WT and Trp-57 spectra to the Trp-less mutant shows strong signal from tryptophan modes W18 (~760 cm^{-1}), W17 (~879 cm^{-1}), W13 (~1130 cm^{-1}), W10 (~1240 cm^{-1}), W7 Fermi doublet (~1340 and ~1361 cm^{-1}), and W3 (~1548 cm^{-1}). Unique tyrosine peaks are also evident, such as the Y1+2Y16a Fermi doublet (~833 and ~854 cm^{-1}), Y9a (~1180 cm^{-1}), and Y7a (~1211 cm^{-1}). Strong signal from overlapping trp and tyr peaks appears near 1611 cm^{-1} (Y8a and W1). Because Trp-57 OmpA has a single tryptophan residue at position 57, our Trp-57 spectra unambiguously illustrate vibrational spectra of this single residue under the current folding and unfolding conditions. The frequency of the indole ring vibration (W3) quantitatively reflects the torsional angle, $\chi 2,1$ about the C-2-C-3-Cβ-Cα linkage.[33] The calculation of the angle from our UVRR spectra yields a $\chi 2,1$ value of ~ 91° for Trp-57 folded in vesicle and detergent, which is similar to the value of 93° from the crystal structure of detergent-solubilized OmpA.[38,39]

In addition to structure, peak positions are sensitive to microenvironment. The W17 band at ~879 cm^{-1} is sensitive to hydrogen bonding by the N_1H group of the indole.[32] In Trp-57 OmpA, decomposition of the peaks near W17 into three Gaussian bands centered at ~833 and ~854 cm^{-1} (Y1+Y16a Fermi double), and ~879 cm^{-1} yield W17 frequencies of 874 and 878 cm^{-1} in unfolded and folded states, respectively. The 4 cm^{-1} increase in W17 frequency illustrates a loss of hydrogen-bonding character of the

indole N_1H upon folding into detergent micelles.[32] Our result coincides with the crystal structure that shows no hydrogen-bonding partners within 4Å of the indole N_1H. Presumably, this loss in hydrogen-bonding structure is due to the expulsion of hydrogen-bonding water partners upon transfer of OmpA from aqueous solution, where it remains unfolded, to detergent micelles, where it forms β-barrel. The removal of water upon folding in detergent is consistent with the observed increase in hydrophobicity as measured via steady-state fluorescence experiments.[11]

An expanded region of the Fermi resonance doublet of trp near 1340-1360 cm^{-1} is illustrated in Figure 5.4 for WT and Trp-57 OmpA. Only features from trp contribute to these spectra because a W0 spectrum was subtracted from the corresponding WT or Trp-57 spectra. The doublet has been decomposed into two Gaussian peaks centered at 1340 and 1361 cm^{-1} (20 cm^{-1} breadth for each peak). The relative intensity, *R*, of this doublet resonance (I_{1361}/I_{1340}) is sensitive to local environment; excitation with 488 nm results in a value of *R* that ranges from 0.65-0.92 in hydrophilic solvents such as methanol, 1.02-1.11 in benzene, and 1.23-1.32 in saturated hydrocarbons.[26] This ratio is also wavelength-dependent, but remains a sensitive indicator of local environment with UV excitation. For WT OmpA, the ratios, *R*, when OmpA is folded in detergent, folded in SUV, and unfolded in KP_i, are 1.6, 1.8, and 1.1, respectively. These large values for *R* averaged over all five native trp residues in folded OmpA are consistent with burial of the trp residues in a highly hydrophobic region, such as in a local hydrophobic pocket or in the hydrocarbon core of the vesicle. For Trp-57 OmpA, *R* is 1.2 (folded in detergent), 1.3 (folded in SUV), and 0.9 (unfolded in KP_i). These data support a picture in which the single trp residue at position 57 remains in a relatively hydrophilic region when unfolded,

and transfers to a hydrophobic microenvironment upon folding into vesicles or detergent, consistent with burial of the trp residue upon folding.

In addition to the single trp residue in Trp-57, the remaining four native tryptophan residues also undergo structural changes upon folding; these shifts can be determined from further comparison of WT, Trp-57, and Trp-less OmpA UVRR spectra. In Trp-57, the combined Y8a and W1 peak near 1611 cm^{-1} appears in the same spectral region as the isolated Y8a peak in Trp-less spectra, suggesting that any change in W1 frequency caused by protein folding is masked by the large signal from tyrosine. In WT OmpA, however, frequency shifts of the W1 tryptophan band are evident in this spectral region; the large peak appears at 1614, 1609, and 1612 cm^{-1} for protein folded in detergent, protein folded in SUV, and unfolded protein, respectively. This W1 mode has contributions from the phenyl ring and pyrrole N_1C_8 stretch,[26] and the frequency shift from 1614 to 1609 cm^{-1} of protein folded in detergent and vesicle, respectively, suggests different folded structures in these two media. Additional support for distinguishable folded structures is evident in the W3 peak of WT OmpA. Unlike the fixed W3 peak of Trp-57 OmpA at 1548 cm^{-1}, the W3 peak of WT OmpA shifts from 1548 (folded in detergent) to 1544 (folded in SUV) cm^{-1}. This shift may reflect a change in the average torsional angle, $\chi 2,1$, from ~91° to ~79° for the remaining four trp residues in OmpA folded in vesicle and detergent, respectively. Alternatively, the shift of W3 frequency in WT OmpA could be attributed to a large change in $\chi 2,1$ of a single trp residue for the protein folded in vesicle vs. detergent.

Inspection of the Trp-less OmpA UVRR spectra indicates that tyrosine residues also undergo changes upon folding. The large peak near 1611 cm^{-1} is dominated by the

seventeen native tyrosine residues; in Trp-less, the isolated tyrosine peak, Y8a, appears at 1612 (folded in detergent), 1612 (folded in SUV) and 1609 (unfolded) cm^{-1}. The Y8a ring-stretching mode is sensitive to hydrogen bonding, and has been shown to undergo a systematic decrease in frequency with increasing hydrogen bond strength.[19] The observed shift in Y8a frequency suggests that on average, the tyrosine residues have weaker hydrogen bonds in folded OmpA than in unfolded OmpA. This loss of tyrosine hydrogen bonding is consistent with our conclusion, based on W17 analysis above, that trp-57 also experiences decreased hydrogen bonding upon folding. Comparison of the Y8a frequency in unfolded OmpA to the model compound (Y8a for L-tyr in 0.5M urea/KP_i appears at ~1609 cm^{-1}) shows similar hydrogen bonding in the unfolded protein relative to the fully solvent-exposed model compound. Collectively, these data support a picture in which solvent exposure to aromatic amino acids is decreased in the folded state because of water expulsion upon folding.

5.4 Summary

UVRR spectroscopy is a powerful technique that is capable of elucidating site-specific, molecular changes associated with protein folding. Here, we report 230-nm excitation UVRR spectra of an integral membrane protein folded in a synthetic bilayer vesicle for the first time. Comparison of these UVRR spectra to those of protein folded in detergent micelles and protein unfolded in buffer reveals structural changes for these different conformations, including modifications in tryptophan hydrogen-bonding strength and microenvironment. Our results coincide with previous studies based on other techniques. However, UVRR spectroscopy is unique because the spectra yield *residue-specific*, *structural* details of a protein in the native environment of a bilayer

membrane. These and other ongoing studies, including UVRR spectroscopy of additional OmpA mutants in our own lab, will contribute to the growing understanding of membrane protein folding.

5.5 Continued Studies

After publication of this paper, improvements were made to our system. In addition, the excitation wavelength study described in Chapter 4 illustrated that 228-nm excitation, not 230-nm excitation, is the ideal wavelength. Here, we present improved UVRR spectra with 228-nm excitation of wild type, full-length single-trp mutants (Trp-7, Trp-15, Trp-57, Trp-102, Trp-143, and Trp-170), and the Trp-less mutant. Figure 5.5 and Figure 5.6 show the corrected UVRR spectra of full-length OmpA mutants unfolded in buffer, and folded in DMPC vesicles, respectively. The tryptophan W18, W17, W10, W7, and W3 modes are indicated. The trp mode intensities are enhanced when protein is folded the hydrophobic environment of the vesicle due to a red-shift in the absorption spectra.

Changes are observed in the frequencies of the W17, W10, and W3 modes, and in intensity ratios of the W7 Fermi doublet and the W17/W18 modes. These changes are consistent with increases in hydrophobicity of trp environment when protein is folded in vesicle. A detailed investigation of select single-trp mutants will be further analyzed in Chapter 6 in this dissertation. A short analysis will be presented here.

Studies in our lab have shown that the ratio of the W17 mode (~ 879 cm^{-1}) intensity and W18 mode (~760 cm^{-1}) intensity, $R_{W17:W18}$, is a sensitive reporter of hydrogen bonding in nonpolar or polar environments.[40] These studies on skatole showed $R_{W17:W18}$ values that increased from 0.15 to 0.26 with hydrogen-bonding in a hydrophobic

environment, and increased from 0.26 to 0.30 with hydrogen bonding in a hydrophilic environment. For all the single-trp mutants, except Trp-15, this ratio decreased from ~0.40 to ~0.35 when the protein was folded in vesicle, indicating decreased hydrogen bonding in the vesicle. The W7 mode Fermi doublet ratio, R_{FD}, for these OmpA trp mutants increased when the protein was in the lipid bilayer. This result, combined with the observed blue-shift of the fluorescence, is consistent with an increase in hydrophobic environment of trp residues when the protein is folded in the lipid bilayer. Tabulated frequencies and ratios of trp modes, and fluorescence maxima are found in Table 5.1 for full-length mutants.

UVRR steady-state spectra of the truncated single-trp mutants, Trp-7t, Trp-15t, Trp-57t, Trp-102t, Trp-143t, Trp-170t, and WTt, and full-length Trp-less mutant, were also collected, and are shown in Figure 5.7 and Figure 5.8 for unfolded and folded protein, respectively. Tabulated trp mode frequencies and intensity ratios are found in Table 5.2. The same trends were observed in trp frequency shifts and intensity ratios for the truncated versions of these single-trp mutants, showing the quadruple mutations did not drastically affect protein structure.

Tyrosine modes in OmpA at 230-nm excitation showed differences between the unfolded and folded UVRR spectra, consistent with tyr residues undergoing changes in environment upon folding into the lipid bilayer. At 228-nm excitation, however, the tyr mode frequencies do not change significantly. One reason for this difference on observations is that 230-nm excitation is closer to the maximum of the tyrosine REP than 228-nm; Tyrosine show the greatest enhancement at 233-nm excitation, as determined in Chapter 4.

5.6 Acknowledgements

Chapter 5, in part, is a reprint of the material as it appears in the Journal of Physical Chemistry *B* **112**, 9507 (2008). K. M. Sanchez, T. J. Neary, and J. E. Kim, American Chemical Society, 2008. The dissertation author was the primary investigator and author of this paper.

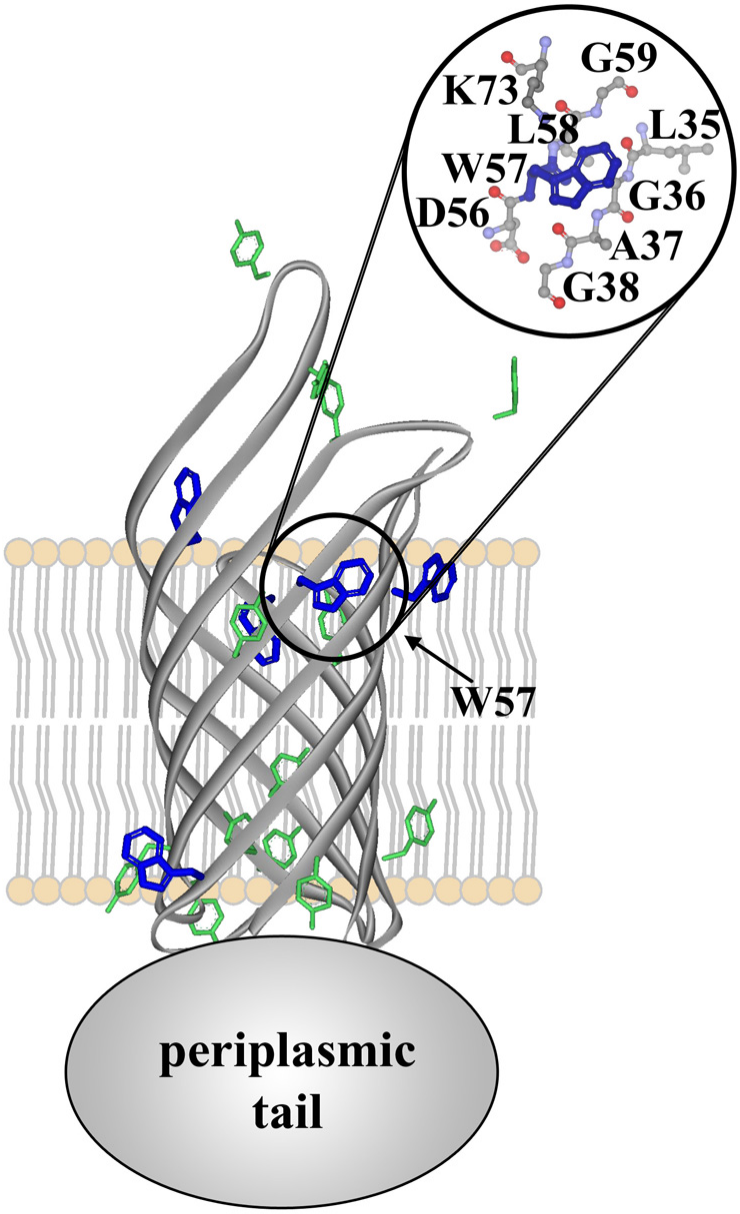

Figure 5.1: Structural representation of the OmpA transmembrane domain (residues 1-171; PDB file 1QJP13) highlighting the five native tryptophan residues (blue) and thirteen native tyrosine residues (green) in the truncated protein. An expanded region of the local residues within 5Å of the indole group of W57 is also shown. Cartoon representations of the periplasmic tail and lipid bilayer are included.

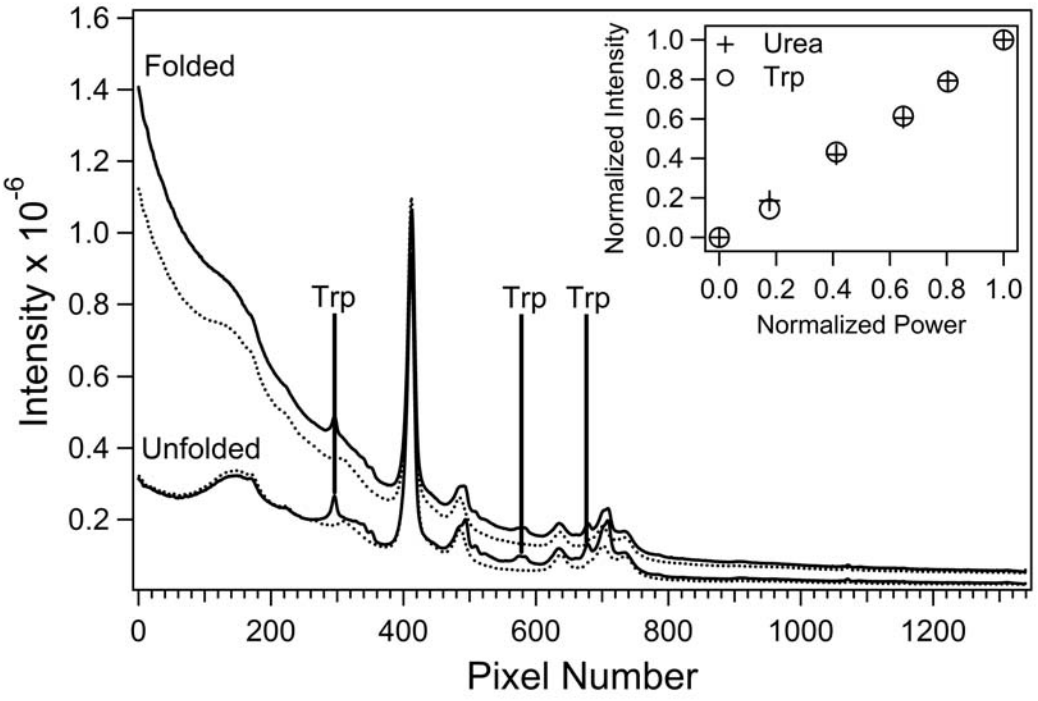

Figure 5.2: Raw UVRR spectra of WT OmpA folded in vesicle and unfolded in KP_i buffer, at 230-nm excitation. The solid curves are spectra of protein solution; dotted curves are spectra of corresponding buffer solution. Unique protein peaks from tryptophan are indicated; the large peak near pixel 400 is due to urea. Inset: Normalized urea and trp peak intensities as a function of normalized power.

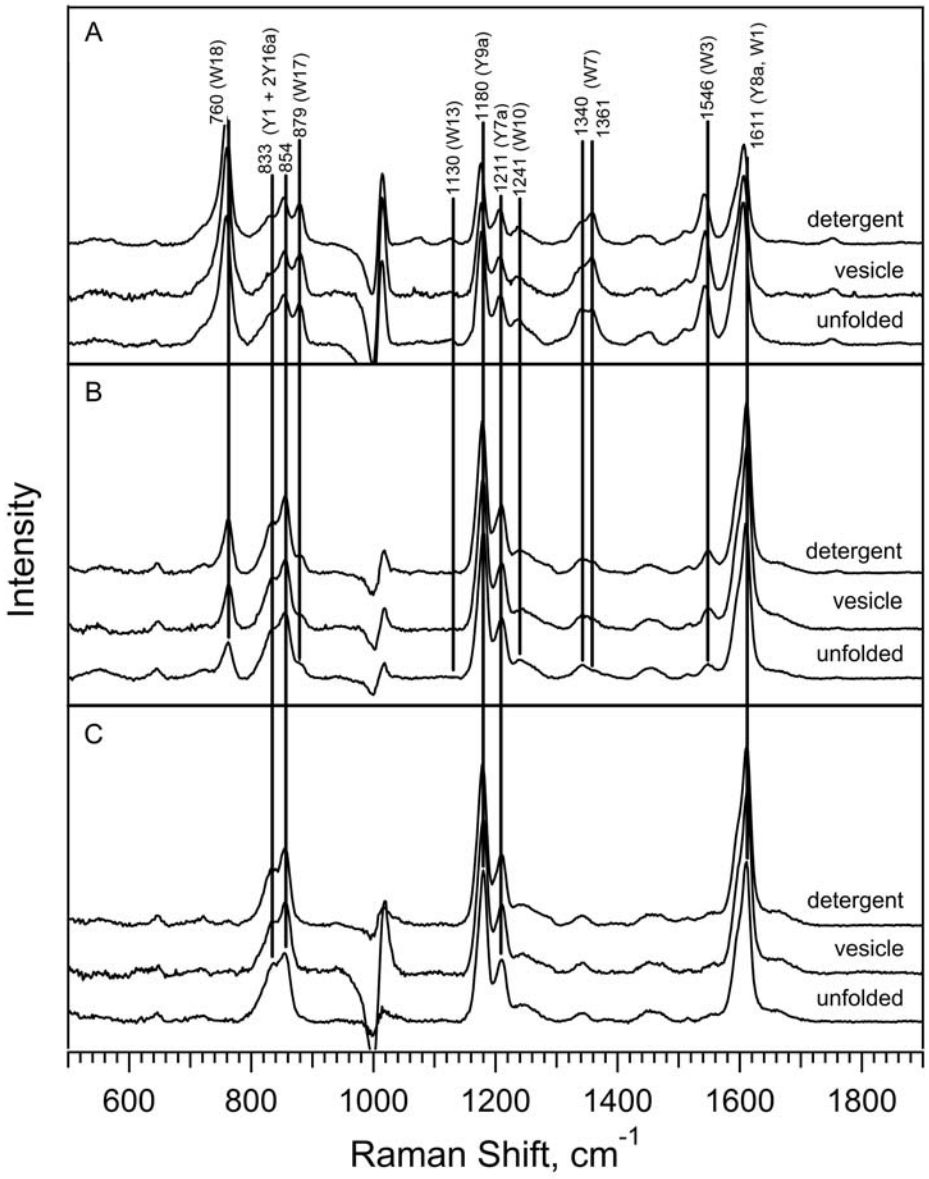

Figure 5.3: Corrected UVRR spectra of WT OmpA (A), W57 OmpA (B), and W0 OmpA (C) folded in detergent, folded in vesicle, and unfolded in KP_i buffer, at 230-nm excitation. Trp and tyr peaks are indicated. The feature near 1000 cm^{-1} is due to incomplete subtraction of the large urea peak.

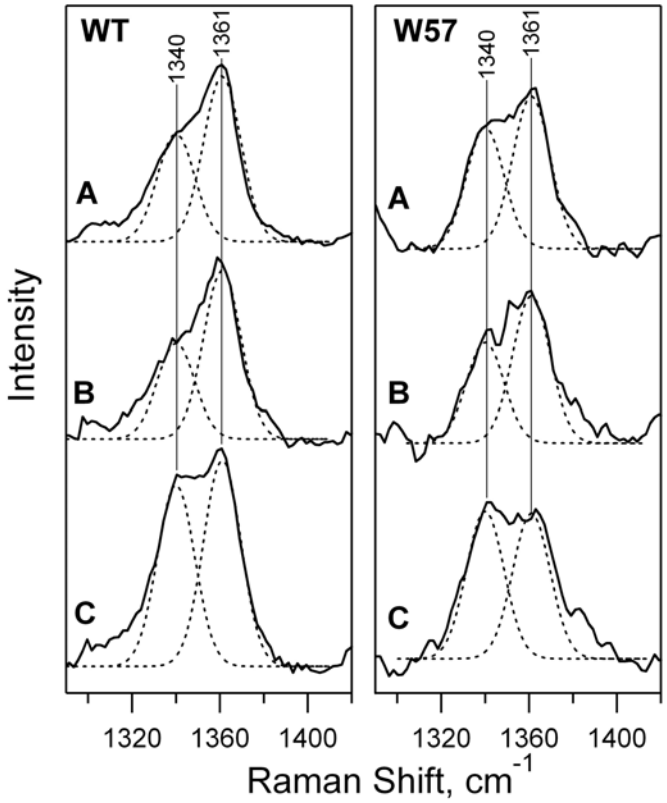

Figure 5.4: Expanded region of W7 Fermi doublet for wild type (WT; left) and Trp-57 (W57; right) OmpA folded in detergent (A), folded in vesicle (B), and unfolded in KP_i buffer (A). Tyrosine and protein signal observed in Trp-less spectra were removed. Gaussian decompositions are indicated by the dotted curves.

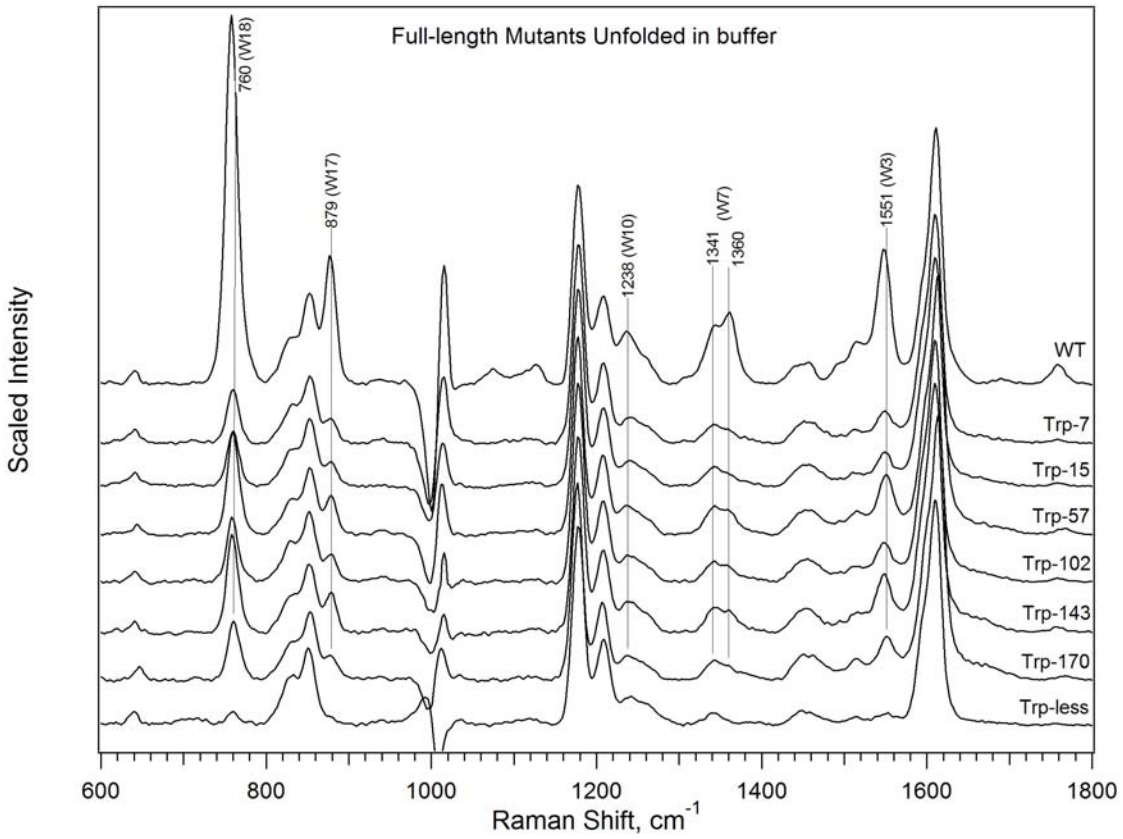

Figure 5.5: Corrected UVRR spectra of wild type (WT), full-length single-trp mutants, and trp-less mutants unfolded in phosphate buffer, at 228-nm excitation. Select trp peaks are indicated. The large feature at ~1000 cm^{-1} is due to incomplete subtraction of urea.

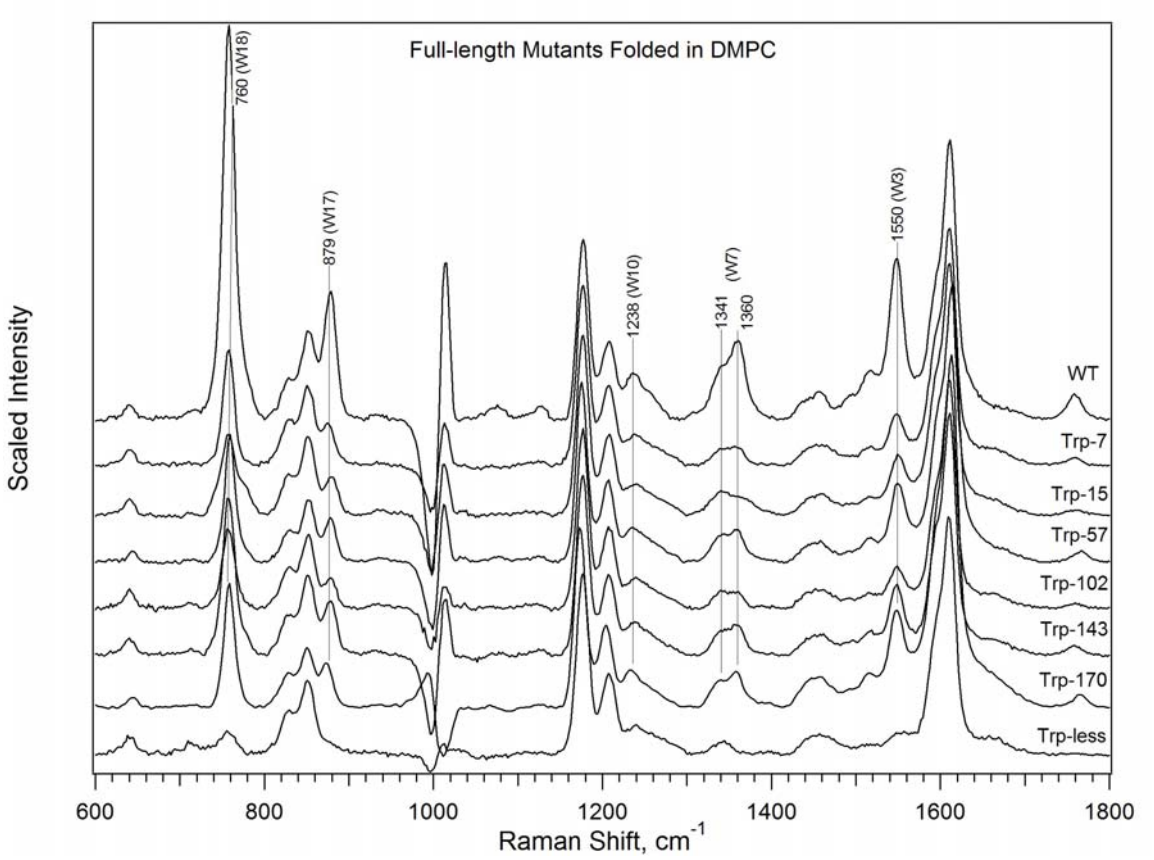

Figure 5.6: Corrected UVRR spectra of wild type (WT), full-length single trp mutants, and trp-less mutant folded in DMPC vesicles, at 228-nm excitation. Select trp peaks are indicated. The large feature at ~1000 cm^{-1} is due to incomplete subtraction of urea.

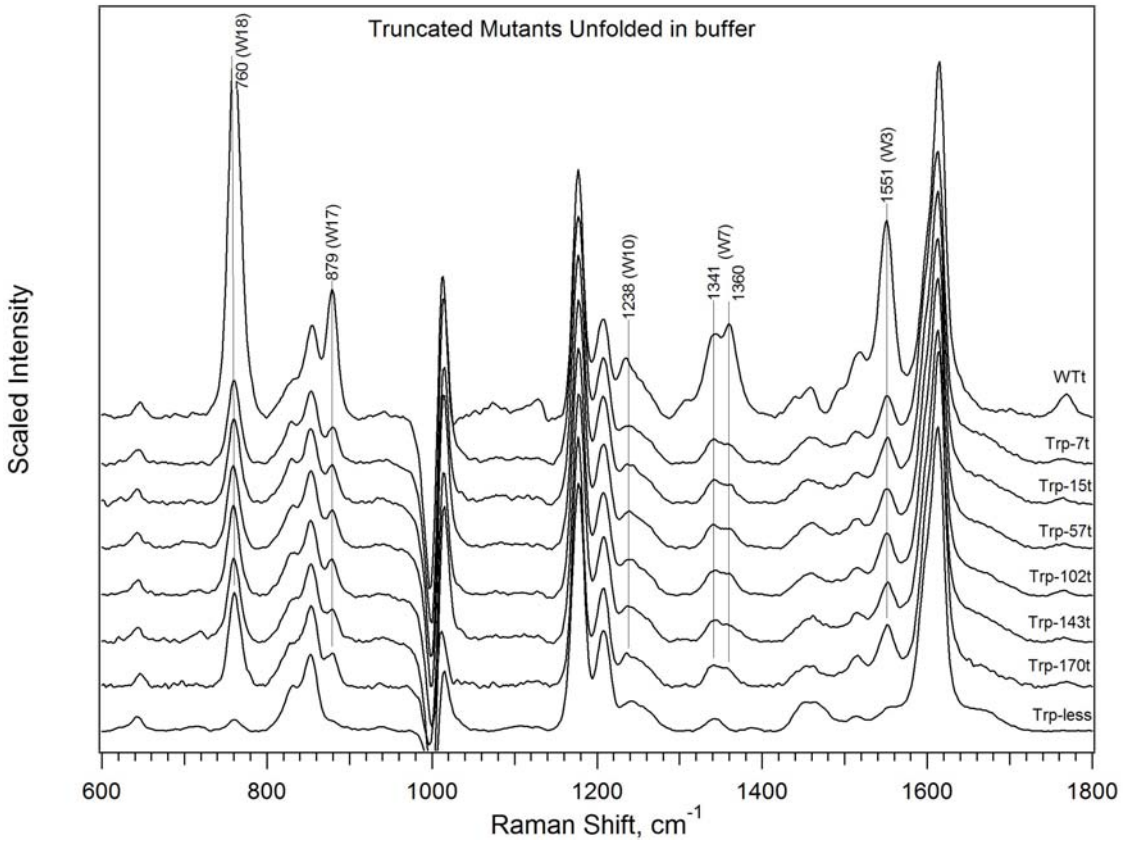

Figure 5.7: Corrected UVRR spectra of truncated wild type, truncated single-trp mutants, unfolded in phosphate buffer, at 228-nm excitation. The full-length trp-less mutant is shown for comparison. Select trp modes are indicated. The large feature at ~1000 cm^{-1} is due to incomplete subtraction of urea.

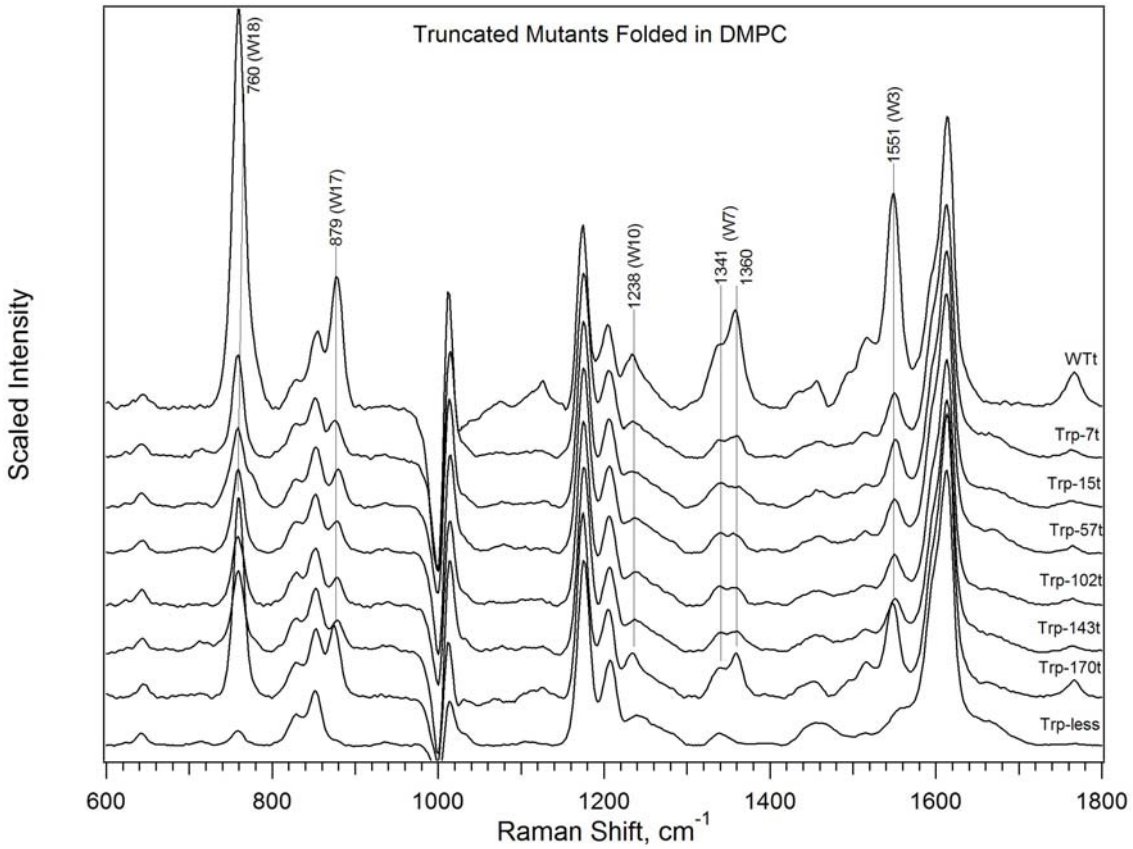

Figure 5.8: Corrected UVRR spectra of truncated wild type, truncated single-trp mutants, folded in DMPC vesicles, at 228-nm excitation. The full-length trp-less mutant is shown for comparison. Select trp modes are indicated. The large feature at ~1000 cm^{-1} is due to incomplete subtraction of urea.

Table 5.1: Trp mode frequencies of unfolded (U) and folded (F) full-length mutants at 228-nm excitation. All frequencies are reported in cm^{-1}. The $R_{W17:W18}$ is the ratio of intensities of the W17 mode and the W18 mode. The R_{FD} is the ratio of the W7 Fermi doublet. Fluorescence λ_{max} is also included.

Full-length Protein	W18	W17	$R_{W17:W18}$	R_{FD}	W3	λ_{max}
Trp-7 (U)	758	879	0.46	1.0	1549	354
Trp-7 (F)	758	875	0.36	1.9	1549	327
Trp-15 (U)	760	881	0.44	1.1	1549	353
Trp-15 (F)	758	881	0.47	1.2	1549	333
Trp-57 (U)	759	879	0.38	1.3	1551	353
Trp-57 (F)	759	879	0.35	1.9	1549	335
Trp-102 (U)	758	879	0.43	1.3	1547	352
Trp-102 (F)	758	879	0.37	1.5	1549	332
Trp-143 (U)	758	879	0.41	1.1	1549	352
Trp-143 (F)	758	879	0.35	1.8	1549	333
Trp-170 (U)	760	879	0.42	1.3	1551	352
Trp-170 (F)	760	875	0.35	1.9	1549	327
WT (U)	758	877	0.35	1.4	1547	350
WT (F)	758	879	0.33	1.8	1549	336

Table 5.2: Trp mode frequencies of unfolded (U) and folded (F) truncated mutants at 228-nm excitation. All frequencies are reported in cm^{-1}. The $R_{W17:W18}$ is the ratio of intensities of the W17 mode and the W18 mode. The R_{FD} is the ratio of the W7 Fermi doublet. Fluorescence λ_{max} is also included.

Truncated Protein	W18	W17	$R_{W17:W18}$	R_{FD}	W3	Fluor Max
Trp-7t (U)	760	879	0.44	1.2	1552	354
Trp-7t (F)	760	877	0.35	2.0	1550	329
Trp-15t (U)	760	879	0.46	1.2	1552	353
Trp-15t (F)	760	879	0.48	1.2	1550	332
Trp-57t (U)	760	879	0.47	1.5	1552	351
Trp-57t (F)	760	879	0.37	1.8	1550	332
Trp-102t (U)	760	879	0.40	1.3	1552	351
Trp-102t (F)	760	879	0.40	1.7	1550	332
Trp-143t (U)	760	879	0.39	1.5	1552	354
Trp-143t (F)	760	879	0.38	1.9	1550	335
Trp-170t (U)	760	881	0.34	1.8	1551	350
Trp-170t (F)	760	875	0.36	2.1	1547	329
WTt (U)	760	879	0.33	1.3	1551	352
WTt (F)	760	879	0.33	1.9	1549	335

Table 5.3: Tyrosine mode frequencies of unfolded (U) and folded (F) full-length mutants at 228-nm excitation. All frequencies are reported in cm^{-1}. The ratio of intensities of the Y1 and 2Y16a modes is indicated, $R_{Y1:2Y16a}$.

Full-length Protein	Y1, 2Y16a	$R_{Y1:2Y16a}$	Y9a	Y7a	Y8a
Trp-7 (U)	835, 855	0.59	1179	1209	1611
Trp-7 (F)	833, 855	0.56	1177	1209	1611
Trp-15 (U)	833, 855	0.65	1179	1209	1611
Trp-15 (F)	831, 855	0.50	1177	1209	1611
Trp-57 (U)	833, 853	0.53	1177	1207	1612
Trp-57 (F)	833, 853	0.49	1176	1207	1612
Trp-102 (U)	831, 853	0.55	1177	1209	1613
Trp-102 (F)	831, 853	0.54	1175	1207	1613
Trp-143 (U)	833, 855	0.56	1177	1207	1609
Trp-143 (F)	831, 853	0.51	1177	1207	1611
Trp-170 (U)	833, 853	0.57	1177	1207	1613
Trp-170 (F)	831, 851	0.55	1177	1207	1613
WT (U)	833, 855	0.52	1177	1209	1611
WT (F)	831, 853	0.45	1177	1207	1611
Trp-less (U)	833, 853	0.64	1179	1209	1611
Trp-less (F)	831, 855	0.61	1179	1209	1611

Table 5.4: Tyrosine mode frequencies of unfolded (U) and folded (F) truncated mutants at 228-nm excitation. All frequencies are reported in cm^{-1}. The ratio of intensities of the Y1 and 2Y16a modes is indicated, $R_{Y1:2Y16a}$.

Truncated Protein	Y1, 2Y16a	$R_{Y1:2Y16a}$	Y9a	Y7a	Y8a
Trp-7t (U)	833, 855	0.57	1179	1209	1611
Trp-7t (F)	831, 855	0.56	1177	1209	1609
Trp-15t (U)	833, 855	0.57	1179	1209	1611
Trp-15t (F)	829, 853	0.49	1177	1209	1611
Trp-57t (U)	831, 853	0.56	1177	1207	1611
Trp-57t (F)	831, 853	0.53	1177	1207	1613
Trp-102t (U)	831, 853	0.53	1177	1209	1613
Trp-102t (F)	829, 853	0.55	1175	1207	1613
Trp-143t (U)	831, 853	0.55	1177	1207	1613
Trp-143t (F)	831, 853	0.52	1177	1207	1613
Trp-170t (U)	830, 853	0.57	1177	1207	1615
Trp-170t (F)	830, 853	0.53	1175	1205	1613
WTt (U)	833, 855	0.42	1177	1207	1615
WTt (F)	831, 855	0.36	1175	1205	1613

5.7 References

(1) Ash, W. L.; Zlomistic, M. R.; Oloo, E. O.; Tieleman, D. P. *Biochim. Biophys. Acta* **2004**, *1666*, 158.

(2) Bond, P. J.; Cutherbertson, J. M.; Deol, S. S.; Sansom, M. S. P. *J. Am. Chem. Soc.* **2004**, *126*, 15948.

(3) Booth, P. J.; Templer, R. H.; Meijberg, W.; Allen, S. J.; Curran, A. R.; Lorch, M. *Crit. Rev. in Biochem. and Mol. Biol.* **2001**, *36*, 501.

(4) White, S. H.; Wimley, W. C. *Annu. Rev. Biophys. Biomol. Struct.* **1999**, *28*, 319.

(5) MacKenzie, K. R. *Chem. Rev.* **2006**, *106*, 1931.

(6) Lee, A. G. *Biochim. Biophys. Acta* **2003**, *1612*, 1.

(7) Hong, H.; Tamm, L. K. *Proc. Natl. Acad. Sci. U.S.A.* **2004**, *101*, 4065.

(8) Sanchez, K. M.; Gable, J. E.; Schlamadinger, D. E.; Kim, J. E. *Biochemistry* **2008**, *47*, 12844.

(9) Kleinschmidt, J. H.; den Blaauwen, T.; Driessen, A. J. M.; Tamm, L. K. *Biochemistry* **1999**, *38*, 5006.

(10) Surrey, T.; Jahnig, F. *Proc. Natl. Acad. Sci. U.S.A.* **1992**, *89*, 7457.

(11) Kim, J. E.; Arjara, G.; Richards, J. H.; Gray, H. B.; Winkler, J. R. *J. Phys. Chem. B* **2006**, *110*, 17656.

(12) Ramakrishnan, M.; Qu, J.; Pocanschi, C. L.; Kleinschmidt, J. H.; Marsh, D. *Biochemistry* **2005**, *44*, 3515.

(13) Dornmair, K.; Kiefer, H.; Jahnig, F. *J. Biol. Chem.* **1990**, *265*, 18907.

(14) Pocanschi, C. L.; Patel, G. J.; Marsh, D.; Kleinschmidt, J. H. *Biophys. J.* **2006**, *91*, L75.

(15) Ahmed, A.; Beta, I. A.; Mikhonin, A. V.; Asher, S. A. *J. Am. Chem. Soc.* **2005**, *127*, 10943.

(16) Chi, Z.; Asher, S. A. *Biochem.* **1999**, *38*, 8196.

(17) Rodriguez-Mendieta, I. R.; Spence, G. R.; Gell, C.; Randford, S. E.; Smith, D. A. *Biochem.* **2005**, *44*, 3306.

(18) Huang, C. Y.; Balakrishnan, G.; Spiro, T. G. *Biochem.* **2005**, *44*, 15734.

(19) Rodgers, K. R.; Su, C.; Subramaniam, S.; Spiro, T. G. *J. Am. Chem. Soc.* **1992**, *114*, 3697.

(20) Jayaraman, V.; Rodgers, K. R.; Mukerji, I.; Spiro, T. G. *Science* **1995**, *269*, 1843.

(21) Kochendoerfer, G. G.; Kaminaka, S.; Mathies, R. A. *Biochem.* **1997**, *36*, 13153.

(22) Kim, J. E.; Pan, D. H.; Mathies, R. A. *Biochem.* **2003**, *42*, 5169.

(23) Mizuno, M.; Hamada, N.; Tokunaga, F.; Mizutani, Y. *J. Phys. Chem. B* **2007**, *111*, 6293.

(24) Sato, A.; Gao, Y.; Kitagawa, T.; Mitzutani, Y. *Proc. Natl. Acad. Sci. U.S.A.* **2007**, *104*, 9627.

(25) Austin, J. C.; Jordan, T.; Spiro, T. G. *Ultraviolet Resonance Raman Studies of Proteins and Related Model Compounds*; John Wiley and Sons: New York, 1993.

(26) Harada, I.; Takeuchi, H. *Raman and Ultraviolet Resonance Raman Spectra of Proteins and Related Compounds*; John Wiley & Sons, Ltd.: Chichester, 1986; Vol. 13.

(27) Huang, C. Y.; Balakrishnan, G.; Spiro, T. G. *J. Ram. Spect.* **2006**, *37*, 277.

(28) Chi, Z.; Asher, S. A. *J. Phys. Chem. B* **1998**, *102*, 9595

(29) Fodor, S. P. S.; Copeland, R. A.; Grygon, C. A.; Spiro, T. G. *J. Am. Chem. Soc.* **1989**, *111*, 5509.

(30) Sweeney, J. A.; Asher, S. A. *J. Phys. Chem.* **1990**, *94*, 4784.

(31) Efremov, R. G. F., A.V. ; Nabiev, I.R. *Journal of Raman Spectroscopy* **1992**, *23*, 69.

(32) Miura, T. T., H. ; Harada, I. *Biochemistry* **1988**, *27*, 88.

(33) Miura, T. T., H. ; Harada, I. *Journal of Raman Spectroscopy* **1989**, *20*, 667.

(34) Babakhani, A.; Gorfe, A. A.; Gullingsrud, J.; Kim, J. E.; McCammon, J. A. *Biopolymers* **2007**, *85*, 490.

(35) Hong, H.; Park, S.; Flores Jimenez, R. H.; Rinehart, D.; Tamm, L. K. *J. Am. Chem. Soc.* **2007**, *129*, 8320.

(36) Wimley, W. C.; Creamer, T. P.; White, S. H. *Biochemistry* **1996**, *35*, 5109.

(37) Yau, W.-M.; Wimley, W. C.; Gawrisch, K.; White, S. H. *Biochemistry* **1998**, *37*, 14713.

(38) Pautsch, A.; Schulz, G. E. *Nat. Struct. Biol.* **1998**, *5*, 1013.

(39) Pautsch, A.; Schulz, G. E. *J. Mol. Biol.* **2000**, *298*, 273.

(40) Schlamadinger, D. E.; Gable, J. E.; Kim, J. E. *J. Phys. Chem.* **2009**, *accepted*.

Chapter 6

Evolution of molecular changes of trp residues in OmpA: A UV resonance Raman folding kinetics study

6.1. Introduction

Proteins are known to spontaneously fold *in vivo* into the native conformation. All of the necessary information to correctly fold into its native structure is contained in the protein primary sequence.[1] But, how is it possible for a polypeptide chain to fold into its functional form on a biologically relevant timescale? And by what mechanism does the protein fold?

Its *in vivo* folding mechanism is assisted by molecular chaperones and folds on a very fast time scale.[2] However, the *in vitro* folding mechanism of OmpA into synthetic lipid bilayers occurs on a much slower timescale (~100 minutes).[3-5] Its *in vitro* folding mechanism is thought to occur in three stages: First, the hydrophobic collapse of protein in aqueous solution (seconds), followed by adsorption onto the membrane surface (minutes), and the final step includes a concerted folding/insertion mechanism into the membrane to its final native structure (~ hour).[6] This mechanism is described in Figure 1.5. Detailed folding and insertion kinetics experiments have lead to the discovery of folding intermediates in OmpA, some of which have been attributed to the above folding stages.[4,7-10]

Despite the wealth of knowledge gained from previous folding studies on OmpA, critical molecular information, such as the intermolecular interactions that stabilize the

protein during the folding/insertion process and relevant timescales are still missing. UVRR spectroscopy is a powerful technique that can provide this molecular detail. Changes in trp environmental hydrophobicity, hydrogen bonding, and dihedral torsion angle about the protein backbone can be monitored using this technique.[11-15] Significant changes occur in trp environment in OmpA during the folding process as the protein inserts into the complex water-bilayer interface and folds to its final structure in the hydrophobic lipid bilayer. Applying UVRR kinetics to the folding/insertion mechanism of OmpA will allow us to determine the interactions of anchoring trp residues on the relevant timescales.

As determined in Chapter 5, the first UVRR steady-state spectra of a membrane protein in highly scattering synthetic lipid bilayers were collected of wild type and the single-trp mutants of OmpA.[16] The UVRR data showed modest changes in the trp vibrational modes between unfolded and folded states of different single-trp mutants. To probe these environment-dependent changes over the folding timescale, UVRR spectra of single-trp mutants were collected at different time points during the folding and insertion process. The current kinetics study expands on the previous work by monitoring UVRR changes during folding/insertion into vesicles. In addition to folding kinetics experiments, an adsorbed form of the protein was probed to determine the relationship, if any, between the folding pathway and this adsorbed intermediate.

The single-trp mutants under investigation in this paper are three native trp residues Trp-7, Trp-15, Trp-102, and one non-native trp residue Trp-170. These single-trp mutants were chosen due to unique environment and/or the thermodynamic properties determined from our previous work.[17] Trp-7 and Trp-170 are located on the bottom of

the β-barrel, on the N-terminus and C-terminus, respectively. Trp-15 is located on the top of the β-barrel and has a likely hydrogen bonding partner with a residue on a neighboring strand. Trp-102 is also located on the top of the barrel, but is the only trp residue located on a loop and that faces the interior of the barrel. Each trp will likely experience different environmental changes and/or folding timescales due to these unique locations. The trp residues located at the top of the barrel (Trp-15 and Trp-102) insert and traverse through the center of the bilayer, while the trp residues located on the bottom of the barrel (Trp-7, and conceivably Trp-170) remain on one side of the lipid bilayer and do not cross the bilayer center during the folding process.[10] Truncated versions of the single-trp mutants were also studied to determine how the folding and insertion mechanism is affected by the presence/absence of the soluble tail, which encompasses roughly half of the protein.

6.2. Experimental Methods

6.2.1 Preparation of small unilamellar vesicles

Small unilamellar vesicles (SUVs) of diameter ~50 nm were prepared using a previously published procedure and is discussed in detail in Chapter 2.[17,18] Different SUV solutions were made for different folding conditions of OmpA: OmpA folds into DMPC (1,2-dimyristoyl-*sn*-glycero-3-phosphocholine) SUVs; OmpA adsorbs onto DPPC (1,2-dipalmitoyl-sn-glycerocholine) SUVs; and 7:3 DMPC:DMPE (1,2-dimyristoyl-*sn*-glycero-3-phosphoethanolamine) SUVs were used for biologically relevant lipid head groups (PE).[19] SUV solutions were diluted to a final lipid concentration of 1 mg/mL in 20 mM KP_i buffer for all experiments. Vesicle solutions containing DMPC lipids were equilibrated overnight at 35 ^{0}C, and used the following day. Vesicle solutions containing

DPPC or 7:3 DMPC:DMPE lipids were made the morning of experiments. DPPC lipid solutions were equilibrated at room temperature for 30 minutes prior to spectroscopic measurements to ensure gel-phase vesicles for protein adsorption studies.

6.2.2 Preparation of unfolded, adsorbed, and folded OmpA Mutants

Unfolded OmpA mutants were made by dilution of stock (unfolded) protein into 20 mM KP_i buffer (no vesicles). Spectra of unfolded protein in KP_i were collected immediately after addition of unfolded protein to buffer to prevent aggregation of protein. Adsorbed OmpA mutants were made by dilution of stock protein into buffer solution containing DPPC vesicles at 23 ºC, which is below the phase transition temperature of DPPC lipids, and were equilibrated at room temperature for 30 minutes prior to spectroscopic measurements. For folding into DMPC vesicles, individual DMPC solutions (no protein) were made for each time point and equilibrated overnight at 37 ºC. The folding process was initiated by addition of stock unfolded protein into DMPC vesicles. Spectra were collected immediately (t = 0 min) or incubated at 37 ºC until the appropriate time point. Adsorbed forms of the protein were verified using fluorescence spectroscopy and SDS-PAGE gel electrophoresis. The adsorbed protein has an apparent molecular weight of ~35 kDa on the gels, similar to the unfolded protein, but different from folded protein (~30 kDa). The fluorescence maximum was ~340 nm for adsorbed protein, compared to ~350 nm for unfolded protein, or ~330 nm for folded protein. Protein samples and blanks containing DMPC:DMPE vesicle mixtures were equilibrated at 50 ºC for 3 hours to ensure equilibrium conditions.

6.2.3 Fluorescence and absorption measurements.

Details of fluorescence and absorbance measurements are discussed in detail in Chapter 2, and will be briefly discussed here. Fluorescence measurements were collected using 290-nm excitation, for all sample and blank solutions, at the same time points as the UVRR spectra (see below). Sample and blank solutions containing DMPC vesicles were kept above 30 ºC, which is greater than the phase transition temperature of DMPC. Sample and blank solutions containing DPPC vesicles were kept at 23 ºC, which is lower than the phase transition temperature of DPPC. Sample and blank solutions containing DMPC:DMPE vesicle mixtures were collected at 50 ºC, which is above the phase transition temperature of DMPE vesicles.

Absorbance measurements were collected of all protein and blank samples. Protein concentrations were nominally ~ 20 μM in all samples, using molar absorptivities in Chapter 2. Spectral contribution from buffer and vesicles was subtracted from protein containing samples using Igor Pro data analysis software (WaveMetrics).

6.2.4 UVRR measurements.

A detailed description of the Raman instrumentation can be found in Chapter 2. UVRR spectra were collected of the full-length (and truncated) single trp mutants, Trp-7(t), Trp-15(t), Trp-102-(t), and Trp-170(t), and Trp-less, at different time points after initiation of folding into DMPC bilayers. UVRR spectra were collected at the following time points of t = 0, 20, 40, 60, and 180 minutes after addition of protein to DMPC vesicle solution. Steady-state UVRR spectra of unfolded and adsorbed forms of the protein were also collected. UVRR spectra were collected of blank solutions (with and without urea) to remove spectral contributions from quartz capillary, buffer, and urea from protein containing samples. Each sample and blank UVRR spectrum was collected

for a total of five minutes. UVRR spectra were collected at the time points corresponding to t = 1-6 min, 20-25min, 40-45 min, 60-65 min, and 180-185 min following initiation of the folding event. Each one-minute spectrum was compared to the previous to confirm that no variation was observed during the 5 minute collection window.

6.3 Results

6.3.1 Steady-state UVRR spectra of full-length trp mutants of OmpA

As a reminder, tryptophan residues in general will be referred to as *trp*; the single-trp OmpA mutants will be referred to as *Trp-X* (e.g. Trp-7); the tryptophan vibrational modes in the UVRR spectra will be referred to as *WX* (e.g. W18). Figure 6.1 shows the steady-state UVRR spectra for the trp mutants Trp-7, Trp-15, Trp-102, and Trp-170, and the Trp-less mutant unfolded in KP_i buffer (6.1.A) and folded in DMPC vesicles (6.1.B) after subtraction of the appropriate buffer. The feature found at ~1000 cm^{-1} is due to incomplete subtraction of the urea. All spectra have been scaled to the intensity of the Y9a mode (~1177 cm^{-1}), which does not change significantly between unfolded and folded protein. Isolated tyr (Y) modes are observed in the Trp-less mutant and the single-trp mutants, and appear at ~833 and ~853 cm^{-1} (Y1 + 2Y16a), ~1177 cm^{-1} (Y9a), ~1209 cm^{-1} (Y7a), and ~1611 cm^{-1} (Y8a, with strong overlap of the trp mode W1). The vibrational modes for the unique trp residues located at position 7, 15, 102, and 170 in the primary sequence are clearly distinguishable from the tyr modes, and are found at ~ 760 cm^{-1} (W18), ~ 880 cm^{-1} (W17), ~1240 cm^{-1} (W10), ~1340/1360 cm^{-1} (W7), ~1550 cm^{-1} (W3), and ~1611 cm^{-1} (W1 with strong overlap with Y8a). Minimal changes were observed with the seventeen tyrosines between unfolded, adsorbed, and folded protein and will not be discussed further.

There are modest differences in trp modes frequencies and intensities between the unfolded and folded UVRR spectra of the single-trp mutants. The trp modes that are useful markers are the W17, W7, and W3 modes. Tabulated frequencies for select tyr and trp modes from the steady-state spectra are found in Table 6.1. The W17 mode frequency is often used a hydrogen bonding marker for the trp N_1H group.[13] Frequencies of ~875 cm^{-1} correlate to strong H-bonding, ~878 cm^{-1} correlates to medium H-bonding, and ~880 cm^{-1} correlates to weak-to-no H-bonding. The steady-state spectra of Trp-7 and Trp-170 show the largest decrease in frequency, - 4 cm^{-1}, when folded in vesicle, to a final value of 877 cm^{-1} and 875 cm^{-1}, respectively. There is also a small decrease in the W17 mode frequency for Trp-102 to a value of 877 cm^{-1} when folded in vesicle. Trp-15 has a value of 881 cm^{-1} in both unfolded and folded protein.

The W7 mode is a sensitive marker for trp environmental hydrophobicity.[12] The ratio of the intensities of the Fermi doublet, R_{FD} (I_{1360}/I_{1340}), is larger when trp is in a more hydrophobic environment. R_{FD} values obtained for model compound using 514.5 nm excitation are < 1.0 for trp in aqueous solvents, 1.02-1.11 for trp in benzene, and 1.23-1.32 for trp in saturated hydrocarbons. The R_{FD} values determined for the trp residues in OmpA all increase with varying degrees when the protein is folded in vesicle. Trp-7 and Trp-170 report the largest values at 1.9 when folded in buffer, followed by Trp-102 at 1.5, and Trp-15 at 1.2.

Another mode that is frequently used as a structural marker in proteins is the W3 mode. The W3 mode is used as a conformational marker, and its frequency reflecting the dihedral torsion angle, $\chi^{2,1}$, about the C2-C3-Cβ-Cα linkage.[14] Minimal changes are observed in frequency between unfolded and folded protein, within 2 cm^{-1}, which is our

experimental error. The W3 mode frequencies obtained for the folded protein correlate to torsion angles of 90º, 96º, 100º, and 90º for Trp-7, Trp-15, Trp-102, and Trp-170, respectively. The values obtained from the crystal structure show deviation from those determined from UVRR and report values of 83º, 45º, and 93º, for Trp-7, Trp-15, and Trp-102, respectively. Trp-170 is a non-native trp residue and does not have a known crystal structure, therefore the dihedral angle is not known.

6.3.2 UVRR kinetics spectra of Trp-15

Representative UVRR kinetics spectra are shown in Figure 6.2 for the single trp mutant, Trp-15, highlighting three regions of interest, the W18 mode, the W17 mode, and the W7 mode. The steady-state UVRR spectra of Trp-15 unfolded in KP_i buffer and adsorbed on DPPC vesicles are shown on the top graphs for comparison; the kinetics spectra of Trp-15 folding into DMPC vesicles at different time points (t = 0 , 20, 40, 60, and 180 min) are shown below. The spectrum of Trp-15 in DMPC vesicles at 180 minutes is the steady-state folded form of the protein. Spectra have been corrected for buffer contribution, and scaled to the intensity of the Y9a peak. The location of Trp-15 in OmpA is shown in Figure 6.3, highlighting the location 2 neighboring residues, Gln17 and Asn33.

A shoulder appears on the high frequency side of the W18 mode at ~778 cm^{-1}. The spectra have been decomposed into two Gaussian peaks centered at 760 cm^{-1} and 778 cm^{-1}. This shoulder is visible in the spectra by the 20 minute time point and increases in intensity during the folding process until the final folded structure at 180 minutes. The W17 mode appears at ~881 cm^{-1} at all time points in the folding process. This frequency indicates weak/no hydrogen bonding of the indole N_1H.

The R_{FD} values in the steady-state spectra are 1.1 and 1.2 for unfolded and folded protein, respectively. The R_{FD} values showed minimal change during the folding process in DMPC vesicles at the different time points, and remains at ~1.1. The largest R_{FD} was found in the adsorbed form, with a value of 1.3. The W7 mode frequencies also show distinct shifts and become broader during the folding process. The W7 mode was decomposed into Gaussian fits, shown as dashed gray lines, in the right panel of Figure 6.2. Unfolded Trp-15 had W7 frequencies of 1343 cm^{-1} and 1363 cm^{-1}, with FWHM values of ~18 cm^{-1}. These peaks moved away from each other and became increasingly broad during later time points in the folding process. The frequencies of these peaks in the folded protein were 1336 cm^{-1} (-7 cm^{-1} vs. unfolded) and 1366 cm^{-1} (+3 cm^{-1} vs. unfolded), with FWHM values ~30 cm^{-1} (+12 cm^{-1}) for both peaks. Table 6.2 shows the R_{FD} values, the W7 mode frequencies, and FWHM values from the Gaussian fits during the folding process. The peaks start to shift and broaden by the t = 20 min in the folding process, followed by another change occurring between the 40 min and 60 min spectra. The peak frequencies and widths do not change after the 60 min time point. Tabulated trp mode frequencies of Trp-15 from the kinetics studies are found in Table 6.3.

6.3.3 UVRR kinetics spectra of Trp-7

The location of Trp-7 in the crystal structure of OmpA is shown in Figure 6.4, showing its location in the membrane, with distances to neighboring aromatic residues. The UVRR kinetics spectra collected of Trp-7 and are shown in Figure 6.5. All spectra were corrected for buffer contribution and baseline subtraction, and were scaled to the Y9a peak at ~1179 cm^{-1}.

The W17 mode shifts to lower frequencies during the folding process; this frequency shift is shown in Figure 6.6. The W17 mode unfolded in buffer has a value of 881 cm^{-1} and remains at this value immediately after addition of protein to DMPC vesicles (t = 0 min). The frequency shifts to 879 cm^{-1} by t = 20 min in the folding process, and further shifts to 877 cm^{-1} by t = 60 min into the folding process. No further change in position is observed between 60 min and 180 min in the folding process.

UVRR difference spectra of the W7 Fermi doublet region are shown in the left panel of Figure 6.7. Contribution from the 17 native tyrosine residues was removed by subtraction of the Trp-less mutant, resulting in the tyrosine-free difference spectra. The Fermi doublet was decomposed into two Gaussian peaks, shown as dashed gray lines. Trp-7 has a R_{FD} value of 1.0 and 1.1, unfolded in buffer, and adsorbed to DPPC vesicles, respectively. Immediately after initiation of folding in vesicle, this value increases to 1.3. By the 40 min time point, the R_{FD} ratio increased to 1.6, and reaches a final value of 1.9 in the folded form of the protein, by t = 180 min. Tabulated UVRR frequencies and intensity ratios for Trp-7 are found in Table 6.3. Peak frequencies remain within our experimental error.

6.3.4 UVRR kinetics spectra of Trp-170

Trp-170 is a non-native trp mutant located near the soluble domain of the protein. Its location in the crystal structure is shown in Figure 6.4. Trp-170 mutant has a single trp residue at position 170, with a phenylalanine residue located at position 7. The UVRR kinetics spectra were collected for Trp-170 at different time points in the folding process. UVRR spectra for Trp-170, in different buffer conditions and the kinetics spectra, are similar to those obtained for Trp-7 mutant and will not be shown here.

Tabulated UVRR frequencies and intensity ratios for the trp modes of Trp-170 at the different time points are found in Table 6.3.

When Trp-170 is unfolded in buffer, or adsorbed to DPPC vesicles, the W17 mode frequency is at 879 cm^{-1}. By t = 20 min, the peaks shifts to 875 cm^{-1}, and remains at this value for the duration of the folding process. No further change is observed for this mode for the remainder of the folding process.

The difference spectra to isolate the W7 mode Fermi doublets for Trp-170, are shown in accompanying panel (right) of Figure 6.7. The W7 mode was decomposed into two Gaussian peaks, shown in dashed gray lines. The R_{FD} of Trp-170 unfolded in buffer has a value of 1.3 and increases to a value of 1.5 immediately after addition of unfolded protein to vesicle (t = 0 min). The R_{FD} continues to increase in small increments from 1.3 to 1.9 for the duration of the folding process. The R_{FD} has a final value of 1.9 in the folded protein.

6.3.5 UVRR kinetics spectra of Trp-102

The location of Trp-102 in the crystal structure of OmpA is shown in Figure 6.8, and shows the residues immediately surrounding the trp residue. The UVRR kinetics spectra for Trp-102 show similar trp and tyr mode frequencies found in the UVRR kinetics spectra for the other single-trp mutants; the full UVRR spectra for Trp-102 will not be shown. The W17 mode shifts during the folding process. The frequency remains at 879 cm^{-1} for Trp-102 unfolded in buffer, adsorbed in DPPC vesicles, and during the first 20 minutes in the folding process in DMPC vesicles. The W17 mode shifts to 877 cm^{-1} by t = 40 min in the folding process and remains at this frequency for the duration of the folding process. The isolated W7 Fermi doublets for the UVRR kinetics experiments

for Trp-102 are shown in the left panel in Figure 6.8. The Fermi doublets for the corresponding spectra of the truncated mutant, Trp-102t, are shown for comparison. The R_{FD} values increase from 1.3 for unfolded protein to 1.5 for completely folded protein. During the course of the folding timescale, the R_{FD} increased from 1.3 at initiation of folding to a value of 1.4 at t = 20 min. Another increase was observed at t = 60 min, from 1.4 to 1.5. The adsorbed protein had the lowest R_{FD} with a value of 1.1. Tabulated frequencies of trp modes for the Trp-102 mutants are found in Table 6.3.

6.3.6 UVRR kinetics spectra of truncated OmpA mutants

UVRR kinetics and steady-state spectra were collected for the corresponding truncated single-trp mutants Trp-7t, Trp-15t, Trp-102t, and Trp-170t. UVRR spectra were collected for these proteins unfolded in buffer, adsorbed onto DPPC vesicles, and taken at different time points during the folding process into DMPC vesicles (t = 0 – 180 min). Representative UVRR spectra of the truncated mutant, Trp-15t, are shown in Figure 6.10. Tabulated UVRR trp mode frequencies and intensity ratios, along with tryptophan emission maxima, can be found in Table 6.4 for all the truncated mutants studied here. It is worthwhile to note that the shoulder on the W18 mode is seen in the UVRR spectrum of Trp-15t folded in vesicle. Other changes observed for full-length protein are generally reproduced for the truncated counterparts.

6.4 Discussion

Non-covalent interactions are the main driving force behind formation of protein secondary structure and are crucial to the stability of proteins in the membrane.[17,20] These interactions can occur between neighboring amino acid residues, in close proximity in the primary sequence or quite distant along the polypeptide chain, and can

also occur between amino acid residues and the lipid bilayer.[1,7,21] These interactions include a variety of hydrogen bonds between amino acid side-chains and protein backbone, energetic contributions from residues partitioning into the lipid bilayer, and electrostatic and nonpolar interactions.[22-27]

Non-covalent interactions were investigated in OmpA (Chapter 3), to determine their affects on the thermodynamic stability of different mutants.[17] From these thermodynamic studies, it was determined that pairwise aromatic interactions with trp residues, hydrogen bonds with the trp N_1H group, and the amphiphilic nature of trp contribute to protein stability. These non-covalent interactions were further monitored during the folding/insertion process of OmpA to obtain a better understanding of the roles these trp residues play in folding and insertion mechanisms in the membrane.

6.4.1 Trp-15: Hydrogen bonds and amino-aromatic interactions

The trp residue at position 15 is located at the top of the β-barrel and directionally folds/inserts into the vesicle from this "top" side of the barrel.[9,18] Due to this location, this trp residue must traverse the lipid bilayer as it folds into its native structure.[10] Trp-15 contributes to the thermodynamic stability of OmpA in the membrane through a hydrogen bond between the indole N_1H moiety on the trp residue and the carbonyl group on the Asn33 side-chain from a neighboring β-strand, with distance < 2 Å (figure 6.3).[17,28] Here we use UVRR to probe the evolution of this hydrogen bond.

The crystal structure of Trp-15 shows a likely hydrogen bond between the N_1H group of the indole and the carbonyl side-chain of Asn33. The W17 mode frequency does not provide evidence for this hydrogen bond. During the folding process, no change is observed in frequency and remains at a value that indicates weak/no hydrogen bonding.

This inconsistency could arise from protein structural differences when the protein is folded in detergent micelle in the static crystal structure vs. folded in fluid lipid bilayers for these experiments. Perhaps the increased mobility of the protein in the fluid lipid bilayer causes the distance between the trp residue and Asn33 to increase, thereby preventing formation of this hydrogen bond. Alternatively, other studies from our group have recently suggested that W17 is not an ideal indicator of H-bonding; the range over which this mode shifts is much smaller than previously reported.[29]

The W6, W4, and W10 modes also show correlations between frequency shifts and hydrogen bond strength of the N_1H group.[14,29] The W6 and W4 modes occur at frequencies (~1430 cm^{-1} and ~1490 cm^{-1}) with strong spectral overlap with tyr modes (see Figure 6.11) and cannot be analyzed easily. The W10 mode is more easily distinguished from tyr modes, although it also has significant overlap with tyr signal. Figure 6.12 shows the W10 mode of unfolded and folded Trp-15 and Trp-less mutants; adsorbed protein is shown for comparison. A decrease in W10 frequency is correlated to increasing hydrogen bonding strength.[29] For Trp-15, the W10 mode shows increased hydrogen bonding strength when folded in vesicle, as determined from the frequency shift from 1240 cm^{-1} to 1236 cm^{-1}. The Ratio of the W17 mode (~ 879 cm^{-1}) and W18 mode (~760 cm^{-1}), $R_{W17:W18}$, is also a sensitive reporter of hydrogen bonding in a nonpolar or polar environments.[29] Increasing ratios are observed with increasing hydrogen bonding strength, with a more drastic effect in hydrophobic pockets. The $R_{W17:W18}$ value increases for Trp-15 during the folding process, showing increased hydrogen bond strength. Together, the $R_{W17:W18}$ increase and shift in W10 mode provides evidence for the hydrogen bond with Trp-15, consistent with the crystal structure.

The R_{FD} values indicate an aqueous environment for this trp residue during all folding timescales, and also display the lowest R_{FD} values of all the trp residues in this study. Given its location in the hydrophobic bilayer in the folded form, one would expect an increase in environmental hydrophobicity for trp residues folded in vesicle. During the course of the folding event, the following environments might be expected for the trp residues that cross the bilayer center (Trp-15) during folding: at the beginning of the folding process before addition of vesicle, trp residues are in an aqueous environment. The hydrophobicity should increase upon adsorption to the vesicle surface due decreased solvent exposed surface area and expulsion of water molecules from the protein. The most hydrophobic environment would be observed for trp residues when the protein traverses through the membrane and crosses the center of the lipid bilayer. Water is least expected at this location due to the extremely hydrophobic nature of the lipid tails. Finally, the hydrophobicity might be expected to decrease in the native state due to trp preference for the more aqueous water-bilayer interface. This proposed change in hydrophobicity was not observed for Trp-15, nor for any of the trp residues in this study.

Trp-15 has a 79% solvent accessible surface area (SASA), which suggests it is accessible to and could interact with lipid heads and/or lipid tails. Since the R_{FD} values report an aqueous environment, the presence of the lipid bilayer in later folding timescales does not appear to directly affect this ratio. The crystal structure of Trp-15 shows both polar and nonpolar residues within ~ 7 Å of the trp residue and is located between two polar residues, Ser16 and Gly14. The close proximity to polar residues may result in the aqueous R_{FD} values for Trp-15, and helps explain the relatively constant,

polar R_{FD} values during the folding process for this mutant. Trends in the R_{FD} values at each time point in the kinetics experiments are shown in Figure 6.14.

Trp fluorescence is also used to determine hydrophobicity of trp environment and/or solvent exposure in proteins. The emission maximum, λ_{max}, shifts with hydrophobicity, with values of ~355 nm for solvent exposed trp in aqueous environment, ~340 nm for trp partially buried in a hydrophobic environment, and ~330 nm for trp fully buried in a hydrophobic environment.[30] The fluorescence λ_{max} value for Trp-15 blue-shift during the folding/insertion process, consistent with an increase in hydrophobicity. This fluorescence result conflicts with an aqueous environment determined from the R_{FD} values. However, we note that a previous study in our group showed that fluorescence maxima strongly correlate with both H-bonding and hydrophobicity. Specifically, the blue-shift in fluorescence maxima may be explained by loss of H-bond strength of the indole NH group during folding.

One of the most unique features found in the UVRR spectra of Trp-15 is the appearance of a shoulder on the W18 mode at ~778 cm^{-1}. This shoulder is not observed in any of the single-trp spectra, and is only observed in the partially folded/folded structure of Trp-15 in preformed vesicles. It cannot be attributed to a specific molecular interaction solely due to the folded structure, since this shoulder is not observed in the UVRR spectrum of Trp-15 folded in detergent micelle (data not shown). The appearance of this shoulder must arise from a unique molecular interaction found only for this trp residue and only when Trp-15 is folded in vesicle. This shoulder has very rarely been observed in other UVRR spectra of trp residues in proteins.[31-33] Studies on the partially folded A-state of Ferricytochrome *c* at pH 2.2 showed a shoulder on the high frequency

side on the W18 mode (Figure 3 in the paper). Although they fit the mode to two peaks, with frequencies of 758 cm^{-1} and 765 cm^{-1}, no attempt was made to discuss or propose its origin.[31] UVRR spectra of the synthetic 20 residue polypeptide, Trp-Cage, also showed this shoulder (Figure 7 in the paper), and was only observed in the spectrum collected at 4 ºC.[33] This shoulder is at a similar frequency as ours, ~780 cm^{-1}, but was not mentioned in the paper. A W18 shoulder was also observed in UVRR spectra of myoglobin, and was attributed to the contribution from twp trp residues present in the protein with 2 different W18 mode frequencies.[32] This is an unlikely explanation for our results since OmpA Trp-15 mutant, contains a single trp residue. In the current study, this shoulder appears by within the first 20 minutes in the folding process, and continues to increase in intensity for the duration of the folding kinetics.

The possible non-covalent interactions with trp, tyr, or phe residues were investigated to determine possible interactions that could give rise to this shoulder. The types of interactions and energetic contributions are described in detail in Chapter 1; only a few will be discussed here. The π-face of the aromatic ring can favorably interact with other aromatic rings (aromatic-aromatic interactions), or form hydrogen bonds with neighboring residues (amino-aromatic or cation-π interactions).[26,27] The aromatic ring can act as both a hydrogen bond donor (C-H groups in the plane of the aromatic ring) and a hydrogen bond acceptor (π-face of the aromatic ring). Amino-aromatic interactions occur between aromatic residues (trp, tyr, and phe) and the amino groups of side-chains (Lys, Arg, Asn, Gln, His) at distances of ~3 – 6 Å.[27,34] The charged side-chains of Lys or Arg, or the choline head groups of lipid bilayers for the more specific cation-π interactions with the aromatic residues.[34,35] Cation-π interactions have already been

shown to play a role in stabilizing OmpA structure.[19] Previous UVRR studies show correlations of trp mode frequencies and intensities changes with cation-π interactions in biological systems.[36-39] Some of the observed changes include increases in intensity for several modes.[29,38] Unfortunately, the intensities of many of the trp modes also increase when the protein is folded in vesicle due to a red-shift in the absorption spectrum in a hydrophobic environment; any intensity increases due to cation-π interactions cannot be distinguished from the other effects.[11] Therefore, we performed additional experiments to identify the origin of this new marker.

UVRR spectra were collected for the single-trp mutants, Trp-15 and Trp-143 in different vesicle compositions with different head groups, to observe spectral changes possibly associated with lipid – cation-π interactions. Spectra were collected in 70%:30% mol ratio of DMPC:DMPE vesicles and 100% DMPC vesicles. DMPC vesicles have larger head groups ($-N(CH_3)_3^+$) than DMPE vesicles ($-NH_3^+$). Binding energies for cation-π interactions are typically greater with smaller cations than for larger cations, likely due to closer contact between the cation and the π-face.[40] Lipid effects also show significant changes in thermodynamic properties and folding efficiencies of OmpA due to different lipid composition and size.[6,7] Specifically, addition of PE vesicles to PC vesicles increases the thermodynamic stability of OmpA.[19] Figure 6.13 shows UVRR spectra of Trp-15 and Trp-143 in 100% PC (DMPC) vesicles and 70%:30% PC:PE (DMPC:DMPE) vesicles. No significant spectral changes were observed between the different lipid compositions. Changes may only be observed at higher mol fractions of DMPE vesicles, however, the protein has decreased folding efficiency at higher ratios of DMPE vesicles, seen in SDS-PAGE gels (unpublished lab results). If a cation-π

interaction occurs between the lipid head groups and Trp-15, it does not appear to be affected by changes in head group size.

Although our results do not conclusively prove or disprove the possibility of cation-π interactions with Trp-15, we do believe it is not responsible for the observed shoulder on W18 since a cation is not located near Trp-15.[29,36,37,41] Instead, we propose that this shoulder reflects an amino-aromatic interaction between Gln17 and Trp-15, where the $-NH_2$ group of Gln17 acts as the hydrogen bond donor with the π-face of the aromatic ring as the hydrogen bond acceptor.[27] The distance between these two residues in the crystal structure is ~5 Å, which is within range for this type of interaction.[34,42] In addition to the shoulder on the W18 mode, the unique spectral changes observed in the W7 mode. The W7 mode shows distinct peak shifts and peak broadening during the folding process. The spectral changes in the W7 Fermi doublets occur within the first 20 minutes of the folding process, a similar timescale as the appearance of the shoulder on the W18 mode. Since other studies have shown changes in the W7 mode with cation-π interactions, it seems likely the encompassing amino-aromatic interaction can also affect the W7 mode.[38]

UVRR spectra were collected of Trp-15 in a solution of DPPC vesicles to create an adsorbed protein. This spectrum was compared to protein unfolded in KP_i buffer, and to the spectrum immediately after initiation of the folding/insertion process (t = 0 min). UVRR and fluorescence data indicates the adsorbed form of the protein in DPPC vesicles is neither like the unfolded protein structure, nor like that found in DMPC vesicles at initiation of folding (t = 0 min). SDS gels showed adsorbed protein has an apparent molecular weight of the unfolded protein (~35 kDa), yet the fluorescence indicates trp

environment in adsorbed protein is similar to that in DMPC vesicles at t = 0 min. The UVRR spectral changes indicate a very different environment for Trp-15 in the adsorbed form, compared to the unfolded protein or immediately after initiation of folding into DMPC vesicles (t = 0 min). Additionally, the adsorbed Trp-15 has the most hydrophobic environment according to the R_{FD} value, no shoulder is observed on the W18 mode for the adsorbed protein, and the hydrogen bonding indicators, the W17 and W10 modes, have frequencies that are more similar to the unfolded protein. All evidence suggests the adsorbed form of the protein in DPPC vesicles has similar spectroscopic evidence to both the unfolded protein and the adsorbed/partially inserted form in DMPC vesicles at t = 0 min into the folding process. The species formed in DPPC vesicles may be a unique folding intermediate that forms along the folding pathway, with distinct spectral features.

The W3 mode frequency is often used as the conformational marker. A torsion angle of 95º was determined from the W3 mode in folded protein, which is different from the $\chi^{2,1}$ angle determined from the crystal structure of 45º (PDB 1QJP). A 2 cm^{-1} shift was observed during the folding process, but this is within our experimental error. Recent studies show deviation from the W3 frequency and $\chi^{2,1}$ due to hydrogen bonding effects, cation-π interactions, and weak electrostatic and nonpolar interactions.[43] These same interactions are also likely to influence the trp residues in our studies and could affect the W3 frequency. Minimal rotation of trp residues is observed when inserted in the membrane.[44] This result is consistent with previous MD simulations, and suggests the trp residue anchor the protein in the membrane at early time scales and maintains the correct orientation/position in the bilayer during the folding process.[45]

6.4.2 Trp-7 and Trp-170: aromatic-aromatic interactions

Trp-7 and Trp-170 were chosen for this study for their unique location in the protein, and their contribution to the stability of OmpA. Trp-7 is the only native trp residue located at the bottom of the β-barrel near the N-terminus and is located in a unique hydrophobic pocket consisting of the aromatic residues Tyr8, Tyr43, Tyr168, and Phe170. Its location in the crystal structure of OmpA is shown in Figure 6.4, with distances between neighboring aromatic centroids.[46,47] This cluster of aromatic residues was determined to provide stability to the protein through these pairwise aromatic interactions.[17] During the folding/insertion process into the membrane, Trp-7 remains on the periplasmic side (the outer leaflet of the lipid bilayer) and does not cross the bilayer center.[10] Figure 6.4 shows two trp residues in this hydrophobic pocket. In the Trp-7 mutant, the native residue at position 170 is a phenylalanine residue.

Trp-170 is a non-native trp residue in OmpA and resides in the transmembrane domain in the same hydrophobic pocket as Trp-7 on a neighboring β-sheet. Thermodynamic studies show this trp residue also contributes to OmpA stability through the same aromatic-aromatic interactions with the neighboring aromatic residues as Trp-7. Trp-170 is located near the boundary between the transmembrane domain and the soluble domain of the protein. Due to its location near Trp-7, it likely remains on the same side of the lipid bilayer during the folding process and does not cross the bilayer center. The folding kinetics of these two trp residues at the bottom of the transmembrane domain are likely to be different than those determined for the trp residues at the top.

The W17 mode hydrogen bonding indicator shows increasing hydrogen bonding strength during the folding process for Trp-7 and Trp-170, and shows a strong hydrogen bond in the hydrophobic bilayer. The crystal structure does not show hydrogen bond

partners with the N_1H of trp and typical hydrogen bond acceptors. However, the π electrons of aromatic rings can act as a proton acceptor.[13] Trp-7 and Trp-170 are located near a variety of aromatic residues in this pocket. The flexible nature of the lipid bilayer may allow H-bonding to occur even though it is not seen in the crystal structure. Hydrogen-bonding interactions occur between aromatic residues and the lipid bilayer. Both trp residues face towards the lipid bilayer and have high solvent accessible surface areas (SASA), with values of ~84% and ~80% (determined using the phe residue at this location), for Trp-7 and Trp-170, respectively. Since these trp residues face towards the lipid bilayer, and have high SASA values, hydrogen bonds with the lipid bilayer are likely sources.[21,48-50] Possible hydrogen-bond acceptors are phosphate head groups or lipid acyl carbonyl groups. A final possible interpretation for the shifts in W17 mode can be due to π-stacking of the aromatic residues in this aromatic belt.

The changes in the W17 mode from the kinetics spectra indicate different folding timescales for Trp-7 and Trp-170. The W17 mode in Trp-7 shifts within the first 20 minutes of the folding process, followed by another shift to lower frequency by 60 minutes into the folding process. The W17 mode for Trp-170 shifts within the first 20 minutes of folding, and remains constant for the duration of the folding process. This suggests different kinetics for these two residues.

The R_{FD} values indicate a hydrophobic environment for Trp-7 and Trp-170. In fact, these two trp residues have the most hydrophobic environments of all the trp residues under investigation in this study. This is consistent with the hydrophobic pocket in the crystal structure. Over the course of the folding kinetics, the R_{FD} value for Trp-7 increases from 1.0 to 1.3 immediately after initiation of the folding process and shows

Trp-7 is in a hydrophobic environment at the start of the folding process. The R_{FD} value continues to increase during the folding process and hydrophobicity is likely attributed to the formation of the aromatic pocket with the Tyr8, Tyr43, Tyr168, and Phe170 residues. This data is consistent with Trp-7 immediately associates with the water/bilayer interface.

Trp-170 appears to be in a more hydrophobic environment than Trp-7 at earlier time scales, as evidenced by larger R_{FD} values. By completion of the folding process, both Trp-7 and Trp-170 experience the same degree of hydrophobicity, as would be expected in the aromatic pocket from the crystal structure. Initial differences in R_{FD} values between Trp-7 and Trp-170 could result from the environmental effects.

The blue-shifted fluorescence values agree with the increasing hydrophobic environment for Trp-7 and Trp-170 determined from the R_{FD} values. Trp-7 has the most blue-shifted fluorescence of all the trp mutants when folded in vesicle. Although Trp-170 is also located in this hydrophobic pocket, its fluorescence value is 331 nm when folded in vesicle. The long timescales in the fluorescence shifts correlate nicely with the long timescales of the UVRR kinetics spectra.

The W3 conformational marker reports a torsion angle for Trp-7 of 90º, which is similar to the angle determined from the crystal structure of 83°. The frequency of the W3 mode does not shift outside our experimental error, and any rotation of Trp-7 is not observed during the folding process. The adsorbed protein shows the most deviation from unfolded or folded protein, with a frequency of 1554 cm^{-1}. This corresponds to a torsion angle of 106º, and indicates the adsorbed form of the protein is different from the unfolded state or the structure immediately after initiation of folding.

Since Trp-170 is a novel mutant, there is no crystal structure for Trp-170, and hence no $\chi^{2,1}$ value. The W3 frequency can be utilized in this case to provide additional structural information of this new trp residue in OmpA. A value of 90º was determined for Trp-170from the W3 frequency. In the crystal structure shown in Figure 6.4, a similar $\chi^{2,1}$ angle was calculated with a value of 83º for this non-native trp residue. This small difference in consistent with variations in torsion angle determined from crystal structure and W3 frequency for the other trp residues in OmpA. A Trp-170 is the only trp residue that shows a significant change in W3 mode between unfolded and folded structures. The frequency shifts from 1553 cm^{-1} in unfolded protein to 1549 cm^{-1} at initiation of folding, corresponding to torsion angles of 100º and 90º, respectively.

6.4.3 Trp-102: Hydrogen bonds with protein backbone

The location of Trp-102 is different from the other trp residues in this study. It is the only trp residue that located at the top of the β-barrel that is on a loop and resides in the interior of the barrel.[51,52] The long flexible loops at the top of OmpA show large fluctuations in the NMR structure and do not appear to be sterically hindered by the presence of the micelles.[47,53] One would expect an aqueous environment for Trp-102 during the folding process, given its location in the interior of the barrel. The barrel forms an aqueous pore through the center of the barrel.[54,55]

The W17 hydrogen bond marker indicates medium-to-strong hydrogen bond for Trp-102 unfolded in buffer, and during the entire folding process. This observation is consistent with a hydrogen bond between Trp-102 and solvent in unfolded protein. As the protein folds/inserts into the bilayer, Trp-102 maintains this hydrogen bond in the aqueous pore, and shows increased strength between 20 – 40 minutes in the folding

process. Analysis of the crystal structure in Figure 6.8 shows possible hydrogen bond acceptors within < 6Å of the N_1H Trp-102. Acceptors include the backbone carbonyl groups of Asn145 (6 Å), Val119 (4.5 Å), or Gly118 (4.5 Å). Although typical hydrogen bond distance range from ~2 – 3.6 Å and the H-bonding geometry is ideally linear, the flexible structure of the protein in the membrane may cause shorter distances and better geometries that indicated from the crystal structure between the hydrogen bond donor and the acceptor.[51] Since Trp-102 is located in the aqueous interior of the protein on a loop, hydrogen bonds to water molecules may also exist.

Although the location of Trp-102 in the protein suggests an aqueous environment, the UVRR data does not reflect this. Trp-102 has the smallest solvent accessible surface area (SASA) of all the trp residues, with a value of 64%. The R_{FD} value of Trp-102 unfolded in buffer indicates that this trp is in a hydrophobic environment. During this folding/insertion process into DMPC vesicles, the R_{FD} increases from 1.3 to 1.5. This increase in hydrophobicity during the folding process could be attributed to formation of the β-sheets, and the influence of the residues on Trp-102 environment. What is surprising is R_{FD} values never report an aqueous environment for Trp-102 either before or after the folding process as one would expect given its location in the protein. This suggests that local residues may influence the R_{FD} values.

The fluorescence values indicate an aqueous environment for Trp-102 unfolded in buffer, and a more hydrophobic environment upon initiation of the folding process in vesicles. These results are slightly different than those determined from the R_{FD} values that show a hydrophobic environment in both cases. Again, this result highlights different sensitivities of fluorescence and Raman.

The W3 mode frequency reports on the $\chi^{2,1}$ torsion angle about the protein backbone. The values determined from the W3 mode frequency are consistent with the torsion angle determined from the crystal structure. W3 mode of 1550 cm^{-1} correlates to a $\chi^{2,1}$ torsion angle of a 93º, the same value from the crystal structure. Our results indicate minimal changes in rotation during the folding process.

6.4.4 Truncated Mutants

UVRR kinetics studies were performed on the truncated single-trp mutants to determine the affects of the soluble tail on the folding/insertion process of OmpA. The soluble tail is roughly half of the protein and consists of ~150 out of the 325 residues of OmpA. The tail has been proposed to be involved in pore formation: a larger pore in formed with the influence of the tail, a smaller pore is formed without its contribution.[52,56,57] It seems likely that the presence or absence of the soluble tail would affect the folding kinetics.

The UVRR spectra collected for the truncated mutants were similar to their full-length forms. The same general trends in hydrogen bond strength, trp hydrophobicity, and other structural markers for these trp mutants are observed for both the full-length and truncated proteins. One noticeable change is the magnitude of the R_{FD} values. Figure 6.15 shows the calculated R_{FD} values for each time point in the folding process for all of the truncated OmpA mutants. These values are larger in the truncated mutants. This suggests the soluble tail may interact with the transmembrane domain, possibly through formation of a larger pore. The kinetics for were different for the truncated mutants compared to the full-length versions. In general, the spectral changes occurred on a faster timescale for truncated mutants. Truncated mutants showed a larger degree of

spectroscopic change within 0 – 20 min in the folding process, whereas the full-length mutants showed comparable changes between 20 – 40 min in the folding process. Previous studies in our lab suggest the soluble tail helps to stabilize the unfolded transmembrane domain of the protein.[17] Our evidence can support this claim.

6.4.5 Proposed Folding Mechanism

The overall folding kinetics determined for trp residues in OmpA in this study show spectroscopic changes on a similar folding timescale as previous kinetics studies.[4,10] On average, it takes OmpA ~ 60 – 80 minutes to fully fold into the lipid bilayer from a denatured state, depending on temperature, vesicle size, and vesicle composition.[4,6,58,59] Our results are consistent with these findings and show minimal spectroscopic changes after 60 minutes in DMPC vesicles.

Spectral changes in Trp-15 are observed within the first 20 minutes after initiation of folding, with continued changes for the remainder of the folding process, ~60 – 180 min, consistent with formation of amino-aromatic interactions in the early timescales followed by continued folding/insertion into the membrane. Trp-7 and Trp-170 data reflect the formation of the hydrophobic pocket in the protein 20 – 40 minutes of folding. The UVRR data suggests the hydrophobic pocket starts forming within the first 20 minutes of folding, and provides evolution of high-order structures in OmpA. The three β-sheets containing the aromatic residues, Tyr8, Tyr43, Tyr168, and Phe170, come together to form this hydrophobic pocket within the first 20 minutes. Minimal changes are observed in Trp-7 and Trp-170 spectra after the 40-min time point, consistent with these trp residues remaining on the same side of the lipid bilayer during the folding process.[10] The small observed changes likely result from movement of the protein in the

lipid bilayer or slow formation of this pocket over long timescales. Formation of the hydrogen bonds with Trp-102 and protein backbone occur on a longer timescale, ~40 minutes, and could indicate higher degree of flexibility in this portion of the protein during the folding process. The spectroscopic properties of the adsorbed protein are both different and similar to unfolded protein and protein immediately after initiation of folding. These similarities and differences suggest this is a unique intermediate along the folding pathway.

6.5 Summary

UVRR kinetics studies were performed on select trp residues in OmpA to monitor vibrational changes in trp residues during the folding/insertion process into lipid vesicles. The spectral changes were correlated to different inter-molecular interactions with the trp residues and neighboring amino acids and provide evidence for the formation of higher order structure in the protein in the membrane. The amino-aromatic interaction between the trp15and the $–NH_2$ group of the Gln17 side chain, as observed by the shoulder on the W18 mode and the W7 peaks shifts, starts to form within the first 20 minutes of the folding process in DMPC vesicles. The hydrophobic pocket of Trp-7, Tyr8, Tyr43, Phe170, and Tyr168, as evidenced by the increase in R_{FD} values, also starts to form within the first 20 minutes in the folding process. The hydrogen bond with Trp-102 starts to form after 40 minutes in the folding process. Our results show non-covalent interactions between complementary beta-sheets on similar timescales, consistent with a picture of cooperative folding/insertion of OmpA in the lipid bilayer.[6,10]

6.6 Acknowledgements

I thank Beijing Wu and Nadhia Gotama for help with protein expression, and Brian Leigh for help with DS Viewer Pro.

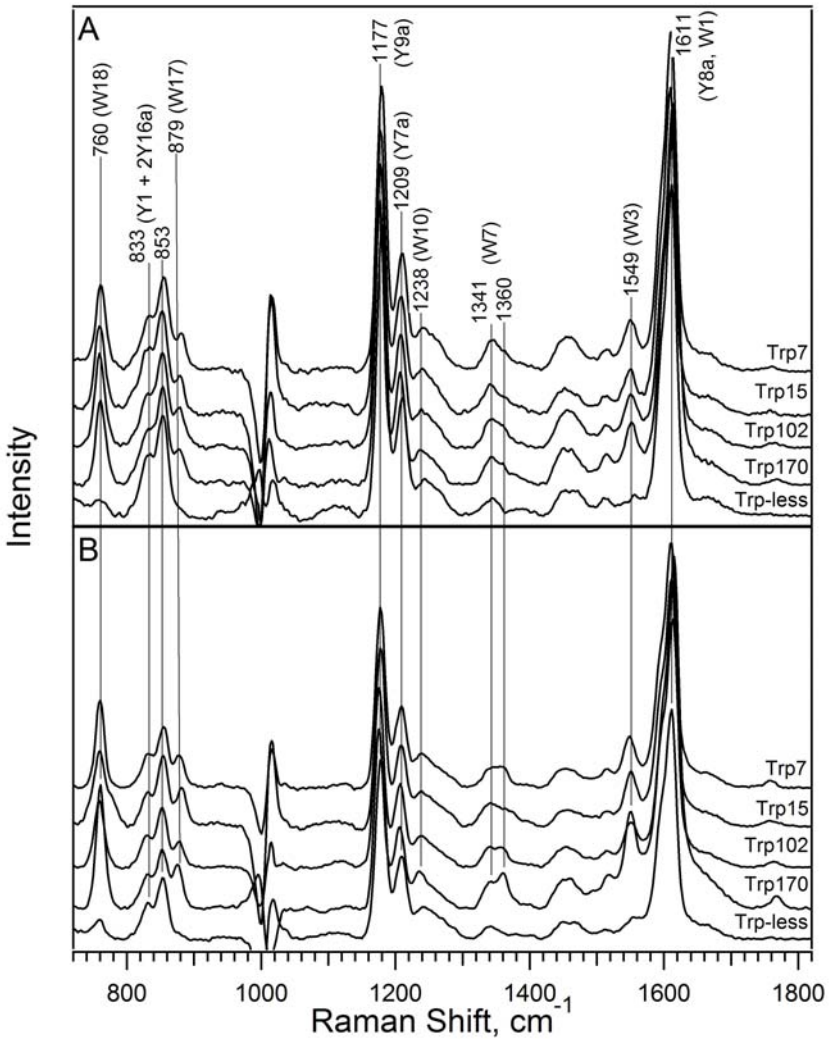

Figure 6.1: Steady-state UVRR spectra of the single-trp mutants Trp-7, Trp-15, Trp-102, and Trp-170, and the Trp-less mutant (no trp residues) at 228-nm excitation. Protein samples unfolded in buffer (A), and folded in DMPC vesicles (B). Some tryptophan (W) and tyrosine (Y) vibrational modes are highlighted. The feature at ~1000 cm^{-1} is due to incomplete subtraction of urea. All spectra are scaled to the intensity of the Y9a mode.

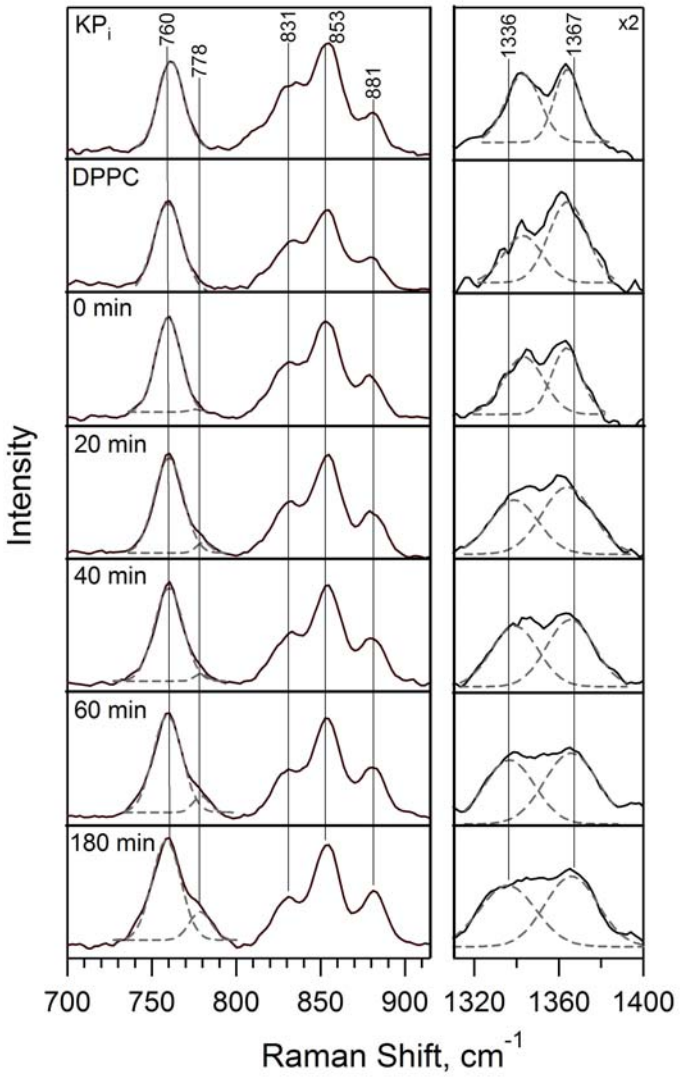

Figure 6.2: UVRR kinetics spectra of full-length OmpA-Trp-15 mutant unfolded in KP_i buffer, adsorbed in DPPC vesicles, and folding into DMPC vesicles at different time points during the folding process (t = 0 –180 min). W18 mode (760 cm^{-1}) and W7 Fermi doublet modes(~1340 cm^{-1}, ~1360 cm^{-1}) are decomposed into Gaussian peaks, shown as dashed gray lines. W7 modes are difference spectra (after removing contribution from tyrosine peaks reported by the Trp-less mutant) and are scaled x2.

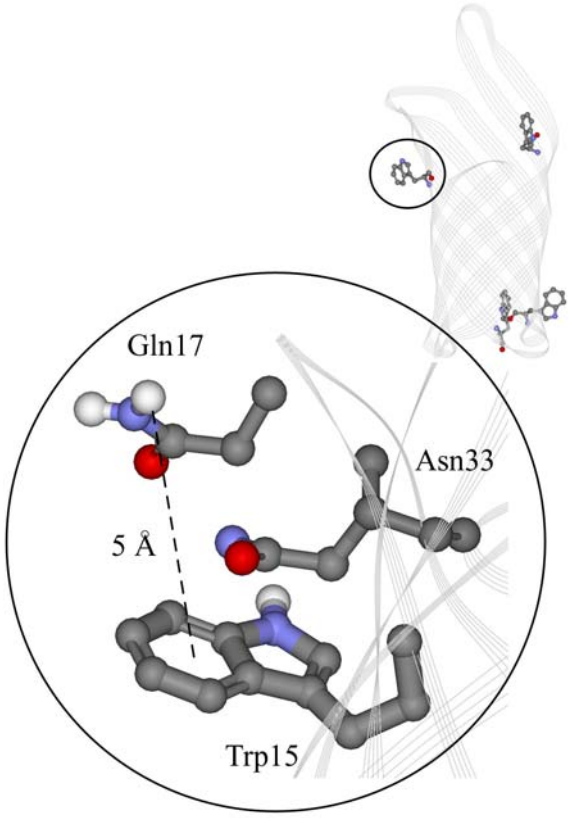

Figure 6.3: Crystal structure of the transmembrane domain of OmpA (PDB 1QJP), showing location of trp-15 in the protein. The highlighted region has been rotated 90 º counterclockwise from inset. The distance between aromatic centroid of Trp-15 and side-chain of Gln17 is ~5 Å. A hydrogen bond forms between the side-chain carbonyl group of Asn33 and the N_1H of the indole, ~ 2 Å apart.

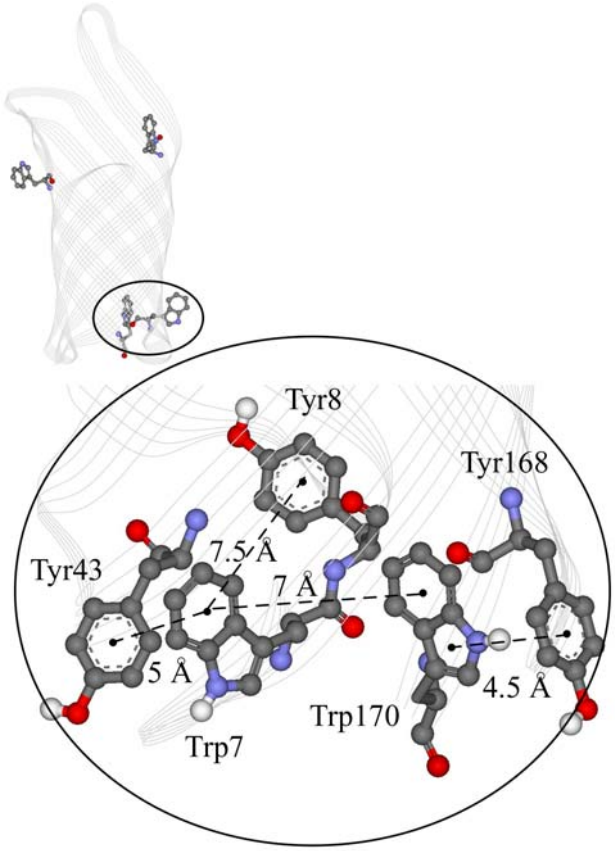

Figure 6.4: The crystal structure of OmpA, showing the native trp-7 and the non-native trp-170. In the Trp-7 mutant, the residue at position 170 is a phe. In the Trp-170 mutant, the residue at position 7 is a phe. The distances between aromatic centroids are indicated.

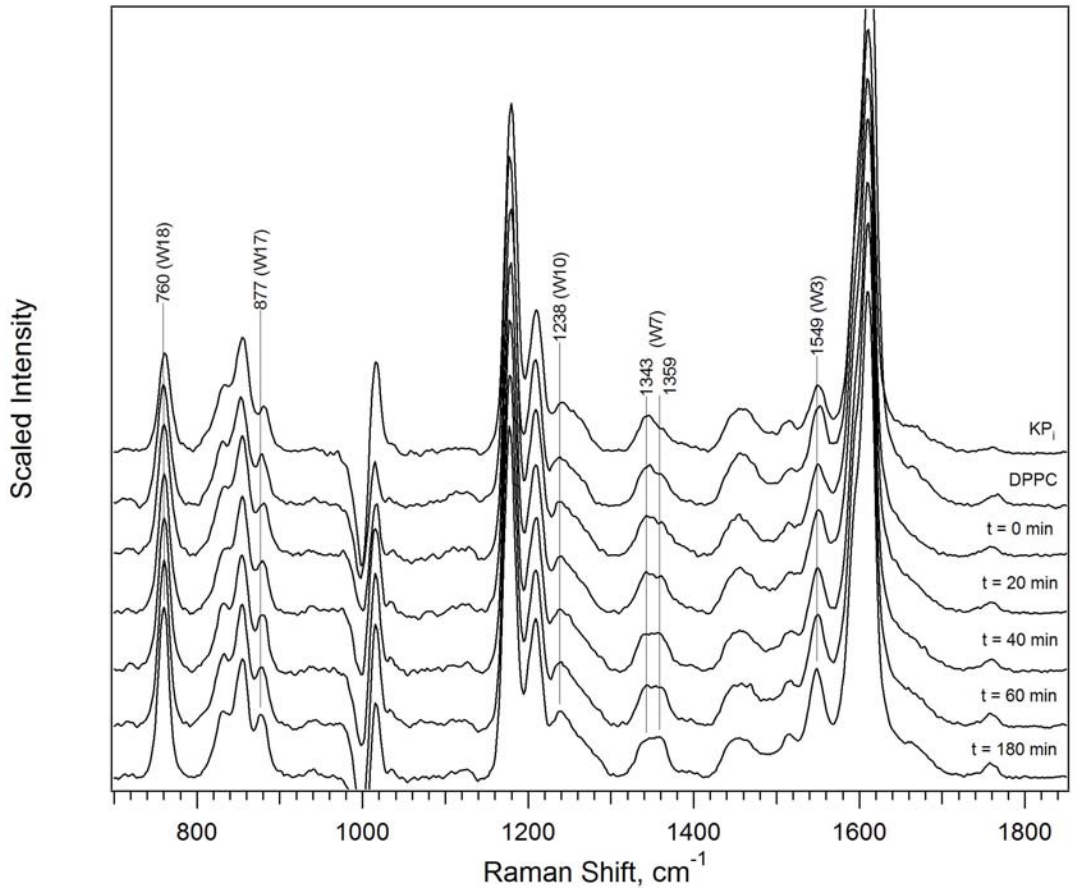

Figure 6.5: UVRR kinetics spectra of Trp-7 unfolded in KP_i buffer, adsorbed on DPPC vesicles, and folding into DMPC vesicles at different time points. A few trp vibrational modes are indicated (W#).

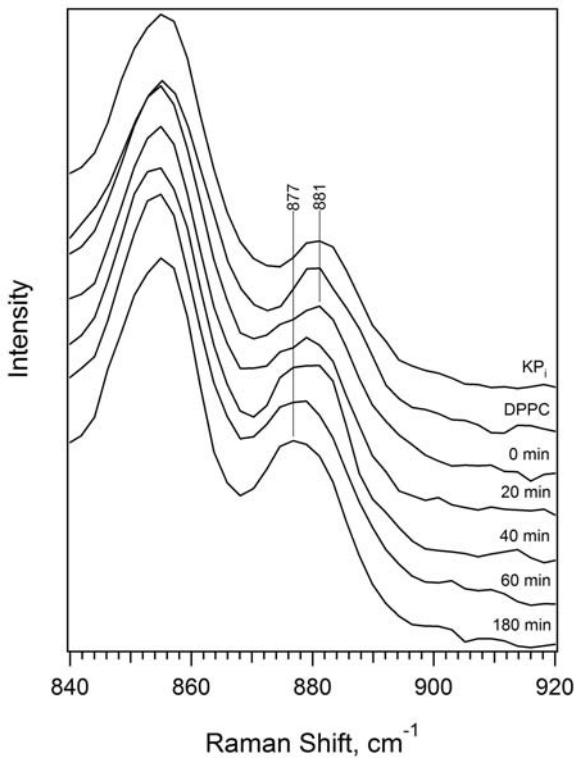

Figure 6.6: UVRR kinetics spectra of Trp-7 of the W17 mode frequency shift. Protein is unfolded in KP_i buffer, adsorbed on DPPC vesicles, and folded into DMPC vesicles at different time points (t = 0 – 180 min following initiation of folding event).

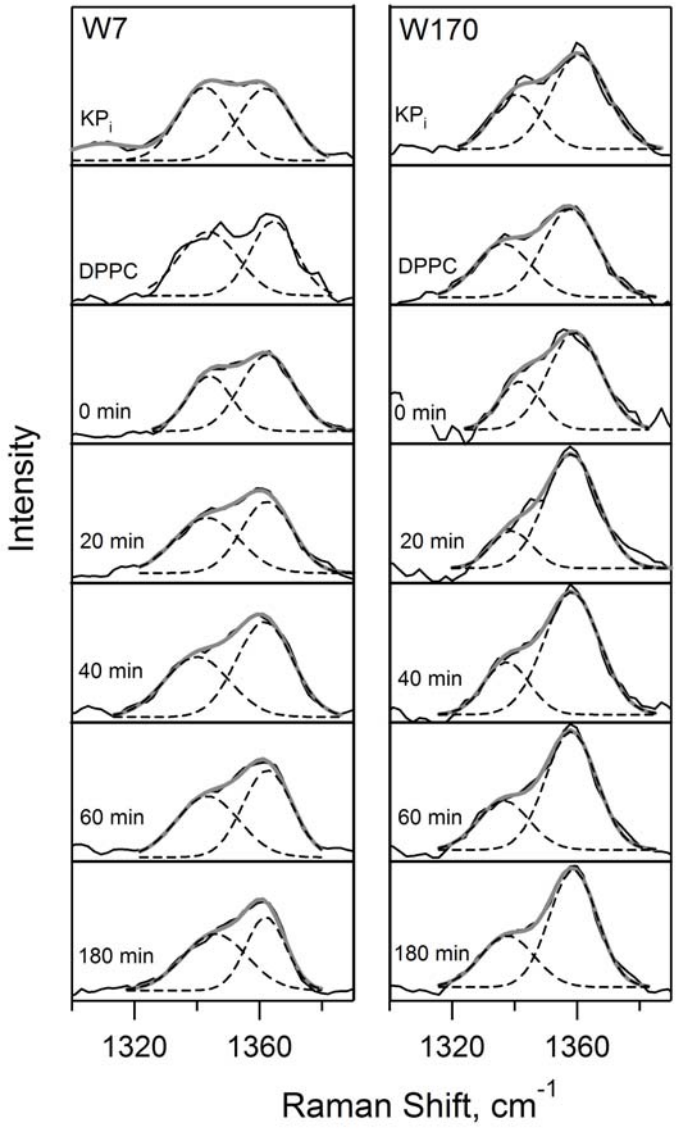

Figure 6.7: UVRR difference spectra of Trp-7 and Trp-170 Fermi doublet. Proteins are unfolded in KP_i buffer, adsorbed on DPPC vesicles, and different time points in the folding process in DMPC vesicles (t = 0 – 180 min). Trp-less mutant in the appropriate buffer was subtracted to remove contribution from 17 tyrosine residues. Peaks were decomposed into Gaussian peaks, shown as dashed gray lines. Fits are shown in solid gray.

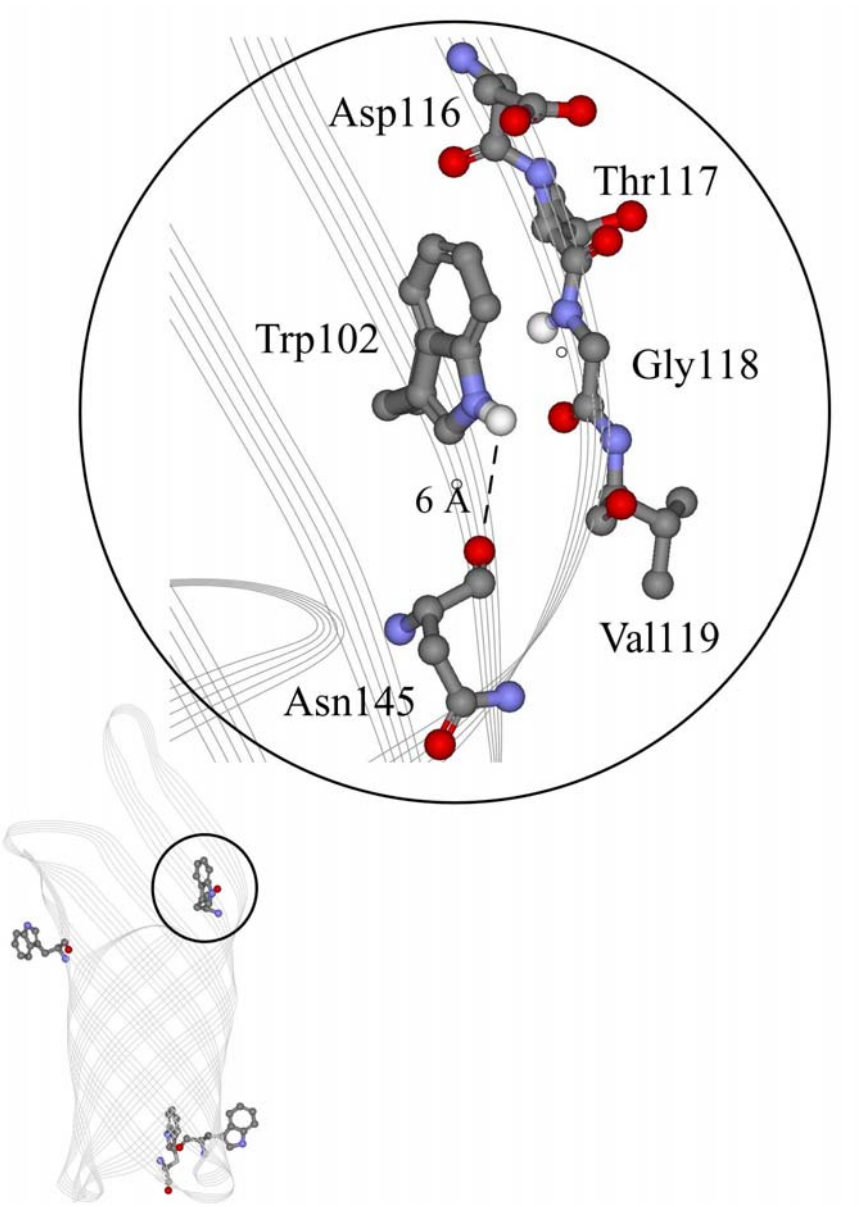

Figure 6.8: Crystal structure of the transmembrane domain of OmpA (PDB 1QJP), showing the location of Trp-102 at the top of the barrel. A possible hydrogen bond between the carbonyl of the Asn145 backbone and the N_1H of the indole.

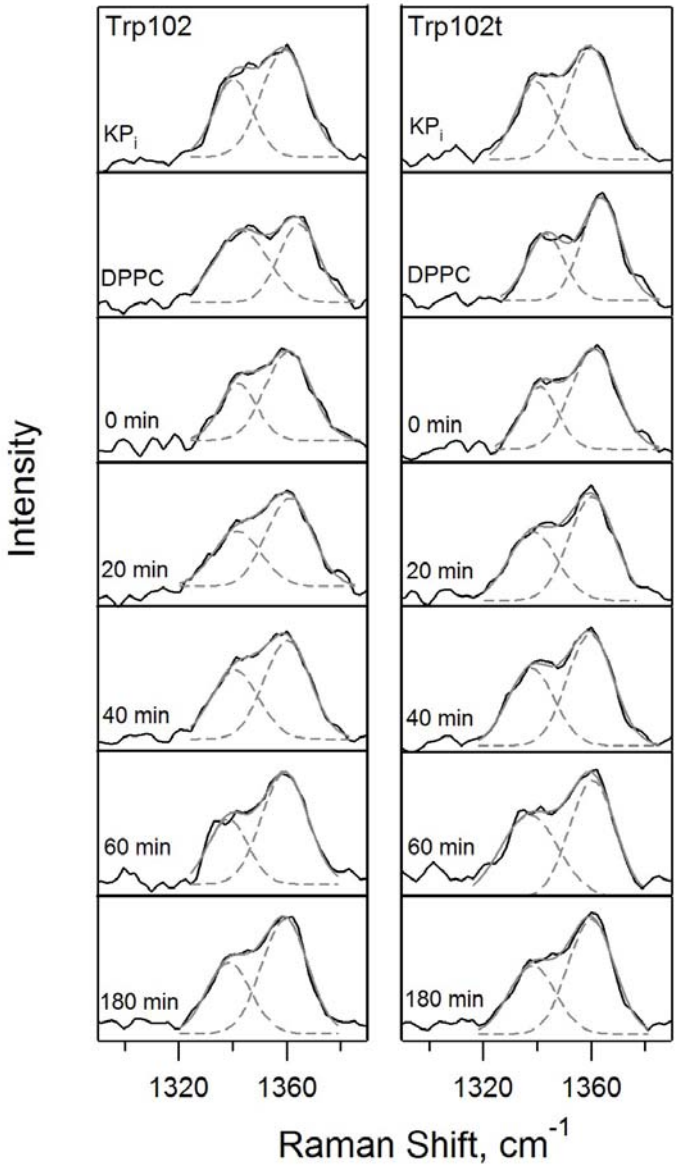

Figure 6.9: UVRR difference spectra of Trp-102 and Trp-102t W7 mode Fermi doublet, unfolded in KP_i buffer, adsorbed on DPPC vesicles, and different time points (t = 0 – 180 min) in the folding process. Contribution from tyrosine residues has been removed. UVRR spectra are shown in black; Gaussian fits are shown in dashed gray lines; summed fits are shown in solid gray lines.

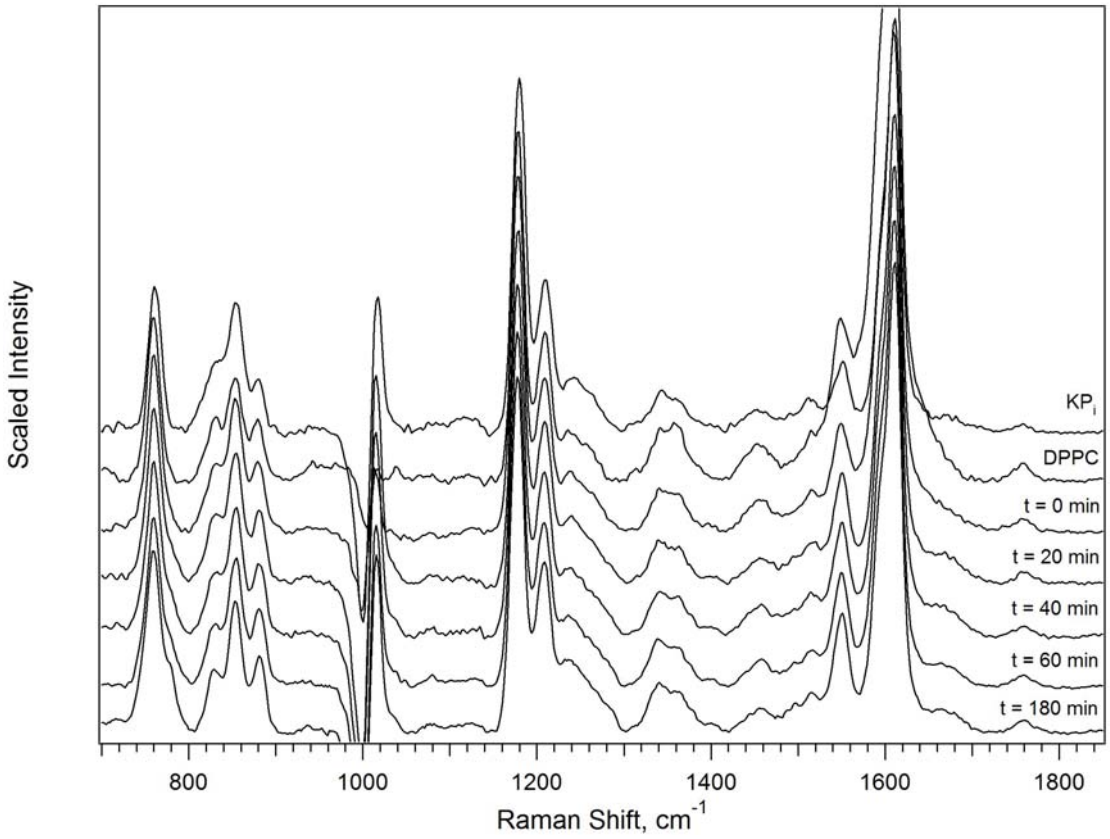

Figure 6.10: Representative UVRR kinetics spectra of truncated OmpA single-trp mutant (Trp-15t), unfolded in KP_i buffer, adsorbed on DPPC vesicles, and at different time points in the folding process (t = 0 – 180 min). The large feature at ~1000 cm^{-1} is from over-subtraction of urea buffer.

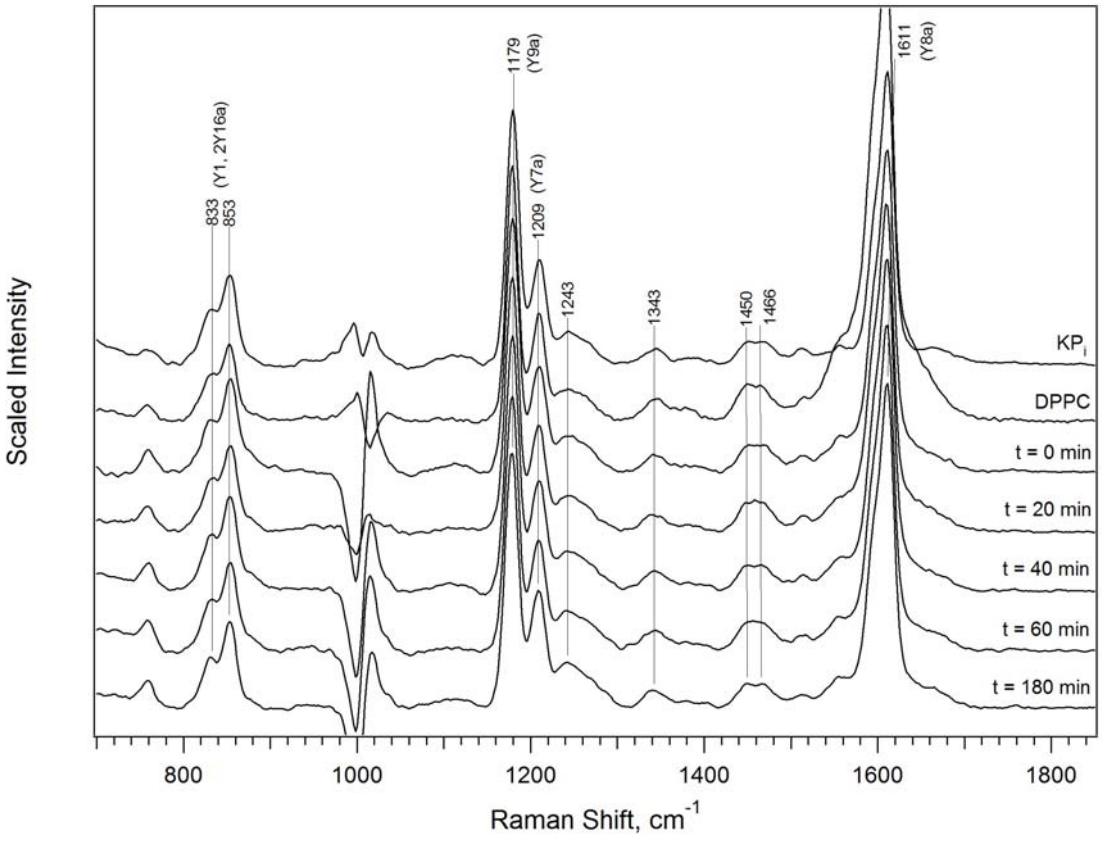

Figure 6.11: UVRR spectra of Trp-less OmpA, unfolded in KP_i buffer, adsorbed on DPPC vesicles, and at different time points in the folding process into DMPC vesicles. Tyr vibrational modes are indicated. The feature at ~1000 cm^{-1} is from incomplete subtraction of urea buffer.

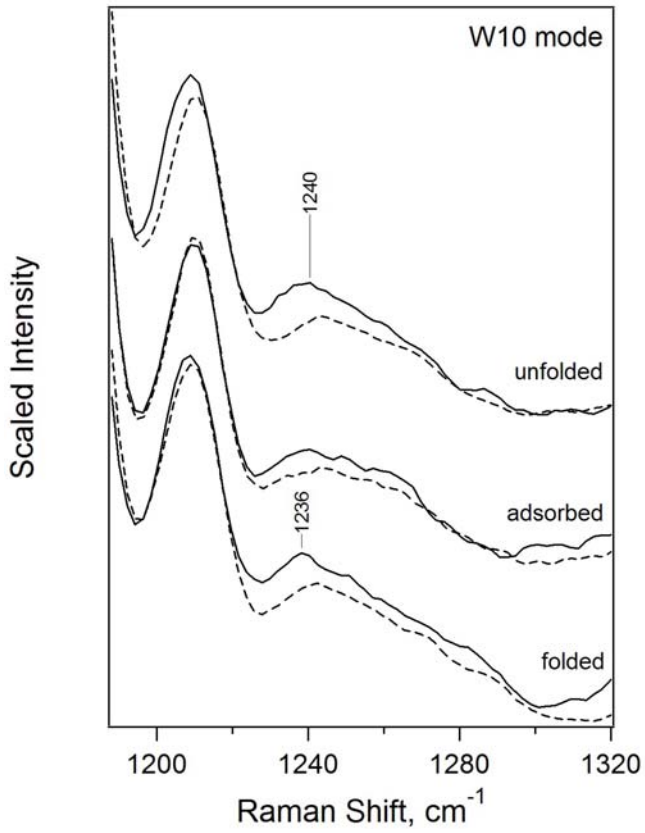

Figure 6.12: The W10 mode found in the UVRR spectra of Trp-15 (solid black curves) and Trp-less (dashed black curves) mutants unfolded in buffer, adsorbed to DPPC vesicles, and folded in DMPC vesicles.

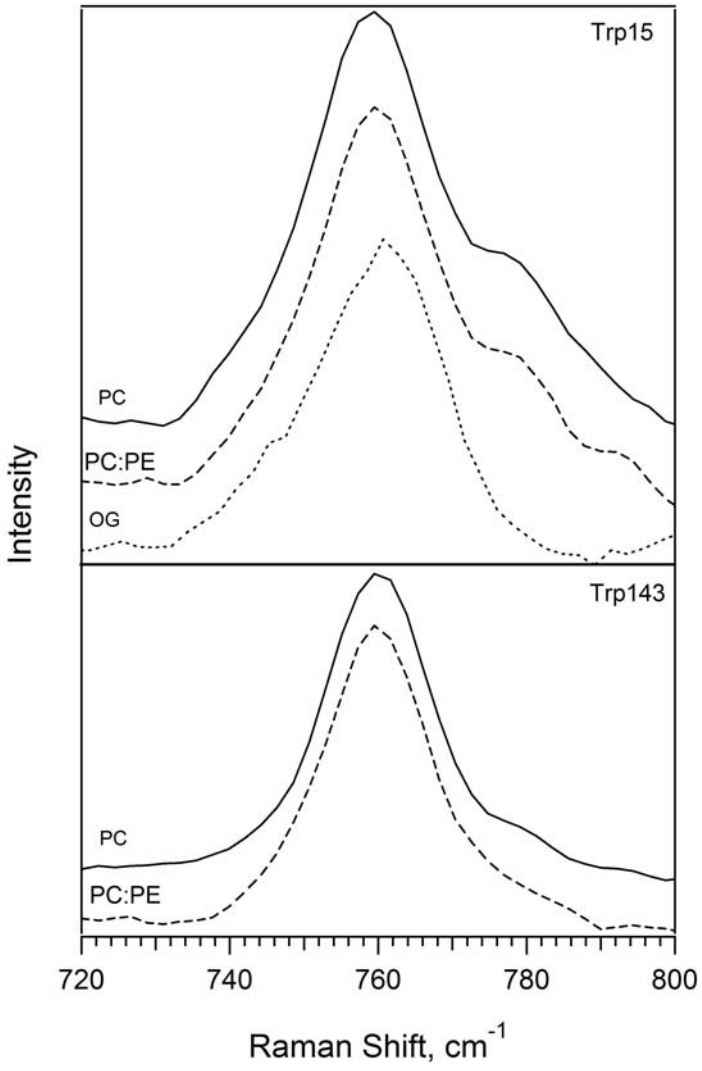

Figure 6.13: The W18 mode region of Trp-15 and Trp-143 in 100% PC (DMPC) and 70%:30% PC:PE (DMPC:DMPE) vesicles. Trp-15 in detergent micelles (OG) is added for comparison. UVRR spectra are offset for clarity.

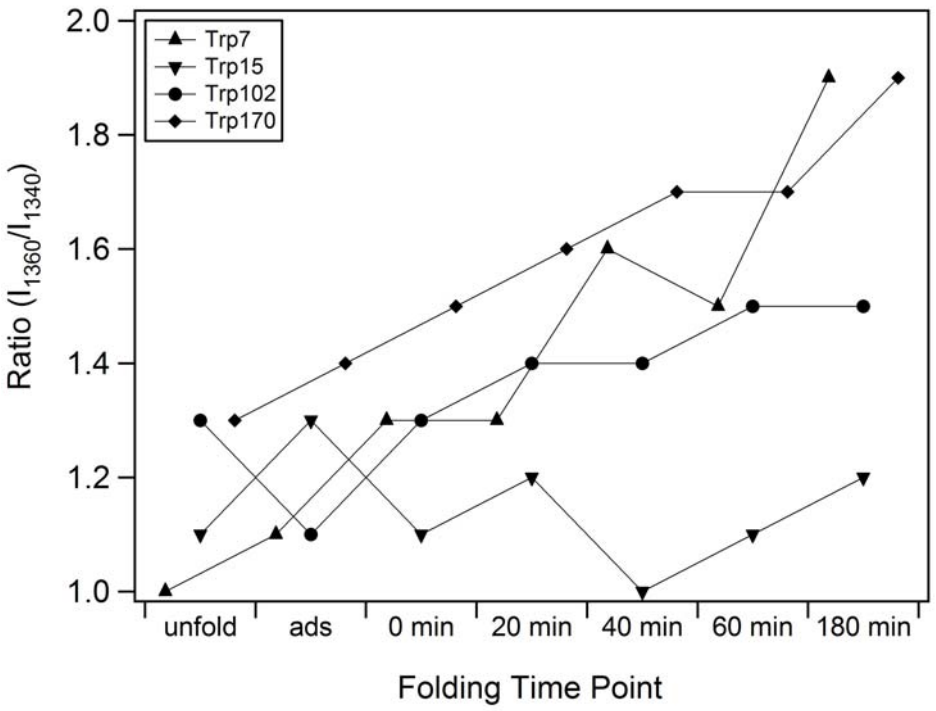

Figure 6.14: UVRR Fermi doublet ratios of the full-length single trp mutants in this study in different folding conditions. Protein is unfolded in buffer (unfold), adsorbed on DPPC vesicles (ads), and folding into DMPC vesicles at different time points (t = 0 – 180 min).

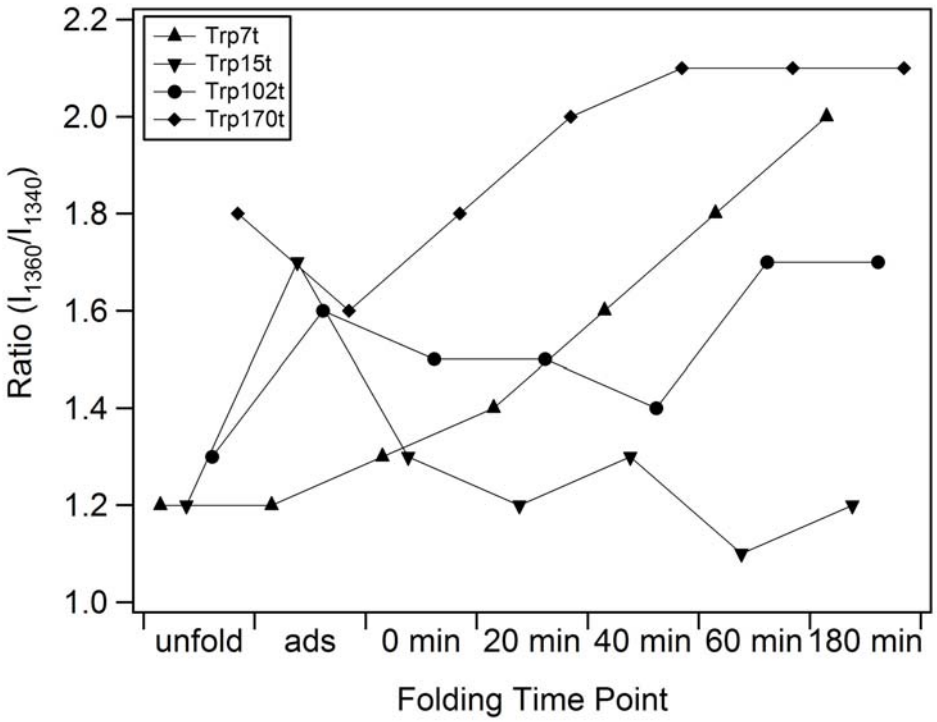

Figure 6.15: UVRR Fermi doublet ratios of the truncated single trp mutants in this study in different folding conditions. Protein is unfolded in buffer (unfold), adsorbed on DPPC vesicles (ads), and folding into DMPC vesicles at different time points (t = 0 – 180 min).

Table 6.1: Steady-state UVRR trp and tyr vibrational mode frequencies and intensity ratios for trp mutants and trp-less mutants of OmpA, unfolded in buffer (U) and folded in DMPC vesicles (F). $R_{Y1:2Y16a}$ is the intensity ratio of the Y1 and 2Y16a modes. $R_{W17:W18}$ is the intensity ratio of the W17 and W18 modes. R_{FD} is the ratio of the W7 mode Fermi doublet (I_{1360}/I_{1340}). Accuracy was determined to be 2 cm^{-1}.

Mutant	U/F	W18	Y1, 2Y16a	$R_{Y1:2Y16a}$	W17	$R_{W17:W18}$	Y9a	Y7a	R_{FD}	W3	Y8a/Y8b + W1
Trp7	U	760	835, 855	0.59	881	0.46	1179	1209	1.0	1549	1611
	F	760	833, 855	0.56	877	0.38	1177	1209	1.9	1549	1611
Trp15	U	762	833, 855	0.65	881	0.46	1179	1209	1.1	1551	1611
	F	760	831, 855	0.50	881	0.50	1177	1209	1.2	1551	1611
Trp102	U	759	831, 853	0.55	879	0.44	1177	1209	1.3	1550	1613
	F	759	831, 853	0.54	877	0.37	1175	1207	1.5	1552	1613
Trp170	U	760	832, 853	0.57	879	0.40	1177	1207	1.3	1553	1613
	F	758	831, 851	0.55	875	0.36	1177	1207	1.9	1549	1613
Trpless	U	-	833, 853	0.64	-	-	1179	1209	-	-	1611
	F	-	831, 855	0.61	-	-	1179	1209	-	-	1611

Table 6.2: W7 mode Fermi doublet ratios, R_{FD}, with corresponding peak frequencies and widths from Gaussian peak fits in Figure 6.2. OmpA Trp-15 was unfolded in buffer, adsorbed to DPPC vesicles, and folding into DMPC vesicles at different time points in the folding process. Folded protein is protein in DMPC at t = 180 min. Accuracy is 2 cm^{-1}.

Trp15	R_{FD}	1340 cm^{-1} (FWHM, cm^{-1})	1360 cm^{-1} (FWHM, cm^{-1})
Unfolded (KP_i)	1.1	1343 (18)	1363 (15)
Adsorbed (DPPC)	1.3	1343 (21)	1364 (21)
DMPC, t = 0 min	1.1	1343 (22)	1364 (16)
DMPC, t = 20 min	1.2	1339 (25)	1364 (28)
DMPC, t = 40 min	1.0	1339 (26)	1365 (26)
DMPC, t = 60 min	1.1	1336 (28)	1366 (29)
DMPC, t = 180 min	1.2	1336 (31)	1366 (29)

Table 6.3: Tabulated UVRR trp mode frequencies for full-length single-trp mutants, unfolded in KP_i buffer, adsorbed on DPPC vesicles, and folding in DMPC vesicles at different time points (t = 0 – 180 min). $R_{W17:W17}$ is the intensity ratio of the W17/W18 modes. R_{FD} is the ratio of W7 Fermi doublet, I_{1360}/I_{1340}. UVRR frequency accuracy is 2 cm^{-1}. Tryptophan fluorescence for each sample is given by λ_{max}.

Mutant	Description	W18	W17	$R_{W17:W18}$	R_{FD}	W3	λ_{max} (nm)
Trp7	unfolded	760	881	0.46	1.0	1549	353
	adsorbed	760	879	0.44	1.1	1554	344
	DMPC, t = 0 min	760	881	0.39	1.3	1551	339
	DMPC, t = 20 min	760	879	0.36	1.3	1551	335
	DMPC, t = 40 min	760	879	0.36	1.6	1549	329
	DMPC, t = 60 min	760	877	0.37	1.5	1549	329
	DMPC, t = 180 min	760	877	0.38	1.9	1549	327
Trp15	unfolded	762	881	0.46	1.1	1551	350
	adsorbed	760	881	0.37	1.3	1555	345
	DMPC, t = 0 min	760	879	0.44	1.1	1549	344
	DMPC, t = 20 min	760	879	0.43	1.2	1551	341
	DMPC, t = 40 min	760	879	0.46	1.0	1551	338
	DMPC, t = 60 min	760	881	0.49	1.1	1549	338
	DMPC, t = 180 min	760	881	0.50	1.2	1551	335
Trp102	unfolded	759	879	0.44	1.3	1550	352
	adsorbed	759	879	0.44	1.1	1552	347
	DMPC, t = 0 min	759	879	0.46	1.3	1552	337
	DMPC, t = 20 min	759	879	0.43	1.4	1552	333
	DMPC, t = 40 min	759	877	0.41	1.4	1550	335
	DMPC, t = 60 min	759	877	0.38	1.5	1550	334
	DMPC, t = 180 min	759	877	0.37	1.5	1552	330
Trp170	unfolded	760	879	0.40	1.3	1553	353
	adsorbed	758	879	0.36	1.4	1549	340
	DMPC, t = 0 min	760	879	0.39	1.5	1551	337
	DMPC, t = 20 min	758	875	0.36	1.6	1551	338
	DMPC, t = 40 min	758	875	0.37	1.7	1549	336
	DMPC, t = 60 min	758	875	0.34	1.7	1549	333
	DMPC, t = 180 min	758	875	0.36	1.9	1549	331

Table 6.4: Tabulated UVRR trp mode frequencies for truncated single-trp mutants, unfolded in KP_i buffer, adsorbed on DPPC vesicles, and folding in DMPC vesicles at different time points (t = 0 – 180 min). $R_{W17:W18}$ is the intensity ratio of the W17/W18 modes. R_{FD} is the ratio of the W7 Fermi doublet, I_{1360}/I_{1340}. UVRR frequency accuracy is 2 cm^{-1}. Tryptophan fluorescence for each sample is given by λ_{max}.

Mutant	Description	W18	W17	$R_{W17:W18}$	R_{FD}	W3	λ_{max}
Trp7t	unfolded	760	879	0.45	1.2	1551	355
	adsorbed	760	879	0.44	1.2	1554	352
	DMPC, t = 0 min	760	879	0.40	1.3	1549	342
	DMPC, t = 20 min	760	879	0.39	1.4	1549	336
	DMPC, t = 40 min	760	879	0.38	1.6	1549	330
	DMPC, t = 60 min	760	877	0.35	1.8	1549	330
	DMPC, t = 180 min	760	877	0.36	2.0	1549	326
Trp15t	unfolded	760	881	0.37	1.2	1551	350
	adsorbed	760	879	0.38	1.7	1549	339
	DMPC, t = 0 min	760	879	0.39	1.3	1549	340
	DMPC, t = 20 min	760	881	0.41	1.2	1551	332
	DMPC, t = 40 min	760	881	0.42	1.3	1549	332
	DMPC, t = 60 min	760	881	0.46	1.1	1549	328
	DMPC, t = 180 min	760	881	0.40	1.2	1551	328
Trp102t	unfolded	759	879	0.42	1.3	1550	352
	adsorbed	759	881	0.39	1.6	1552	348
	DMPC, t = 0 min	759	879	0.41	1.5	1552	342
	DMPC, t = 20 min	759	879	0.42	1.5	1550	341
	DMPC, t = 40 min	759	879	0.40	1.4	1550	342
	DMPC, t = 60 min	759	879	0.40	1.7	1550	332
	DMPC, t = 180 min	759	879	0.41	1.7	1550	331
Trp170t	unfolded	760	879	0.35	1.8	1551	350
	adsorbed	758	877	0.36	1.6	1549	341
	DMPC, t = 0 min	760	877	0.33	1.8	1551	335
	DMPC, t = 20 min	758	873	0.35	2.0	1549	332
	DMPC, t = 40 min	758	875	0.33	2.1	1549	334
	DMPC, t = 60 min	758	873	0.35	2.1	1549	334
	DMPC, t = 180 min	758	875	0.37	2.1	1549	329

Table 6.5: Tabulated UVRR tyrosine modes for kinetics studies of full-length OmpA single-trp and trp-less mutants. All frequencies are in cm^{-1}. $R_{Y1:2Y16a}$ is the ratio of intensities of the Y1 and 2Y16a modes. Accuracy is 2 cm^{-1}.

Mutant	Description	Y1, 2Y16a	$R_{Y1:2Y16a}$	Y9a	Y7a	Y8a
Trp7	unfolded	835, 855	0.59	1179	1209	1611
	adsorbed	831, 853	0.59	1177	1209	1613
	DMPC, t = 0 min	833, 855	0.59	1179	1209	1611
	DMPC, t = 20 min	835, 855	0.56	1179	1209	1611
	DMPC, t = 40 min	833, 853	0.59	1179	1211	1611
	DMPC, t = 60 min	833, 855	0.59	1179	1209	1611
	DMPC, t = 180 min	833, 855	0.56	1177	1209	1611
Trp15	unfolded	833, 855	0.65	1179	1209	1611
	adsorbed	833, 855	0.61	1179	1209	1609
	DMPC, t = 0 min	833, 853	0.59	1179	1209	1611
	DMPC, t = 20 min	831, 855	0.56	1179	1209	1611
	DMPC, t = 40 min	833, 853	0.53	1179	1209	1611
	DMPC, t = 60 min	833, 855	0.51	1179	1209	1611
	DMPC, t = 180 min	831, 855	0.50	1177	1209	1611
Trp102	unfolded	831, 853	0.55	1177	1209	1613
	adsorbed	831, 853	0.58	1179	1209	1613
	DMPC, t = 0 min	831, 853	0.57	1177	1209	1613
	DMPC, t = 20 min	833, 853	0.55	1177	1209	1613
	DMPC, t = 40 min	831, 853	0.54	1177	1207	1613
	DMPC, t = 60 min	833, 853	0.54	1177	1207	1613
	DMPC, t = 180 min	831, 853	0.54	1175	1207	1613
Trp170	unfolded	832, 853	0.57	1177	1207	1613
	adsorbed	832, 855	0.61	1179	1209	1611
	DMPC, t = 0 min	832, 853	0.55	1177	1207	1613
	DMPC, t = 20 min	830, 851	0.58	1175	1205	1613
	DMPC, t = 40 min	830, 851	0.61	1175	1205	1613
	DMPC, t = 60 min	830, 851	0.60	1175	1205	1613
	DMPC, t = 180 min	830, 851	0.59	1175	1205	1613
Trp-less	unfolded	833, 853	0.64	1179	1209	1611
	adsorbed	833, 853	0.61	1179	1209	1609
	DMPC, t = 0 min	833, 855	0.63	1179	1209	1611
	DMPC, t = 20 min	831, 855	0.57	1179	1209	1611
	DMPC, t = 40 min	833, 853	0.57	1179	1209	1611
	DMPC, t = 60 min	833, 855	0.59	1179	1209	1611
	DMPC, t = 180 min	831, 855	0.61	1179	1209	1611

Table 6.6: Tabulated UVRR tyrosine modes for kinetics studies of OmpA truncated single-trp mutants. All frequencies are in cm^{-1}. $R_{Y1:2Y16a}$ is the ratio of intensities of the Y1 and 2Y16a modes. Accuracy is 2 cm^{-1}.

Mutant	Description	Y1, 2Y16a	$R_{Y1:2Y16a}$	Y9a	Y7a	Y8a
Trp7t	unfolded	833, 855	0.57	1179	1209	1611
	adsorbed	831, 853	0.52	1179	1209	1613
	DMPC, t = 0 min	833, 855	0.59	1179	1209	1609
	DMPC, t = 20 min	835, 855	0.60	1179	1209	1611
	DMPC, t = 40 min	831, 855	0.57	1179	1209	1611
	DMPC, t = 60 min	831, 855	0.61	1177	1209	1611
	DMPC, t = 180 min	831, 855	0.56	1177	1209	1609
Trp15t	unfolded	833, 855	0.57	1179	1209	1611
	adsorbed	831, 853	0.63	1179	1209	1609
	DMPC, t = 0 min	833, 855	0.52	1179	1209	1609
	DMPC, t = 20 min	833, 855	0.54	1179	1209	1611
	DMPC, t = 40 min	831, 855	0.51	1177	1209	1609
	DMPC, t = 60 min	831, 855	0.52	1177	1209	1611
	DMPC, t = 180 min	829, 853	0.49	1177	1209	1611
Trp102t	unfolded	831, 853	0.53	1177	1209	1613
	adsorbed	831, 855	0.61	1179	1209	1613
	DMPC, t = 0 min	831, 853	0.53	1177	1209	1613
	DMPC, t = 20 min	831, 853	0.54	1175	1207	1613
	DMPC, t = 40 min	831, 853	0.52	1175	1207	1613
	DMPC, t = 60 min	829, 853	0.53	1175	1207	1613
	DMPC, t = 180 min	829, 853	0.55	1175	1207	1613
Trp170t	unfolded	830, 853	0.57	1177	1207	1615
	adsorbed	831, 851	0.59	1175	1207	1613
	DMPC, t = 0 min	830, 853	0.53	1177	1207	1615
	DMPC, t = 20 min	830, 851	0.50	1175	1205	1613
	DMPC, t = 40 min	830, 851	0.54	1175	1205	1613
	DMPC, t = 60 min	830, 851	0.50	1175	1205	1613
	DMPC, t = 180 min	830, 853	0.52	1175	1205	1613

6.7 References

(1) Anfinsen, C. B. *Science* **1973**, *181*, 223.

(2) Bulieris, P. V.; Behrens, S.; Holst, O.; Kleinschmidt, J. H. *J. Biol. Chem.* **2003**, *278*, 9092

(3) Kleinschmidt, J. H.; Wiener, M. C.; Tamm, L. K. *Protein Science* **1999**, *8*, 2065.

(4) Surrey, T.; Jahnig, F. *J. Biol. Chem.* **1995**, *270*, 28199.

(5) Surrey, T.; Schmid, A.; Jahnig, F. *Biochem.* **1996**, *35*, 2283.

(6) Kleinschmidt, J. H.; Tamm, L. K. *J. Mol. Biol.* **2002**, *324*, 319.

(7) Tamm, L. K.; Arora, A.; Kleinschmidt, J. H. *Journal of Biological Chemistry* **2001**, *276*, 32399.

(8) Rodionova, N. A.; Tatulian, S. A.; Surrey, T.; Jahnig, F.; Tamm, L. K. *Biochem.* **1995**, *34*, 1921.

(9) Kleinschmidt, J. H.; Tamm, L. K. *Biochem.* **1996**, *35*, 12993.

(10) Kleinschmidt, J. H.; den Blaauwen, T.; Driessen, A. J. M.; Tamm, L. K. *Biochemistry* **1999**, *38*, 5006.

(11) Chi, Z.; Asher, S. A. *J. Phys. Chem. B* **1998**, *102*, 9595

(12) Harada, I. M., T. ; Takeuchi, H. *Spectrochimica Acta* **1986**, *42A*, 307.

(13) Miura, T. T., H. ; Harada, I. *Biochemistry* **1988**, *27*, 88.

(14) Miura, T. T., H. ; Harada, I. *Journal of Raman Spectroscopy* **1989**, *20*, 667.

(15) Spiro, T. G.; Grygon, C. A. *Journal of Molecular Structure* **1988**, *173*, 79.

(16) Sanchez, K. M.; Neary, T. J.; Kim, J. E. *J. Phys. Chem. B* **2008**, *112*, 9507.

(17) Sanchez, K. M.; Gable, J. E.; Schlamadinger, D. E.; Kim, J. E. *Biochemistry* **2008**, *47*, 12844.

(18) Surrey, T.; Jahnig, F. *Proc. Natl. Acad. Sci. U.S.A.* **1992**, *89*, 7457.

(19) Hong, H.; Tamm, L. K. *Proc. Natl. Acad. Sci. U.S.A.* **2004**, *101*, 4065.

(20) White, S. H.; Wimley, W. C. *Annu. Rev. Biophys. Biomol. Struct.* **1999**, *28*, 319.

(21) Lee, A. G. *Biochim. Biophys. Acta* **2003**, *1612*, 1.

(22) Scheiner, S.; Kar, T.; Pattanayak, J. *J. Am. Chem. Soc.* **2002**, *124*, 13257.

(23) Brandl, M.; Weiss, M. S.; Jabs, A.; Suhnel, J.; Hilgenfeld, R. *J. Mol. Biol.* **2001**, *307*, 357.

(24) Serrano, L.; Bycroft, M.; Fersht, A. R. *J. Mol. Biol.* **1991**, *218*, 465.

(25) Wimley, W. C.; Creamer, T. P.; White, S. H. *Biochemistry* **1996**, *35*, 5109.

(26) Burley, S. K.; Petsko, G. A. *Science* **1985**, *229*, 23.

(27) Burley, S. K.; Petsko, G. A. *FEBS Lett.* **1986**, *203*, 139.

(28) Hong, H.; Park, S.; Flores Jimenez, R. H.; Rinehart, D.; Tamm, L. K. *J. Am. Chem. Soc.* **2007**, *129*, 8320.

(29) Schlamadinger, D. E.; Gable, J. E.; Kim, J. E. *J. Phys. Chem.* **2009**, *accepted*.

(30) Burnstein, E. A.; Vedenkina, N. S.; Ivkova, M. N. *Photochem. and Photobiol.* **1973**, *18*, 263.

(31) Jordan, T.; Eads, J. C.; Spiro, T. G. *Protein Sci.* **1995**, *4*, 716.

(32) Gao, Y.; El-Mashtoly, S. F.; Pal, B.; Hayashi, T.; Harada, K.; Kitagawa, T. *J. Biol. Chem.* **2006**, *281*, 24637

(33) Ahmed, A.; Beta, I. A.; Mikhonin, A. V.; Asher, S. A. *J. Am. Chem. Soc.* **2005**, *127*, 10943.

(34) Dougherty, D. A. *Science* **1996**, *271*, 163.

(35) Gallivan, J. P.; Dougherty, D. A. *Proc. Natl. Acad. Sci. U.S.A.* **1999**, *96*, 9459.

(36) Xue, Y.; Davis, A. V.; Balakrishnan, G.; Stasser, J. P.; Staehlin, B. M.; Focia, P.; Spiro, T. G.; Penner-Hahn, J. E.; O'Halloran, T. V. *Nat. Chem. Biol.* **2008**, *4*, 107

(37) Thomas, G. J. J. *Biopolymers* **2002**, *67*, 214.

(38) Wen, Z. Q.; Thomas, G. J. J. *Biochem.* **2000**, *39*, 146.

(39) Yorita, H.; Otomo, K.; Hiramatsu, H.; Toyama, A.; Miura, T.; Takeuchi, H. *J. Am. Chem. Soc.* **2008**, 15266.

(40) Ma, J. C.; Dougherty, D. A. *Chem. Rev.* **1997**, *97*, 1303.

(41) Takeuchi, H. *Biopolymers* **2003**, *72*, 305

(42) Duan, G.; Smith Jr., V. H.; Weaver, D. F. *J. Phys. Chem. A* **2000**, *104*, 4521.

(43) Juszczak, L. J.; Desamero, R. Z. B. *Biochem.* **2009**, *48*, 2777.

(44) Kim, J. E.; Arjara, G.; Richards, J. H.; Gray, H. B.; Winkler, J. R. *J. Phys. Chem. B* **2006**, *110*, 17656.

(45) Babakhani, A.; Gorfe, A. A.; Gullingsrud, J.; Kim, J. E.; McCammon, J. A. *Biopolymers* **2007**, *85*, 490.

(46) Pautsch, A.; Schulz, G. E. *Nat. Struct. Biol.* **1998**, *5*, 1013.

(47) Pautsch, A.; Schulz, G. E. *J. Mol. Biol.* **2000**, *298*, 273.

(48) White, S. H. *Adv. Protein Chem.* **2006**, *72*, 157.

(49) Sanderson, J. M. *Org. Biomol. Chem.* **2007**, *5*, 3276

(50) van der Wel, P. C. A.; Reed, N. D.; Greathouse, D. V.; Koeppe II, R. E. *Biochem.* **2007**, *46*, 5714.

(51) Bond, P. J.; Sansom, M. S. P. *J. Mol. Biol.* **2003**, *329*, 1035.

(52) Zakharian, E.; Reusch, R. N. *Biochemistry* **2005**, *44*, 6701.

(53) Tamm, L. K.; Liang, B. *Prog. NMR Spect.* **2006**, *48*, 201.

(54) Sugawara, E.; Nikaido, H. *J. Mol. Biol.* **1992**, *267*, 2507.

(55) Sugawara, E.; Nikaido, H. *J. Biol. Chem.* **1994**, *269*, 17981

(56) DeMot, R.; Vanderleyden, J. *Mol. Microbiol.* **1994**, *12*, 333

(57) Koebnik, R. *Mol. Microbiol.* **1995**, *16*, 1269

(58) Kleinschmidt, J. H.; Tamm, L. K. *Biochem.* **1999**, *38*, 4996

(59) Pocanschi, C. L.; Patel, G. J.; Marsh, D.; Kleinschmidt, J. H. *Biophys. J.* **2006**, *91*, L75.

Chapter 7

Summary and Future Experiments

7.1 Thermodynamic studies of OmpA

One of the goals of membrane protein folding studies is to ascertain the molecular interactions of anchoring trp residues that promote conformational stability of proteins in the membrane. A variety of non-covalent interactions that promote protein stability have been determined for soluble proteins and a few membrane proteins. Hydrogen bonds are the main driving force for formation of protein secondary structure, and also include hydrogen bonds with side-chains and lipid bilayer.[1-5] Free energies of transfer from water to the bilayer interface determined from White-Wimley hydrophobicity scales, in addition to the anchoring roles aromatic residues play in the membrane are additional stabilizing interactions.[6-9] Steady-state fluorescence measurements of the anchoring tryptophan residues in OmpA were used to directly measure the relative populations of folded and unfolded protein. The conformational stabilities from these fluorescence studies were calculated for wild type and single-trp mutants, and the trends were discussed in terms of important non-covalent interactions. Wild type OmpA reported the largest stability. The full-length single-trp mutants had lower stabilities, consistent with removal of four of the five native stabilizing trp residues. The trends in free energies of unfolding are likely a combination of non-covalent interactions. Neighboring aromatic residues favorably interact to contribute to the stability of the protein. Trp-7, Trp-57, and Trp-143 have neighboring aromatic residues that likely contribute to protein stability.

chain is also important, as shown in our study if Trp-15. The unique amphiphilic nature of trp residues provides additional stability in the case of Trp-102. The overall contribution of individual trp residues to OmpA stability ranges from 2 – 4 kcal/mol, consistent with previous studies.[10] Thermodynamic studies were also performed on truncated single-trp mutants. For these studies, the C-terminal soluble domain of the protein was removed. The thermodynamic stabilities increased for these truncated mutants. Our results indicated the importance of the unfolded state of the protein. Removal of the tail destabilized the unfolded transmembrane domain of the protein and resulted with increased stabilities for these truncated mutants.[11]

7.2 Wavelength Dependence Studies

The first UVRR excitation wavelength dependence was performed on the membrane protein OmpA, using excitation wavelengths ranging from 206.5 nm – 236.5 nm. The excitation wavelength dependence was performed on tyrosine and tryptophan residues in OmpA, using a single-trp mutant and a trp-less mutant, to determine the wavelength with the greatest enhancement of trp signal in OmpA. These studies were also performed on the aqueous model compounds tryptophan, tyrosine, and phenylalanine. The largest Raman cross sections for aqueous model compounds, trp, tyr, and phe, were found using 220-nm excitation, consistent with previous measurements.[12,13] Raman cross sections for aromatic residues in OmpA were different. The greatest enhancement of signal from tryptophan residues in OmpA was obtained with 228-nm excitation; the greatest enhancement of tyrosine signal in OmpA was obtained with 233-nm excitation. Our results are comparable excitation profile studies on soluble proteins.[14] Differences observed in cross sections between trp and tyr residues in the

protein and for aqueous model compounds can be attributed to the local environment effects that have been shown to influence Raman cross sections.[14]

7.3 UVRR steady-state studies of folded and unfolded OmpA

The first UVRR spectra of OmpA under *in vitro* folding and unfolding conditions were presented, and showed the applicability of using UVRR to study protein folding. UVRR spectra were collected of wild type OmpA, unfolded in buffer and folded in the highly-scattering environments of detergent micelles or lipid bilayers. These aromatic residues, trp, tyr, and phe, are preferentially located at the water/bilayer interface.[7,10,15] Modification in trp vibrational structure and microenvironment is expected and was observed when protein is transferred from an unfolded structure in aqueous environment to a folded structure in the membrane. Future UVRR steady-state studies can probe OmpA backbone to provide secondary structure information on the soluble tail. Currently, only the crystal structure of the transmembrane domain has been determined for OmpA.[16,17] In the current studies, UVRR spectra were collected of OmpA using an excitation wavelength of 206.5 nm. Small changes were observed in spectra of folded and unfolded protein. However, using an excitation wavelength closer to the absorption band of the peptide backbone should provide more conclusive results. Increased enhancement should be observed using excitation wavelengths closer to the absorption band of the peptide group at ~190 nm.[12,18-20] Differences in UVRR spectra for full-length and truncated OmpA unfolded in buffer and folded could provide some additional structural information of the soluble tail not observed using longer excitation wavelengths (206.5 nm).

7.4 UVRR folding kinetics studies of OmpA

UVRR spectra of single-trp mutants of OmpA were collected at different time points during the folding/insertion process. The trp residues under investigation were chosen for their unique environment and/or thermodynamic properties determined from our previous work.[11] Spectral changes were correlated to different intermolecular interactions, including amino-aromatic interactions (Trp-15), formation of hydrophobic pocket (Trp-7 and Trp-170), and hydrogen bonds. These results show non-covalent interactions between complementary beta-sheets on similar timescales, consistent with a picture of cooperative folding/insertion of OmpA in the lipid bilayer.[21,22] An adsorbed protein was also monitored to determine the relationship, if any, between the folding pathway and this adsorbed intermediate. Spectra of the adsorbed species have similarities to both unfolded protein and pf protein immediately after initiation of folding. This result suggests the adsorbed protein is a unique intermediate along our folding pathway.

In the current study, we attributed the spectroscopic changes observed in the Trp-15 spectra to amino-aromatic interaction between Trp-15 and Gln17. To further investigate the source of these spectroscopic changes, we can remove the Gln17 from the sequence and replace it with asparagine (Asn) or isoleucine (Ile). Asn residue is a shorter version of Gln. It maintains the $–NH_2$ group, but lacks an additional $–CH_2$ group in the side-chain. Isoleucine (Ile) has a similar chain length but replaces the $–NH_2$ group, with a $–CH_3$ group. Both mutations potentially disrupt this amino-aromatic interaction; if this interaction is responsible for the spectral features in the Trp-15 then spectral changes would be observed. Cation-π interactions have already been identified in stabilizing OmpA structure.[23] Additional cation-π interactions can be probed in OmpA by replacing

the Gln17 with Lys or Arg residues which form these interactions.[24] Additional UVRR kinetics studies on millisecond or second timescales could provide valuable information on intermolecular interactions that form on these shorter timescales.

7.5 Future Directions: Badan-labeled OmpA fluorescence

Tryptophan residues are frequently utilized as reporters of environment in biological systems because the spectroscopic properties of these intrinsic fluorophores are highly sensitive to environment.[25] In addition, few trp residues are found in the primary sequence of proteins, allowing site-specific information to be obtained.[26] The dynamic range of the tryptophan residues in OmpA is ~25 nm between folded (~330 nm) and unfolded (~355 nm) protein.

Badan can also provide site-specific environmental information of membrane proteins.[27] It is a thiol reactive probe that is highly sensitive to its environment. Badan emission is ~500 nm in a hydrophobic environment and ~550 nm in an aqueous environment. It has a much larger dynamic range observed in fluorescence values compared to trp residues in OmpA, thereby making it a more sensitive probe for local environment.

Badan specifically labels cysteine residues. Only two native cysteine residues are located in OmpA and both residue in the soluble domain. As proof of concept, two different locations in OmpA were chosen for Badan labeling to observe changes in fluorescence in two different environments. The phe residue at position 15 or at position 40 were mutated to cys residues in the truncated Trp-less mutant for Badan labeling and are referred to as W0t-F15C (F15C) and W0t-F40C (F40C). F15C is located at the top of the barrel and faces the lipid bilayer; F40C is located in the center of the barrel and faces

the interior of the aqueous pore. Figure 7.1 shows the location of these two mutants in the crystal structure of OmpA. Absorbance ratios determined a labeling efficiency of ~50%. Badan-labeled protein obtained a folded structure in the presence of DMPC vesicles, as determined from CD measurements and SDS-PAGE gel mobility (data not shown).

Fluorescence experiments were performed on free Badan in the same conditions as OmpA folding studies. Using 380-nm excitation, fluorescence spectra were collected of free Badan in DMPC vesicles at 30 ºC, DPPC vesicles at 25 ºC (room temp), 8 M urea, and KP_i buffer. The fluorescence spectra of free Badan in these conditions are shown in Figure 7.2. Free Badan in aqueous environment reports a fluorescence value of ~550 nm, and reports a value of ~500 nm in hydrophobic environments. Fluorescence spectra of free Badan in hydrophobic environments shows at least two populations, consistent with previous studies that indicate multiple excited states for Badan.[27] Tabulated emission maxima is found in Table 7.1.

Fluorescence spectra of Badan in OmpA are considerably different. Spectra of Badan-labeled W0t-F15C OmpA in different folding conditions are shown in Figure 7.3. Spectra were collected at different time points in the folding process in DMPC vesicles, t = 0 – 180 min following initiation of folding. A shift in emission maxima and increase in quantum yield are observed when protein folds into DMPC vesicles. These spectral changes are consistent with those observed for trp residues in OmpA (see Figure 7.4). The timescales for spectral changes in Badan fluorescence occur on similar timescales as trp fluorescence spectral changes.[22] This result implies the addition of an organic fluorophore to OmpA does not drastically change the folding kinetics.

Emission maxima of Badan-labeled OmpA shift from 510 nm to 477 nm at t = 0 min to t = 180 min incubation time in DMPC vesicles. Unfolded labeled protein has an emission value of 543 nm in 8 M urea, and adsorbed labeled protein has a value of 450 nm in DPPC vesicles. Emission maxima for free Badan are different from Badan in the protein as observed by changes the emission maxima. These results provide evidence for protein effects on Badan fluorescence. Tabulated emission maxima are found in Table 7.1.

Fluorescence spectra of Badan-labeled F40C OmpA in different conditions are shown in Figure 7.5. F40C is located in the center of lipid bilayer and faces the center of the barrel. The environment of Badan at this location is different than the environment located at residue position 15. The fluorescence values for Badan at residue position 40 report values of 537 nm, 519 nm, 481 nm, and 474 nm, for protein unfolded in 8 M urea, unfolded in KP_i, folded in DMPC vesicles, and adsorbed in DPPC vesicles, respectively. Fluorescence values are consistent with a more aqueous environment for the Badan label in the protein. Surprisingly, Badan fluorescence in F40C OmpA in 8 M urea is different from the value determined for labeled F15C in 8 M urea and suggests different environments in unfolded protein at these two locations. Tabulated emission maxima are found in Table 7.1.

In addition to steady-state fluorescence measurements of free Badan and Badan in OmpA, anisotropy values were also determined. The anisotropy spectra for free Badan, and Badan-labeled W0t-F15C are shown in Figures 7.6 and 7.7, respectively. Hindered rotation of fluorophore is expected when protein is folded in vesicle, and free rotation is expected when protein in unfolded in buffer. Free Badan shows the highest anisotropy in

glycerol, consistent with hindered rotation of the fluorophore in this viscous solvent. Free Badan in the presence of vesicle also has a non-zero anisotropy value, and indicates some interaction of free Badan with vesicle. Negligible anisotropy was found for free Badan in water and 8 M urea.

The anisotropy of Badan in F15C OmpA has the highest values folded in DMPC vesicles, folded in DPPC vesicles, and adsorbed on DPPC vesicles. A non-zero anisotropy value is also found for labeled protein in KP_i buffer, and indicates hindered rotation of Badan in this environment. Interestingly, the anisotropy shows a wavelength dependence for labeled protein in 8 M urea, and indicates the presence of two excited states.[28]

Fluorescence values of Badan-labeled protein shift in the presence of denaturant. This shift with increasing concentrations of urea can be used to calculate the free energy of unfolding for Badan-labeled W0t-F15C. The refolding curve for W0t-F15C is shown in Figure 7.8. The $\Delta G^{\circ}_{H_2O}$ for labeled protein was determined to be 1.1 kcal/mol, a value much smaller than that determined for wild type OmpA protein using trp fluorescence. These results for the Badan labeled protein are consistent with removal of all five native anchoring trp residues in OmpA.

In summary, these preliminary results from the steady-state fluorescence spectra and anisotropy data show the applicability of using Badan fluorescence to determine environmental information in the membrane protein OmpA.

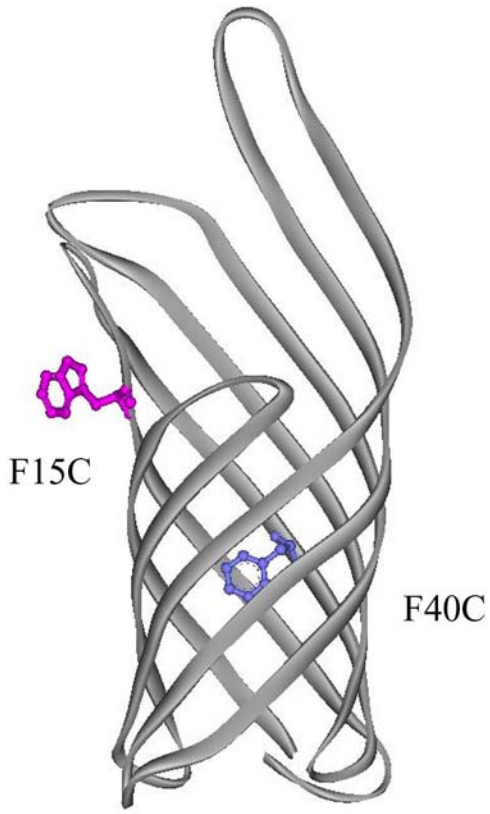

Figure 7.1: Crystal structure of OmpA highlighting the location of the cysteine residues for Badan labeling. A trp residue is located at position 15 in wild type OmpA. In the Trp-less mutant, it replaced with a phe residue.

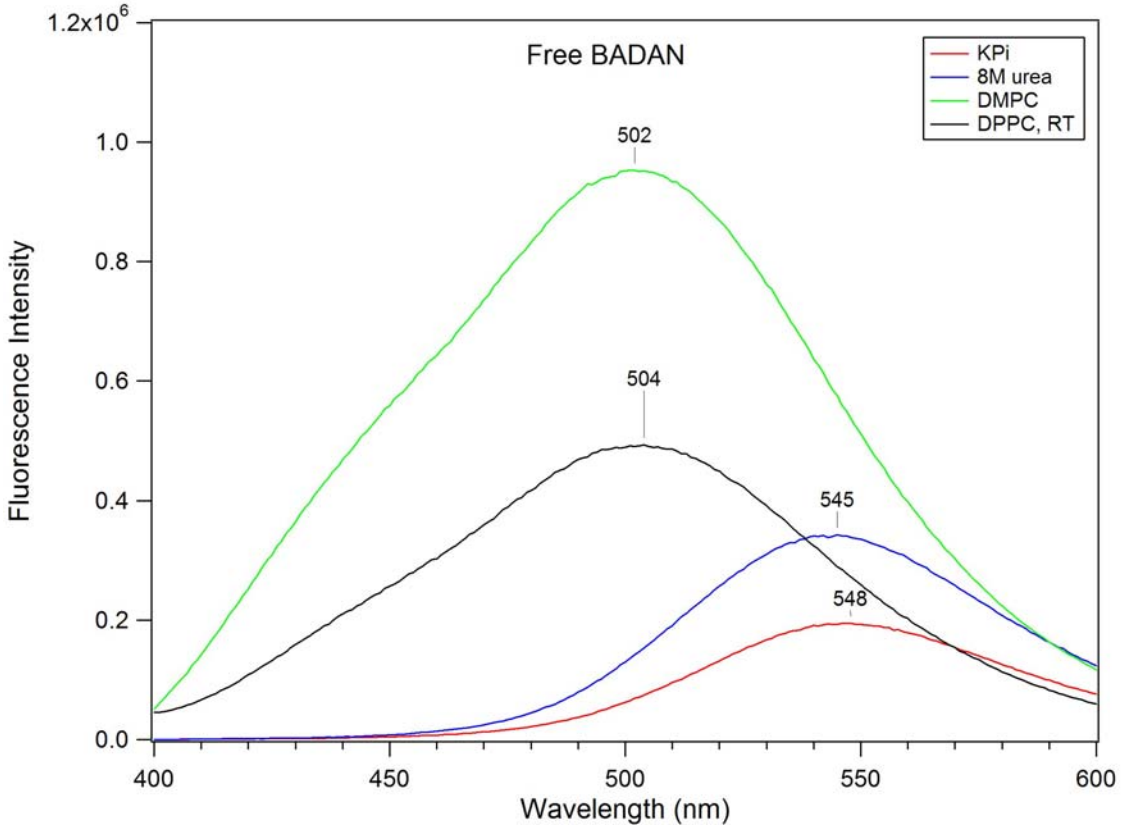

Figure 7.2: Free Badan label in KP_i buffer, 8 M urea, DMPC vesicles, and DPPC vesicles at room temperature (RT).

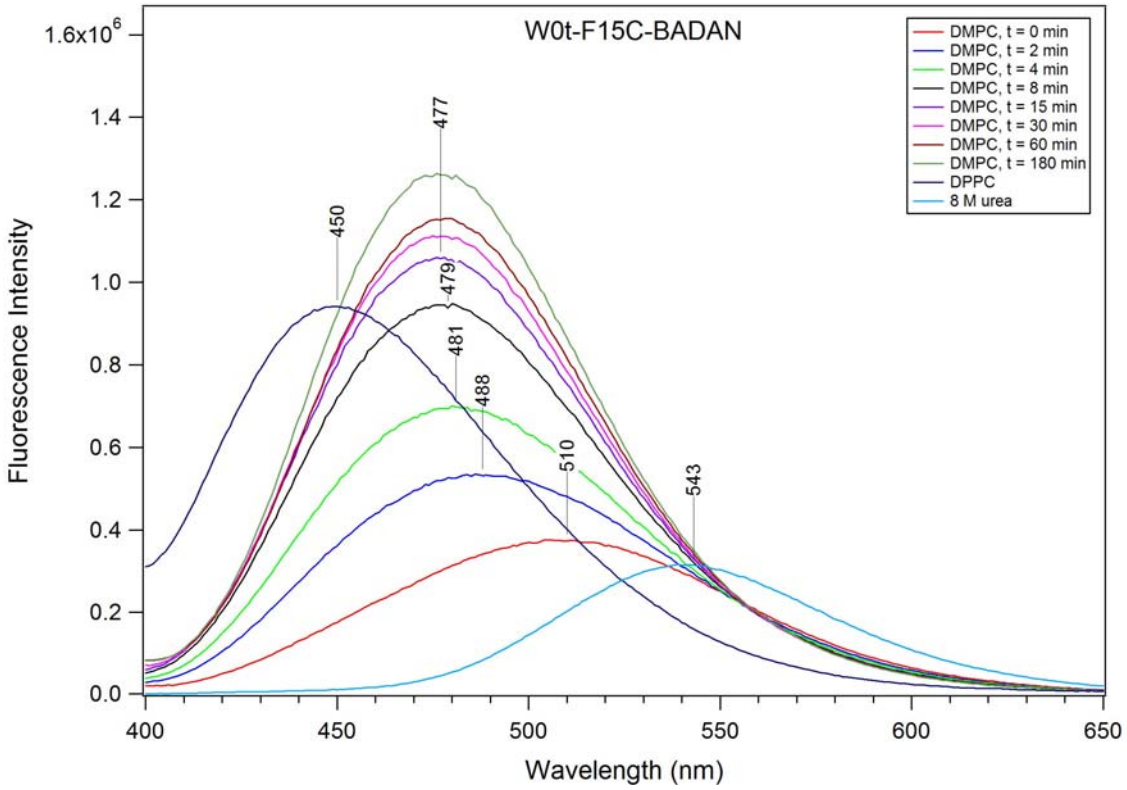

Figure 7.3: Fluorescence spectra of W0t-F15C Badan-labeled protein at different time points in the folding process in DMPC vesicles. Protein was folded in DMPC at t = 180 min, adsorbed on DPPC vesicles, and unfolded in 8 M urea.

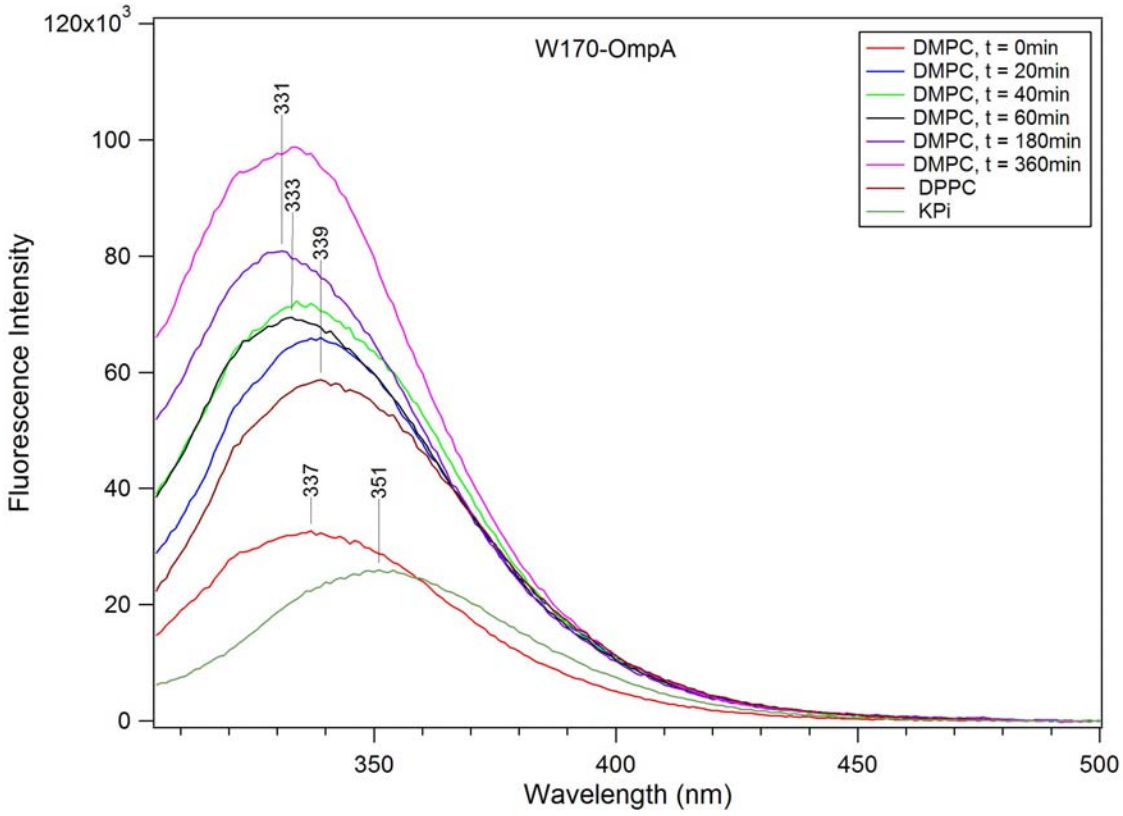

Figure 7.4: Representative tryptophan fluorescence spectra of the single-trp mutant Trp-170 at different time points in the folding process in DMPC vesicles (t = 0 – 180 min), protein adsorbed to DPPC vesicles, and unfolded in KP_i buffer.

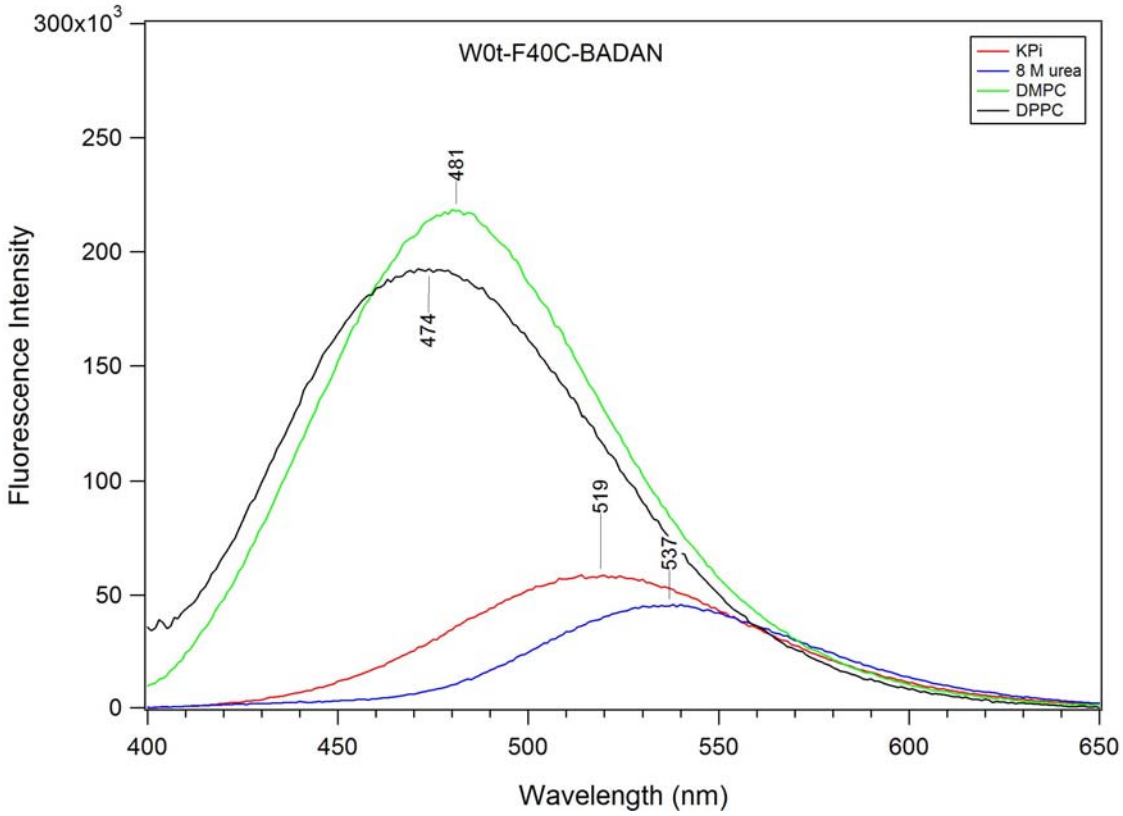

Figure 7.5: Fluorescence spectra of W0t-F40C Badan-labeled protein unfolded in KP_i buffer and 8 M urea, folded in DMPC vesicles, and adsorbed in DPPC vesicles.

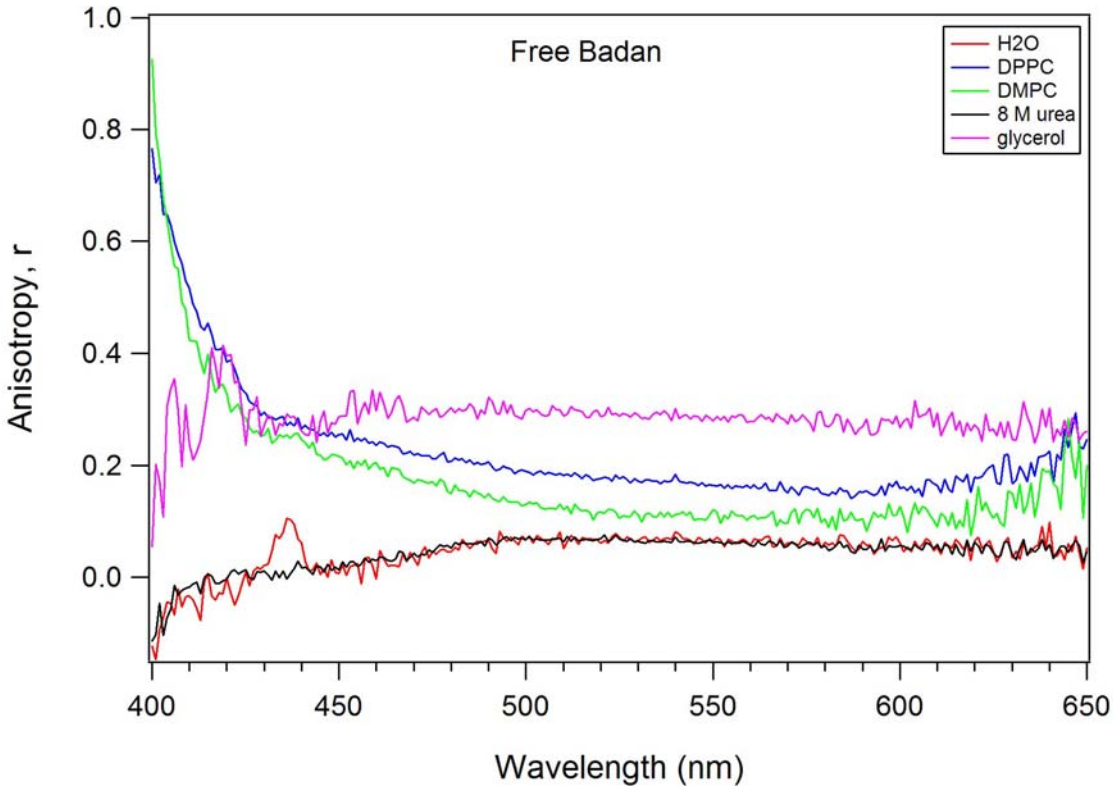

Figure 7.6: Steady-state anisotropy values determined for free Badan in water, DPPC vesicles, DMPC vesicles, 8 M urea, and glycerol.

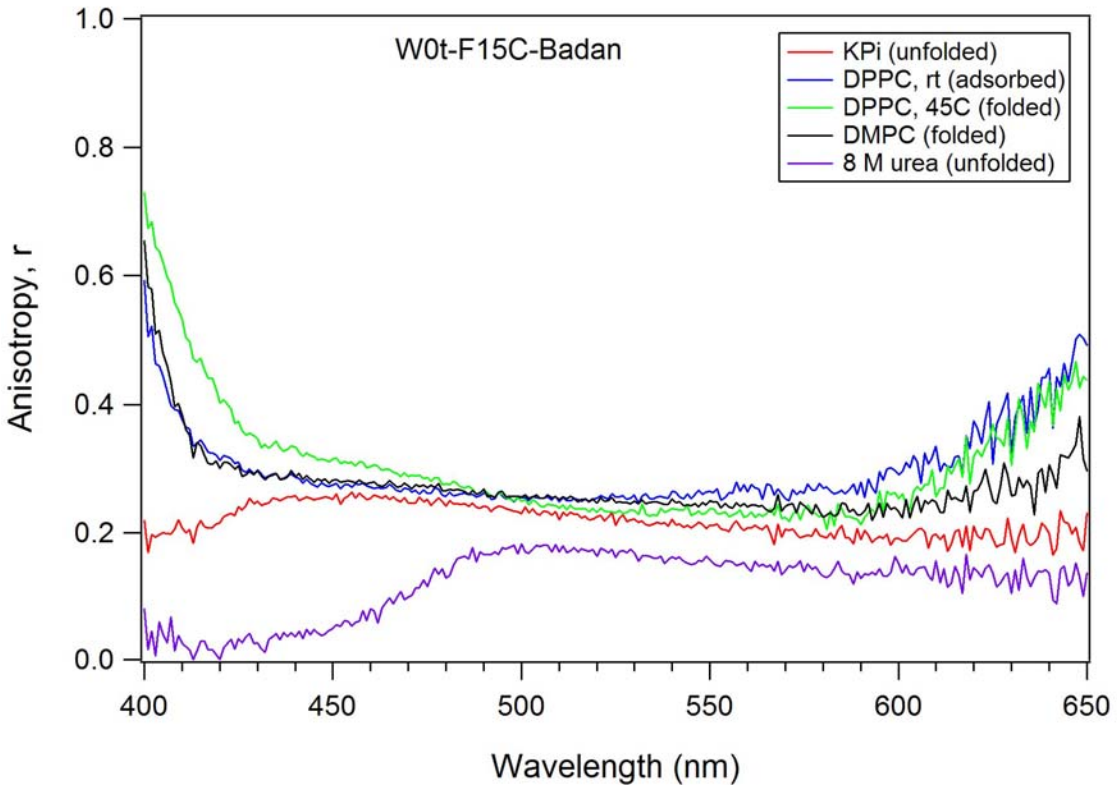

Figure 7.7: Steady-state anisotropy values determined for Badan-labeled W0t-F15C OmpA unfolded in KP_i buffer, adsorbed to DPPC vesicles, folded in DPPC vesicles, folded in DMPC vesicles, and unfolded in 8 M urea.

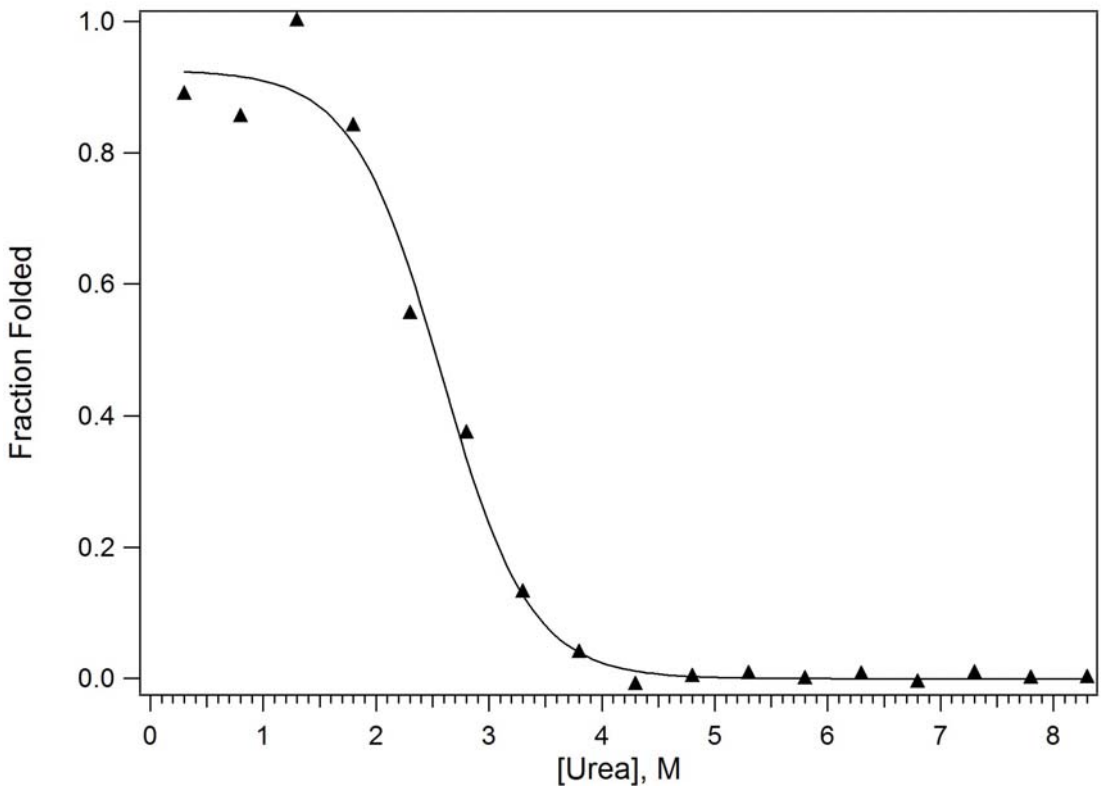

Figure 7.8: Refolding curve of Badan-labeled W0t-F15C OmpA. Protein was equilibrated overnight in 50-nm diameter DMPC vesicles and increasing concentrations of urea, at 37 ºC.

Table 7.1: Tabulated emission maxima for free Badan, Badan-labeled W0t-F15C OmpA, and Badan-labeled W0t-F40C OmpA. Values are reported in nm.

	free Badan	F15C-Badan	F40C-Badan
KPi	548	519	519
8 M urea	545	543	537
DMPC	504	477	481
DPPC	502	450	474

7.6 References

(1) White, S. H. *Adv. Protein Chem.* **2006**, *72*, 157.

(2) Baker, E. N.; Hubbard, R. E. *Prog. Biophys. mole. Biol.* **1984**, *44*, 97.

(3) Burley, S. K.; Petsko, G. A. *Science* **1985**, *229*, 23.

(4) Burley, S. K.; Petsko, G. A. *FEBS Lett.* **1986**, *203*, 139.

(5) Derewenda, Z. S.; Lee, L.; Derewenda, U. *J. Mol. Biol.* **1995**, *252*, 248.

(6) Wimley, W. C.; White, S. H. *Nat. Struct. Biol.* **1996**, *3*, 842.

(7) Wimley, W. C.; Creamer, T. P.; White, S. H. *Biochemistry* **1996**, *35*, 5109.

(8) Yau, W.-M.; Wimley, W. C.; Gawrisch, K.; White, S. H. *Biochemistry* **1998**, *37*, 14713.

(9) Lee, A. G. *Biochim. Biophys. Acta* **2003**, *1612*, 1.

(10) Hong, H.; Park, S.; Flores Jimenez, R. H.; Rinehart, D.; Tamm, L. K. *J. Am. Chem. Soc.* **2007**, *129*, 8320.

(11) Sanchez, K. M.; Gable, J. E.; Schlamadinger, D. E.; Kim, J. E. *Biochemistry* **2008**, *47*, 12844.

(12) Rava, R. P. S., T.G. *J. Phys. Chem.* **1985**, *89*, 1856.

(13) Fodor, S. P. S.; Copeland, R. A.; Grygon, C. A.; Spiro, T. G. *J. Am. Chem. Soc.* **1989**, *111*, 5509.

(14) Chi, Z.; Asher, S. A. *J. Phys. Chem. B* **1998**, *102*, 9595

(15) Babakhani, A.; Gorfe, A. A.; Gullingsrud, J.; Kim, J. E.; McCammon, J. A. *Biopolymers* **2007**, *85*, 490.

(16) Pautsch, A.; Schulz, G. E. *Nat. Struct. Biol.* **1998**, *5*, 1013.

(17) Pautsch, A.; Schulz, G. E. *J. Mol. Biol.* **2000**, *298*, 273.

(18) Dudik, J. M.; Johnson, C. R.; Asher, S. A. *J. Phys. Chem.* **1985**, *89*, 3805

(19) Huang, C. Y.; Balakrishnan, G.; Spiro, T. G. *J. Ram. Spect.* **2006**, *37*, 277.

(20) Chi, Z.; Chen, X. G.; Holtz, J. S.; Asher, S. A. *Biochem.* **1998**, *37*, 2854.

(21) Kleinschmidt, J. H.; Tamm, L. K. *J. Mol. Biol.* **2002**, *324*, 319.

(22) Kleinschmidt, J. H.; den Blaauwen, T.; Driessen, A. J. M.; Tamm, L. K. *Biochemistry* **1999**, *38*, 5006.

(23) Hong, H.; Tamm, L. K. *Proc. Natl. Acad. Sci. U.S.A.* **2004**, *101*, 4065.

(24) Dougherty, D. A. *Science* **1996**, *271*, 163.

(25) Burnstein, E. A.; Vedenkina, N. S.; Ivkova, M. N. *Photochem. and Photobiol.* **1973**, *18*, 263.

(26) Jayasinghe, S.; Hristova, K.; White, S. H. *Protein Sci.* **2001**, *10*, 455.

(27) Koehorst, R. B. M.; Sprujit, R. B.; Hemminga, M. A. *Biophys. J.* **2008**, *94*, 3945

(28) Lakowicz, J. R. *Principles of Fluorescence Spectroscopy*, 3rd ed.; Springer: New York, 2006.

Appendix A

Procedure for the Expression, Isolation, and Purification of Mutants of OmpA

Growth and Isolation of Cells: (1.5 days)

1) Solutions and Supplies (1 growth)

8 mL Stock 1mg/mL Ampicillin*
6 mL Stock 1M IPTG*
10 mL Stock Glucose 33% (by weight)*
300 mL LB broth** + 50µg/mL Ampicillin* + 0.5% glucose*
500 mL LB broth** + 50µg/mL Amp*
6 x 1L LB broth** + 50µg/mL Amp* + 1mM IPTG*
2 x 250 mL centrifuge bottles**
1 box 200-µL pipette tips**
1 box 1000-µL pipette tips**
500 mL 10mM Tris-HCl buffer, pH 7.8 (need not be sterilized

* STERILIZE by filtration through 0.22um filter
** STERILIZE by autoclaving

2) Recipes

Solution	Concentration	Mass (g)	Final Volume (mL)	pH
Glucose	33% by weight	9.93	30	-
Ampicillin	50mg/mL	0.40	8	-
IPTG	1M	1.43	6	-
Tris-HCl*	10mM	0.788	500	7.8

* Adjust the pH of the solution with 1M NaOH drop wise while stirring the solution; use the pH meter.

LB Solutions	300mL	500mL	6 x 1L
Container Needed	1L flask	1L bottle	Large flasks (4L or 6L)
Mass bacto-tryptone	3g	5g	10g
Mass yeast extract	1.5g	2.5g	5g
Mass NaCl	3g	5g	10g
Volume 1M NaOH	0.3mL	0.5mL	1mL
Volume 50mg/mL ampicillin*	0.3mL	0.5mL	1mL
Volume 1M IPTG**	-	-	1mL
Volume 33% glucose*	4.5mL	-	-

*** ADD only after autoclaving LB and allowing solutions to cool to ~50^{0}C.**
**** ADD on Day 2, morning after 300mL overnight growth**

Growth for Wild Type OmpA (JF701 cell, #6045 cell stock in -80 C freezer)

LB Solutions For Wild Type	50mL	500mL	6 x 1L
Container Needed	200 mL flask	1L bottle	Large flasks (4L or 6L)
Mass bacto-tryptone	3g	5g	10g
Mass yeast extract	1.5g	2.5g	5g
Mass NaCl	-	-	-
Volume 1M NaOH	0.05 mL	0.5mL	1mL
Volume 25 mg/mL Streptomycin*	0.05 mL	0.5mL	1mL
Volume 1M IPTG**	-	-	-
Volume 33% glucose*	-	-	-

Notes for LB solutions:
-LB Broth: 1% bacto-tryptone, 0.5% yeast extract, pH 7
-Pour 100mL of MilliQ water into containers first, then add powdered chemicals, then the rest of the Milli-Q water.
-Loosely cap bottles, and cover all containers loosely with aluminum foil, and label with autoclave tape before autoclaving. (Words "autoclaved" will appear on the tape after the autoclaving cycle has been run.)
-All autoclaved solutions should be in containers at least twice as large as the volume of solution.
- Grow starter growth overnight for 16 hrs, transfer to large flasks the next day

3) Procedure:
DAY 1: (~2 hours)
1. Sterilize all LB solutions, pipette tips, and centrifuge bottles in the afternoon of DAY 1, by AUTOCLAVING, using Method 3 (30 minutes liquid cycle) in autoclave on 6th floor of Urey Hall. Run Method 3 by pressing the number 3 button twice. This will take ~1 hour: 30 minute cycle, 15 minute decompression, 10 minute cool down. Forty-five minutes after the start of the cycle, open the door to the autoclave, and let solutions cool down for 10 minutes before removing, as indicated on the autoclave display.

2. When solutions have cooled down (cool enough to hold the flasks with gloved hands) wipe down countertops and the 1000-µL and the 200-µL pipettes with isopropanol. Wipe everything dry with paper towels. Light a flame on the Bunsen Burner.

3. Add the appropriate amount of stock ampicillin to all solutions of LB (300mL, 500mL, and 6 x 1000mL solutions) using sterilized 1000-uL pipette tips. Add glucose (with a sterilized pipette tip) to the 300mL solution of LB. (IPTG will be added to the 6 x 1L LB solutions in the large flasks the following day.) Make sure the flasks are tightly covered with aluminum foil, and the bottle is tightly closed overnight.

4. To start overnight growth: thoroughly clean the 200-uL pipette with isopropanol first, then gently touch a **sterilized** 200-uL pipette tip to the stock cells of the correct OmpA mutant (stored in the -80 ^{0}C freezer found in the "Stock" box), and eject the tip into the 300mL LB solution (containing Amp and glucose). Return stock cells immediately to -80 ^{0}C. Keep the flask covered with aluminum foil, but make sure it is loosely placed over the flask to allow sufficient oxygen to reach the cells. Put the flask into the small Shaker at 37 ^{0}C for **8-10 hours** ("overnight growth"), at 180 rpm.

5. Have the flame on while adding extras to the LB solutions; extinguish flame after everything has been added.

DAY 2: (~9 hours)

1. Wipe down all countertops with isopropanol and wipe dry. Light a flame and keep it on while working with cells/broth.

2. After **8-10** hours in the Shaker, the overnight growth should be cloudy yellow in appearance. Remove overnight growth (300mL flask) from small Shaker.

3. Take the OD_{600} of the overnight growth: Turn on the lamps (2 of them) to the UV-Vis Absorption Spectrometer and let them warm up at least twenty minutes before collecting a spectrum. With a sterile pipette, add 1 mL of LB + Amp (from the 500 mL solution) to a clean labeled disposable cuvette, and use this as the "blank." (Keep the blank solution until the growth is done.) With another sterile pipette tip, take out 1mL of the overnight growth and put it into a separate disposable cuvette. Take a "sample" spectrum of this, and record the OD ("optical density" or absorption) of the solution at 600 nm in the OmpA Growth Logbook (pg 5).

4. Pass the mouth of the flask over the flame a few times, and pour the LB + cells evenly between the two sterilized centrifuge bottles. Ensure volumes are approximately equal by a visual inspection of liquid levels.

5. Centrifuge for 10 minutes at 6000 rpm, 4 ^{0}C, using the JA-14 rotor. Make sure lid is on tight. To run the centrifuge:

a. Flip the switch to the ON position.
b. Determine the rotor size: either JA-17 (small tubes) or JA-14 (large tubes)
c. Press the **Rotor** button, type 17 (for the JA-17 rotor) or 14 (for the JA-14 rotor) on the number pad, and press **Enter/Recall**
d. Press the **Speed** button, type in the correct speed in RPM, press **Enter/Recall**
e. Press the **Time** button, type in the correct time (min or hr), press **Enter/Recall**

f. Press the **Temp** button, type in the temperature (degrees C), press **Enter/Recall**

6. Remove bottles from centrifuge. There should be a small off-white pellet of cells on one side of the centrifuge bottles at the bottom. If there is no pellet visible, centrifuge again using the same parameters in #5 above. If a pellet is clearly visible, pour off the supernatant (liquid) into a bucket of bleach water in the sink. Fill centrifuge bottles half-full with fresh LB + Amp (from the 500mLs LB + Amp); spin down for 10 minutes at 6000 rpm, at 4 ^{0}C. This is the first "wash."

7. After the centrifuge cycle is done, pour off the supernatant and fill the centrifuge bottles half full again using the rest of the 500mLs of LB + Amp. Spin down using the same conditions as #5 above. The cells have now been "washed" twice with LB + Amp.

8. Pour off all but ~10mLs of supernatant in each bottle. With a sterile 1000-uL pipette tip, gently re-suspend the pelleted cells in the LB by gently sucking up and down supernatant (using STERILE) and pushing out the liquid onto the pelleted cells. *Care must be taken to keep the pipette and tip from touching the sides of the centrifuge bottle or directly touching the pellet.

9. Evenly distribute re-suspended cells into the 6 x 1L LB solutions (with Amp), using a sterile disposable large volume pipette and a red bulb.

10. Add 1 mL of stock IPTG (using a sterilized pipette tip) to each 1000mLs of LB+ Amp in the large volume flasks.

11. Place the six flasks into the large Shaker, and place the springs over the flasks and secure them to the holders, making sure the rubber is on the flasks, and not under the metal pieces. MAKE sure the aluminum foil is loosely placed over lid to allow sufficient oxygen to reach the cells. Shake at 37 ^{0} C at 180 rpm.

12. Check the OD (optical density) of the cells at 600 nm, using the UV-Vis Spectrometer, after every hour for the first two hours, and every half hour after until the $OD_{600} \approx 1.0$. (This can take anywhere from 3-5 hours after transfer to the large flasks, depending on the starting OD_{600} of the overnight 300mL growth.*The lower the OD of the overnight growth is, the better!*)

13. When $OD_{600} \approx 1.0$ (or starts to decrease) start "spinning down" the cells. Start with one flask: Pass the mouth of the bottle over the flame a few times first, and then pour ~250mLs of broth into 6 (250-mL) centrifuge bottles (non-sterile, but clean). (Put the other flasks into the fridge in the mean time.) Keep the flasks covered with aluminum foil when centrifuging bottles; flame the inside of the aluminum foil before placing it back on the flask to cover it. Make sure the centrifuge bottles with similar liquid levels are placed directly across from each other in the rotor, to balance the centrifuge. Centrifuge for 10 min, at 6000rpm and 4 ^{0}C.

14. After the centrifuge cycle is complete, pour off supernatant into the bucket of bleach water in the sink. There should now be tan-gray pelleted cells at the bottom of each bottle. Flame the mouth of the flask again and pour more broth (cells) into the centrifuge bottles, and run the centrifuge cycle again, pour off the supernatant, etc. Continue "spinning down" until all six liters of broth (cells) are spun down. Pour off supernant. There should now be fairly large tan-gray pelleted cells at the bottom of each bottle.

15. Take a clean centrifuge bottle. Label it with a piece of colored tape, and weigh the bottle with the cap on. Write down the mass of the (empty) bottle + cap directly on the tape.

16. Gently scoop out the pellet from each bottle and combine them in the weighed centrifuge bottle, using a spoonula.

17. Add ~1mL of 10mM Tris buffer to re-suspend the remaining cells left in the centrifuge bottle. Re-suspend cells, then transfer to next bottle, and re-suspend those left-over cells, etc. Continue on with this process until the 1-mL Tris buffer becomes very cloudy, and then transfer it to the bottle containing the combined cells. Add another mL of Tris buffer, rinse out the bottles, etc. Do this until all of the left-over cells have been transferred to weighed centrifuge bottle, and nothing remains in the bottles.

18. Fill the centrifuge bottle to half full (~125 mLs) with 10mM Tris-HCl buffer. To balance the centrifuge, place an equally filled (water) centrifuge bottle across in the rotor. Centrifuge for 10 minutes at 6000rpm, and 4 ^{0}C.

19. Pour off supernatant in the bleach water, and fill half-full again with Tris buffer. Spin down. (The cells have now been "washed" twice with Tris buffer.)

20. Pour off the supernatant. Weigh the bottle + "wet cells", and record the mass directly on the tape. Record the mass of the wet cells in the logbook (pg 7).

Mass of bottle + cap + wet cells = 69.688 g
Mass of bottle + cap = -59.007 g
10.68 g wet cells

21. Place the centrifuge bottle into the -80 C freezer until ready to continue with the cell-lysis procedure.

22. Throw away all pipette tips, aluminum foil, gloves, etc into the (autoclaveable) red Biohazard trash that has be in contact with any bacteria.

23. Wash all flasks, bottles, etc with bleach water first (to kill bacteria). Then wash thoroughly with warm soapy water. Pat dry and return to cabinet.

**Keep flame on while pouring 6 x 1L of LB + cells into centrifuge bottles

**Always keep the flasks covered with aluminum foil
**When adding extras (like Amp, IPTG, etc) to bottles or flasks, keep pipette and tip away from the sides, and add solutions to the center of the container (to ensure the pipette does not contaminate the container, and also that no solution ends up on the sides).
**Spinning down six liters of LB broth/cells will take 2-3 hours

Cell Lysis and Protein Isolation: (~6 hours)

1) Solutions and Supplies (1 growth)

150 mL 0.75M Sucrose/10mM Tris-HCl, pH 7.8 (COLD)
150 mL 20mM EDTA/0.5 mg/mL Lysozyme (COLD)
100 mM PMSF (*protease inhibitor….really bad stuff!)
8 x 30 mL centrifuge tubes
250 mL centrifuge bottle
ice bath
sonicator with ½" horn (tip)

2) Recipes

Solution	Final Volume (mL)	Components	Mass (g)
Sucrose/Tris/pH 7.8	150	0.75M sucrose	38.5g sucrose
		10mM Tris-HCl	0.236g Tris-HCl
EDTA/Lysozyme	150	20mM EDTA	1.117g EDTA
		0.5 mg/mL Lysozyme	0.075g lysozyme

*Volume of sucrose is NOT trivial! (1g sucrose ≈ 1mL sucrose) A 150ml solution will require ~120mls of water

Notes:
Add all dry chemicals first to container, then add water.
Make all solutions with MilliQ water.
Adjust the pH of the solution using 1M NaOH drop wise (with pH-meter).
Store both solutions in the refrigerator.

3) Procedure:

1. Defrost cells in an ice bath. (Add a few mLs of Tris buffer to help defrost if necessary.) Add a stir bar, and stir for ~1-2 hours (or until cells are defrosted). The cells are now long, slimy, off-white/gray, stringy clumps.

2. While stirring over an ice bath, and add 55mL of COLD Sucrose/Tris solution.

3. Next, add 55mL of COLD EDTA/Lysozyme solution, slowly over 1 minute.

4. Add 1mL of 100mM PMSF.

5. Stir until the cells are completely dissolved for ~1 hour, over ice, or no more clumps are visible.

6. Lyse the cells fully, by sonicating the solution. Place the sonicator tip (1/2" horn) into the solution, but keep tip away from the sides and bottom of bottle. Place a clamp around the bottle to keep it from moving, and place the bottle in an ice bath. Close the door of the sonicator. Sonicate the solution at a 50% duty cycle for 5 minutes (10 minutes total time), with 70% Maximum Amplitude. Solution should be cloudy yellowish/brown, with no visible clumps. If clumps are visible, re-sonicate for another 5 min. cycle.

*** See Drawing 1 below.

Drawing 1: Diagram of placement of Sonicator Tip in centrifuge bottle

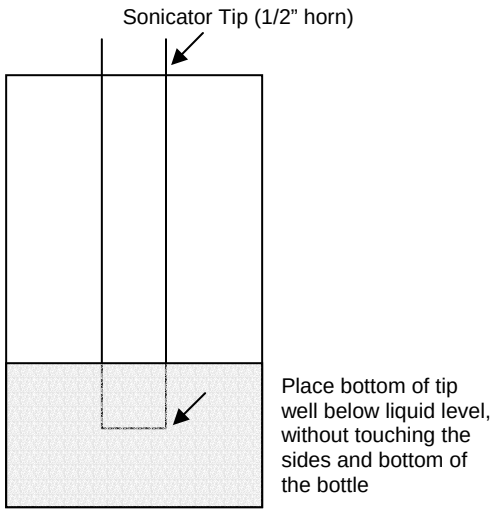

7. Remove centrifuge bottle from sonicator. Rinse the sonicator tip with isopropanol first, then rinse with water, and dry.

8. Distribute the sonicated solution evenly between 4 (30mL) centrifuge tubes, and spin for 15 minutes, 5000 rpm, 4 ^{0}C. (Balance tubes in JF-17 rotor by placing tubes of roughly equal weight across from each other.)

9. Transfer the **SUPERNATANT** to four clean 30mL centrifuge tubes. Balance the weight of the tubes to exactly 0.01 decimal places:
Weigh each tube in Styrofoam holder individually, with cap on. Pair up the tubes closest in weight. Transfer liquid from the heavier tube to the lighter tube until the tubes of one pair are the exact same weight to two decimal places (0.01g). Place these SAME WIGHT tubes across from each other in the rotor to balance the centrifuge. Do the same for the next pair of tubes.

Tube 1: 55.16 g	**Tube 2**: 55.05 g
Tube 3: 55.16 g	**Tube 4**: 55.05 g

* Place Tube 1 and Tube 3 directly across from each other in the rotor, and place Tube 2 and Tube 4 directly across from each other in the rotor.

10. Using the JA-17 rotor, centrifuge the four tubes for 90 minutes at 17,000 rpm (maximum revolutions/min with this rotor), 4 ^{0}C.

11. Pour off the supernatant into a separate container and SAVE it. Label it "**Soluble Protein**", and include the mutant name (OmpA-W_), the date, and your initials. Store the bottle in the chromatography fridge in the equipment room until the entire lysis/ pre-extraction/extraction process is complete. (You will run a gel on all saved supernatant solutions at the end.)

12. The pellets inside the centrifuge tubes should be brownish-red in color with gray in the middle (titanium dust from the sonicator tip). It will have jello-like consistency on the outer edges of the pellet. The pellet should now contain the OmpA membrane protein (and other membrane proteins).

13. Weigh a centrifuge bottle, and label its mass on a piece of tape on top of the lid.

14. The pellets now contain all the membrane proteins from the cells. Combine the pellets into one centrifuge bottle (250mL), by gently scooping out the pellet using a small spatula. Add 1 mL of the pre-extraction buffer to the fist tube, and re-dissolve the remaining pellet fragments. Transfer the mL to the next tube, re-dissolve the pellet fragments, and transfer to the next tube, etc. Continue this process until all the tubes have been washed with the one mL of pre-extraction buffer. Transfer the one mL to the large centrifuge bottle containing the pellets.

15. Add one more mL of pre-extraction buffer, and rinse all the tubes once more, following the above procedure (#15 above). Combine the mL with the pellets. If there are still some remnants of the pellets left in the tubes, rinse with one addition mL of pre-extraction buffer. *A total of two mLs of pre-extraction buffer should have been added (unless one more mL was needed).

16. Weigh the bottle + pellets + 2 mL pre-extraction buffer, and record the mass on the tape. Assuming 1 mL of pre-extraction buffer (urea) = 1 g, subtract out the mass of the urea and the mass of the empty centrifuge bottle from the total mass of bottle + cells + urea, to determine the mass of the membrane proteins.

Mass of bottle + cap + protein + 2mL urea = 62.688 g
Mass of bottle + cap = -59.007 g
Mass of 2 mL Urea = - 2 g
1.68 g membrane proteins

17. Store the bottle in the -80 ^{0}C until ready to continue on with the Pre-extraction and Extraction steps.

Pre-Extraction: (~ 6 hours)

1) Solutions and Supplies

70 mL Pre-extraction buffer
70 mL 1:1 Extraction buffer/Isopropanol
50 ^{0}C water bath
4 x 30mL centrifuge bottles
250-mL centrifuge bottle

2) Recipes

Solution	Final Volume (mL)	Components	Mass (g)
Pre-Extraction Buffer	150	3.5 M Urea*	31.55g urea
		20 mM Tris-HCl	0.473g Tris-HCl
		0.05% 2-ME	75 uL 2-ME
		pH 9	-
Extraction Buffer	150	8 M urea*	72.12g urea
		20 mM Tris-HCl	0.473g Tris-HCl
		0.1% 2-ME	150 uL 2-ME
		pH 8.5	-

***** The volume of urea is not trivial! (**1g urea ≈ 1 mL urea**). A 150 mL solution of 8M urea will require ~80mLs of Milli-Q water.

Notes:
Add all dry chemicals first, then add water.
Adjust the pH of the solution using 1M NaOH drop wise (with pH-meter).
2-ME is stored in the hood, and should be distributed in the hood.
The 1:1 Extraction buffer/isopropanol is made with 35 mL Extraction buffer and 35 mL isopropanol.

3) Procedure

1. Remove the pellets from the freezer, and defrost in a 50 ^{0}C water bath. Add the rest of the 70 mLs of Pre-Extraction buffer. (*If 2 mLs were added previously to dissolve the left-over pellets after the cell-lysis procedure, add 68mLs more.) Stir using with a stir bar. The solution should turn yellowish/brown in color.

2. When no more clumps are visible, distribute the dissolved solution evenly into four centrifuge tubes. Weigh the tubes. (Follow the same procedure from the cell-lysis section.) Pair up the similarly weighed tubes, and adjust the weight until the two tubes have the same weight to two decimal places (0.01g). Place the tubes with the SAME WIGHT across from each other in the rotor to balance. Repeat for the other pair of tubes.

3. Centrifuge in the JA-17 rotor for 2 hours, at 17,000 rpm, and 4^{0}C.

4. Pour off the supernatant from the three tubes (containing the membrane proteins) into a separate bottle and SAVE it. Label it "**Peripheral Proteins**", and include the mutant name (OmpA-W_), the date, and your initials on a piece of tape. Store the bottle in the chromatography fridge in the equipment room until the entire lysis/ pre-

extraction/extraction process is complete. (You will run a gel on these saved solutions at the end.) Dump out the water from the fourth tube.

5. The pellet should be reddish/brown in color, and contains the integral membrane proteins only. Combine the pellets into a clean 250mL centrifuge bottle.

6. Rinse the centrifuge tubes with 2-3 mLs total of (1:1) extraction buffer: isopropanol, to remove the remaining pellet fragments: Add 1 mL of the extraction buffer/isopropanol solution (0.5mL Extraction Buffer + 0.5mL isopropanol) to one tube and dissolve the remaining pellet fragments. Transfer the mL of solution to the next tube, dissolve the fragments, and transfer to the next tube, etc. When all three tubes have been rinsed once, transfer the mL to the bottle containing the pellets. Add another (fresh) mL of extraction buffer/isopropanol solution and repeat the above process until the tubes have been rinsed with 2-3mL total of extraction buffer/isopropanol. Combine the "rinses" with the pellets in the centrifuge bottle, and store in the -20 ^{0}C freezer until the next day.

Extraction: (~ 4-5 hours)

1) Solutions and Supplies

35 mL Extraction buffer
35 mL isopropanol
50 ^{0}C water bath
4 x 30mL centrifuge bottles
100-mL bottle

2) Recipes

Solution	Final Volume (mL)	Components	Mass (g)
Extraction Buffer*	150	8 M urea	72.12g urea
		20 mM Tris-HCl	0.473g Tris-HCl
		0.1% 2-ME	150 uL 2-ME
		pH 8.5	-

*Final working solution is a 1:1 solution of Extraction Buffer: Isopropanol
(35mL Extraction buffer + 35mL isopropanol)
*Add all dry components first, then add appropriate amount of Milli-Q water.

3) Procedure

1. Add the remaining 1:1 Extraction buffer/isopropanol solution to the frozen pellets and defrost in a 50 ^{0}C water bath (~1hour), while stirring. (*If 2 mLs were added previously to dissolve the left-over pellets after the Pre-Extraction procedure, add 68mLs more.)

2. To help remove the protein from the membrane, it is helpful to break up the pellets with a spatula. After the red/brown pellets are completely dissolved, there will be fatty white clumps floating in solution. This is the remaining insoluble membrane/lipids.

3. When no more clumps are visible, distribute the solution evenly into three centrifuge tubes. Fill another tube with water (to balance). There will be four tubes total now, three with protein solution and one with water. Weigh the tubes. (Follow the same procedure from the cell-lysis section.) Pair up the similarly weighed tubes, and adjust the weight until the two tubes have the same weight to two decimal places (0.01g). Place the tubes with the SAME WIGHT across from each other in the rotor to balance. Repeat for the other pair of tubes.

4. Centrifuge in the JA-17 rotor for 1.5 hours, at 17,000 rpm, and 4^{0}C.

5. After the centrifuge cycle is complete, pour the supernatant into a bottle and label it "**Crude Protein**", and include the mutant name (OmpA-W_), the date, and your initials on a piece of tape. Store the bottle in the chromatography fridge in the equipment room until ready for purification. This is the crude OmpA membrane protein. Save some of the pellet in a 1.5-mLEppendorf tube, label it "membrane", (include mutant name, date, initials) and place it in the fridge.

6. Determine the concentration of the crude protein: Use UV-Vis absorption spectrometer (the two lamps should warm up at least for twenty minutes before collecting a spectrum).

In the (black) quartz absorption cuvettes, **blank** on 1 mL of (1:1) Extraction buffer:isopropanol. Collect a **sample** spectrum of 0.5 mL crude protein + 0.5 mL (1:1) extraction buffer:isopropanol (2xdilution). Pour the "sample" + extraction buffer/isopropanol back into the bottle containing the crude protein. The additional extraction buffer/isopropanol that gets added to the "crude protein" does not affect the purification process. Label (and save) the spectrum in the UV-Vis software as follows: your initials, the month, the date, and the sample number.

> **Example**: ks012401, ks012402, ks012403, … indicating ks took the spectra on January 24th, on samples 1, 2, 3…

7. Calculate the concentration using the OD at 280 nm. See Figure 1 below for a sample absorption spectrum of a single Tryptophan truncated OmpA mutant, and Table 1 below for determination of concentrations in µM and mg/mL.

Figure 1: Absorption spectrum of crude OmpA-W57t mutant. Blanked on (1:1) extraction buffer: isopropanol. OD_{280} = 0.55 (2x dilution). Final concentration of crude OmpA-W57t = **42.2 uM** = **0.8 mg/mL**.

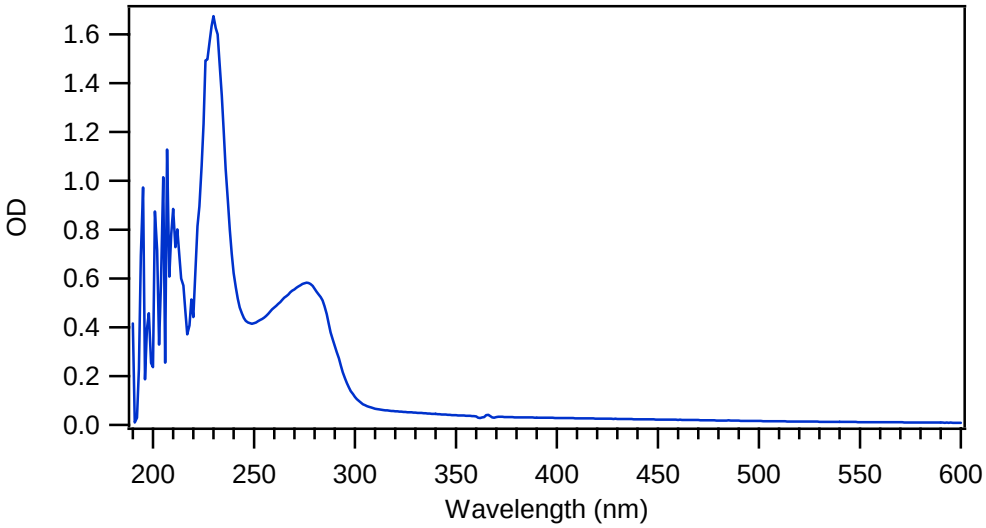

Table 1: ε, µM, and mg/mL for OmpA mutants

OmpA	ε ($M^{-1}cm^{-1}$)	1 OD_{280} = (µM)	1 OD_{280} = (mg/mL)
Wild Type	54,394	18.38 µM	0.646 mg/mL
1 W mutant	32,326	30.93 µM	1.083 mg/mL
0 W mutant	26, 809	37.30 µM	1.300 mg/mL
1 W truncated mutant	26,018	38.44 µM	0.732 mg/mL

8. Print out a copy of the absorption spectrum of the crude protein. Tape it in the OmpA Logbook and record the OD_{280} of the Crude Protein, the OmpA mutant name, the date, your initials, and the UV-Vis filename next to the spectrum.

Purification: (~ 8 hours)

1) Solutions and Supplies

Buffer A (filtered)
Buffer B (filtered)
Cleaning Buffer (filtered)
1000 mL Milli-Q water (filtered)
Crude Protein (filtered)
150-mL Superloop
FPLC with 5-mL QSFF anion exchange column
60 Test tubes (12mm x 75mm)

2) Recipes

Solution	Volume	Components	Mass (g)
Buffer A*	1000 mL	8 M urea	480.8
		15 mM Tris-HCl	2.364
		0.05% 2-ME	500 uL
		pH 8.5	-
Buffer B*	500 mL	8 M urea	240.4
		15 mM Tris-HCl	1.182
		0.05% 2-ME	250 uL
		200 mM NaCl	5.844
		pH 8.5	-
Cleaning Buffer*	500 mL	8 M urea	240.4
		20 mM KPi	0.8709 g K_2HPO_4
			0.6805 g KH_2PO_4
		2M NaCl	58.44
		pH 7.3	-

* All solutions must be filtered first before using! See Procedure section below for details.

Notes:
Add all dry components first, and then add the appropriate amount of Milli-Q water.
The volume of urea is NOT trivial! (**1g urea ≈ 1 mL urea)**
Adjust the pH of the solutions using the pH meter and 1M NaOH.

3) Procedure

1. Filter (separately) Buffer A, Buffer B, the Cleaning Buffer, 1000 mL of Milli-Q water, and the Crude Protein. (All the solutions need to be dust free and particle free to prevent clogging the tubing.) See Figure 1 below.

Figure 1: Part of the filtration set-up.

2. Place the tubing from **Pump A** into the **Buffer A** bottle, and the tubing from **Pump B** into the **Buffer B** bottle. Cover both bottles with aluminum foil.

3. The purification method used to purify OmpA mutants has been programmed into the FPLC Controller (LLC-500) as Method 1. To run the OmpA Purification Method, make sure the tubing is in the correct bottle (see number 2 above) and then press **#1** and then press the **do/store** button. See Method 1 below for the entire purification method.

Method 1: OmpA Purification

Volume	Function	Value	Notes
0.0	conc % B	0.0	100% Buffer A
0.0	mL/min	2.0	flow rate
0.0	cm/mL	0.5	chart recorder rate (don't have one!)
0.0	**valve.pos**	1.3	WASH (switch out buffers in pumps)
25.0	conc % B	0.0	
25.0	conc % B	100.0	100% Buffer B
50.0	conc % B	100.0	
50.0	conc % B	0.0	
50.0	**valve.pos**	1.1	LOAD (equilibrate column w/ buffers)
75.0	conc % B	0.0	
75.0	conc % B	100.0	
100.0	conc % B	100.0	
100.0	conc % B	0.0	

150.0	**valve.pos**	1.2	INJECT (inject protein onto column)
225.0	**valve.pos**	1.1	LOAD (wash column with Buffer A)
246.0	**port.set**	6.1	fraction collector ON
250.0	conc % B	0.0	Concentration gradient [0-200] mM NaCl
350.0	conc % B	100.0	
354.0	**port.set**	6.0	fraction collector OFF
375.0	conc % B	100.0	
375.0	conc % B	0.0	
425.0	conc % B	0.0	

4. In the mean time, prep the 150-mL Superloop with Buffer A. With a 60-mL syringe, load Buffer A into the top of the superloop, then reverse it, and load buffer A into the bottom